THE UNIVERSITY
of EDINBURGH

This thesis has been submitted in fulfilment of the requirements for a postgraduate degree (e.g. PhD, MPhil, DClinPsychol) at the University of Edinburgh. Please note the following terms and conditions of use:

This work is protected by copyright and other intellectual property rights, which are retained by the thesis author, unless otherwise stated.
A copy can be downloaded for personal non-commercial research or study, without prior permission or charge.
This thesis cannot be reproduced or quoted extensively from without first obtaining permission in writing from the author.
The content must not be changed in any way or sold commercially in any format or medium without the formal permission of the author.
When referring to this work, full bibliographic details including the author, title, awarding institution and date of the thesis must be given.

Apoptotic cell interaction with IgM antibodies and modulation of ischaemic tissue injury

A thesis submitted by

Emily E. Hesketh

to

The College of Medicine and Veterinary Medicine
in fulfillment of the requirements for the degree of

Doctor of Philosophy
in the subject of
Clinical Sciences – Inflammation

MRC Centre for Inflammation Research, University of Edinburgh,
Queen's Medial Research Institute, Edinburgh, United Kingdom

March 2015

“If we knew what it was we were doing, it would not be called research, would it?”

— Albert Einstein

“You cannot pass,” he said. The orcs stood still, and a dead silence fell. “I am a servant of the Secret Fire, wielder of the flame of Anor. You cannot pass. The dark fire will not avail you, flame of Udûn. Go back to the Shadow! You cannot pass.”

— J.R.R. Tolkien, *The Fellowship of the Ring*

Declaration

This is to declare that this thesis has been composed by me and presents my own original research. Wherever contributions of others are involved every effort is made to indicate this clearly and instances of collaborative research are acknowledged. No part of this thesis has been submitted for any other degree or professional qualification. Publications and presentations arising from this work have also been acknowledged.

This work was performed under the supervision and guidance of Professor Jeremy Hughes and Dr David C Kluth at the MRC Centre for Inflammation Research, University of Edinburgh, Queen's Medical Research Institute.

Signed: …… **Date:** …….

Emily E. Hesketh

Abstract

Acute kidney injury (AKI) induced by renal ischaemia reperfusion injury (IRI) is characterised by renal failure, acute tubular necrosis (ATN), inflammation and microvascular congestion. Apoptotic cell administration reduces inflammation in experimental models of acute inflammation in the lung, joints and peritoneum. Preliminary data suggested that administration of $20x10^6$ apoptotic thymocytes to mice 24-hours prior to renal IRI ameliorated renal function without affecting ATN 24-hours following IRI. This thesis attempted to validate these finding and explore underlying hypothetical mechanisms. These studies examined if functional protection was conferred by apoptotic cell modulation of (a) circulating IgM antibodies or (b) coagulation status leading to improved intrarenal microvascular blood flow.

Pathogenic IgM antibodies bind ischaemic cardiac or skeletal muscle and the intestine leading to complement activation and worse injury. We examined IgM binding to human renal (HK-2) cells by flow cytometry and to ischaemic murine kidney tissue. H_2O_2 or Antimycin A treated HK-2 cells incubated with human serum (IgM source) exhibited no IgM binding. Medullary IgM deposition assessed by immunofluorescence was minimal following IRI. We also assessed IgM deposition by immunohistochemistry following hepatic IRI and discovered dramatic deposition. These data suggest that IgM antibodies exhibit differential binding to injured tissues and are not directly involved in renal IRI, but may have a role in hepatic IRI.

To support our second hypothesis we studied apoptotic cell modulation of coagulation. A thrombin generation assay revealed that early apoptotic cell-treated mice exhibited delayed thrombin generation. Furthermore, *in vitro* studies confirmed direct apoptotic cell-platelet binding. To replicate apoptotic cell derived functional protection Balb/c mice underwent 20, 24 or 25-minutes of ischaemia to induce mild, moderate or severe kidney dysfunction. Renal function and injury was determined 24-hours following IRI by plasma creatinine measurement and ATN scoring. Unexpectedly,

intravenous pretreatment of mice with apoptotic thymocytes conferred no protection. Indeed, apoptotic thymocytes further impaired renal function depending upon injury severity. Impairment of renal function was not secondary to increased microvascular congestion, inferred by fibrin and platelet deposition, neither increased ATN nor inflammation, assessed by neutrophil infiltration. These data indicate that apoptotic cell administration does not protect from subsequent renal IRI and that apoptotic cells are thus not inherently anti-inflammatory in all models of acute inflammation.

Unable to replicate apoptotic cell derived functional protection we explored the binding of IgM antibodies to apoptotic cells which acts to facilitate dead cell clearance. We characterised IgM binding to non-apoptotic and apoptotic murine thymocytes and human Jurkat cells using flow cytometry, confocal and electron microscopy. We demonstrated specific IgM binding to a subset of late apoptotic cells. Electron microscopy indicated that IgM^{+} apoptotic cells exhibited marked plasma membrane disruption, suggesting that access to intracellular epitopes was required for IgM binding. Binding of IgM to permeabilised non-apoptotic and apoptotic cells suggested that IgM bound epitopes are 'apoptosis independent' such that IgM may bind any cell with profound plasma membrane disruption. Interestingly, permeabilised erythrocytes exhibited significant IgM binding thus supporting the importance of cell membrane epitopes. These data suggest that IgM may recognise and tag damaged nucleated cells or erythrocytes that exhibit significant cell membrane disruption.

Lay Abstract

Acute kidney injury (AKI) is common and may affect many critically ill patients when it increases morbidity and mortality. Current treatments for AKI are purely supportive with no specific treatment options available. AKI involves acute inflammation and disruption of blood flow through the microvasculature (system of small blood vessels) and these areas urgently require novel treatments. Apoptotic cells (dying cells) can influence inflammation and the coagulation system with apoptotic cell treatment improving outcome in several experimental animal models of disease. Preliminary data that gave rise to these studies suggested that the administration of apoptotic cells to mice prior to the experimental induction of AKI protected mice from functional injury. In this thesis, we investigated two hypothetical mechanisms that may explain how apoptotic cells can protect mice from AKI. These examined the interaction of apoptotic cells with (a) a specific type of antibody known as IgM and (b) the blood clotting system.

IgM antibodies are known to be harmful in heart, skeletal muscle and intestinal injury. We first aimed to confirm that IgM antibodies were involved in AKI. Studies in a mouse model of AKI and human kidney cell culture assays clearly indicated that IgM antibody did not bind to injured kidney cells. Our findings suggested that IgM is not a key player in AKI. As the role of IgM in liver injury was unknown, we also studied the involvement of IgM antibodies in a mouse model of liver injury. In contrast to the kidney, IgM antibodies bound strongly to injured liver tissue. Perplexed by this we next wanted to try and explain why IgM bound differently to different cells. Using cell culture assays, flow cytometry, confocal and electron microscopy we investigated IgM binding to a range of different cell types. These included healthy, apoptotic and permeabilised human and mouse immune cells and mouse red blood cells. We discovered that before IgM binding can take place, the outside surface of the cell must be sufficiently ‘open’ to allow the large IgM antibodies access to the cell interior.

We next focused our attention to how apoptotic cells might alter blood clotting. Through the use of blood clotting assays and flow cytometry we demonstrated that apoptotic cells could directly bind platelets (key particles that affect clotting) and modify the rate at which blood clots. These findings indicated that apoptotic cells might be able to alter blood clotting such that blood flow after AKI was improved resulting in protected renal function. Lastly, multiple experiments attempted to unequivocally determine whether apoptotic cell administration prior to mice prior to AKI was protective but no protection was seen. Indeed, the injury was actually worsened in some settings. This was found not to be the result of increased blood clotting in the microvasculature, increased structural injury or inflammation.

The totality of these results indicates that IgM antibodies are not likely to be viable targets of novel therapeutics in the treatment of AKI. In addition 'apoptotic cell therapy' does not have translational relevance for patients with AKI.

Acknowledgements

I would like to express my gratitude towards my supervisors Professor Jeremy Hughes and Dr David Kluth who made my project possible. I would like to sincerely thank Jeremy whose thoughtful advice, guidance and pioneering attitude has made me a better scientist. I will endeavor to complete all future experiments and papers with my 'reviewer's cap' on.

I must acknowledge Professor Ian Dransfield for the valuable insight, critique and advice he provided throughout my studies. I am grateful for the help I received from the talented experimental surgeons that are Gary Borthwick and Spike Clay. Their vast expertise greatly improved my *in vivo* skills. I would like to especially thank Gary for his assistance and patience that was vital for all of my *in vivo* experiments. I must also thank Shonna Johnston and Fiona Rossi whose impressive knowledge of everything flow cytometry was crucial in the design and implementation of many experiments.

The Phagocyte Interest Group (The PIG Lab) is one of the most highly functioning, talented and good-natured research groups that I have seen. I feel extremely fortunate to have been a member. I am indebted to many of the members whose contributions ranged from reagents and advice to humor and coffee. The entertainment provided by past and current members of office W2.29 was much appreciated. I extend a special mention to my friend George Tse as we both started and managed to finish our PhD studies together.

Finally I would like to say cheers to my parents for their continued support, interest and genuine efforts to understand my research. Sorry for being a tad moody sometimes.

My studies were supported by grants awarded by Kidney Research UK, the Mrs AE Hogg Charitable Trust for Kidney Research and the Renal Endowment Fund of the Royal Infirmary of Edinburgh.

Publications and Presentations

Publications arising from this work

Hesketh EE, Dransfield I, Kluth DC, Hughes J: Circulating IgM requires plasma membrane disruption to bind apoptotic and non-apoptotic nucleated cells and erythrocytes. *Submitted*

Hesketh EE, Kluth DC, Hughes J: Apoptotic cell administration is detrimental in murine renal ischaemia reperfusion injury. *Journal of inflammation (London, England)* 2014, **11**:31.

Hesketh EE, Czopek A, Clay M, Borthwick G, Ferenbach D, Kluth D, Hughes J: Renal ischaemia reperfusion injury: a mouse model of injury and regeneration. *JoVE* 2014, **88**:e51816

Presentations (Poster) of this work:

Apoptotic cell administration to mice is detrimental to renal function following renal ischaemia reperfusion injury.
Emily E. Hesketh, David Kluth & Jeremy Hughes.
British Society for Immunology, Inflammation and Disease Meeting 2014, University of Manchester

Apoptotic cell administration to mice modulates thrombin generation but is detrimental to renal function following renal ischaemia reperfusion injury.
Emily E. Hesketh, Roger Preston, David Kluth & Jeremy Hughes.
UK Kidney Week 2014, Scottish Exhibition Conference Centre, Glasgow

The interaction of IgM with apoptotic cells and differential IgM deposition in ischaemic kidney and liver tissue.

Emily E. Hesketh, James Richards, Martina Bucsaiova, Mark Dockrell, David Kluth & Jeremy Hughes.

UK Kidney Week 2014, Scottish Exhibition Conference Centre, Glasgow

Acute Kidney Injury and Dying Cells.

Emily E. Hesketh, Roger Preston, David Kluth & Jeremy Hughes.

Kidney Research UK Fellowship Day 2013, University of Durham

Contents

Figure and Table List

Abbreviations

AC(s)	Apoptotic cell(s)
AIH	Autoimmune Hepatitis
AKI	Acute Kidney Injury
ALF	Acute liver failure
AnnV	Annexin-V
ANOVA	Analysis of variance
APC	Allophycocyanin
APC	Activated protein C
APCs	Antigen presenting cells
ATN	Acute tubular necrosis
BSA	Bovine serum albumin
BUN	Blood urea nitrogen
C#	Complement protein #
CD#	Cluster differentiation#
CIA	Collagen induced arthritis
CLP	Caecal ligation and puncture
CMFDA	5-chloromethylfluorescein diacetate
ConA	Concanavalin A
DAB	3,3'-Diaminobenzidine
DAF	Complement decay accelerating factor
DAMP	Damage associated molecular pattern
DAPI	4',6-diamidino-2-phenylindole
Dex	Dexamethasone
EDTA	Ethylenediaminetetraacetic acid
FACS	Fluorescence-activated cell sorting
FCS	Fetal calf serum
FITC	Fluorescein isothiocyanate
FMO	Fluorescent minus one

FRET	Fluorescence resonance energy transfer
FSC	Forward scatter
H&E	Haematoxylin and eosin
H_2O_2	Hydrogen Peroxide
HCl	Hydrochloric acid
HGF	Hepatic growth factor
HK-2	Human proximal tubular epithelial cells
i.t	Intratracheal
i.v	Intravenous
IF	Immunofluoresce
IFN-γ	Interferon-γ
Ig	Immunoglobulin
IHC	Immunohistochemistry
IL-#	Interleukin-#
iNOS	Inducible nitric oxide
IRI	Ischaemia reperfusion injury
KO	Knock out
LDL	Low-density lipoprotein
LPS	Lipopolysaccharide
MAC	Membrane attack complex
MBL	Mannose binding lectin
MetOH	Methanol
MFI	Median fluorescent intensity
NF-kβ	Nuclear factor- kβ
NMHC-II	Non-muscle myosin heavy chain II
OSOM	Outer stripe of the outer medulla
PAF	Platelet activating factor
PBS	Phosphate buffered saline
PDGF	Platelet-derived growth factor

PE	Phycoerythrin
PerCp-Cy5.5	Peridinin-chlorophyll-protein Complex
PFA	Paraformaldehyde
PI	Propidium Iodide
PtdSer	Phosphatidylserine
RAG-1	Recombination Activation Gene-1
ROS	Reactive oxygen species
RPMI	Roswell Park Memorial Institute medium
sCR1	Soluble complement receptor type 1
SEM	Standard error of mean
SLE	Systemic lupus erythematosus
SSC	Side scatter
TEM	Transmission electron microscopy
TGA	Thrombin generation assay
TGF-β	Transforming growth factor-β
Th-#	T helper-#
TLR-4	Toll like receptor-4
TNF-α	Tumour necrosis factor-α
μMT	B-cell deficient

Chapter 1. Introduction

1.1 Basic overview of acute injury

1.1.1 What is acute injury?

Acute injury is a specific type of injury with symptoms or signs that manifest suddenly. Despite being termed 'acute', these injuries may be life threatening. Patients with acute injuries to the lung, brain, liver, heart or kidney are challenging to care for and are vulnerable to complications such as downstream organ dysfunction. This is a particular concern for patients with acute kidney injury (AKI). Unfortunately, injury pathogenesis is often complex with only partial recovery of organ function.

1.1.2 What are the causes of acute injury?

Acute injury can arise as the result of multiple and varied insults including trauma, ischaemia reperfusion injury, drug toxicity, sepsis and autoimmunity. The kidney receives a large blood supply in order to effectively filter the blood and is particularly vulnerable to injury resulting from drug toxicity and ischaemia reperfusion injury (IRI) with the latter being of particular relevance to this thesis. The adverse impact of IRI is often evident following organ transplantation or cardiac surgery that inevitably result in a localized or global restriction of blood supply (Eltzschig and Eckle, 2011). All tissues are vulnerable to IRI including the intestine, kidney, liver, brain, cardiac muscle and skeletal muscle. IRI results in two phases of injury (Eltzschig and Eckle, 2011). Initial injury occurs due to ischaemia and the resultant tissue de-oxygenation and reduced cellular metabolism that may lead to cell death. The second phase of injury occurs when blood supply is restored and tissue is reperfused as this may lead to oxidative stress and the generation of reactive oxygen species and subsequent inflammation and cell injury.

1.1.3 What are the key players in acute injury?

Although the exact pathogenesis of acute injury may vary depending upon the mode

of injury and the tissues affected, the molecular and cellular pathways of acute inflammation are always a key driving force.

1.1.3.1 Mediators of inflammation

Reactive oxygen species (ROS) are key signaling molecules and mediators of acute inflammation at sites of tissue injury (Mittal et al., 2014). These are highly reactive compounds produced following tissue damage, such as hydrogen peroxide (H_2O_2). ROS can induce the secretion of pro-inflammatory cytokines such as tumour necrosis factor-α (TNF-α) and interleukin-1 (Vinay et al., 2012). Through broad signaling pathways, mediated by the transcriptional regulator nuclear factor-κB (NF-κB), these cytokines stimulate the production of chemokines. These chemotactic factors act to promote the rapid infiltration of key immune cells to sites of inflammation (Kindt et al., 2007).

1.1.3.2 Immune cells

Rapid leukocyte infiltration is often a hallmark of acute injury. Whilst the exact composition of this infiltrate varies depending upon the injury, key inflammatory cells are prevalent in the pathogenesis of tissue injury. These include monocytes, macrophages, neutrophils and platelets (Kindt et al., 2007). Monocytes infiltrate into the tissue and may differentiation into macrophages depending upon the local pro-inflammatory mediators (Shi and Pamer, 2011). Neutrophils are usually the first leukocyte to reach sites of tissue injury and can potentiate injury by the secretion of pro-inflammatory mediators that drive further inflammation and cellular injury (Kindt et al., 2007, Mittal et al., 2014).

1.1.3.3 Cellular injury

Cellular injury can be reversible or irreversible leading to cell death depending upon the cell type and the duration and severity of the injurious insult (Vinay et al., 2012). For instance short periods of ischaemia may result in reversible or sublethal damage characterised by cell and mitochondria swelling and membrane blebbing. Conversely

damage induced by longer durations of ischaemia can be irreversible and lethal leading to apoptosis and/or necrosis.

This thesis will primarily study acute kidney injury (AKI), and to a lesser extent acute liver injury, induced by ischaemia reperfusion injury.

1.2 Acute Kidney Injury and Renal Ischaemic Reperfusion Injury

1.2.1 The kidney

The kidneys are the principal site of blood filtration and the regulation of water and salt balance in the excretory system of mammals (Campbell and Reece, 2011). A diagrammatic representation of the major anatomical features of the kidney is provided in figure 1.1A. These paired bean shaped organs receive approximately 20% of resting cardiac blood flow, which is supplied by a renal artery and drained by a renal vein. Urine flows from an individual kidney through a thin muscular tube, known as a ureter, and drains into a urinary bladder.

The kidney can be divided into two anatomically distinct regions comprising the renal cortex and medulla. Travelling through both of these regions is the major functional filtration unit of the kidney – the nephron (Figure 1.1B). In the mammalian kidney the nephron is an approximately 30-55 mm long thin tubule. This tubule begins in the cortex where one end is folded into a cuplike structure named the Bowman's capsule. This surrounds a ball of capillaries that forms the glomerulus. At this point filtration begins as, due to hydrostatic pressure, fluid from the glomerular capillaries is forced across the glomerular basement membrane into the lumen of the Bowman's capsule. The filtrate then passes into the proximal convoluted tubule. The nephron then performs a hairpin bend into the renal medulla in an area of the tubule known as the loop of Henle. Exiting the loop of Henle the filtrate then passes though the distal convoluted tubule, located back in the renal cortex, before travelling to the renal pelvis and ureter via a collecting duct which transverses both the renal medulla and

cortex. The composition of the filtrate is altered to produce urine as the filtrate passes through the nephron by a combination of active and passive transport of water, salts, amino acids and glucose. As the kidneys perform a crucial function an acute injury can be devastating.

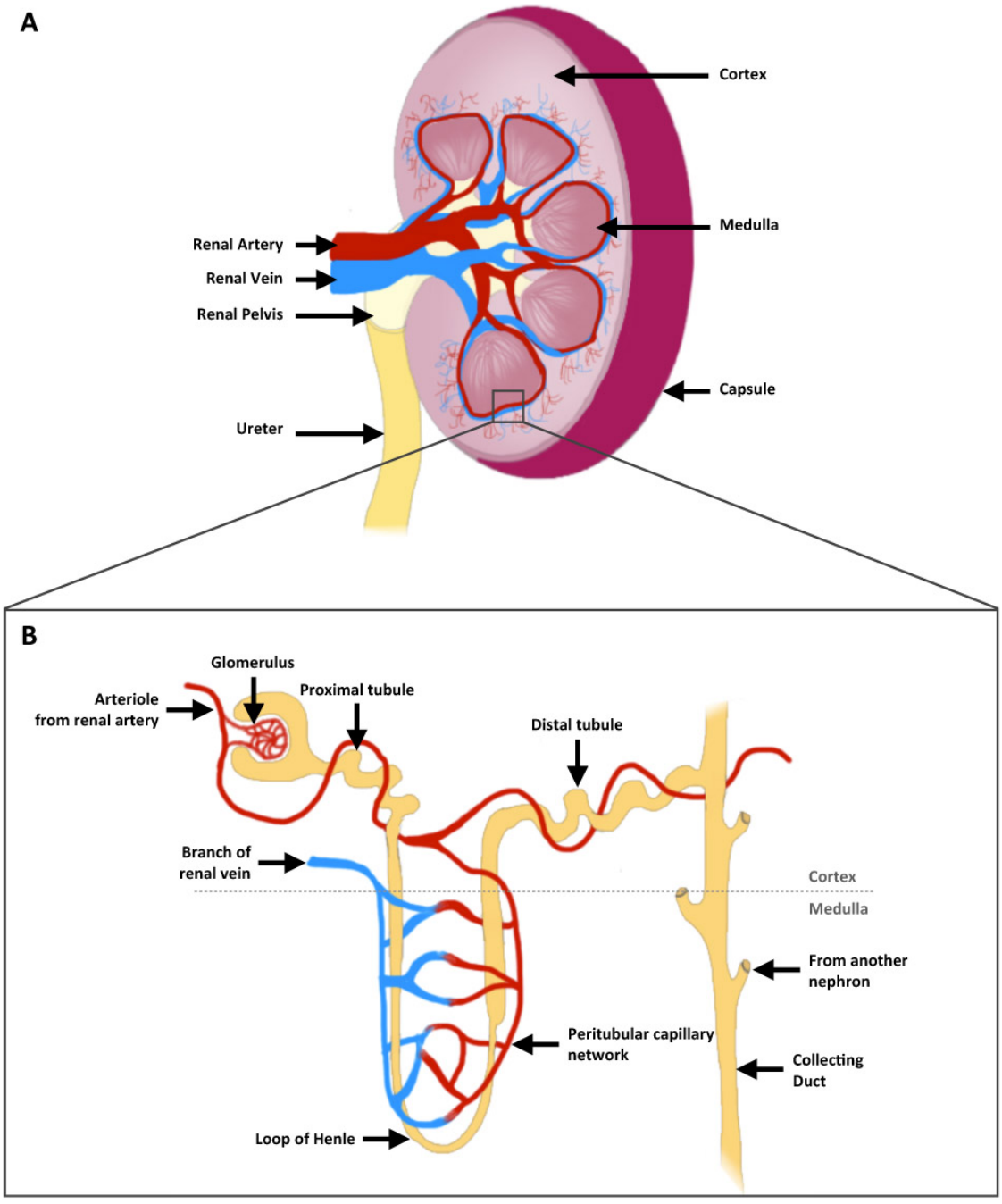

Figure 1.1 Overview of the kidney (A) and the functional unit of the kidney – the nephron (B). Drawn on the basis of the information provided in Chapter 44: Osmoregulation and Excretion in Campbell Biology (Seventh Edition) by Campbell and Reece (2011).

1.2.2 Acute Kidney Injury (AKI)

AKI is a serious and unfortunately common condition that affects hospital inpatients worldwide and is associated with a high mortality and long-term complications (Kerr et al., 2014). The typical clinical characteristics of AKI include a rapid reduction in renal excretory function, diagnosed by elevated levels of serum creatinine and blood urea (products of muscle and nitrogen metabolism, respectively), accumulation of metabolic acids and reduced urine output (Bellomo et al., 2012, Lameire et al., 2013). AKI can arise as the result of extrarenal events, such as cardiac dysfunction, or due to direct intrinsic kidney damage, such as renal IRI (Lameire et al., 2013).

1.2.3 Current treatments

Renal IRI and acute kidney injury place a significant burden upon the health service with an estimated annual AKI-related inpatient cost of £1.02 billion in England alone (Kerr et al., 2014). There is an urgent need for novel AKI treatments, as current clinical treatments still remain purely supportive with no specific therapy available. Acute renal failure may necessitate dialysis but this has no effect upon the underlying AKI and a significant proportion of affected patients will either die or be left with chronic kidney disease. As inflammation plays a key role following renal IRI it is not surprising that the resultant injury may be attenuated by anti-inflammatory treatments (Lutz et al., 2010). Reduced chemokine generation by caspase, NF-κB, and p38 MAPK inhibition ameliorates renal injury following ischaemia (Furuichi et al., 2008). Inflammatory pathways and the microvascular system are two avenues in which novel therapeutics can be developed.

1.2.4 Renal ischaemia reperfusion (IRI) injury pathophysiology

AKI induced by renal IRI is a significant risk factor for patients undergoing renal transplantation or any major surgery that may transiently reduce renal blood flow, such as cardiac surgery. Ischaemic AKI has a complex pathogenesis involving acute inflammatory responses, endothelial and tubular epithelial cell injury (Patschan et al., 2012a, Bonventre and Zuk, 2004, Kinsey et al., 2008). Figure 1.2 provides a

diagrammatic representation of the major changes that occur relevant to this thesis following ischaemic injury.

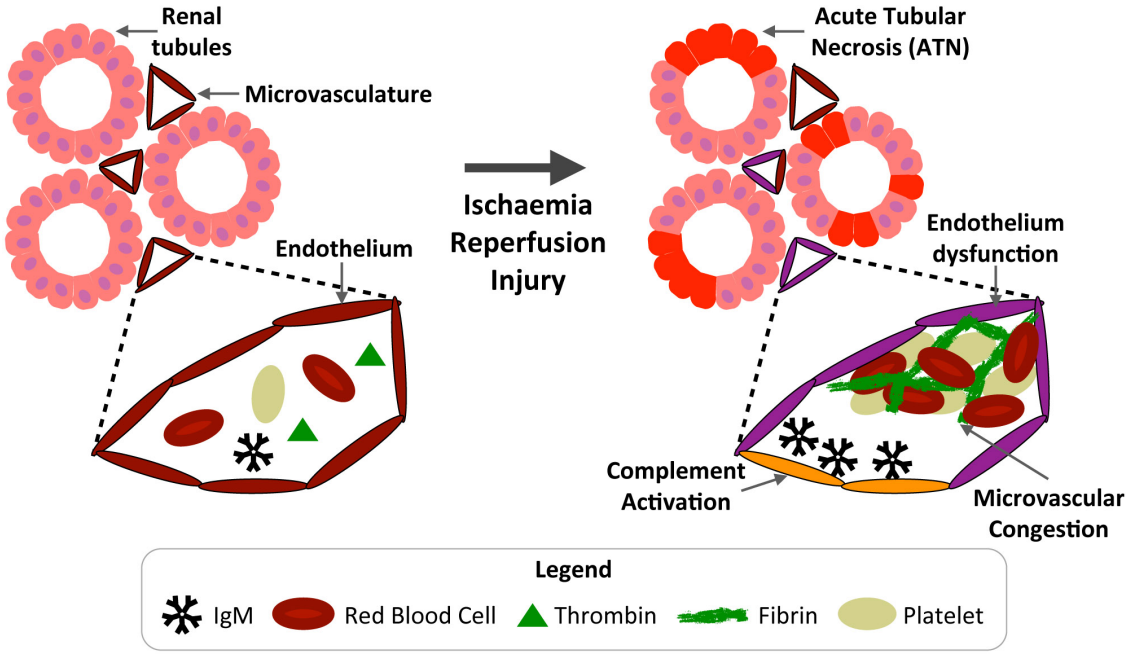

Figure 1.2 – Normal and ischaemic renal microvasculature. Within small peritubular capillaries the endothelium maintains a patent microvascular system by regulating inflammatory cell migration, blood fluidity and preventing thrombus formation. Upon IRI acute tubular necrosis occurs along with endothelial dysfunction. These alterations lead to fibrin and platelet deposition, red blood cell sludging ultimately leading to microvascular congestion, which impairs reperfusion and glomerular filtration. Reperfused injured cells may express autoantigens that are recognised and bound by IgM leading to complement activation that intensifies injury and delays the restoration of renal function. Note that the presentation of autoantigens and IgM antibody binding is introduced in '1.4 IgM Antibodies and Ischaemic Tissue Injury'.

1.2.4.1 Inflammation and acute tubular necrosis

Inflammation has a major influence on the initiation and amplification of IRI, with both the innate and adaptive immune system influencing the pathogenesis of renal IRI (Jang et al., 2010). Pro-inflammatory cytokines such as TNF-α, interleukin (IL)-1β and IL-6 are released by infiltrating leukocytes and injured tubular epithelial cells and act to potentiate inflammation and associated injury (Daha and van Kooten, 2000, Ramesh and Reeves, 2004, Thurman, 2007). Immune cell infiltration is a hallmark of renal IRI with neutrophils and macrophages infiltrating into the interstitium (Patschan et al.,

2012a, Friedewald and Rabb, 2004). Inflammatory responses lead to further endothelial dysfunction and injury with increased leukocyte infiltration and reduced blood flow (Bonventre and Zuk, 2004). Impaired renal blood flow, contributing to a reduction in glomerular filtration rate, promotes renal medullary hypoxia and amplification of cellular injury (Basile, 2011). As a result of ischaemia the structure and function of tubular epithelial cells are significantly altered, as they progress through apoptosis or necrosis, leading to acute tubular necrosis (ATN) (Patschan et al., 2012b, Patschan et al., 2012a). These alterations have a direct impact on the microvasculature.

1.2.4.2 Ischaemic microvascular tissue injury

Alterations to the highly specialized renal microvascular architecture contribute to both the initiation and exacerbation of renal IRI (Becherucci et al., 2009, Patschan et al., 2012b). These microvascular effects are first observed in the medulla, which receives only 10% of the renal blood flow rendering it vulnerable to ischaemic damage (Munshi et al., 2011, Friedewald and Rabb, 2004). Endothelial cells regulate inflammatory cell migration, blood fluidity and actively prevent thrombus formation by controlling fluid, solutes, platelet and blood cell extravasation (Sutton et al., 2002). The endothelium regulates tissue perfusion by controlling local vasoregulation (van Hinsbergh, 2012). Ischaemia results in multiple changes in endothelial morphology including cell swelling, basement membrane detachment, increased leukocyte adhesion molecule expression and blebbing (Sutton et al., 2002). This endothelial dysfunction promotes inflammation, perturbs coagulation control and thrombus formation thereby creating a prothrombotic environment (Becherucci et al., 2009, van Hinsbergh, 2012). These deleterious changes to the microvasculature can be further complicated by the actions of platelets.

1.2.4.3 Platelets

Platelets, which accumulate in the vascular bed, become active following reperfusion and may have a pathophysiological role in IRI. Platelets contain many pro-

inflammatory mediators and cell surface ligands (Morrell et al., 2007). Upon activation platelets release ROS and pro-inflammatory mediators including thromboxane A_2, leukotrienes and platelet-derived growth factor (PDGF) and the chemokine mediator platelet activating factor (PAF) (Massberg et al., 1998, Eppihimer and Granger, 1997). Through the selectin family of adhesion molecules, such as P-selectin (ligand – PGSL-1) platelets are able to bind to subendothelial matrixes (Eppihimer and Granger, 1997).

1.2.4.4 Microvascular congestion

The cumulative effect of the above alterations ultimately leads to the microvasculature becoming congested with erythrocytes and platelet/fibrin aggregates. This limits perfusion and propagates ischaemic injury (Patschan et al., 2012b, Eneström et al., 1988), a phenomenon termed 'no-reflow'. By reducing microvascular congestion reperfusion can occur more effectively eliminating prolonged ischaemic periods (Patschan et al., 2012b). Studies have indicated that a reduced pre-injury hematocrit improves renal blood flow post ischaemia (Mason et al., 1987, Hellberg et al., 1990). These studies suggest that microvascular congestion does indeed contribute to poor re-flow following ischaemia.

1.2.5 Experimental model of renal IRI

Experimental models that accurately and reproducibly recapitulate renal IRI are crucial in dissecting the pathophysiology of AKI and the development of novel therapeutic agents. In this thesis a surgical mouse model of renal IRI was used (Hesketh et al., 2014, Wei and Dong, 2012, Kumar et al., 2009, Oxburgh and de Caestecker, 2012). This model utilizes a midline laparotomy approach for the surgery with one incision allowing both a right nephrectomy, which provides control tissue, and clamping of the left renal pedicle to induce ischaemia of the left kidney. Sham controls are performed by manipulation of the left and right renal pedicle only following a laparotomy. By carefully monitoring the body temperature during the period of ischaemia this model achieves reproducible functional and structural injury. In contrast to models that utilise bilateral kidney ischaemia (Wei and Dong, 2012) the unilateral model has the

advantage of a right nephrectomy being undertaken at the time of surgery. The right nephrectomy tissue serves as non-injured control tissue.

1.3 Acute Liver Failure (ALF)

1.3.1 The Liver

As the largest organ in vertebrates the human liver can be broadly divided into two lobes; however, the exact form of the liver can vary between species (Campbell and Reece, 2011). The liver receives a dual blood supply from the hepatic artery and hepatic portal vein. Approximately 60% of the liver consists of cells termed hepatocytes that enable the liver to perform a diverse range of functions including filtration of blood arising the digestive tract, blood detoxification, bile secretion and synthesis of major complement and blood clotting proteins. As the liver performs a diverse range of functions acute injuries can be devastating.

1.3.2 Overview and pathophysiology

Although rare, with a worldwide incidence of below 10 cases per million persons a year, acute liver injury or acute liver failure (ALF) is a life threatening condition that arises as a result of sudden and severe hepatic injury (Bernal et al., 2010, Bernal and Wendon, 2013). ALF is associated with a mortality rate of 50%, with most patients presenting with hepatic dysfunction, abnormal liver biochemical values, and coagulopathy with some patients developing multi-organ failure, including renal dysfunction (Bernal and Wendon, 2013, Moore, 1999). Hepatic injury can originate as the result of multiple causes; however, relevant to this thesis are IRI (hypoxic hepatitis) and autoimmune hepatitis (AIH) both of which are highly inflammatory. Hypoxic hepatitis is characterised by hepatocyte necrosis, neutrophil and Kupffer cell activation, production of cytokines, chemokines and ROS with increased lymphocyte and monocyte infiltration (Zhai et al., 2013). Ischaemic injury is an important form of hepatic injury that may occur during hepatic tumour resections and liver transplant surgery as interruption of the hepatic blood supply is unavoidable (Mendes-Braz et al.,

2012). AIH is a chronic inflammatory condition, involving progressive fibrosis and loss of self tolerance with the development of autoantibodies (Mieli-Vergani and Vergani, 2011). The pathogenesis is thought to involve antigen-presenting cells (APCs) that present liver peptides derived from self-antigens to the T-cell receptor of T-helper cells (Mieli-Vergani and Vergani, 2011, Liberal et al., 2013). Resultant autoantibodies contribute to antibody-mediated cellular cytotoxicity and complement mediated tissue injury (Liberal et al., 2013). AIH patients often have elevated serum globulin levels with IgG levels generally elevated 1.2 to 3.0 times (Krawitt, 2006). To further dissect the pathogenesis of ALF and AIH researchers need to study animal models that accurately and reproducibly replicate the human disease.

1.3.3 Models of ALI

In this thesis hypoxic hepatitis was modeled in mice by warm (*in situ*) partial hepatic IRI. To induce ischaemia the hepatic artery, portal vein and bile duct of the left liver lobe are occluded. This results in only partial liver ischaemia as blood flow is still supplied to the patent right and caudal lobes (Mendes-Braz et al., 2012). AIH was modeled in mice using the plant lectin Concanavalin A (ConA) model (Tiegs et al., 1992, Wang et al., 2012). This model exhibits T-cell activation and cytokine upregulation indicative of chronic inflammation and autoantibody generation and closely replicates human disease (Wang et al., 2012, Sass et al., 2002, Nakano et al., 2013). Tissue necrosis occurs in both models, accompanied by elevated plasma levels of alanine aminotransferase (ALT) that represents a useful biochemical marker of liver injury.

1.4 IgM Antibodies and Ischaemic Tissue Injury

With autoantibodies present in patients with AIH, it is important to note that autoantibodies of the IgM isotype are implicated in the pathogenesis of ischaemic injury to the intestine, skeletal and cardiac muscle. Thus, the role of IgM antibodies in AIH, renal and liver IRI merits investigation.

1.4.1 Function, structure and IgM production

Immunoglobulin class M (IgM) antibodies are produced by a subset of B cells (B1 Cells) and exist as two forms – a) on the surface membrane of B-cells where it forms the B cell receptor and b) as a secreted circulating form found in the blood (Ehrenstein and Notley, 2010). Circulating IgM can be further divided into immune, produced following foreign antigen exposure, and IgM antibodies that are detectable in the absence of antigenic stimuli and are present at birth (Lobo et al., 2010, Ehrenstein and Notley, 2010). The focus of this thesis is circulating IgM. Unlike IgG antibodies, IgM is not transferred from mothers to newborns and as such newborns demonstrate a similar IgM antibody repertoire that becomes highly diverse with age (Madi et al., 2012, Madi et al., 2009). Encoded by minimally or non-mutated germ line genes (Lobo et al., 2010) IgM antibodies are polyreactive with low-binding affinity (Fu et al., 2007, Ehrenstein and Notley, 2010). Circulating IgM has unique properties owing to its pentameric form (Czajkowsky and Shao, 2009), hence it can interact with several binding partners and participate in diverse pathophysiologies such as infection, B cell homeostasis, inflammation, atherosclerosis and autoimmunity (Ehrenstein and Notley, 2010). Using cryo-atomic force microscopy of individual human IgM, Czajkowsky *et al.,* (2009) revealed that IgM antibodies are mushroom-shaped with a central protruding region containing binding sites for complement protein C1q. IgM antibody-antigen complexes (immune complexes) have fully exposed C1q binding sites, allowing activated C1q to bind and interact with downstream complement components.

1.4.2 The complement system

The complement system is a highly regulated major effector of humoral immunity and consists of numerous interacting soluble serum and membrane proteins (Campbell and Reece, 2011). It should be appreciated that the complement system is quite complex and this thesis will only provide a simplified overview of the major components necessary to understand and interpret the data presented.

1.4.2.1 Three pathways of complement activation

The complement system becomes active and responsive upon the cleavage of complement protein 3 (C3) into C3a, and importantly C3b. Three pathways can initiate this: classical, mannose binding lectin (MBL), and the alternative pathway (Figure 1.3).

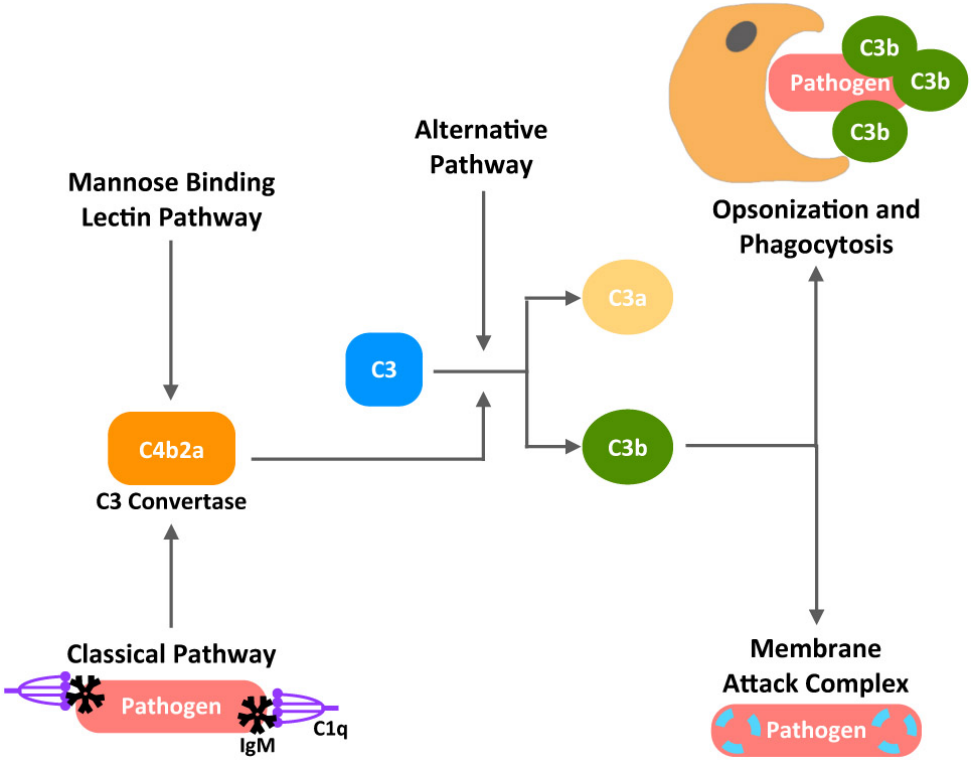

Figure 1.3 – Simplified overview of the major steps and components of the complement system. Three distinct pathways can activate the complement system: alternative, mannose binding lectin and the classical pathway. All three pathways result in increased production of C3b from C3. The final steps of each pathway ultimately lead to formation of the membrane attack complex, with subsequent cell lysis, or complement protein opsonisation and phagocytosis of a number of different cells including pathogens and apoptotic cells. Figure created on the basis of information in Chapter 7: The complement System of Immunology (Sixth Edition) by Kindt *et al.,* (2007).

1.4.2.2 The classical pathway

Of particular relevance to this thesis is the classical pathway of complement activation. IgM and certain IgG subclasses (IgG_1, IgG_2 and IgG_3) activate the complement cascade by binding to soluble antigens or antigenic surfaces such as bacterial cell walls. As previously mentioned, the formation of IgM antibody/immune complexes exposes

binding sites for C1q, which together with complement proteins C1r and C1s, forms the macromolecular complex C1. C1 facilitates the formation of complex C4b2a, called C3 convertase, which acts to catalyze the formation of C3b.

1.4.2.3 The mannose binding lectin pathway

The MBL pathway becomes activated following the binding of MBL, a member of the collectin family, to mannose polysaccharide (mannans) containing bacterial surfaces. Similar to the classical pathway this binding initiates the activation of a C1-like macromolecular complex which facilities C3 convertase formation with subsequent C3b production.

1.4.2.4 The alternative pathway

The alternative pathway does not require antibodies for activation. Due to spontaneous cleavage of C3, low levels of C3b fragments are continuously present in the serum. However, the complement cascade is only activated once stable C3b binding to a variety of antigenic surfaces, such as bacterial lipopolysaccharides.

1.4.2.5 Termination of the cascade and effector functions

Although the initiating steps differ, all three pathways culminate in the increased production of C3b. This leads to a number of basic functions; however, of relevance to this thesis is increased phagocytosis and or cellular lysis. One of the terminal events of the complement cascade is the requirement of complement proteins C5–C9 to form a macromolecular structure known as the membrane-attack complex (MAC) in the cell membranes of targeted cells. MAC mediates cell lysis by forming membrane pores that allows unrestrictive ion and small molecule diffusion ultimately leading to a loss of osmotic stability and subsequent cell death. Binding of complement factors to antigenic cell surfaces including apoptotic cells also leads to opsonisation that acts to promote phagocytosis.

1.4.3 Complement and IgM in ischaemic injury

Despite forming the first line of defense against foreign and endogenous antigens evidence is accumulating for the pathogenic involvement of circulating IgM following ischaemic injury. IgM antibodies have an important role in classical complement activation that leads to organ and tissue injury as indicated by studies of ischaemia in various organs (Burne-Taney et al., 2003, Czajkowsky and Shao, 2009, Zhang et al., 2004, Weiser et al., 1996, Zhang et al., 2006a) (summarised in detail in Table 1.1). For instance, intestinal ischaemia reperfusion injury is dependent upon the classical complement pathway and IgM (Williams et al., 1999). Weiser *et al.,* (1996) indicated that complement may be activated by a natural antibody as Recombination Activation Gene-1 (RAG-1-/1) mice, deficient in both mature B and T lymphocytes, did not develop injury following hind limb ischaemia. Injury was, however, restored following reconstitution of RAG-1 mice with fresh-pooled serum. Williams *et al,* (1999) subsequently demonstrated that mice deficient in Ig had significantly reduced intestinal injury following IRI that was restored to wild-type levels when reconstituted with IgM. Furthermore IgM bound the reperfused injured endothelium, colocalizing with C3 in wild-type mice, whilst minimal C3 and IgM deposition was observed in Ig-deficient mice. Reperfusion injured cells express autoantigens, such as annexin IV (intestinal villi) and non-muscle myosin heavy chain II (NMHC-II) (cardiac muscle, skeletal endothelium and muscle fiber bundles and intestinal mucosa). These autoantigens are recognised and bound by IgM antibodies leading to subsequent classical complement activation that acts to promote further tissue injury (Ehrenstein and Notley, 2010, Zhang and Carroll, 2007, Haas et al., 2010, Zhang et al., 2006b, Chan et al., 2006). The exact role, if any, of IgM antibodies in renal or liver IRI is unknown. It is possible that cells in the reperfused and injured renal microvasculature or the renal tubules may also express neo-epitopes that are recognised and bound by IgM (Figure 1.2 provides a diagrammatic representation of this). Lastly, Burne-Taney (2003) discovered that B cell deficient mice (μMT) were protected from renal IRI, with injury restored by serum reconstitution, but not by B cell transfer, suggesting a circulating factor such as IgG or IgM may be involved. It should also be noted that a

Table 1.1 – Summary of key papers demonstrating a pathogenic role for IgM during ischaemic injury

Model	Key Findings	Reference(s)
Myocardial ischaemia	- Cr2-/- (mice with a defective IgM repertoire due to defective B-1 cells), RAG-1 and sIgM mice had significantly reduced infarct size, with injury restored following IgM reconstitution	(Zhang et al., 2006b) (Busche et al., 2009)
	- Pathogenic B-1 cell hybridoma clone IgM_{cm-22} identified - Cardiac injury restored in RAG-1 mice reconstituted with IgM_{cm-22} - Self reactive neo-epitope non-muscle myosin heavy chain II (NMHC-II) identified as IgM_{cm-22} target in cardiac muscle cells - Synthetic peptide mimetope (N2) directed against NMHC-II administered 60-90min post ischaemia attenuated cardiac injury - N2 treated mice demonstrated reduced infarct size, IgM and C3d deposition with reduced monocyte and neutrophil infiltration	(Haas et al., 2010)
Skeletal muscle Ischaemia	- Cr2, C3, C4 deficient mice protected from injury - RAG-2 mice protected, injury restored following serum transfer - Endothelial C3 and IgM deposition observed in wild type mice	(Weiser et al., 1996)
	- IgM deposited after 5mins of ischaemia and increased up until 6hrs, and diminished during reperfusion	(Chan et al., 2004)
	- IgM_{cm-22} bound to NMHC-II in injured endothelial and muscle fiber - Injury, IgM and C3 deposition restored in Cr2-/- mice reconstituted with IgM_{cm-22}	(Austen et al., 2004)
	- Synthetic peptide mimetope (N2) treatment attenuated skeletal ischaemic injury with decreased numbers of injured muscle fibers	(Chan et al., 2006) (Zhang et al., 2006a)
Intestinal ischaemia	- C3 and RAG-1 deficient mice had attenuated injury with reduced IgM and C3 deposition in ischaemic tissue - Injury restored in RAG-1 mice following IgM reconstitution - C3 and IgM colocalized to reperfused mucosa in wild type mice	(Williams et al., 1999)
	- IgM_{cm-22} found to bind to NMHC-II in injured skeletal muscle - IgM_{cm-22} restored injury in RAG-1 mice with significant IgM, C4 and C3 deposition that co-localized with IgM in injured villi and mucosa	(Zhang et al., 2004)
	- N2 treatment attenuated skeletal ischaemic injury in mice in a dose dependent manner	(Zhang et al., 2006a)
	- IgM clone (mAb B4) identified which could restore injury in RAG-1 mice by binding to annexin-IV resulting in complement activation and neutrophil infiltration	(Kulik et al., 2009)
Renal tubular cells	- Used *in vitro* ischaemic reperfusion injury model in human and murine proximal tubular epithelial cells to investigate role of IgM and C3 deposition - Following hypoxic injury to human renal tubular cells C3 deposition occurred which was dependent on IgM and C1q activation of the classical complement pathway - Alternative pathway required for C3 deposition on necrotic human renal tubular cells - C3 deposition following ischaemic and necrotic injury to murine renal tubular cells occurs via the alternative pathway	(van der Pol et al., 2011)

recent paper by van der Pol *et al.,* (2011) suggested that IgM may bind to injured ischaemic human renal tubular cells *in vitro*.

1.4.4 Complement, renal ischaemia and liver injury

Despite the role of IgM in renal ischaemia remaining unclear, there is growing evidence indicating the complement system is a key amplifier of tissue injury during renal ischaemia (Renner et al., 2010, Weisman et al., 1990a). Following ischaemia, circulating complement factor 3a (C3a) increases and C3 deposition is observed along the tubular basement membrane (Thurman, 2007). Furthermore, mice deficient in complement proteins C3, C5 and C6 are protected from renal IRI (Zhou et al., 2000a). Similarly, as the main site of C3 synthesis it is unsurprising that rat models have suggested that complement may have an important role in liver injury (Lehmann et al., 2001, Chavez-Cartaya et al., 1995, Fondevila et al., 2008, Alper et al., 1969, Tu et al., 2011). With complement seemingly implicated in renal ischaemia and liver injury it may be possible that IgM might play an important role as well as other ischaemic injury models that demonstrate a pathogenic role for IgM also exhibit strong complement involvement. If IgM antibodies are involved in the injury pathogenesis of renal and liver IRI they may representative novel therapeutic targets.

1.4.5 Therapeutic blockage of IgM

Therapeutic strategies designed to block various components of the immune system, such as complement inhibition, have proven effective in experimental IRI (Lutz et al., 2010, Riedemann and Ward, 2003). Use of complement inhibitor recombinant soluble CR1 (sCR1) has prevented complement-mediated tissue injury in experimental intestinal, cardiac and skeletal muscle ischaemia (Riedemann and Ward, 2003, Weisman et al., 1990b, Zacharowski et al., 1999, Hill et al., 1992, Kyriakides et al., 2001). In a similar line studies have successfully blocked IgM binding to injured cells in a variety models of ischaemia. Studies have previously confirmed the involvement of complement activation via a single IgM clone that recognized a neo-epitope on hypoxic cells (Zhang and Carroll, 2007, Haas et al., 2010, Zhang et al., 2006b, Chan et al., 2006).

This was identified as NMHC-II that is accessible to IgM antibodies on cardiac muscle, endothelium and muscle fibers and intestinal mucosa following ischaemia. These studies have since demonstrated reduced IgM deposition and attenuated injury following pretreatment with the synthetic antigenic N2 epitope, which recognizes NMHC-II in a mouse model of acute myocardial infarction and intestinal and skeletal IRI. Such a strategy may be amenable to renal and/or hepatic IRI if IgM does play a key pathogenic role.

1.5 Apoptotic cells and Disease Modulation

As discussed in '1.1.3.3 Cellular Injury' acute injury can result in irreversible lethal tissue damage that leads injured cells to undergo apoptosis and or necrosis.

1.5.1 Overview of apoptosis

Each day billions of cells undergoing programmed cell death, or apoptosis, are cleared in the constant and crucial pursuit of normal tissue homeostasis (Kerr et al., 1972, Elmore, 2007, Wyllie et al., 1980, Savill, 1994). During apoptosis, sequential activation of initiator/effector caspases leads to morphological changes including cell shrinkage and nuclear pyknosis, with maintenance of plasma membrane integrity (Elmore, 2007, Kerr et al., 1972, Galluzzi et al., 2007). In the absence of efficient phagocytic clearance, apoptotic cells ultimately progress to secondary necrosis, with the loss of membrane integrity and release of potentially immunogenic and inflammatory intracellular contents, including organelles. This can be a highly inflammatory process as rapid disruption of both organelle and cellular plasma membrane integrity occurs releasing noxious intracellular contents (Ziegler and Groscurth, 2004). Whilst some diseases are characterised by apoptosis, high levels of necrotic death are found in some diseases, following critical cell damage resulting from hypoxia, toxins or infection. Cells undergoing primary necrosis exhibit catastrophic loss of membrane integrity and rapid release of potentially pro-inflammatory intracellular components (Savill et al., 2002, Zong and Thompson, 2006). Such a situations occurs in patients with thrombotic

microangiopathy syndromes (George and Nester, 2014) in which microvascular thrombus formation and enhanced shear stress (Camus et al., 2012, Dhaliwal et al., 2004) disrupt and fragment erythrocytes (Dhaliwal et al., 2004, Radhi and Carpenter, 2012, Colman, 1969). Erythrocyte fragmentation with the release of cytotoxic cell-free haemoglobin and damage associated molecular pattern (DAMP) exposure would be predicted to further drive inflammation (Chen et al., 2014, Gladwin and Ofori-Acquah, 2014, Gladwin et al., 2012). It is therefore critical that apoptotic cells, necrotic cells and severely damaged erythrocytes are rapidly removed in order to limit potential autoimmunity and tissue and vascular inflammation.

1.5.2 Dead cell clearance

The immunogenicity of dying cells is not simply determined by the mode of cell death (apoptosis versus necrosis), suggesting that there are additional molecular determinants that influence autoantibody generation. The repertoire of membrane alterations associated with cell death, (Fadeel, 2004) including exposure of phosphatidylserine (PtdSer) (Fadok et al., 2001) on the outer plasma membrane leaflet together with binding of specific opsonins or bridging molecules, such as C-reactive protein, Protein S, milk fat globule-EGF factor 8, C1q, mannose-binding lectin or IgM antibodies (Ogden et al., 2001, Gershov et al., 2000, Hart et al., 2004) determine the molecular pathways utilised in phagocytic uptake. Furthermore, the opsonisation status of apoptotic or necrotic cells will govern the ultimate fate of internalised cellular material within phagocytes and the capacity for presentation of antigens to T cells that is necessary for B cell activation and autoantibody production (Savill et al., 2002).

1.5.3 Studies demonstrating modulation of disease by apoptotic cell administration

A key event in apoptosis is the surface exposure of PtdSer that signals the clearance of apoptotic cells by macrophages (Fadok et al., 1992) and promotes the resolution of inflammation (Serhan and Savill, 2005, Fadok et al., 1998). Macrophages that ingest apoptotic cells adopt an anti-inflammatory and immunosuppressive phenotype with secretion of anti-inflammatory cytokines, including transforming growth factor-β (TGF-

Table 1.2 – Summary of papers demonstrating apoptotic cell modulation of experiment disease models. Abbreviations are as follows: apoptotic cell(s) (AC(s)); Lipopolysaccharide (LPS); Caecal ligation and puncture (CLP); Hepatocyte growth factor (HGF); Inducible nitric oxide (iNOS).

Model	Key Methodology	Key Findings	Ref.
LPS induced lung inflammation and thioglycollate induced peritoneal inflammation	- **Cells:** UV irradiated human Jurkat cells or human monomyelocyte PLB-985 cells - **Administration:** Peritoneal = $40x10^6$ after 3 days Lung = i.t $20x10^6$ after 36-48hrs of LPS - **Apoptotic:** 60-80% apoptotic	- Mice treated with apoptotic Jurkat cells following peritoneal or lung inflammation had raised TGF-β1 levels in lavage fluids - In both models apoptotic cell clearing macrophages were confirmed to be responsible for elevated TGF-β1 levels - Reduced intra-alveolar neutrophil counts and TNF-α levels in broncho-alveolar lavages were observed 1-3 days following AC administration - Administration of apoptotic PLB cells (which do not express PtdSer) did not induce elevated TGF-β1 levels	(Huynh et al., 2002)
LPS induced shock and CLP	- **Cells:** aged human polymorphonuclear neutrophils (PMNs) - **Administration:** i.v For LPS = $2x10^6$, $10x10^6$, $20x10^6$ immediately after LPS For CLP = $10x10^6$ 1hr later - **Apoptotic:** early	- Mice treated with $10x10^6$ ACs following LPS & CLP exhibited improved health & survival rate - ACs given 1, 3, 6 & 24hrs following LPS were still protective - AC treatment following LPS reduced PMN infiltration, lowered IL-12, TNF-α, IFN-γ whilst IL-10 was upregulated - $10x10^6$ & $20x10^6$ ACs reduced [LPS], whilst $2x10^6$ ACs had no effect	(Ren et al., 2008)
Collagen Induced Arthritis (CIA)	- **Cells**: aged apoptotic thymocytes - **Administration**: i.v $20x10^6$ 0,1,2 days prior to CIA - **Apoptotic:** early, but late ACs also protective	- AC treated mice had antigen-specific CD4+ T cells producing IL-10 or IFN-γ - AC contact induced B cells to activate IL-10 secreting T cells - AC treated mice had a significantly lower mean arthritis score - AC administration after onset of CIA conferred no protection - AC protection is dependent on IL-10	(Gray et al., 2007)
Bleomycin induced lung inflammation	- **Cells**: UV irradiated human Jurkat cells - **Administration**: i.t $10x10^6$ 2 days after bleomycin treatment - **Apoptotic:** early	- AC exposure increased HGF production which attenuated lung injury in mice - 2 days following AC administration HGF mRNA production and alveolar macrophage clearance was enhanced - HGF remained elevated 21 days post AC administration - Levels of fibrosis reduced in lung tissue - Anti-HGF antibody abolished protection	(Lee et al., 2012)

LPS induced hepatitis	- **Cells**: UV irradiated apoptotic splenocytes - **Administration**: 3 days prior to LPS treatment Main experiment 1.5 x10^7 via portal vein Sub experiments: 1x10^7 to 3x10^7 ACs, and 2x10^8 ACs - **Apoptotic:** early	- ACs primarily captured by Kupffer cells - ACs significantly attenuated liver injury in both C57BL/6 & Balb/c mice - ACs administration 3-7days prior to LPS was maximally protective - Maximum protection conferred with 1x10^7 to 3x10^7 ACs, 2x10^8 ACs conferred no protection - Pro-inflammatory cytokines (TNF-α, IL-6, IL-1 β) reduced, whilst anti-inflammatory cytokines (IL-4, IL-10, TGF- β) significantly elevated	(Zhang et al., 2011)
Pneumococcal Pneumonia	- **Cells**: UV irradiated alveolar macrophages - **Administration**: i.t 1x10^4 immediately following infection - **Apoptotic:** early	- ACs had no antimicrobial effect on bacterial colonies - However at 12-48hrs following administration AC treated mice had reduced lung inflammation indicated by reduced neutrophil infiltration in iNOS$^{-/-}$ and C57BL/6 mice - TNF-α expression was reduced in AC treated mice	(Marriott et al., 2006)
Rat allogeneic whole-heart transplant	- **Cells**: UV irradiated donor splenocytes - **Administration**: 50x10^6 via penile vein 14, 7 or 3 days prior to transplant - **Apoptotic:** 50% apoptotic	- Mice treated with donor ACs exhibited prolonged graft survival with reduced lymphocyte infiltration and tissue necrosis - ACs administered 7 days prior to transplant were most effective - Inhibition of phagocytosis by gadolinium chloride treatment and PtdSer blockage abolished prolonged graft survival following AC treatment	(Sun et al., 2004)

β) and IL-10 (Savill et al., 2002). The consequences of apoptotic cell phagocytosis has been reviewed by Erwig and Henson (2007). Apoptotic cells were first suspected to be immuneregulatory due to the observation that kidney allograft survival was greatly improved following repeated blood transfusions (Opelz and Terasaki, 1978, Opelz et al., 1997). Blood stored for clinical transfusions are known to contain apoptotic granulocytes and lymphocytes (van Prooijen et al., 1994, Smit Sibinga, 1999). To this end the exogenous administration of apoptotic cells reduces inflammation in various experimental models of disease including lipopolysaccharide (LPS)-induced shock (Ren et al., 2008), collagen induced arthritis (CIA) (Gray et al., 2007) as well as lung (Lee et al., 2012, Huynh et al., 2002, Marriott et al., 2006) and liver inflammation (Zhang et al.,

2011) (summarised in detail in Table 1.2). The potential anti-inflammatory mechanisms of exogenous apoptotic cell administration are diverse and include:

(i) PtdSer dependent induction of TGF-β1 secreting apoptotic cell ingested macrophages in lung and peritoneal inflammation (Huynh et al., 2002),

(ii) the induction of IL-10 production by Kupffer cells by TGF-β bound to the apoptotic cell surface (Zhang et al., 2011),

(iii) the induction of IL-10 producing $CD19^+$ regulatory B cells that stimulate a population of IL-10 secreting antigen-specific $CD4^+$ T cells in CIA (Gray et al., 2007) and

(iv) binding of LPS to apoptotic cells accompanied by reduced serum TNF-α levels and increased serum IL-10 levels in LPS shock (Ren et al., 2008). Ren *et al.,* also observed reduced neutrophil infiltration in the kidney following apoptotic cell administration in LPS-induced shock.

In addition, it has been shown that both apoptotic and necrotic cells exert anti-inflammatory effects (Miles et al., 2009) suggesting that these effects are not confined to intact apoptotic cells.

1.6 Apoptotic cells and IgM antibodies

1.6.1 Perturbations of dead cell clearance

Perturbations of the complex regulated process of dead cell clearance have been implicated in the pathophysiology of many autoimmune disease states. The development of autoantibodies, particularly against cytoplasmic or nuclear antigens which characterises diseases such as systemic lupus erythematosus (SLE), has been suggested to be a consequence of excessive levels of apoptosis and/or compromised clearance (Gaipl et al., 2005). Indeed, numerous developmental defects, neurodegenerative disorders and diseases are characterised by increased cellular turnover with excessive apoptosis including cancer (Elliott and Ravichandran, 2010, Elmore, 2007).

1.6.2 IgM antibodies and phagocytosis

IgM antibodies have been shown to mediate and accelerate the clearance of apoptotic cells by phagocytes (Peng et al., 2005, Ogden et al., 2005, Litvack et al., 2010, Litvack et al., 2011) with this function involving recruitment of C1q (Chen et al., 2009b, Chen et al., 2009a). Phagocytosis of apoptotic cells is markedly reduced in the absence of IgM (Quartier et al., 2005), furthermore these IgM-deficient mice exhibit a clear autoimmune phenotype similar to that seen in SLE (Boes et al., 2000, Ehrenstein et al., 2000).

1.6.3 IgM bound apoptotic cells and epitopes

Circulating IgM antibodies are of relatively low affinity and exhibit polyreactivity (Avrameas et al., 1983, Avrameas, 1991, Casali and Notkins, 1989) as they bind to a diverse range of non-self and self-antigens (summarised in detail in Table 1.3) (Fu et al., 2007, Williams et al., 1999, Zhang et al., 2006a, Briles et al., 1982). Late apoptotic cells (Litvack et al., 2010, Fu et al., 2007, Zwart et al., 2004, Ciurana and Hack, 2006, Porcheray et al., 2013) and derived microparticles (Litvack et al., 2011) are preferentially bound by IgM antibodies. Consequently, IgM antibodies have been reported to bind neo-epitopes that become accessible following plasma membrane alterations associated with apoptosis, (Fu et al., 2007, Grönwall et al., 2012, Kim, 2010) such as exposure of phosphorylcholine (Briles et al., 1981) and PtdSer (Litvack et al., 2011, Fu et al., 2007). In addition, membrane phospholipase (PLA2) has been implicated in phospholipid remodeling and exposure of IgM bound epitopes (Kim et al., 2002). Many IgM antibodies recognise oxidation-specific epitopes and oxidised low-density lipoproteins that are present on apoptotic cells, (Chou et al., 2009a, Rosenes et al., 2013, Chikazawa et al., 2013, Tsiantoulas et al., 2012) representing immunodominant DAMPs (Leibundgut et al., 2013, Hartvigsen et al., 2009). Whilst the precise molecular determinants on apoptotic cells that are recognised by IgM are yet to be fully defined, an important role for IgM in the clearance of apoptotic cells is well established (Peng et al., 2005, Ogden et al., 2005, Litvack et al., 2010, Litvack et al., 2011, Boes et al., 2000, Ehrenstein et al., 2000).

Table 1.3 – Epitopes and proteins bound by IgM. Only epitopes and proteins that are fully identified and described with robust IgM binding are included. Epitopes and proteins are divided into phospholipid/oxidised epitope, carbohydrate, nuclear and protein related groups.

Name	Brief Description	Reference(s)
Phospholipid and oxidized epitope		
Annexin-IV	Phospholipid binding protein	(Kulik et al., 2009)
Cardiolipin	Diphosphatidylglycerol lipid in mitochondria membrane	(Tuominen et al., 2006) (Sorice et al., 2000) (Cvetkovic et al., 2002)
LDL-malondialdehyde	Oxidised low-density lipoprotein produced by reactive aldehyde degradation	(Chou et al., 2009b) (Chen et al., 2009b) (Cvetkovic et al., 2002) (Rouhl et al., 2010)
Lysophosphatidylcholine	Oxidised low-density lipoprotein	(Mercolino et al., 1986) (Kim et al., 2002) (Blanc et al., 2007b)
Phosphatidylserine	Phospholipid exposed during apoptosis	(Fu et al., 2007) (Kim, 2010)
Phosphorylcholine and related 1-pal- mitoyl-2-(5'-oxovaleroyl)-sn-glycero-3-phosphocholine (POVPC)	Oxidised low-density lipoprotein head group exposed during apoptosis	(Chou et al., 2009b) (Shaw et al., 2003) (Briles et al., 1981) (Chen et al., 2009b) (Anania et al., 2010) (Shaw et al., 2000) (Fu et al., 2007) (Vas et al., 2012)
Protein-bound 4-oxo-2-nonenal (ONE), 4-Hydroxynonenal	Reactive aldehyde oxidation specific epitope	(Chikazawa et al., 2013) (Chou et al., 2009b) (Khatoon et al., 2012)
Carbohydrate		
Chitin	Polymeric carbohydrate	(Rapaka et al., 2010)
Collectin surfactant protein D	Carbohydrate-binding collectin group of innate pattern recognition protein	(Litvack et al., 2010)
Pneumococcal bacterial cell wall polysaccharide	Polymeric carbohydrate	(Chou et al., 2009b)
Nuclear		
dsDNA	Nucleic acid	(Witte, 2008) (Wellmann et al., 2005)
Nuclear autoantigen lamin B1	Nuclear envelope protein	(Dieudé et al., 2002) (Senecal et al., 1999)
Protein		
Actin	Cytoskeletal protein	(Fu et al., 2007)
GRP78, BiP (Ig heavy-chain binding protein)	Heat-shock protein 70 family member	(Rosenes et al., 2013)
Non-muscle myosin heavy chain II and myosin	ATP dependent motor proteins	(Zhang et al., 2006a) (Haas et al., 2010) (Fu et al., 2007)
B-tubulin	Cytoskeletal microtubule protein	(Connolly et al., 1997)

1.7 Apoptotic Cells and Coagulation

1.7.1 Relationship of apoptotic cells and coagulation

The surface exposure of PtdSer on apoptotic cells not only signals their clearance by macrophages (Fadok et al., 1992), but also confers apoptotic cells with a procoagulant tendency (Casciola-Rosen et al., 1996). The first indication of a potential relationship between apoptosis and thrombogenicity was seen in cancer patients undergoing chemotherapy (Pickering et al., 2008, Wang et al., 2001). These patients had abnormal levels of coagulation activation markers, and as the intensity of chemotherapy increased, resulting in tumour apoptosis, thromboembolism risk also increased (Wang et al., 2001, Lee and Levine, 1999). This relationship has been further confirmed through human tumour cell lines and non-tumour cell lines (Wang et al., 2001). Wang *et al.,* (2001) demonstrated a correlation between thrombin generation, tissue factor activity and the degree of apoptosis in camptothecin (chemotherapeutic agent) treated cell lines. Furthermore this correlation could be abolished by the addition of Annexin-V (AnnV), which binds to PtdSer. Thrombin can have a significant impact on the progression of IRI as it results in the activation of endothelial cells, platelets, monocytes, dendritic cells and T cells through a family of thrombin protease-activate receptors (Morrell et al., 2007).

1.7.2 Mechanisms of coagulation influence

Through a variety of mechanisms apoptotic cells can affect the coagulation status and interact with components of the clotting system, such as platelets either directly or indirectly. Apoptotic cells, bodies and surface blebs themselves confer procoagulant activity (Casciola-Rosen et al., 1996). Due to exposure of PtdSer, along with other phospholipids, apoptotic cells provide a surface for the assembly of macromolecular coagulation complexes essential for the formation of thrombin (Casciola-Rosen et al., 1996, Pickering et al., 2008). This PtdSer exposure on the apoptotic cells and surface blebs can amplify the catalytic surface available for thrombin assembly (Casciola-Rosen et al., 1996).

1.8 Preliminary Data

Previous unpublished work in the lab by Dr DA Ferenbach, which gave rise to this project, demonstrated that the administration of $20x10^6$ apoptotic thymocytes 24-hours prior to renal IRI significantly preserved renal function (Figure 1.4A), inferred from reduced plasma creatinine, whilst ATN remained unaffected (Figure 1.4B) in both Balb/c and FVB mice.

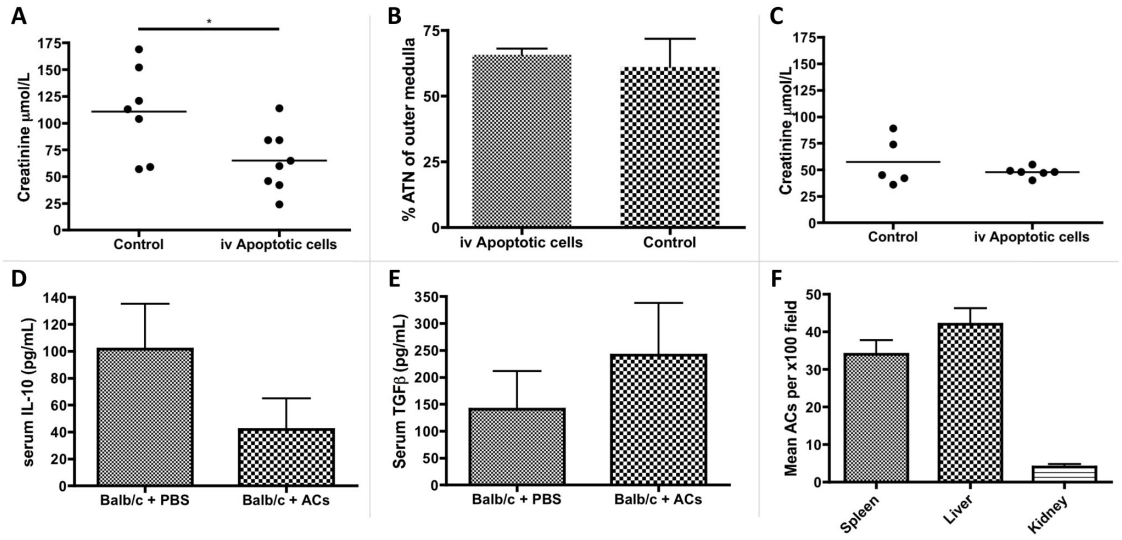

Figure 1.4 – Preliminary data. Administration of $20x10^6$ apoptotic thymocytes 24-hours prior to renal IRI significantly preserved renal function (**A**), whilst ATN remained unaffected (**B**) in Balb/c mice. **C**) Apoptotic cells administered 8 days prior to renal IRI conferred no protection. Apoptotic cell treated mice did not have augmented levels of IL-10 (**D**) and TGF- β (**E**). **F**) The apoptotic cells are detectable in the kidney, spleen and liver 1-hour following injection.

The administration of apoptotic cells 8 days prior to renal IRI conferred no functional or structural protection (Figure 1.4C). This also provides evidence against the involvement of B cells as this is the length of time required for B cell activation of IL-10 secreting antigen-specific T cells, as observed by Gray *et al.,* (2007) in CIA. Previous investigations have suggested that the mechanism eliciting functional protection is not due to an anti-inflammatory tissue environment conferred from immunosuppressive macrophage secreting IL-10 and TGF-β. Apoptotic cell treated mice did not have augmented serum levels of IL-10 (Figure 1.4D) or TGF-β (Figure 1.4E) following renal

IRI. The apoptotic cells were detectable in the blood, kidney, spleen and liver up to 1-hour following administration (Figure 1.4F). Severe Combined Immunodeficiency (SCID) mice, which lack T and B lymphocytes and antibodies, treated with apoptotic cells 24-hours prior to renal IRI are not protected suggesting that the mechanism in part may be antibody mediated. Furthermore, IgM deposition was also evident in the injured kidney.

Although therapeutic interventions usually improve both renal function and structure, protection of renal function alone has been observed in mice administered heme oxygenase-1 overexpressing macrophages (Ferenbach et al., 2010) and was considered to be secondary to improved microvascular blood flow thereby allowing the perfusion of non-injured functioning nephrons.

1.9 Hypothetical mechanisms of apoptotic cell derived functional protection

In the light of the ability of apoptotic cells to interact with both IgM antibodies and coagulation factors, the following two testable hypothetical mechanisms may explain apoptotic cell mediated functional protection (Figure 1.5):

a) Apoptotic cells administered 24-hours before renal IRI actively bind circulating IgM that may also be able to recognise injured cells. At the time of ischaemia the intravascular level of self-reactive IgM is decreased which limits endothelium/epithelial injury and activation (Figure 1.5B).

b) Apoptotic cells administered 24-hours prior to renal IRI results in a transient perturbation of coagulation status that acts to limit microvascular congestion at the time of ischaemia (Figure 1.5C).

Both of these hypothetical mechanisms might improve microvascular flow and thus improve renal function.

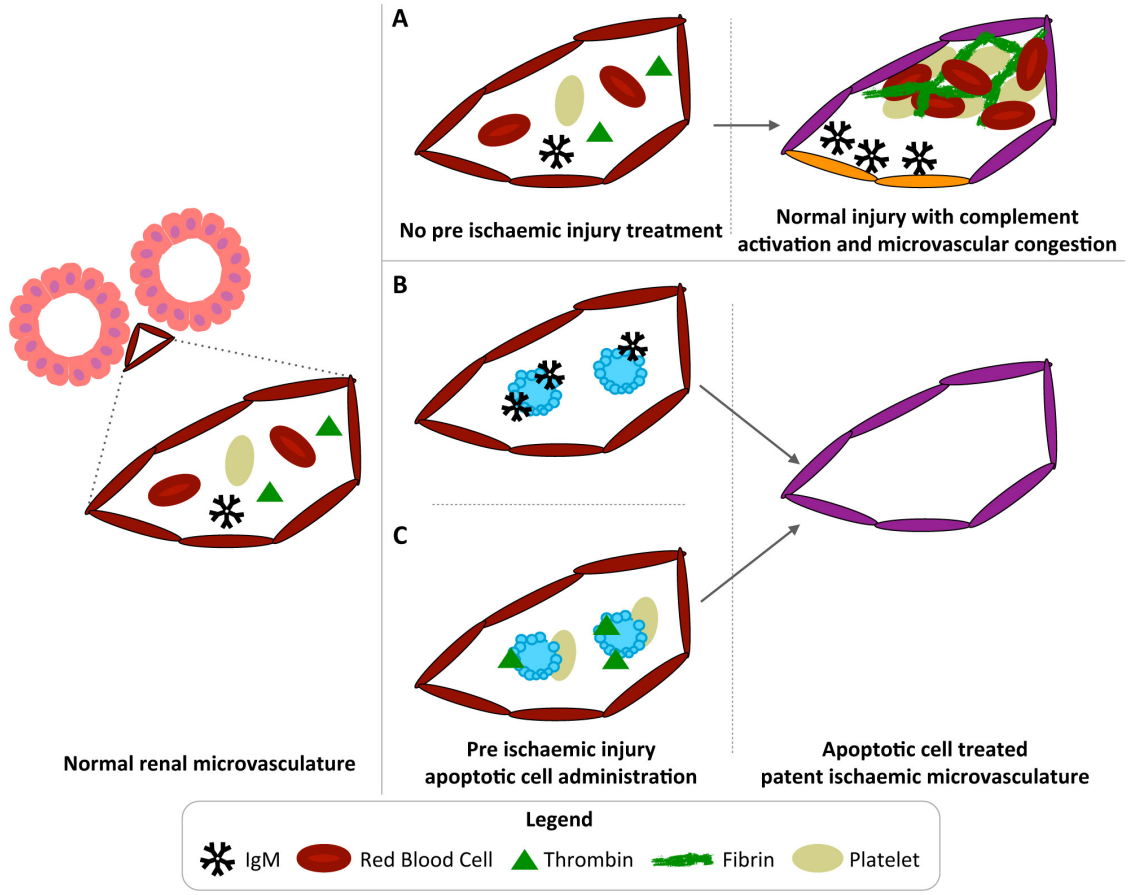

Figure 1.5 - Two hypothetical mechanisms examining whether AC-mediated protection was conferred by modulation of (B) natural IgM antibodies or by (C) coagulation status. A) Normal renal microvasculature with no pre-ischaemic treatment may express IgM bound neo-epitopes and microvascular congestion may occur following ischaemia. **B**) Apoptotic cells given 24-hours before renal IRI actively bind circulating IgM that may also recognise injured cells. At the time of ischaemia the intravascular level of self-reactive IgM is decreased which limits endothelium/epithelial injury and activation. This leads to improved microvascular flow and therefore improved renal function. **C**) Apoptotic cells administered 24-hours prior renal ischaemia results in a transient perturbation of the coagulation system that acts to limit microvascular congestion post ischaemia. This leads to more efficient reperfusion and improved renal function.

1.10 Aims

The main aim of this thesis was to validate the previous findings and to elucidate the mechanism behind the protection conferred from the intravenous administration of apoptotic cells 24-hours prior to renal IRI.

This was to be achieved by the following steps:

1) Investigate IgM deposition following ischaemic injury in kidney and liver tissue
2) Confirm the ability of apoptotic cells to influence coagulation
3) Establish and optimise the murine IRI model
4) Establish and optimise parameters to study microvascular congestion
5) Recapitulate the functional protection conferred by apoptotic cell administration
6) Establish an assay to further investigate IgM antibody binding to apoptotic cells *in vitro*

Chapter 2. Materials and Methods

2.1 General

2.1.1 Chemicals and cell culture reagents – Unless stated otherwise chemicals and cell culture reagents were purchased as detailed here. Cell culture reagents were purchased from PAA Laboratories, UK or Life Technologies, Paisley, UK. Tissue culture plastics were from Corning Incorporate, Netherlands or BD Biosciences, UK. Heat inactivated fetal calf serum (FCS) was purchased from BioSera, Sussex or Life Technologies, Paisley, UK. Chemicals were purchased from Sigma Aldrich, UK.

2.1.2 Mice - Balb/c or RAG1-deficient mice were purchased from Harlan, UK or Charles River. All animal procedures were performed under a Project License (60/3339) and in accordance with guidelines set out by the United Kingdom's Home Office under the Animal (Scientific Procedures) Act of 1986 and the University of Edinburgh's Biological Services Department. All animals were housed in the BRR unit and had free access to food and water.

2.2 General cell culture and induction of apoptosis

2.2.1 Preparation of non-apoptotic and apoptotic thymocytes – Following cervical dislocation thymi were dissected from 4 – 8 week old male Balb/c mice. Thymocytes were dissociated by gently grinding thymi through a cell strainer (40 µM nylon, BD Falcon) and washed through using RPMI 1640 medium. The cell suspension was made up to 10 mL of RPMI, which on average resulted in a cell density of $10x10^6$ cells/mL. Thymocytes were used immediately or aged overnight at 37°C and 5% CO_2 in a T25 cm^2 flask (with 0.2 µM vent cap) to generate a population of cells with variable levels of apoptosis. To elicit a predominantly late apoptotic cell population, thymocytes were treated with 1 µM Dexamethasone for 20-hours. Following incubation, cell suspensions were centrifuged at 230 x *g* for 6-minutes, and washed with PBS before

the cell number per mL was determined using a Nucleocounter (Chemometec). Murine apoptotic thymocytes were used to investigate the influence of apoptotic cells on coagulation, confirm apoptotic cell mediated protection from renal IRI and to explore circulating IgM binding to apoptotic cells. Non-apoptotic cells were used as negative controls or to investigate intracellular IgM antibody binding.

2.2.2 Culture of Jurkat cells and induction of apoptosis – Apoptosis was induced in human Jurkat cells, which were then used to explore human circulating IgM antibody binding. Human Jurkat cells were cultured in RPMI 1640 medium with 10% heat-inactivated FCS, 1% L-glutamine and 1% penicillin-streptomycin at 37°C and 5% CO_2. Cells were cultured at a density of $2x10^6$/mL and apoptosis induced by incubation with 0.5µM camptothecin for 16-hours. In some experiments apoptosis was induced by treatment with 25 µM hydrogen peroxide (H_2O_2) for 2-hours. Cells were then centrifuged at 300 x *g* for 6-minutes, and washed with PBS. These conditions were selected following dose titration experiments.

2.2.3 Culture of human proximal tubular epithelial cells (HK-2) - HK-2 cells were kindly provided by Dr Mark Dockrell (SWT Institute for Renal Research, London). Cells were cultured in RPMI 1640 medium with 5% heat-inactivated FCS, L-glutamine and penicillin-streptomycin at 37°C and 5% CO_2. HK-2 cells were detached with trypsin or cell dissociation buffer. HK-2 cells were used to investigate circulating IgM antibody binding following *in vitro* injury as described in '2.9.1 Induction of ATP depletion in HK-2 cells by Antimycin A' and '2.9.2 Induction of cellular injury in HK-2 cells by H_2O_2'.

2.3 Assessment of apoptosis by flow cytometry

2.3.1 Annexin-V (AnnV) and PI staining – All assessment of apoptosis was inferred from AnnV and PI staining. An overview of where this protocol is placed when performed as part of IgM binding assessment is provided in Figure 2.1B. PtdSer exposure was detected using either Alexa Fluor 647, FITC or PE conjugated Annexin-V (all 1:100,

BioLegend, UK) diluted in AnnV binding buffer (Hanks Balanced Salt Solution H6648 with 5 mM $CaCl_2$ final concentration) and incubated for 15-minutes. Exactly 1 µL propidium iodide (PI) [1mg/mL] (Invitrogen, UK) diluted 1:20 in PBS was added to samples before analysis. Cells were either designated non-apoptotic ($AnnV^-PI^-$), early ($AnnV^+PI^-$) or late ($AnnV^+PI^+$) apoptotic. Staining was assessed by flow cytometry on a BD FACSCalibur (10,000 events collected) and analysed using FlowJo (TreeStar).

2.4 Flow cytometry phenotyping

2.4.1 Thymocyte phenotyping – Cell suspensions generated from dissociated thymi were phenotyped to ensure that cell populations were predominantly T cells. Fresh thymocytes were prepared as described and stained with the following anti-mouse antibodies conjugated to various fluorochromes: FITC CD3 (1:200, Clone: 145-2C11, BioLegend) PE CD4 (1:200, Clone: RM4-5, BD Pharmingen), APC CD8α (1:200, Clone: 53-6.7, eBioscience), PerCp-Cy5.5 CD11b (1:200, Clone: M1/70, eBiosciences) and Pacific Blue B220 (1:100, Clone: RA3-6B2, BD Pharmingen) before analysis by flow cytometry on a BD LSR Fortessa. The following isotype controls were used to confirm primary antibody specificity and cell positivity: PE Rat IgG2a κ (1:200, BioLegend), APC Rat IgG2a κ (1:200, eBioscience), PerCP/Cy5.5 Rat IgG2b κ (1:200, BioLegend) and eFluor450 Rat IgG2a κ (1:100, eBioscience). Fluorescent minus one (FMO) controls were also included.

2.5 Flow cytometry methodology used to study *in vitro* circulating IgM antibodies

2.5.1 Permeabilisation **–** To explore IgM antibody binding to intracellular antigens cells (excluding erythrocytes) were permeabilised using the following saponin based reagents purchased from eBioscience and used according to the manufacturer's instructions: Fixation/Permeabilization Concentrate (Ref: 00-5123-43), Fixation/Permeabilization Diluent (Ref: 00-5223-56) and Permeabilization Buffer 10x (Ref: 00-8333-56). To confirm permeability PI was added to samples, as described in

‘2.3.1 Annexin-V (AnnV) and PI staining’, before analysis by flow cytometry on a BD FACSCalibur.

2.5.2 Assessment of IgM binding to cells – The following techniques were used to detect murine and human IgM antibody binding to cells. An overview of this protocol is provided in Figure 2.1A & B. Approximately $5x10^5$ cells (excluding injured HK-2 cells and erythrocytes) were incubated in PBS or 30% human serum (Jurkat and permeabilised HK-2 cells) or 12.5% Balb/c or RAG1-deficient mouse plasma (thymocytes) for 30-minutes. Some experiments used Balb/c serum. For thymocytes APC Mouse (Balb/c) IgM κ isotype control (25µg/mL, Clone: G155-228, BD Pharmingen) was used as a control irrelevant murine IgM antibody to assess any non-specific interaction. This was used at a high concentration to be comparable to levels of IgM found in murine plasma (0.22±0.036 mg/L – Personal communication: George Tse, University of Edinburgh). IgM binding (including injured HK-2 cells but excluding erythrocytes) was detected by a 30-minute incubation with the following IgM µ chain specific antibodies: FITC mouse anti-human IgM (1:5, Clone: G20-127, BD Pharmingen) and APC rat anti-mouse IgM (1:100, Clone ID: II/41, BD Pharmingen) diluted in 1% BSA. Annexin-V and PI staining was then performed as described in ‘2.3.1 Annexin-V (AnnV) and PI staining’. Cell number, antibody dilutions and diluents were selected following titration and analysed using median fluorescent intensity (MFI). IgM binding was assessed by flow cytometry on a BD Calibur or assay modifications made to allow samples to be viewed by confocal or electron microscopy as described in ‘2.6.1 Confocal microscopy’ and ‘2.6.2 Transmission Electron Microscopy (TEM)’, respectively. In some instances the level of C3 deposition on the cell surface was assessed as described below.

2.5.3 Assessment of C3 deposition on the cell surface – To confirm that C3 deposition was detected following IgM binding, non-apoptotic and apoptotic thymocytes were treated with either 12.5% normal plasma, or heat-inactivated Balb/c plasma (1-hour incubation at 55°C) for 30-minutes. C3 deposition was detected by a 30-minute

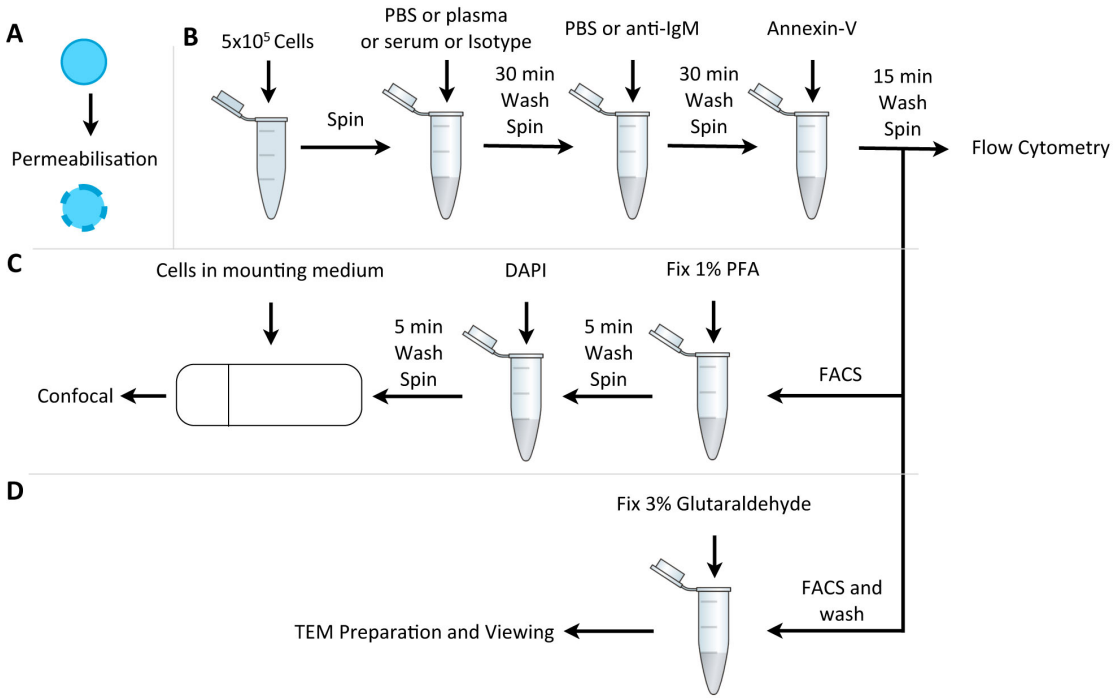

Figure 2.1 – Schematic detailing how the cells binding IgM binding were assessed by flow cytometry (B), confocal (C) and electron (D) microscopy. A) In some experiments non-apoptotic and apoptotic murine thymocytes, human Jurkat cells and human proximal tubular epithelial cells (HK-2) were permeabilised (2.5.1 Permeabilisation) prior to assessment of IgM binding. B) Outline of how IgM binding was assessed and any subsequent modifications made to allow samples to be viewed by confocal (C) or electron (B) microscopy as described in '2.6.1 Confocal microscopy' and '2.6.2 Transmission Electron Microscopy (TEM)', respectively.

incubation with FITC goat anti-mouse C3 (1:100, MP Biomedical). Annexin-V and PI staining was then performed and analysed as described in '2.3.1 Annexin-V (AnnV) and PI staining'.

2.5.4 Fluorescence-Activated Cell Sorting (FACS) - To separate discrete populations of IgM^+ and IgM^- cells, FACS sorting was undertaken. An overview of where this protocol is placed when performed as part of IgM binding assessment is provided in Figure 2.1C & D. Thymocytes, treated and stained as above, were sorted on a BD FACSAria II with a 70µM nozzle. Post-sorting checks were performed to ensure populations remained in original FSC SSC regions and to assess staining. Following sorting thymocytes were either viewed using confocal or electron microscopy.

2.5.5 Permeabilisation and assessment of IgM binding to murine erythrocytes – Murine IgM antibody binding to erythrocytes, as a simple anucleated organelle free cell, was undertaken as follows. As described in '2.8.1 Murine plasma/serum generation and erythrocyte isolation' erythrocytes were isolated and 200µL of the suspension was stained with Alexa Fluor-488 rat anti-mouse TER-119/Erythroid cells antibody (1:100, Biolegend) for 30-minutes before being washed with PBS and centrifuged at 600 *x g* for 10-minutes. Anti-TER-119 recognizes a molecule associated with erythrocyte cell-surface glycophorin A (Kina et al., 2000). Permeabilisation was achieved by a 10-minute incubation in 0.05% saponin after which erythrocytes were washed. Erythrocytes were incubated in PBS or Balb/c or RAG1-deficient mice plasma at a ratio of 1:1 (erythrocyte volume:plasma volume) for 30-minutes before being washed. APC Mouse (Balb/c) IgM κ isotype control was used as control irrelevant murine IgM antibodies. IgM binding was detected by a 30-minute incubation with APC rat anti-mouse IgM. AnnV staining was performed to confirm permeabilisation. Samples were diluted in AnnV binding buffer before staining was assessed by flow cytometry on a BD FACSCalibur. Erythrocytes were identified by TER-119 positivity (cell positivity was defined by isotype control – 1:100, Alexa Fluor-488 Rat IgG2b κ, BioLegend). Between 5000-10000 TER-119$^+$ events were collected and analysed using FlowJo.

2.6 Microscopy used to study *in vitro* circulating IgM antibody binding

2.6.1 Confocal microscopy – To visualise IgM binding to murine and human cells confocal microscopy was performed. An overview of where this protocol is placed when performed as part of IgM binding assessment is provided in Figure 2.1C. Sorted populations of thymocytes were treated with plasma and stained as described in '2.5.2 Assessment of IgM binding to cells', with the following modifications. Prior to apoptosis induction thymocytes were stained with CellTracker Green CMFDA (Invitrogen) according to the manufacturer's instructions. Texas Red goat anti-mouse µ chain specific IgM (SouthernBiotech) was used and samples were stained with DAPI

(Invitrogen) and PI staining was omitted. Jurkat cells were treated and stained as above with the addition of DAPI and omission of PI staining. Samples were mounted using ProLong Gold antifade reagent (Life Technologies) and viewed using a Leica SP5 with an x63/1.4 objective. Single stains were used to check for spectral-bleed through. Whole image contrast/brightness and pseudocolour was adjusted using ImageJ (NIH).

2.6.2 Transmission Electron Microscopy (TEM) – TEM was performed to gain a more detailed view of membrane permeability in IgM^+ and IgM^- cells. An overview of where this protocol is placed when performed as part of IgM binding assessment is provided in Figure 2.1D. TEM sample preparation was performed as follows by Stephen Mitchell (University of Edinburgh). FACS sorted thymocytes were fixed in 3% glutaraldehyde in 0.1 M sodium cacodylate buffer, pH 7.3, for 2-hours and washed thrice in 0.1 M sodium cacodylate for 10-minutes each. Post-fixation was performed by a 45-minute incubation in 1% osmium tetroxide in 0.1 M sodium cacodylate before samples were washed thrice in 0.1 M sodium cacodylate for 10-minutes each. Samples were dehydrated by 10-minute incubations in 50%, 70%, 90% and 100% normal grade acetones before a further two 10-minute washes in analar acetone. Samples were embedded in Araldite resin and 1 µM sections cut on a Reichert OMU4 ultramicrotome. Sections were stained with Toluidine Blue and suitable areas for investigation selected by light microscopy. From selected areas 60 nM ultrathin sections were cut and stained with uranyl acetate and lead citrate before viewing in a Philips CM120 transmission electron microscope. Images were taken on a Gatan Orius CCD camera. Whole image contrast/brightness was adjusted using ImageJ.

2.7 General Histology

2.7.1 Cryosectioning **–** Tissue was snap frozen on dry ice and stored at -20°C overnight prior to sectioning. Tissue was embedded in cryomatrix (Thermo Scientific Shandon) and cut at a thickness of 4 µM and placed on slides.

2.7.2 Paraffin sectioning – Tissue was fixed in 4% PFA or Methacarn (60% methanol, 30% chloroform and 10% glacial acetic acid) at 4°C overnight before being transferred to PBS or methanol respectively and then processed on an automated processor. Kidney tissue was then embedded in paraffin and left to solidify overnight before sectioning. Sections were cut at a thickness of 4µm on a microtome (Thermo Scientific Shandon Finesse 3), and placed on slides. Paraffin embedding and sectioning was performed by SuRF Histology facilities within the Queen's Medical Research Institute (QMRI) or EEH.

2.7.3 Haematoxylin & eosin (H&E) staining – Slides with paraffin embedded mouse kidney sections were de-waxed by two 5-minute washes with xylene. Sections were rehydrated through an ethanol series: 100% - 96% - 75% - 50% once for 20-seconds each and stained with Haematoxylin for 5-minutes. Sections were then washed as follows: water, 10-seconds with 0.1% HCl, 20-seconds with Scotts tap water and counterstained with Eosin for 1-minute and washed with water. An ethanol series was used to dehydrate the sections: 50% - 75% - 96% - 100% once for 20-seconds each. Two 5-minutes washes with xylene were performed to clear the sections prior to mounting with Pertex. H&E staining was performed by EEH using SuRF Histology facilities within the QMRI.

2.7.4 Direct and indirect immunofluorescence (IF) of frozen sections – Frozen sections were air dried for 1-hour. Following two 5-minute washes with PBS samples were fixed with either 4% PFA in PBS (for IgM and C3 staining) or 1% PFA 2% Acetic Acid in PBS (for Fibrin staining) for 10-minutes. Acetic acid degrades non-cross linked fibrin. Samples were washed twice for 5-minutes before being loaded into sequenza slide racks (Thermo Scientific) and blocked for 1-hour in 20% serum obtained from the same species in which the antibody was raised. All serum used was obtained from Sigma. Antibodies were then applied and left to incubate for 1-hour. The following antibodies were used: Polyclonal Rabbit Anti-Human Fibrinogen/FITC (1:200, Dako Cytomation) which cross-reacts with mouse fibrin; polyclonal Goat Anti-Mouse IgM (µ chain

specific) Texas Red® (1:200, SouthernBiotech) and polyclonal FITC goat anti-mouse C3 (1:100, MP Biomedical). Sections were washed twice with PBS before being stained with DAPI (1:20,000, Invitrogen) diluted in PBS for 10-minutes. Samples were washed with PBS prior to mounting with either ProLong®Gold Antifade Reagent (Life Technologies) or VECTASHIELD HardSet Mounting Medium (Vector Laboratories). Samples were examined using a Zeiss Axioskop 2mot+ microsope and images were captured using Openlab v4 (PerkinElmer). Alternatively, the following modifications were performed for indirect IF. For B220 detection endogenous biotin was blocked following a 15-minute incubation with Avidin/Biotin Blocking Kit (Vector Laboratories) before biotinylated anti-mouse CD45R/B220 (1:200, Clone: RA3-6B2, PharMingen) was applied for 1-hour. Samples were washed prior to a 1-hour incubation with streptavidin Alexa Fluor-488 (1:1000, Invitrogen). DAPI staining and mounting was performed as detailed above. With the exception of C3 the conditions described above were selected following optimization. Each antibody was trialed with iced cold 70% methanol, 4% PFA, acetone and no fixative and subjected to a titration of 1:60 – 1:1000. Control tissue, either IRI kidney tissue for fibrin or spleen for IgM and B220 was run in parallel when experimental tissue was stained as a positive control to ensure staining had worked.

2.7.5 Immunohistochemistry (IHC) of frozen and paraffin sections – Frozen sections were air dried for 1-hour, washed twice with PBS for 5-minutes and fixed in iced cold 70% methanol for 10-minutes. Paraffin sections were de-waxed and rehydrated as described in section '2.7.3 Haematoxylin & eosin (H&E) staining'. Following two 5-minute washes with PBS endogenous peroxidase activity was blocked by a 15-minute incubation in 0.3% H_2O_2 diluted in methanol. Samples were washed twice for 5-minutes before being loaded into sequenza slide racks. Endogenous avidin and biotin activity was blocked using a Avidin/Biotin Blocking Kit (Vector Laboratories) performed according to the manufacturer's instructions. Samples were incubated in protein block serum-free ready-to-use (Dako) to block non-specific binding. Primary antibodies, diluted in REAL antibody diluent (Dako), were applied and left to incubate overnight at

4°C. Primary antibodies used were rat anti-mouse CD41 (1:250, Clone: MWReg30, AbDserotec), used either unconjugated or biotinylated, rat anti-mouse Gr1 (1:300, Clone: RB6-8C5, BioLegend), biotinylated rat anti-mouse B220/CD45R (1:100,Clone: RA3-6B2, PharMingen) and polyclonal goat anti-mouse μ chain specific IgM (Vector Laboratories). A biotinylated secondary rabbit anti-rat IgG or rabbit anti-goat IgG (both Vector Laboratories) was applied (1:300), diluted in REAL antibody diluent, for 30-minutes after two 5-minute washes (this step was omitted for biotinylated primary antibodies). After two 5-minute washes samples were incubated for 30-minutes in R.T.U Vectastain Kit Elite Reagent (Vector Laboratories) which contains preformed avidin/biotin enzyme complex. Samples were washed thrice before exposure to Dako Liquid DAB + Substrate Chromogen System (Dako) for 10-minutes and then washed thrice. Samples were counterstained with Haematoxylin for 30-seconds, washed with tap water until clean and blued with Scotts Tap Water for 20-seconds. Paraffin sections were dehydrated and mounted as previously detailed. Frozen sections were mounted with VECTASHIELD HardSet Mounting Medium. The conditions described above were selected following optimization, as described above with the following additions. For frozen sections a small titration of H_2O_2 concentration was performed diluted in either PBS or methanol and a range of DAB incubation times were trialed. Control tissue was also run in parallel when experimental tissue was stained to ensure staining had worked. Isotype controls (Purified Rat IgG2b κ, 1:300, BioLegend; unconjugated and biotinylated Rat IgG1, 1:250, AbDserotec) were used to confirm binding specificity.

2.7.6 Quantification of IF and IHC staining - For each stained section (one per mouse) 5 images of the OSOM were taken at either x100 (fibrin and IgM (IF)) or x200 (for CD41, Gr1, and IgM (IHC)). Positive staining was selected using ImageJ (NIH) and processed using the macros detailed in Table 2.1. Sections were examined using either a Zeiss Axioskop 2mot+ and Hamamatsu Orca-ER camera or a Zeiss Axioskop microscope and QImaging Micropublisher 3.3 RTV camera. The number of positive pixels was expressed as a percentage of the total number of pixels. Quantification was performed in a blinded manner.

Table 2.1 – Image J macros for IF (**A** - Macro for RGB Colour image types and **B** - Macro for 8-bit image types) and DAB (**C**) staining quantification.

A	run("RGB Stack");
	setSlice(**#**);
	setAutoThreshold("Default dark");
	//run("Threshold...");
	setThreshold(**##**, 255);
	run("Convert to Mask", " ");
	run("Set Measurements...", "area area_fraction limit display redirect=None decimal=3");
	run("Measure");

B	setAutoThreshold("Default dark");
	//run("Threshold...");
	setThreshold(0, **###**);
	run("Convert to Mask");
	run("Set Measurements...", "area area_fraction limit display redirect=None decimal=3");
	run("Measure");

C	imgName=getTitle();
	run("Colour Deconvolution", "vectors=[H DAB]");
	selectWindow(imgName + "-(Colour_3)");
	close();
	selectWindow(imgName +"-(Colour_1)");
	close();
	selectWindow("Colour Deconvolution");
	close();
	setAutoThreshold("Default dark");
	//run("Threshold...");
	setAutoThreshold("Default");
	setThreshold(0, **###**);
	run("Convert to Mask");
	run("Set Measurements...", "area area_fraction limit display redirect=None decimal=3");
	run("Measure");

2.8 Blood Collection and Processing

2.8.1 Murine plasma/serum generation and erythrocyte isolation **-** Total blood was collected via cardiac puncture from terminally anaesthetised mice into Multivette® 600 Lithium Heparin coated tubes (Sarstedt). Plasma was collected following centrifugation at 1500 x *g* for 10-minutes. The buffy coat was discarded and the

erythrocyte pellet was washed in PBS and centrifuged at 600 *x g* for 10-minutes thrice before being diluted x3.5 in PBS. Total blood was collected via cardiac puncture from terminally anaesthetised mice into a 2 mL syringe for serum generation, which was later transferred into a 1 mL microfuge tube. Serum was collected by allowing blood to clot overnight at 4°C followed by centrifugation at 10,000 *x g* for 5-minutes.

2.8.2 Preparation of citrated whole blood and platelet-poor- and platelet-rich-plasma - Total blood was collected via cardiac puncture from terminally anaesthetised mice into a syringe containing 3.2% sodium citrate (9:1) diluted in Hanks Balanced Salt Solution H6648. Citrated blood was transferred into 1.5 mL microcentrifuge tubes. Platelet-poor-plasma was obtained following centrifugation at 17,000 x *g* twice for 10-minutes and snap frozen on dry ice and stored at -80°C before use. Platelet rich plasma was collected following centrifugation at 100 x *g* for 10-minutes and was used immediately.

2.9 Assessment of IgM binding in *in vitro* models of renal ischaemia reperfusion injury

2.9.1 Induction of ATP depletion in HK-2 cells by Antimycin A – An overview of this assay is provided in Figure 2.2A. Large-scale intracellular ATP and glucose depletion with elevated intracellular calcium levels are hallmarks of cellular ischaemic injury (Kaushal et al., 2004, Greene and Paller, 1994). In this thesis we used a combination of a mitochondrial inhibitor (Antimycin A), a non-metabolised glucose analogue (2-deoxyglucose), and a calcium ionophore (A23187) to mimic 'ischaemia' in HK-2 cells and investigated IgM binding. Incubation in human serum was used to mimic 'reperfusion'. This is an extensively used and widely accepted *in vitro* model of renal IRI injury (Iwata et al., 1995, Lee and Emala, 2002, Breggia and Himmelfarb, 2008). Detailed methodology is as follows. HK-2 cells, detached with trypsin or cell dissociation buffer, were seeded at a density of $3x10^5$ cells/mL and allowed to adhere overnight before injury was induced by a 1-hour or 3-hour incubation in 10 mM antimycin A plus 10 mM 2-deoxyglucose plus 1 µM calcium ionophore or 20 mM

antimycin A plus 20 mM 2-deoxyglucose plus 2 µM calcium ionophore. Cells were then washed with PBS twice. Morphological injury was assessed by microscopy using a Zeiss Axiovert S100 with a 32x/0.4 objective and imaged using a CoolSnap RS Photometrics camera and OpenLab software. To allow *in vitro* reperfusion HK-2 cells were either incubated in RPMI 1640 supplemented with 5% FCS or 30% human serum for 24-hours. HK-2 cells were washed with PBS and detached before IgM binding was detected as described in '2.5.2 Assessment of IgM binding to cells'.

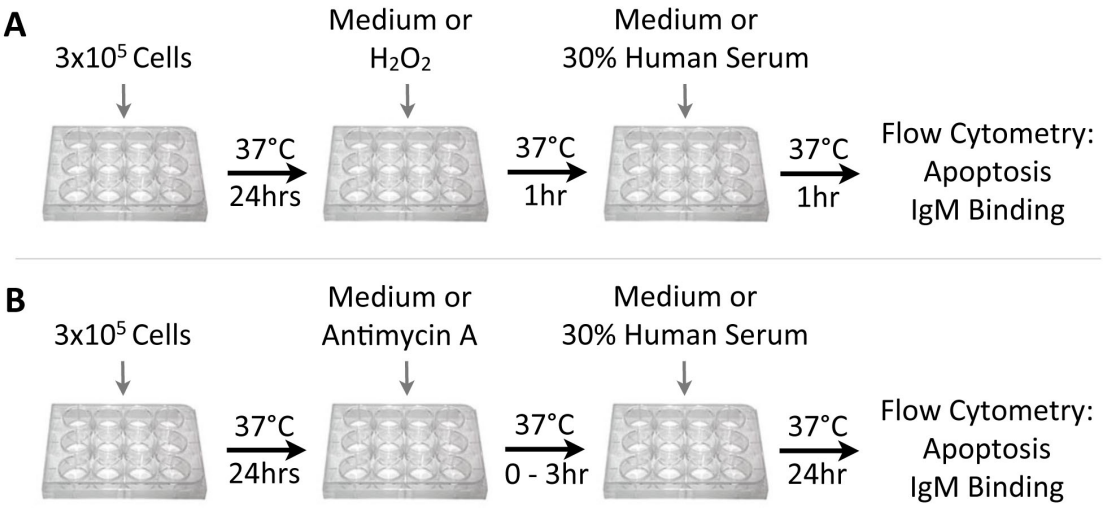

Figure 2.2 – Overview of conditions used to induce cellular injury in human proximal tubular epithelial (HK-2) cells by Antimycin A (A) or H_2O_2 (B). IgM binding was detected as described in '2.5.2 Assessment of IgM binding'. Apoptosis was inferred as described in '2.3.1 Annexin-V (AnnV) and PI staining'.

2.9.2 Induction of cellular injury in HK-2 cells by H_2O_2 – An overview of this assay is provided in Figure 2.2B. Another hallmark of IRI is ROS production, such as H_2O_2, which acts to exacerbate cellular injury (Simonson et al., 1993, Aragno et al., 2003). In this thesis we used an additional *in vitro* model of renal IRI induced by exposure of HK-2 cells to H_2O_2 prior to incubation with human serum, to mimic ischaemia reperfusion injury (Yoshida et al., 2008, Park et al., 2012). Detailed methodology is as follows. HK-2 cells were treated and seeded as above before injury was induced by a 1-hour incubation in serum free RMPI 1640 medium supplemented with either 0, 2.5, 5 or 500 mM H_2O_2. Morphology was assessed as above before HK-2 cells were incubated in

RPMI 1640 supplemented with 5% FCS or 30% human serum for 1-hour. HK-2 cells were washed with PBS and detached before IgM binding was detected as described in '2.5.2 Assessment of IgM binding to cells'. These conditions were selected following dose titration experiments.

2.10 *In vivo* model of renal ischaemia and murine thymocyte administration

2.10.1 Non-apoptotic and apoptotic murine thymocyte administration – To explore the influence of apoptotic cells on renal IRI or coagulation either 200 µL PBS (control) or $20x10^6$ non-apoptotic or apoptotic murine thymocytes, generated from male Balb/c mice as described in '2.2.1 Preparation of non-apoptotic and apoptotic thymocytes', were administered intravenously to mice 24-hours prior to renal IRI or sacrifice.

2.10.2 *In vivo* model of renal IRI **–** Detailed step by step methodology and an accompanying video is described in Hesketh *et al,.* (2014), both of which are included in this thesis. Male 8-week Balb/c mice were anaesthetised using ketamine (70 mg/kg) and medetomadine hydrochloride (1mg/kg) administered by intraperitoneal injection. Subcutaneous buprenorphine analgesia (0.06mg/kg) was given pre-operatively. A contralateral right nephrectomy was performed before the renal pedicle was clamped with an atraumatic clamp for 22, 24 or 25-minutes. Body temperature was maintained at 37°C by a homeostatically controlled blanket (Harvard Apparatus, Boston MA) during the ischaemic period. The peritoneum was then sutured and the skin closed with metallic clips. Anaesthesia was reversed using atipamazole hydrochloride (2mg/kg) and 1 mL sterile saline was administered by a subcutaneous injection post surgery. Sham mice underwent a laparotomy with manipulation of the left and right renal pedicle only. Mice were placed in an incubator at 27°C immediately post-operatively. The left ischaemic kidney, spleen, liver tissue and total blood were collected at the time of sacrifice. Renal function and structural injury was then assessed.

2.10.3 Assessment of renal function – Renal function was inferred from blood urea nitrogen (BUN) [mmol/L] and creatinine [µmol/L] concentration assessed in plasma samples using a creatinase based method by Dr Forbes Howie (MRC Centre for Reproductive Health) on a Cobas Fara Centrifugal Analyser (Roche Diagnostics, UK).

2.10.4 Assessment of acute tubular necrosis (ATN) – ATN scoring was undertaken to quantify the extent of structural injury following renal IRI. The number of viable (intact cell membrane with normal morphology) and necrotic tubules (compromised and disrupted cell membrane) were marked and counted in H&E stained kidney tissue using ImageJ (NIH). The number of necrotic tubules was expressed as a percentage of the total number of tubules (necrotic tubules %). ATN was assessed in 5 images taken at x200 magnification of the outer stripe of the outer medulla (OSOM) per mouse. ATN was scored in a blinded manner.

2.11 Apoptotic cells and coagulation

2.11.1 Thrombin generation assay (TGA) **–** A TGA was used to investigate the ability of apoptotic cells to modulate thrombin generation. The thrombin generated in citrated platelet-poor-plasma collected from male Balb/c mice 24-hours following administration of apoptotic cells was measured by Roger Preston (Department of Clinical Medicine, Trinity College Dublin) as described previously (Tchaikovski et al., 2007).

2.11.2 Detection of platelet binding to apoptotic thymocytes – To explore the ability of apoptotic cells to interact with platelets an *in vitro* assay was established. Murine thymocytes were stained with CellTracker Orange (Invitrogen), according to the manufacturer's instructions, prior to apoptosis induction by overnight ageing. Platelets in 5 µL of citrated whole blood were labeled by a 30-minute incubation with 5 µL of Alexa Fluor-488 Rat Anti-Mouse CD41 (1:200, Clone: MWReg30, BioLegend). Approximately $5x10^5$ CellTracker Orange stained apoptotic thymocytes were then

added to whole blood, containing anti-mouse CD41 labeled platelets, and were incubated for 30-minutes. The sample was then fixed with 500 µL 1% paraformaldehyde (PFA) for 10-minutes before 10,000 $CD41^+$ events were collected by flow cytometry on a BD FACSCalibur. Anti-mouse CD41 binding specificity and positivity was assessed using FITC Rat IgG1 κ isotype control (1:200, BioLegend). Antibody dilutions were selected following titration and analysis undertaken using MFI.

2.12 Statistics

2.12.1 Statistical analysis **–** Results are expressed as means ± SEM. Statistical tests performed were student *t*-test, Kruskal-Wallis one-way ANOVA, standard one-way ANOVA or two-way ANOVA with a Dunn's or Bonferroni multiple comparisons test when appropriate. $P<0.05$ was considered to be statistically significant. Statistical analysis was performed using Prism 6 (GraphPad Software, San Diego).

Chapter 3. Differential IgM deposition following renal and hepatic ischaemic injury

Introduction

The role of IgM antibodies in ischaemic injury is an interesting and evolving area of research meriting further study, as such we aimed to investigate and clarify the potential involvement of IgM in renal and liver injury.

IgM antibodies form an integral and crucial part of our innate immune system, participating in diverse pathophysiologies such as infection, B cell homeostasis, inflammation, and autoimmunity (Ehrenstein and Notley, 2010). However, following ischaemic reperfusion injury, endogenous IgM can be pathogenic by binding injured cardiac muscle, skeletal muscle and the intestine where it activates complement and augments tissue damage (reviewed in Table 1.1). The role of IgM in renal IRI remains unclear, some studies suggest that immunoglobulins may be implicated in injury pathogenesis, whilst others indicate that immunoglobulins have no involvement (van der Pol et al., 2011, Burne-Taney et al., 2003, Park et al., 2002). Lobo *et al.,* (2012) suggested that IgM had a protective role in renal IRI. Following bilateral renal IRI sIgM KO had increased renal inflammation and dysfunction. Reconstitution with purified IgM attenuated renal inflammation. In the same study *in vitro* studies indicated that IgM binding to leukocytes inhibited TLR-4–induced NF-κB nuclear translocation. In addition IgM antibody binding to leukocyte receptors prevented T cell differentiation into pro-inflammatory cells Th-1 and Th-17. In contrast to this paper, there are a number of papers indicating the pathogenic nature of IgM antibodies in ischaemia in other organs (Haas et al., 2010, Zhang et al., 2006b, Zhang et al., 2006a, Zhang et al., 2004, Chan et al., 2004). As such we were still keen to explore the role of IgM antibodies during renal IRI in our own lab. Although ambiguity surrounds the role of IgM antibodies in renal ischaemia reperfusion injury, the involvement of IgM in liver ischaemic injury is unknown. If IgM antibodies are found to be involved then therapeutic strategies designed to inhibit access to IgM bound epitopes may represent

novel treatments for renal and hepatic IRI. Such approaches have been successful in murine models of intestinal, cardiac and skeletal muscle ischaemia in which injury was ameliorated by a synthetic N2 peptide that blocked IgM binding to neo-epitope NMHC-11 (Haas et al., 2010, Zhang et al., 2006a).

In this chapter we explored the binding of IgM antibodies to murine kidney tissue at key time points following renal IRI, and to injured human renal cells *in vitro*. We also characterized the kinetics of IgM deposition in mice following hepatic ischaemic injury, and in a murine model of autoimmune hepatitis (AIH).

Results

3.1 Non-specific staining is evident following IHC detection of IgM in paraffin embedded kidney tissue

Firstly attempts were made to detect IgM in paraffin embedded kidney tissue by IHC as, once optimised, this method results in clear staining with excellent tissue morphology. However, whilst ischaemic kidney tissue harvested 24-hours following renal IRI appeared to show IgM deposition, this staining was also evident in non-injured control kidney tissue (Figure 3.1). Also, some positive staining was observed in immunoglobulin deficient RAG-1 kidney tissue indicating that the anti-IgM antibody used resulted in non-specific staining in kidney tissue (Figure 3.1). This non-specific staining was still detectable at antibody dilutions of 1:20,000 suggesting that IHC based detection of IgM by unconjugated anti-IgM in kidney tissue would not yield optimum accurate results.

3.2 Specific IgM staining is evident following IF detection in frozen kidney tissue

Next, detection of IgM in frozen tissue using IF was trialed using a directly conjugated Texas Red anti-IgM antibody. Frozen spleen tissue was selected as a positive control, due to the presence of membrane bound IgM on B cells, and used to optimise staining conditions. A 1:200 dilution was selected following a titration and the optimum

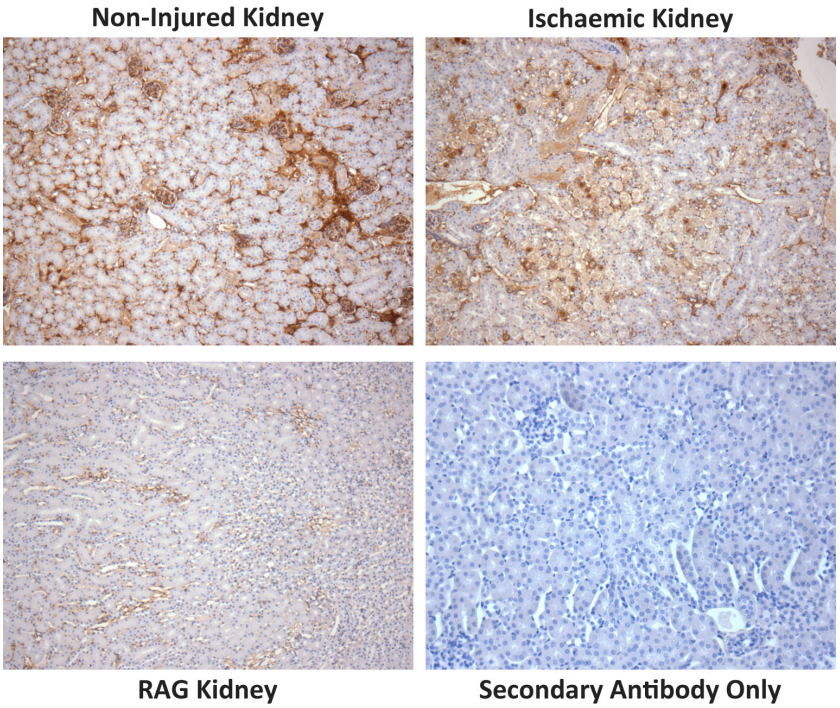

Figure 3.1 – Non-specific staining evident following IHC based detection of IgM in paraffin embedded non-injured, ischaemic and RAG kidney tissue. Trials of unconjugated IHC with an anti-IgM antibody yielded non-specific binding in non-injured, post IRI paraffin embedded kidney tissue. Non-specific binding was also evident in immunoglobulin deficient RAG kidney tissue. Kidney tissue stained with a biotinylated secondary antibody alone illustrated no staining. Magnification: x200.

fixation technique was then determined. Frozen spleen tissue was either left unfixed, or the common fixatives 70% MetOH or 4% PFA were used, the latter of which resulted in strong clear positive IgM staining (Figure 3.2A). The absence of staining in frozen RAG-1 spleen and kidney tissue, and isotype stained spleen tissue, confirmed anti-IgM specificity (Figure 3.2B).

Binding specificity was further confirmed in 4% PFA fixed frozen spleen tissue dual stained for IgM and the B cell marker B220 as similar positive B220 and IgM staining patterns were evident in what appeared to be germinal centers (Figure 3.3). Future experiments therefore detected IgM deposition in 4% PFA fixed kidney tissue using a fluorochrome conjugated anti-IgM antibody.

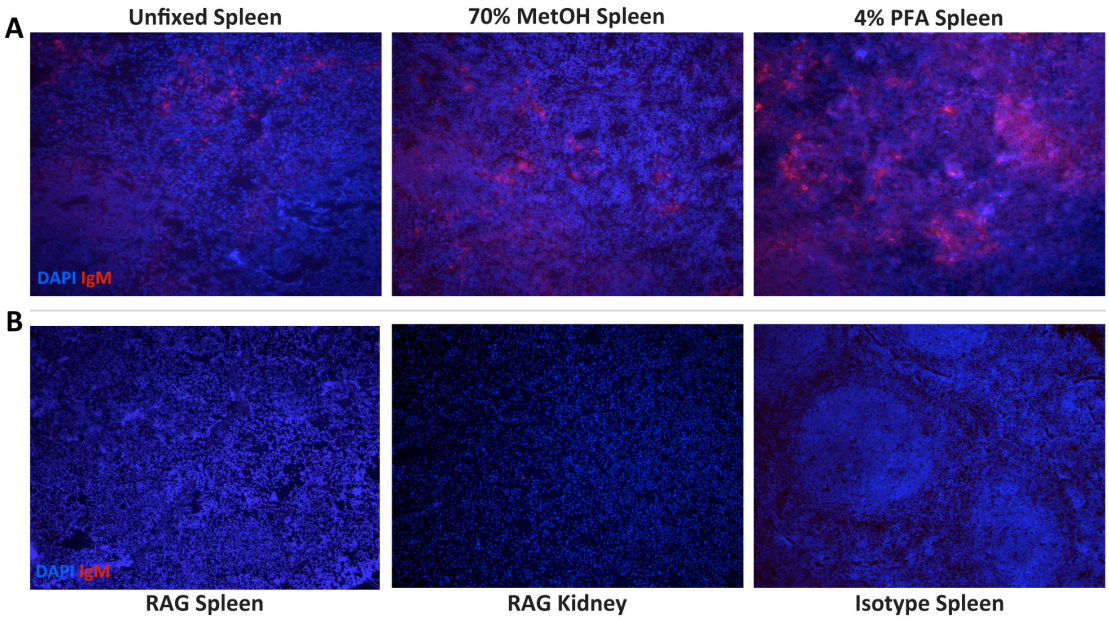

Figure 3.2 – Specific IgM staining evident in frozen spleen tissue fixed with 4% PFA following IF based detection. A) Trials to determine which fixation technique yield optimum staining with a directly conjugated Texas-Red anti-IgM antibody revealed that frozen spleen tissue fixed with 4% PFA exhibited clear positive staining. **B**) No staining was detected in frozen RAG spleen and kidney tissue following anti-IgM staining. Frozen spleen tissue stained with an isotype antibody illustrated no staining. Magnification of all images: x100.

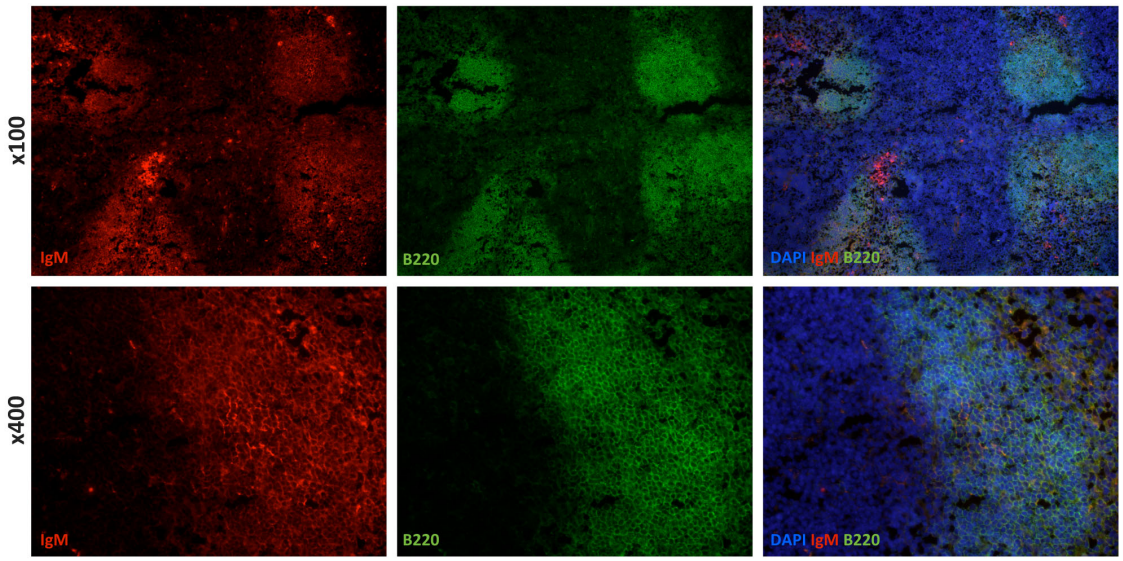

Figure 3.3 – IgM and B220 exhibit similar staining patterns in frozen spleen tissue. To confirm anti-IgM specificity 4% PFA fixed frozen spleen tissue was stained for the B cell marker B220 and IgM. B220 staining was evident in what appeared to be germinal centers with IgM exhibiting a similar staining pattern.

3.3 Despite evident tissue necrosis minimal IgM deposition was detected following renal ischaemic injury

As IgM antibodies have been shown to have a pathogenic role in skeletal, intestinal and cardiac ischaemia (reviewed in Table 1.1), we wanted to ascertain whether IgM might be involved in renal ischaemic injury. To investigate this we first wanted to confirm that IgM was present following injury. Therefore to assess IgM deposition following renal ischaemic injury, 8-week old male Balb/c mice underwent 25-minutes of ischaemia and were sacrificed 30-minutes, 1-hour or 24-hours later. An overview of this experiment is provided in chapter 4 figure 4.5A, however an additional 30-minute time point was studied. Note that the tissue used from this experiment was also used to study baseline injury and microvascular congestion as discussed in chapter 4. As figure 3.4A illustrates tissue necrosis was evident at 1-hour and 24-hours post ischaemia, whilst at 30-minute normal renal tubular morphology, similar to non-injured tissue, was observed. ATN for time points 1-hour and 24-hours was quantified and is presented in figure 4.6B, ATN was not present at 30-minutes. IgM staining was present at 1-hour and 24-hours post ischaemia, but was absent at 30-minutes and in non-injured kidney tissue (Figure 3.4A). As shown in figure 3.4B quantification of IgM^+ staining in the OSOM revealed that, although statistically significant, IgM deposition was minimal at 1-hour with 0.92 ±0.46% IgM^+ and appeared reduced at 24-hours post ischaemia (one-way ANOVA, $P \leq 0.05$, 1-hour and 24-hour ($n = 4$), 30-minutes ($n = 3$), non-injured ($n = 11$)). In addition, quantification confirmed that IgM deposition was largely absent 30-minutes post ischaemia and in non-injured kidney tissue (Figure 3.4B).

3.4 Minimal C3 deposition observed following renal ischaemic injury

As demonstrated in skeletal, intestinal and cardiac ischaemia (reviewed in Table 1.1) C3 deposition is often observed following binding of IgM to injured tissue. We aimed to investigate whether C3 deposition was observed following renal ischaemic injury, the absence of which would further support our data indicating that IgM antibodies are not present in ischaemic kidney tissue. To detect C3 deposition frozen kidney

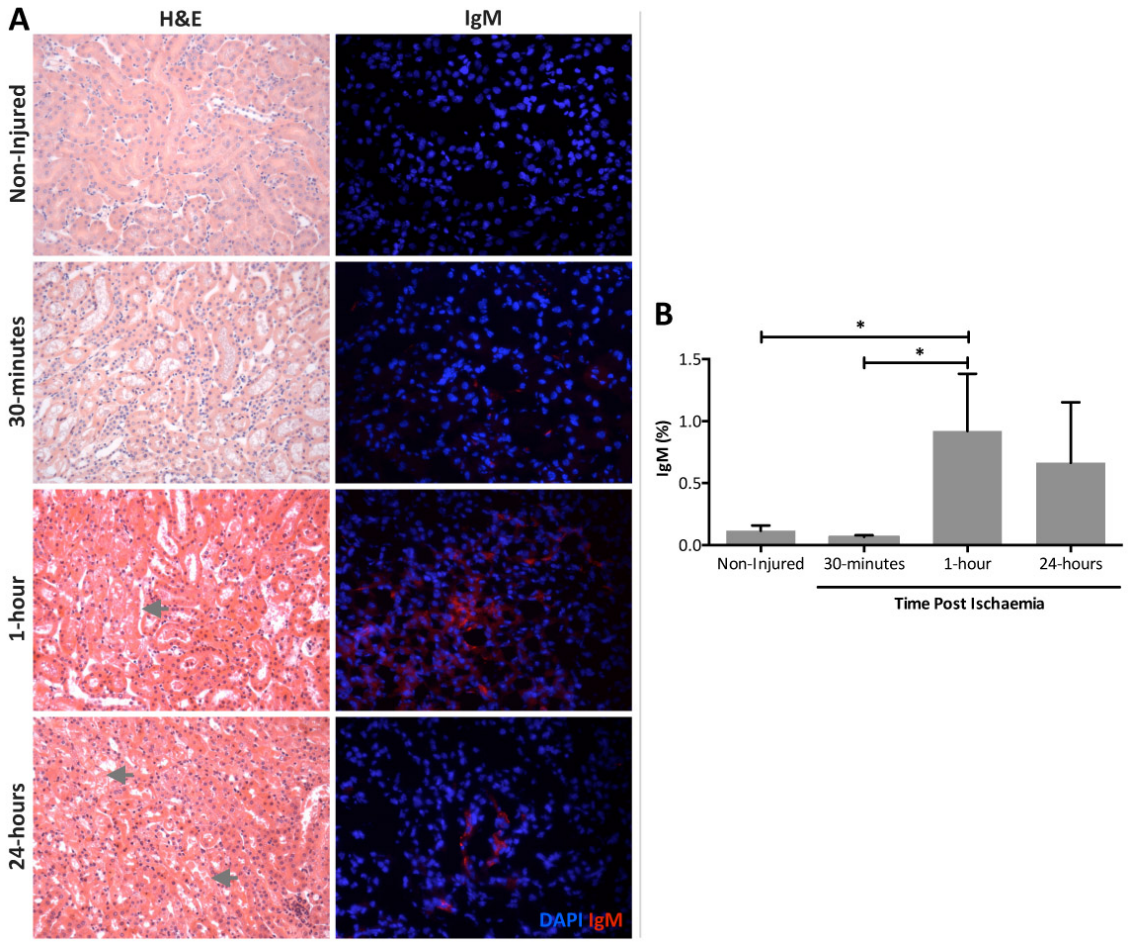

Figure 3.4 – Despite evident tissue necrosis minimal IgM deposition was detected following renal ischaemic injury. To assess IgM deposition following renal ischaemic injury, 8-week old male Balb/c mice underwent 25-minutes of ischaemia and were sacrificed 30-minutes, 1-hour or 24-hours later. **A**) Representative photomicrographs of H&E stained paraffin embedded kidney sections revealed that normal renal tubular morphology is observed at 30-minutes, whilst tissue necrosis was evident at 1-hour and 24-hours (indicated by grey arrows) following renal IRI. Minimal IgM deposition was observed in 4% PFA fixed frozen ischaemic kidney tissue stained with anti-IgM. **B**) Quantification of IgM deposition (expressed as IgM^+ area) in the OSOM demonstrated that IgM was present 1-hour following IRI. Data expressed as ±SEM and analysed by one-way ANOVA. * = $P \leq 0.05$. 1-hour and 24-hour (n = 4), 30-minutes (n = 3), non-injured (n = 11). Magnification H&E: x200. Magnification IgM: x400.

tissue harvested 30-minutes, 1-hour and 24-hours following renal IRI was fixed with 4% PFA and stained with an anti-C3 antibody. As presented in figure 3.5 C3 deposition appeared largely absent at 30-minutes and 24-hours, but was minimally detected at 1-hour post ischaemia. Frozen liver tissue exhibiting injury secondary to carbon tetrachloride administration (kindly provided by Alexandra Thompson) was used as a positive control to validate the anti-C3 antibody (Figure 3.5). Following staining it was

discovered that some tissue from this experiment was all sectioned onto contaminated slides, which interfered with IF staining. It was therefore decided that data from this experiment would not be quantified due to a reduced sample size and as such only representative data is presented.

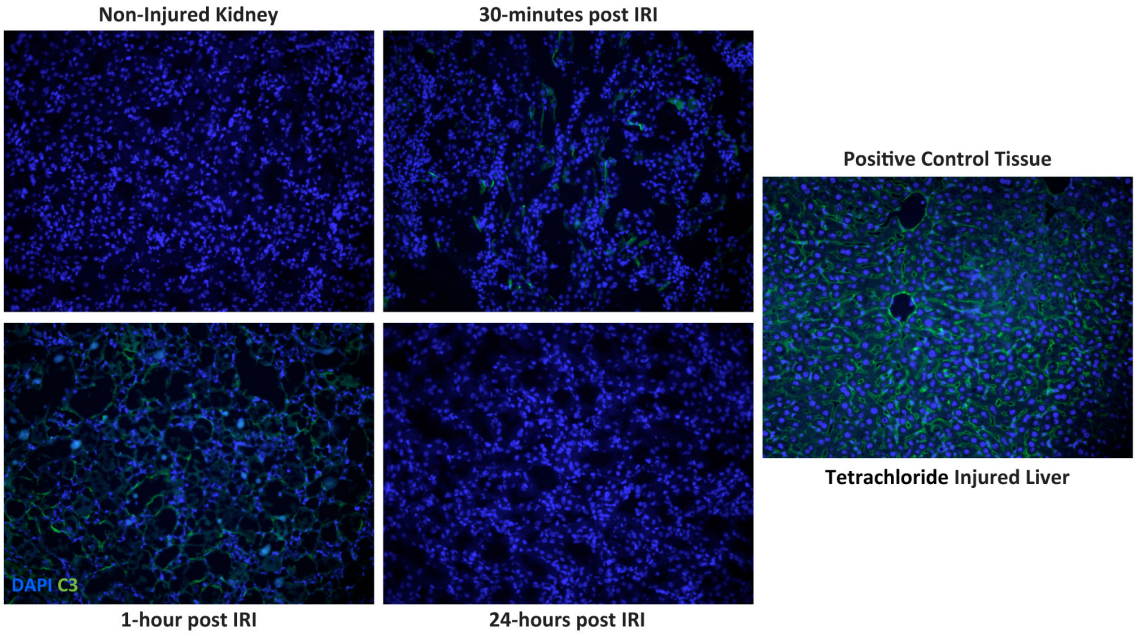

Figure 3.5 - Minimal C3 deposition observed following renal ischaemic injury. C3 deposition was assessed in 4% PFA fixed frozen kidney tissue harvested 30-minutes, 1-hour or 24-hours following 25-minutes of ischaemia in 8-week old male Balb/c mice. Minimal C3 deposition was observed in ischaemic kidney tissue stained with anti-C3. C3 staining was evident in frozen tetrachloride injured liver positive control tissue. Representative photomicrographs. 1-hour and 24-hour (*n* = 4), 30-minutes (*n* = 3), non-injured (*n* = 11). Magnification: x200.

3.5 IgM antibodies reactive to apoptotic cells are not reduced in plasma obtained from mice following apoptotic cell administration or renal ischaemic injury

We sought to determine whether apoptotic cell administration or renal IRI might reduce the level of IgM reactive to apoptotic cells. To assess this plasma samples, obtained following $20x10^6$ apoptotic cell administration or renal IRI, were exposed to apoptotic cells and stained with anti-IgM. The percentage of IgM^+ cells was then assessed by flow cytometry. This technique is designed to determine the level of IgM bound to apoptotic cells and is described in detail in chapter 5. Normal plasma generated from healthy 8-week old male Balb/c mice not undergoing renal IRI was

used as a control. Firstly, plasma samples obtained from 8-week old male Balb/c mice 24-hours following PBS or administration of $20x10^6$ apoptotic cells was studied. This indicated that levels of IgM reactive to apoptotic cells remained similar in plasma samples obtained from normal or PBS/apoptotic cell treated mice (Figure 3.6A). We next determined if IgM levels reactive to apoptotic cells was reduced in plasma samples obtained 1-hour and 24-hours following renal ischaemic injury. Interestingly, whilst levels of IgM^+ cells in plasma obtained from normal mice and mice sacrificed 1-hour following IRI remained similar, a slight non-significant reduction was observed in plasma from mice sacrificed 24-hours following renal ischaemia (Figure 3.6B).

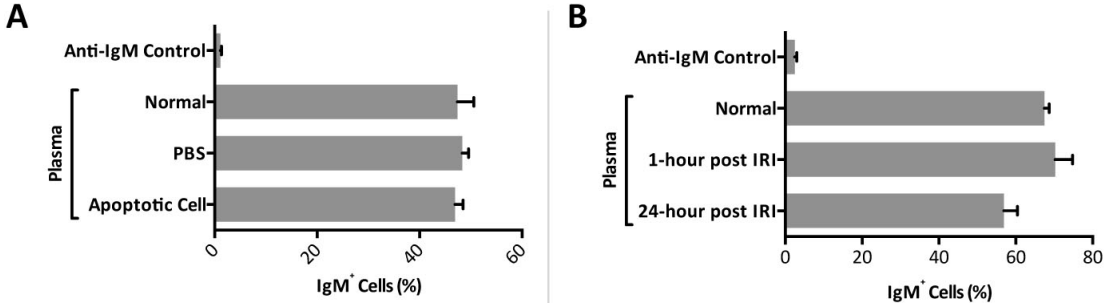

Figure 3.6 – IgM antibodies reactive to apoptotic cells are not reduced in plasma obtained from mice following apoptotic cell administration or renal ischaemic injury. Plasma was obtained from 8-week old male Balb/c mice 24-hours following (**A**) PBS or administration of $20x10^6$ apoptotic cells or (**B**) 1-hour or 24-hours following 25-minutes of ischaemia. Normal plasma was generated from healthy 8-week old male Balb/c mice not undergoing renal IRI or PBS/apoptotic cell administration. The level of apoptotic cell reactive IgM antibodies following apoptotic cell administration or renal IRI was assessed. To do this plasma samples were exposed to apoptotic cells and stained with anti-IgM. The percentage of IgM^+ cells was then assessed by flow cytometry. **A**) Levels of IgM^+ cells remained similar in plasma samples obtained from normal or PBS/apoptotic cell treated mice. **B**) Whilst levels of IgM^+ cells in plasma obtained from normal mice and mice sacrificed 1-hour following IRI remained similar, a slight non-significant trend to a reduction is observed in plasma from mice sacrificed 24-hours following renal IRI. Data expressed as ±SEM and analysed by one-way ANOVA. All groups (*n* = 4 mice).

3.6 H_2O_2 exposure induced morphological injury and apoptosis in HK-2 cells

We next explored the relevance of these findings to human renal ischaemic injury using human proximal tubular epithelial (HK-2) cells; a cell line derived from normal adult human kidney (Ryan et al., 1994). We aimed to validate and further explore the findings of van der Pol *et al.,* (2011) which suggested that IgM bound to HK-2 cells

injured by hypoxia. To further probe IgM binding to injured HK-2 cells we aimed to have three stages of injury: 1) morphological injury with limited apoptosis; 2) morphological injury with evident apoptosis and 3) severe morphological injury with high apoptosis. To induce injury HK-2 cells were exposed to between 0mM to 500mM H_2O_2 for 1-hour. H_2O_2 was selected as this ROS is released during ischaemia and induces cellular injury by oxidative stress (Simonson et al., 1993, Aragno et al., 2003). The use of H_2O_2 to induce cellular injury with subsequent incubation in human serum, to mimic 'ischaemia' and 'reperfusion', respectively, is an accepted *in vitro* model of renal IRI (Yoshida et al., 2008, Park et al., 2012). The resulting degree of morphological injury and apoptosis were assessed by phase contrast microscopy and AnnV and PI staining measured by flow cytometry, respectively. HK-2 cells were classified as non-apoptotic ($AnnV^-PI^-$), early ($AnnV^+PI^-$) or late apoptotic ($AnnV^+PI^+$). Out of the conditions assessed 2.5 mM, 5 mM and 500 mM were selected for future experiments. As illustrated in figure 3.7 these conditions resulted in increasing morphological injury and apoptosis.

3.7 IgM bound minimally to increasingly H_2O_2 injured HK-2 cells

We then aimed to determine whether human IgM would bind to injured HK-2 cells. HK-2 cells were treated with 2.5 mM, 5 mM or 500 mM H_2O_2 for 1-hour to induce injury and were incubated in PBS or human serum as a source of IgM for 1-hour. Samples were then stained with anti-IgM and IgM binding was assessed by flow cytometry. However, IgM did not convincingly bind to any injured HK-2 cells (Figure 3.8). Levels of apoptosis and injury were similar to that illustrated in figure 3.7. Note that these experiments were repeated using both trypsin and non-enzymatic cell dissociation buffer to ensure that the negative result was not due to enzymatic cleavage of cell surface antigens. Upon careful evaluation of the resulting injury and apoptosis it became apparent that following exposure to H_2O_2 the HK-2 cells appeared to progress straight to late apoptosis. As evident in figure 3.7 populations of early apoptotic HK-2 cells were not observed. We hypothesized that IgM may bind to neo-epitopes generated during apoptotic progression and HK-2 cells therefore might need to progress through early apoptosis in order for IgM to bind.

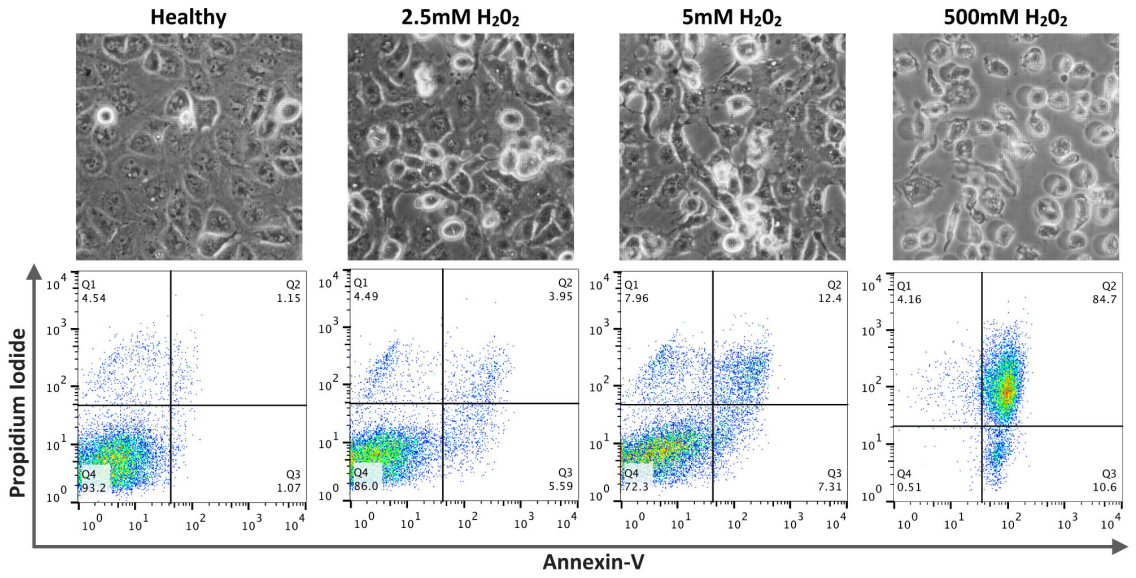

Figure 3.7 – H_2O_2 exposure induced morphological injury and apoptosis in HK-2 cells. HK-2 cells were exposed to 2.5 mM, 5 mM or 500 mM H_2O_2 for 1-hour and the resulting morphological injury and apoptosis was assessed by phase contrast microscopy and AnnV and PI staining measured by flow cytometry, respectively. HK-2 cells were classified as non-apoptotic ($AnnV^-PI^-$), early ($AnnV^+PI^-$) or late apoptotic ($AnnV^+PI^+$). Representative phase contract photomicrographs indicate that 2.5mM and 5mM H_2O_2 exposure induced morphological injury, indicated by cellular disruption and irregular morphology, with limited apoptosis, evident by a large proportion of cells being $AnnV^-PI^-$. A higher degree of injury, associated with increased numbers of $AnnV^+PI^+$ cells and distinct disruption of cells, was induced by incubation in 500 mM H_2O_2. Representative data.

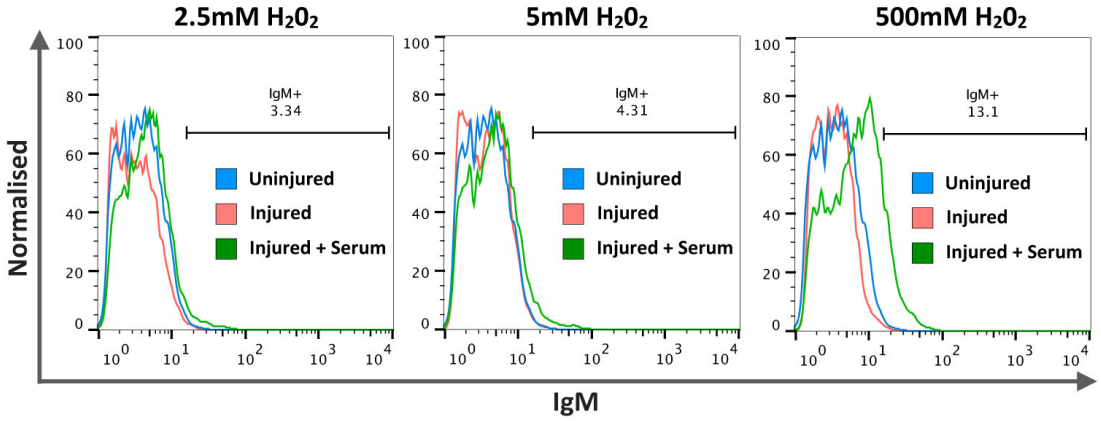

Figure 3.8 – IgM bound minimally to increasingly H_2O_2 injured HK-2 cells. HK-2 cells were exposed to 2.5 mM, 5 mM or 500 mM H_2O_2 for 1-hour. Following this cells were incubated in PBS or human serum (as a source of IgM) for 1-hour. Samples were then stained with anti-IgM and IgM binding was assessed by flow cytometry. Minimal IgM binding was observed in HK-2 cells injured with H_2O_2. Representative histograms and contour plots (n = 3).

3.8 Antimcyin A exposure induced morphological injury and early apoptosis in HK-2 cells

To obtain populations of early apoptotic HK-2 cells, injury was induced by exposure to Antimycin A. Antimycin A is a secondary metabolite which along with 2-Deoxy-D-Glucose chemically depletes ATP inducing oxidative stress via the release of superoxide free radicals and nutrient starvation. Similar to H_2O_2 the use of Antimcyin A to induce cellular injury, with subsequent incubation in human serum to mimic 'ischaemia' and 'reperfusion', respectively, is an accepted *in vitro* model of renal IRI (Iwata et al., 1995, Lee and Emala, 2002, Breggia and Himmelfarb, 2008). A titration of Antimycin A was performed to establish the concentrations necessary to induce increasing morphological injury and increasing apoptosis, with populations of early apoptotic HK-2 cells. HK-2 cells were exposed to between 10 µM to 20 µM Antimycin A for 1-hour or 3-hours. Cellular morphology and apoptosis was evaluated. Exposure to 10 µM Antimycin A for 1-hour and to 10 µM or 20 µM Antimcyin A for 3-hours induced increasing morphological injury and apoptosis as evident in figure 3.9. These conditions were selected for future experiments.

3.9 IgM bound minimally to increasingly Antimcyin A injured HK-2 cells

Following establishment of conditions necessary to induce 'ischaemic' injury by Antimycin A, we then investigated whether IgM would bind to injured HK-2 cells that have progressed through apoptosis. HK-2 cells were treated with 10 µM Antimycin A for 1-hour or 10 µM or 20 µM Antimycin A for 3-hours to induce injury and were incubated in PBS or human serum as a source of IgM for 24-hours. Samples were then stained with anti-IgM and IgM binding was assessed by flow cytometry. Despite HK-2 cells appearing to progress through early apoptosis IgM binding was not detected (Figure 3.10). Levels of apoptosis and injury were similar to that illustrated in figure 3.9. These experiments were also repeated using both trypsin and non-enzymatic cell dissociation buffer to ensure that the negative result was not due to enzymatic cleavage of cell surface antigens.

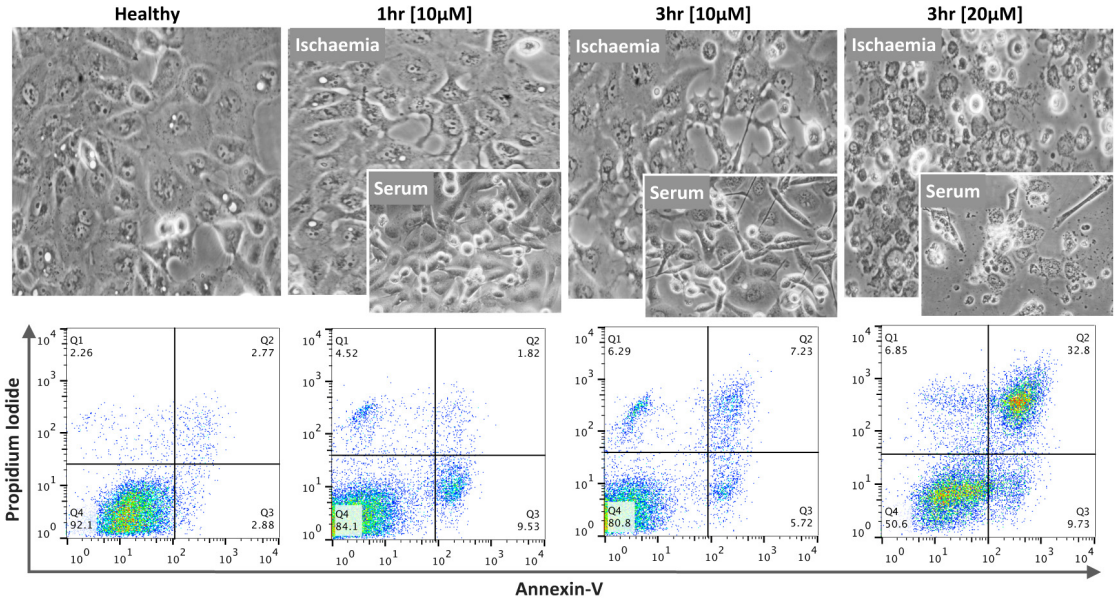

Figure 3.9 – Antimycin A exposure induced morphological injury and apoptosis in HK-2 cells. HK-2 cells were exposed to 10 µM Antimycin A for 1-hour, or incubated in 10 µM or 20 µM Antimcyin A for 3-hours. The resulting morphological injury and apoptosis was assessed by phase contrast microscopy and AnnV and PI staining measured by flow cytometry, respectively. Cells were classified as non-apoptotic ($AnnV^-PI^-$), early ($AnnV^+PI^-$) or late apoptotic ($AnnV^+PI^+$). HK-2 cells were incubated in 10 µM Antimycin A for 3-hours to induce a morphological injury, indicated by cellular disruption and irregular morphology, with limited apoptosis, evident by a large proportion of cells being $AnnV^-PI^-$. A higher degree of injury, associated with increased numbers of $AnnV^+PI^+$ cells and distinct disruption of cells, was induced by a 3-hour incubation in 20 µM Antimycin A. Transient early apoptotic populations of HK-2 cells were observed in all Antimycin A exposed samples. Representative data.

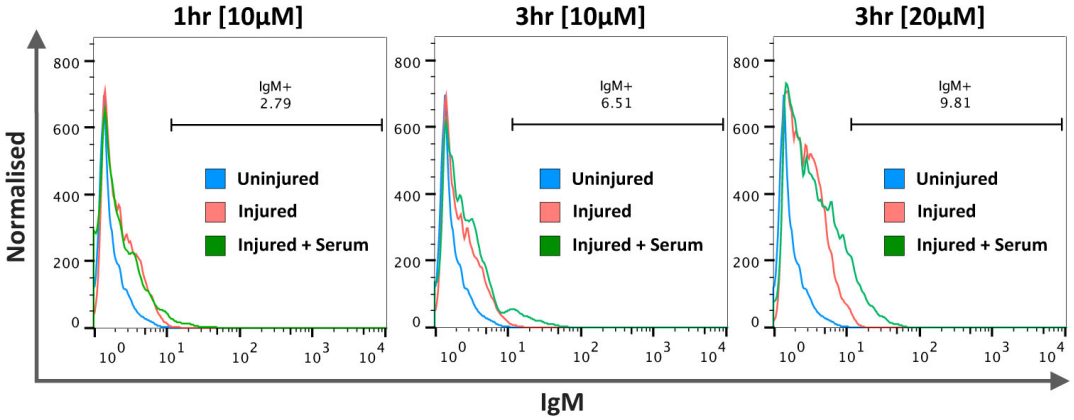

Figure 3.10 – IgM bound minimally to increasingly Antimcyin A injured HK-2 cells. Antimcyin A was used to induce injury in HK-2 cells. Following this cells were incubated in PBS or human serum (as a source of IgM) for 24-hours. Samples were then stained with an anti-IgM antibody and IgM binding was assessed by flow cytometry. Minimal IgM binding was observed in HK-2 cells injured with either 10 µM or 20 µM Antimcyin A. Representative histograms (*n* = 3).

3.10 Specific IgM staining evident following IHC detection in paraffin embedded liver tissue

With data indicating that IgM antibodies do not bind injured tissue following renal ischaemic injury we next sought to determine whether IgM might be involved in hepatic ischaemic injury. To investigate this we first wanted to confirm that we were able to specifically detect IgM in injured liver tissue. Trials of unconjugated polyclonal goat anti-IgM antibody demonstrated positive staining in normal paraffin embedded spleen tissue, with normal liver and immunoglobulin deficient RAG-1 spleen and liver tissue remaining IgM negative (Figure 3.11A). In addition no staining was detected in spleen and ischaemic liver tissue following incubation with a biotinylated antibody alone indicating secondary antibody specificity (Figure 3.11B). Also, anti-IgM antibody specificity was confirmed by exposing spleen and ischaemic liver tissue to goat serum (as an isotype control) with subsequent anti-IgM staining remaining negative (Figure 3.11B).

Similar positive B220 and IgM staining patterns evident in what appeared to be germinal centers in serial paraffin embedded spleen sections stained for IgM or the B cell marker B220 further confirmed anti-IgM specificity (Figure 3.12).

3.11 IgM deposition accumulated over a period of 24-hours following hepatic IRI and visibly declined by 7-days

To assess IgM deposition following hepatic ischaemic injury male C57BL/6 mice underwent 50-minutes of ischaemia induced by clamping of the left liver lobe, mice were sacrificed at various time points between 0-hour and 7-days. James Richards performed the hepatic IRI model and provided tissue used to assess IgM deposition. Assessment of paraffin embedded anti-IgM stained ischaemic liver tissue demonstrated dramatic IgM staining clearly evident at 1-hour and appeared to accumulate until 24-hours post hepatic IRI, but was nearly absent at 7-days (Figure 3.13A). Surprisingly, some IgM staining was detected at 0-hours following hepatic IRI, with IgM appearing to infiltrate into the tissue from central vessels, this was also

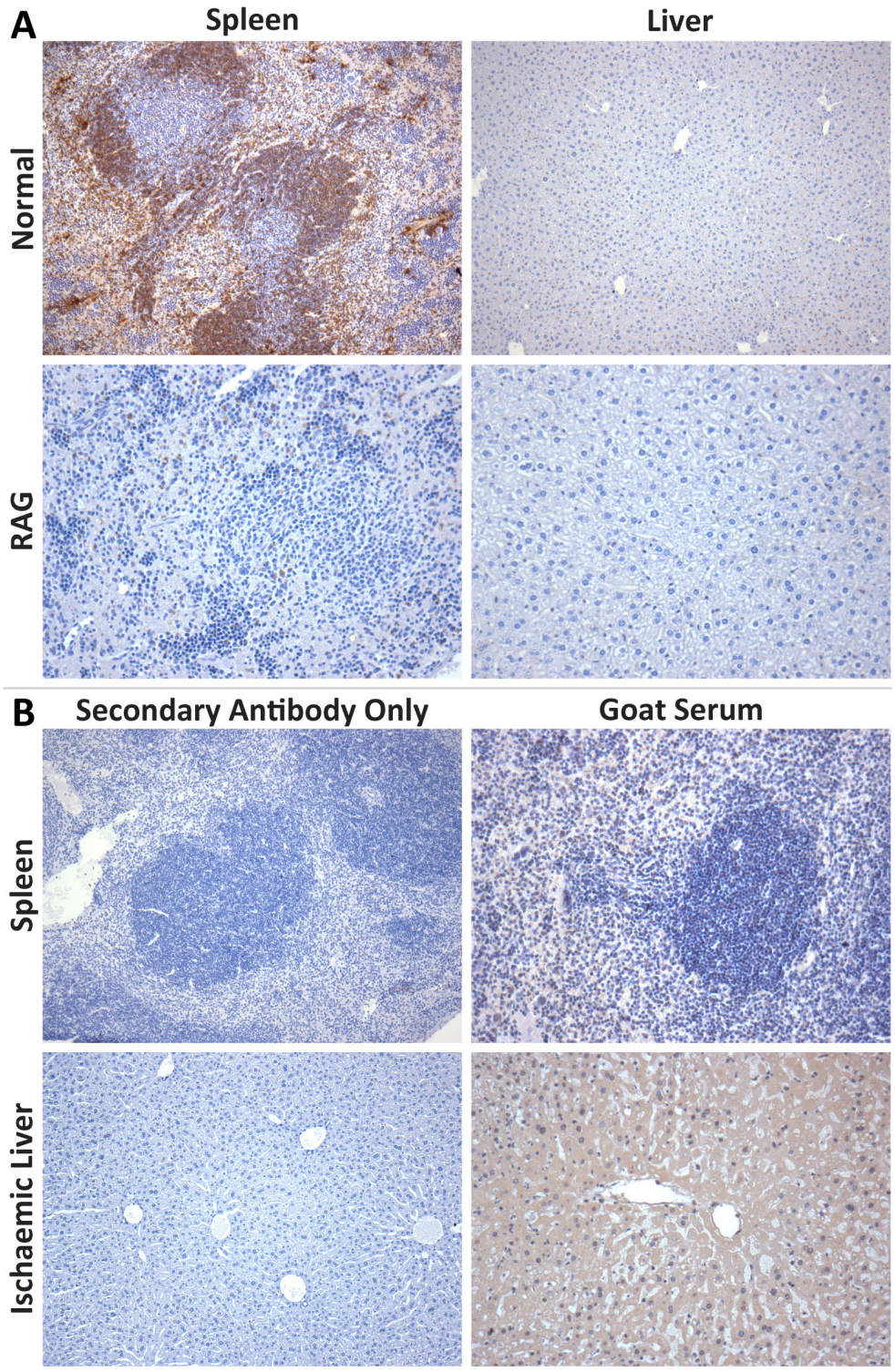

Figure 3.11 – Specific IgM staining evident in paraffin embed liver tissue following IHC based detection. A) Trials of unconjugated IHC anti-IgM antibody yielded positive staining in normal spleen tissue, whilst normal liver and RAG spleen and liver tissue remained IgM negative. **B**) Minimal staining was detected in spleen and ischaemic liver tissue following incubation with a biotinylated secondary antibody alone, or incubation with goat serum (as an isotype control) and subsequent anti-IgM staining. Magnification of all images: x100.

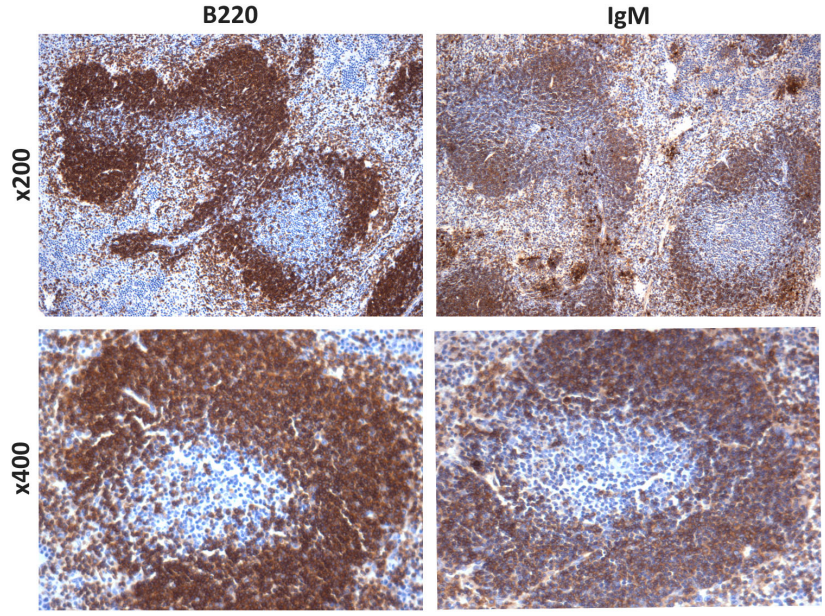

Figure 3.12 – IgM and B220 exhibit similar staining patterns in serial spleen sections. To confirm anti-IgM specificity serial paraffin embedded spleen tissue was stained for the B cell marker B220 or IgM. B220 staining was evident in what appeared to be germinal centers with IgM exhibiting a similar staining pattern in serial spleen sections.

observed at 1-hour and 24-hours post ischaemia (Figure 3.13A black arrows). No IgM deposition was observed in normal or ischaemic RAG-1 liver tissue. These results were confirmed following quantification of IgM deposition (expressed as IgM^+ staining area) which revealed that IgM accumulation reached a maximum at 24-hours with 31.3 ±5.5% IgM^+ staining (Figure 3.13B). Due to a small sample size for some time points the results were not statistically analysed (Non-injured, ischaemic RAG-1 and 0-hour to 24-hour (*n* = 2), 48-hours and 7-days (*n* = 6)).

3.12 IgM deposition following hepatic IRI mapped to areas of liver injury

Inspection of serial H&E and anti-IgM stained paraffin embedded liver sections harvested at various time points between 0-hour and 7-days following hepatic IRI revealed that IgM appeared to bind to areas of injured liver tissue. As indicated by grey arrows in figure 3.14 IgM deposition occurred where injury was observed and this was particularly evident at 24-hours post hepatic IRI.

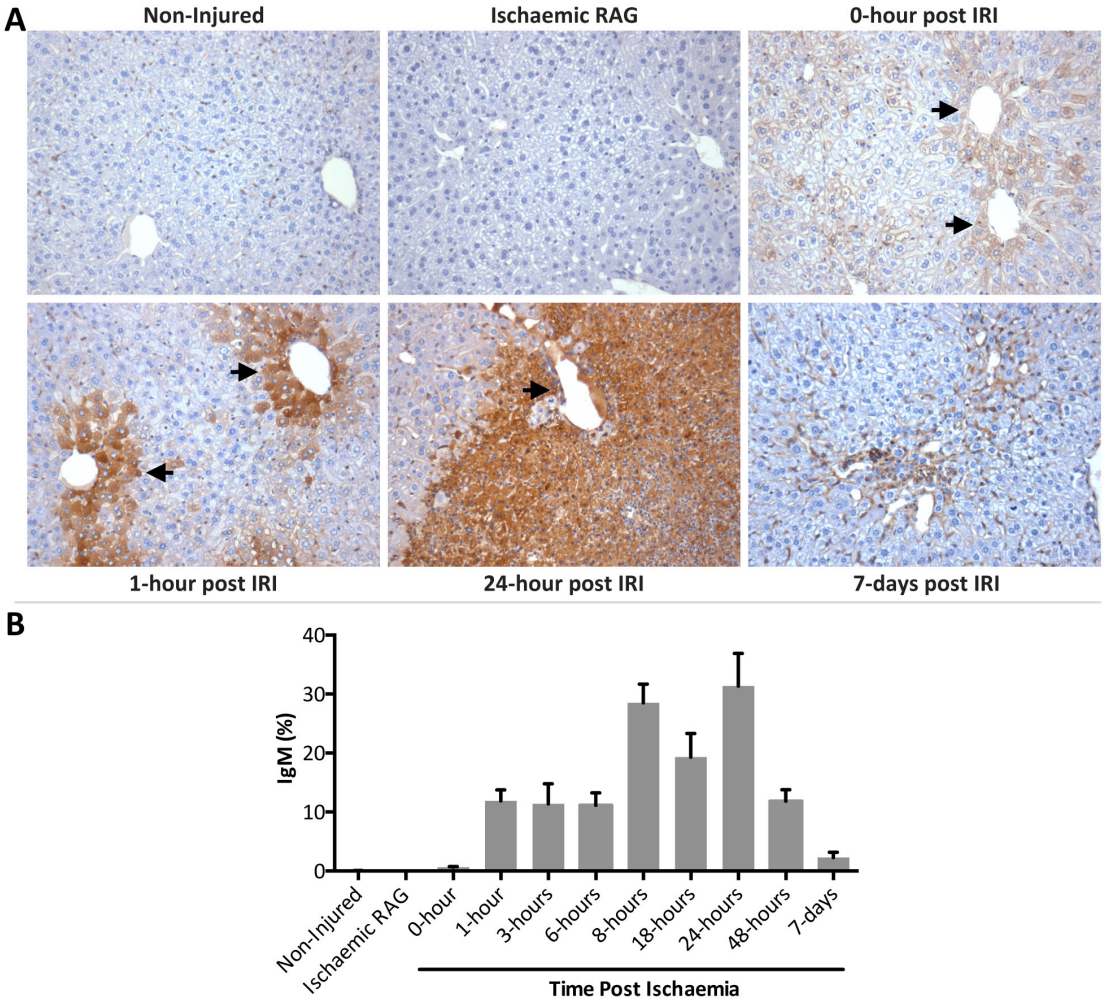

Figure 3.13 – IgM deposition accumulated over a period of 24-hours following hepatic IRI and was visibly declined by 7-days. To assess IgM deposition following hepatic ischaemic injury, male C57BL/6 or RAG mice underwent 50-minutes of liver ischaemia and were sacrificed at various time points between 0-hour and 7-days. **A**) Representative photomicrographs of anti-IgM stained paraffin embedded liver sections revealed that IgM deposition was absent in normal and ischaemic RAG liver tissue. IgM deposition was evident at 1-hour and accumulated until 24-hours following hepatic IRI, and was nearly absent at 7-days. IgM deposition appeared to originate from central veins (indicated by black arrows). **B**) Quantification of IgM deposition (expressed as IgM^+ area) confirmed that IgM was present at 0-hour following hepatic IRI, and accumulated to a maximum at 24-hours. By 7-days IgM deposition had declined. Data expressed as ±SEM. Non-injured, ischaemic RAG and 0-hour to 24-hour (n = 2), 48-hours and 7-days (n = 6). Magnification: x200.

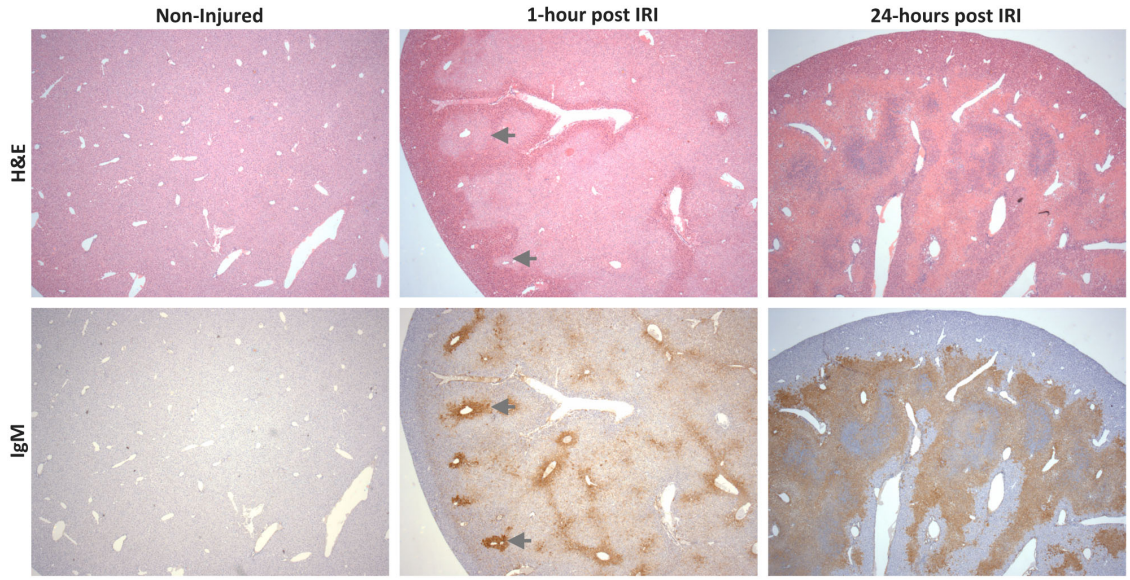

Figure 3.14 – IgM deposition following hepatic IRI mapped to areas of liver injury. To assess IgM deposition following hepatic ischaemic injury, male C57BL/6 mice underwent 50-minutes of ischaemia and were sacrificed at various time points between 0-hour and 7-days. Representative photomicrographs of serial H&E and anti-IgM antibody stained paraffin embedded liver sections demonstrated IgM deposition in areas of liver injury (indicated by grey arrows in 1-hour post IRI). Magnification: x25. Representative of all time points at which IgM deposition was detected.

3.13 IgM deposition mapped to areas of liver necrosis observed following ConA induced liver injury

We then explored whether IgM deposition occurred in a murine model of AIH. AIH is a chronic inflammatory condition characterised by progressive tissue necrosis, and loss of self tolerance with the development of autoantibodies (Mieli-Vergani and Vergani, 2011). AIH was induced in male C57BL/6 mice by an intravenous injection of 10 mg/kg ConA and 24-hours later mice were sacrificed. James Richards performed the ConA model and provided tissue used to assess IgM deposition. Assessment of paraffin embedded anti-IgM stained ConA treated liver tissue demonstrated distinct IgM staining, which as observed in hepatic IRI, also appeared to map to areas of tissue necrosis evident in H&E stained serial liver sections (Figure 3.15A). Quantification of IgM staining (expressed as IgM^+ staining area) revealed that liver tissue harvested from ConA treated C57BL/6 mice was 13.5±1.8% IgM^+, whilst IgM deposition in RAG-1 and non-injured liver tissue remained minimal (Figure 3.15B). Due to a small sample size

for some time points the results were not statistically analysed (Non-injured, RAG (*n* = 2), ConA (*n* = 6)).

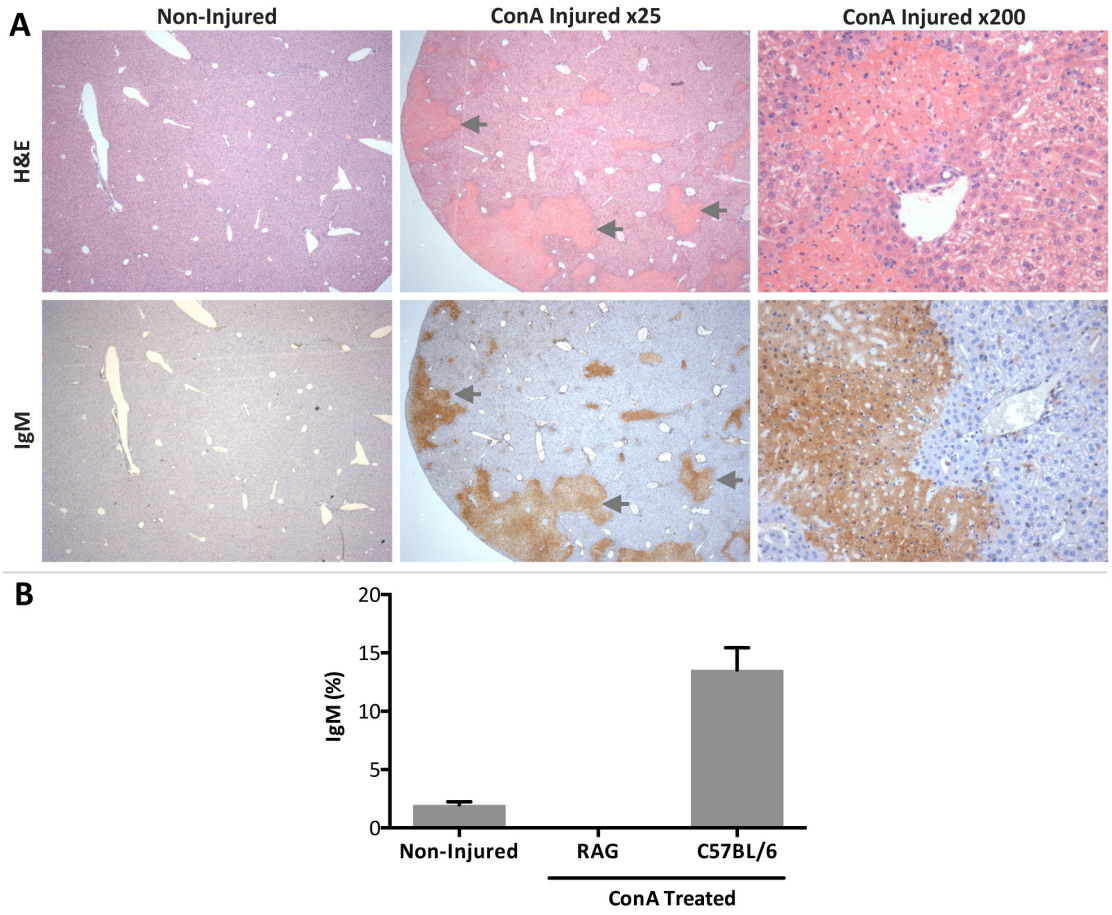

Figure 3.15 – IgM deposition that mapped to areas of liver necrosis observed following ConA induced liver injury. IgM deposition was assessed in male C57BL/6 mice following ConA induced liver injury. **A**) Representative photomicrographs of serial paraffin embedded liver sections stained with either H&E or anti-IgM antibody revealed that IgM deposition occurred in areas of liver necrosis (indicated by grey arrows). **B**) Quantification of IgM deposition (expressed as IgM^+ area) confirmed that IgM was present in ConA injured livers. Data expressed as ±SEM. Non-injured, RAG (*n* = 2), ConA (*n* = 6). Magnification: x25.

3.14 IgM positivity in ConA injured liver tissue is not due to B cell infiltration

To ensure that IgM positivity in ConA injured liver tissue was not due to detection of membrane bound IgM on infiltrating B cells, as occurs in AIH patients, serial paraffin embedded ConA injured liver tissue was stained for IgM or the B cell marker B220 (Vergani and Mieli-Vergani, 2003). IgM and B220 illustrated disparate staining patterns

(Figure 3.16A) with quantification of B220 staining (expressed as $B220^+$ area) confirming that B cell infiltration was not present in ConA injured livers (Figure 3.16B). Due to a small sample size for some time points the results were not statistically analysed (Non-injured, RAG (*n* = 2), ConA (*n* = 6)).

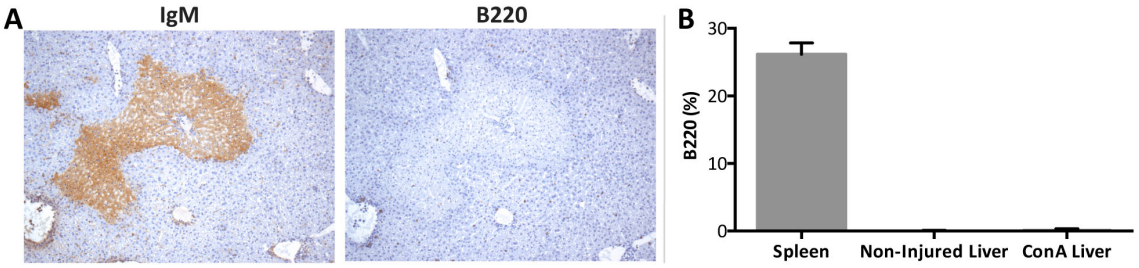

Figure 3.16 – IgM positivity in ConA injured liver tissue is not due to B cell infiltration. To assess whether IgM positivity in ConA injured liver tissue was due to detection of membrane bound IgM on infiltrating B cells serial ConA injured liver tissue was stained for IgM or the B cell marker B220. **A**) Representative photomicrographs of serial paraffin embedded liver sections stained with either anti-B220 or anti-IgM antibody reveal that IgM and B220 illustrated disparate staining patterns. **B**) Quantification of B220 staining (expressed as $B220^+$ area) confirmed that B cells infiltration was not present in ConA injured livers. Spleen tissue was used as a positive control. Data expressed as ±SEM. Non-injured, spleen (*n* = 2), ConA (*n* = 6). Magnification: x100.

Summary

In this chapter we carefully characterised the kinetics of IgM deposition following renal and hepatic ischaemic injury. We discovered striking differences. Whilst IgM deposition was minimal following renal ischaemia, IgM rapidly accumulated over the course of 24-hours post hepatic ischaemia with deposition evident in areas of tissue injury. In additional, similar results were observed in a murine model of AIH with IgM antibodies appearing to strongly bind areas of tissue necrosis.

Despite published work in other organs and dramatic deposition following hepatic IRI, minimal IgM deposition was observed following renal IRI despite the presence of significant ATN. Furthermore, IgM antibodies did not bind injured human renal tubular epithelial cells *in vitro*. The mechanisms underlying the differential nature of IgM

binding to injured liver and kidney *in vivo* are unclear. IgM antibodies are unlikely to play a crucial direct role in renal ischaemia; however, it is clear from this data that IgM might play an important role in the pathogenesis of hepatic injury. In addition, our hypothesis that apoptotic cell-derived protection from renal IRI is due to reduced levels of intravascular self-reactive IgM is unlikely (Section 1.9).

Chapter 4. Apoptotic cell administration to mice is either neutral or detrimental to renal function following renal ischaemia reperfusion injury

Introduction

Renal IRI is an acute inflammatory process and a common cause of AKI in patients. The administration of apoptotic cells has been shown to reduce inflammation in various models including experimental arthritis, bleomycin lung injury, acute hepatitis and LPS-mediated shock (reviewed in Table 1.2). Ischaemic injury also results in activation of the coagulation cascade leading to microvascular congestion (Jennewein et al., 2011) – a process that apoptotic cells may be able to modulate as PtdSer exposures allows interaction with the coagulation cascade (Casciola-Rosen et al., 1996). In view of these previous studies apoptotic cell administration may represent a novel pretreatment for AKI secondary to renal IRI and act to limit the resultant inflammation and modulate microvascular congestion.

Previous work in our lab suggested that intravenous administration of $20x10^6$ apoptotic cells to FVB/n or Balb/c mice 24-hours prior to inducing renal IRI ameliorated renal function without affecting the ATN score 24-hours following IRI. In the work described in this chapter we sought to validate these preliminary findings and explore if modulation of coagulation status leading to improved intrarenal microvascular flow might represent the underlying mechanism eliciting functional protection. We were also interested in further exploring how apoptotic cells may be able to influence and alter coagulation status.

Please note that in this chapter the term apoptotic cells refers specifically to murine apoptotic thymocytes only.

Results

4.1 Establishment and optimisation of an assay to detect platelet binding to apoptotic cells

Platelets can greatly influence thrombogenicity as stimulated platelets are major sites of thrombin generation, and are actively recruited to developing thrombus (Monroe et al., 2002). As PtdSer exposure on apoptotic cells confers pro-coagulant tendencies (Pickering et al., 2008), we hypothesized that apoptotic cells may be able to directly bind platelets. To confirm this we established and optimized an *in vitro* assay designed to detect platelet-apoptotic cell binding. Firstly methods of blood collection were assessed to determine which would yield the best source of platelets. Total blood was collected from male 8-week old Balb/c mice into 0.38% sodium citrate (a common anticoagulant used in platelet studies) and either used immediately as whole blood or used to generate platelet rich plasma. Samples were analysed by flow cytometry FSC SSC dot plots. FSC SSC dot plots of peripheral blood allow easy identification of blood cell types as each lie in very distinct disparate regions. Platelet rich plasma resulted in a poor peripheral blood FSC SSC dot plot, with limited events occurring in the region defined as platelets, however analysis of 1 µL whole blood produced an improved number of events (Figure 4.1A). The volume of whole blood used was increased to 5 µL, which yielded a very typical FSC SSC dot plot with many events designated as platelets (Figure 4.1A). Staining for the platelet surface integrin marker CD41 confirmed that this population was indeed platelets, as approximately 96% events were $CD41^+$ (Figure 4.1B). An anti-CD41 titration was performed and a dilution of 1:200 was selected, on the basis of median fluorescent intensity (MFI) of $CD41^+$ events, for future experiments (Figure 4.1C). Apoptotic cells were stained with the cell tracker CM orange to enable identification during the assay and a concentration titration was performed (Figure 4.1D). Following this 1 µL/mL CM orange was selected, on the basis of MFI of CM $orange^+$ events, for future experiments.

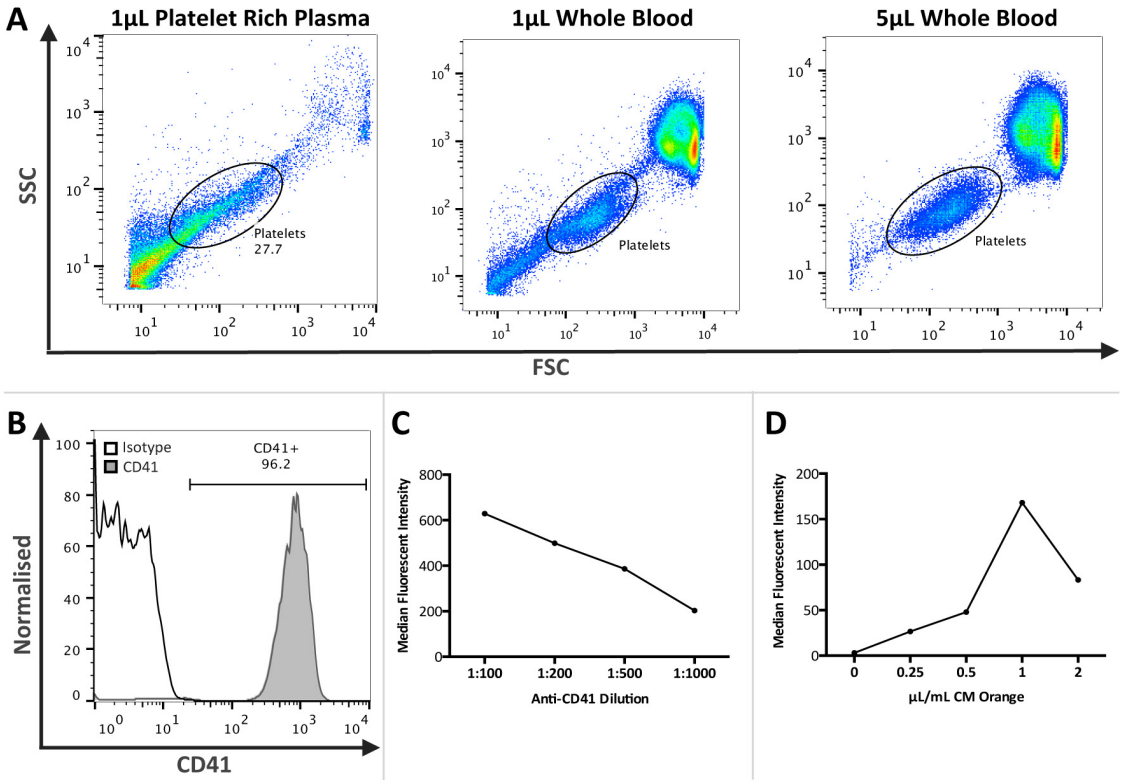

Figure 4.1 – Establishing and optimising an assay to detect murine platelet binding to apoptotic cells. A) Citrated platelet rich plasma and 1µL of whole blood as a source of platelets resulted in a suboptimal peripheral blood FSC SSC dot plot as assessed by flow cytometry. A typical peripheral blood FSC SSC dot plot with a region generally identified as platelets was evident in 5µL of whole blood. **B**) To confirm that the cells within the region designated platelets on FSC SSC dot plots were indeed platelets whole blood was stained with the platelet surface integrin marker CD41. Approximately 96% of events in this region were $CD41^+$. An isotype control antibody confirmed anti-CD41 specificity. **C**) An anti-CD41 titration was performed to determine the correct antibody dilution for IgM detection. Median fluorescent intensity was determined on cells gated for CD41 positivity. **D**) A dilution series was performed for cell tracker CM orange to determine the correct dilution necessary to stain apoptotic cells. Median fluorescent intensity was determined on cells gated for CM orange positivity. Representative of several experiments.

4.2 Apoptotic cells bind to $CD41^+$ platelets

With an assay optimised and established the ability of apoptotic cells to bind to platelets in murine whole blood was determined. Platelets in 5 µL of whole blood were stained with anti-CD41 antibody prior to 30-minute incubation with $5x10^5$ apoptotic cells labeled with the fluorescent cell tracker CM orange. Analysis was performed by flow cytometry (Figure 4.2A). CM $orange^+$ apoptotic cells (Figure 4.2B) and $CD41^+$ platelets (Figure 4.2C) were identified and staining confirmed. Analysis of apoptotic

cells and platelet interaction confirmed apoptotic cell-platelet binding as indicated by the presence of CM Orange^{+} apoptotic cells that were also CD41^{+} (Figure 4.2D).

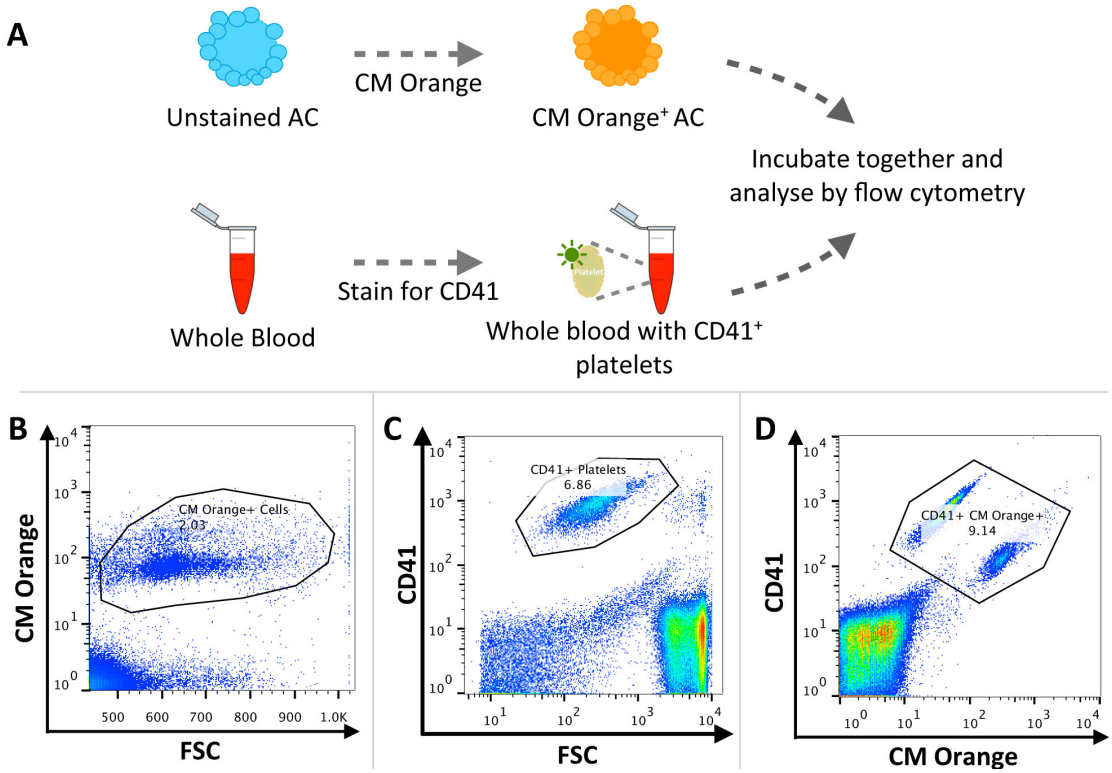

Figure 4.2 – Apoptotic cells bind to CD41^{+} platelets. **A**) Overview of AC-platelet interaction assay. Platelets in whole blood were stained for the platelet surface integrin marker CD41 prior to incubation with apoptotic cells (ACs) labeled with fluorescent cell tracker CM orange. Analysis was performed by flow cytometry. **B**) Confirmation CM Orange staining of ACs. **C**) Confirmation of the presence of CD41^{+} platelets. **D**) AC-platelet binding is indicated by the presence of CM Orange^{+} ACs that were also CD41^{+}. The two populations evident represent differences in platelet-ACs cell size, which was assessed on FSC SSC dot plots. Representative of two experiments.

4.3 Establishment of a technique to count platelets in murine blood

Following the confirmation that apoptotic cells bind platelets we sought to establish a technique that would enable us to quickly perform platelet counts in small volumes of murine blood by flow cytometry. If apoptotic cell derived functional protection from renal IRI was recapitulated we planned to use this technique to determine whether platelets counts were indeed reduced in apoptotic cell treated mice as per our hypothesis (Chapter 1: Introduction Section 1.9). We predicted that apoptotic cells administered prior to renal IRI might bind platelets and transiently reduce counts, therefore limiting platelet deposition post ischaemia such that microvascular

congestion might be attenuated. To determine platelet counts CountBright Absolute Counting Beads (Molecular Probes, Invitrogen), which are broadly fluorescent and detectable by several flow cytometry channels, were added to 5 µL whole blood (stained with anti-CD41) or PBS (negative control). Platelets were identified by FSC SSC dot plots as detailed in figure 4.1A and CD41 positivity confirmed these events to be platelets (Figure 4.3A). Beads were identified by FL3 positivity (Figure 4.3B). According to the reference bead events and manufacturer's instructions platelet counts were determined in murine blood. Due to the inherent variation in platelet counts between mice, replicate values of the same mouse were counted which illustrate minimal variation (Figure 4.3C).

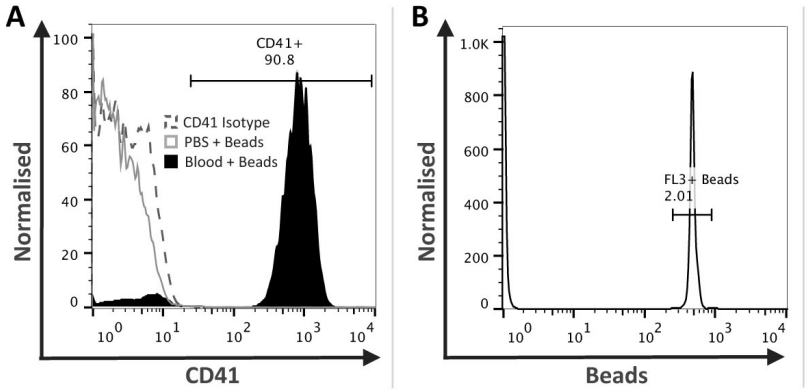

Sample	Platelets µL^{-1}
PBS	405
Whole Blood	490869
Whole Blood	472164
Whole Blood	419908

Figure 4.3 – Establishing a technique to count platelets in murine blood in order to assess whether counts were reduced following apoptotic cell administration. A) Counting beads were added to PBS and whole blood samples. Platelets were identified by FSC SSC dot plots as shown in figure 4.1A and assessment of CD41 positivity confirmed these events were platelets. PBS and beads was used as a negative control. **B**) Beads were identified by FL3 positivity. **C**) Replicate platelet counts (µL^{-1}) in a sample of murine whole blood and PBS.

4.4 Apoptotic cell administration to mice modulates thrombin generation

The inherent coagulability of plasma from mice treated with apoptotic cells was examined to investigate whether coagulation was modified such that microvascular congestion may be reduced following ischaemia. Thrombin is a key procoagulant enzyme that, in addition to activating platelets, catalyzes the formation of fibrin (Monroe et al., 2002). To investigate this a thrombin generation assay (TGA) was performed on citrated platelet-poor-plasma obtained 24-hours after Balb/c mice received PBS (*n* = 6) or 20x10^6 early apoptotic cells (*n* = 6) (approximately 51%

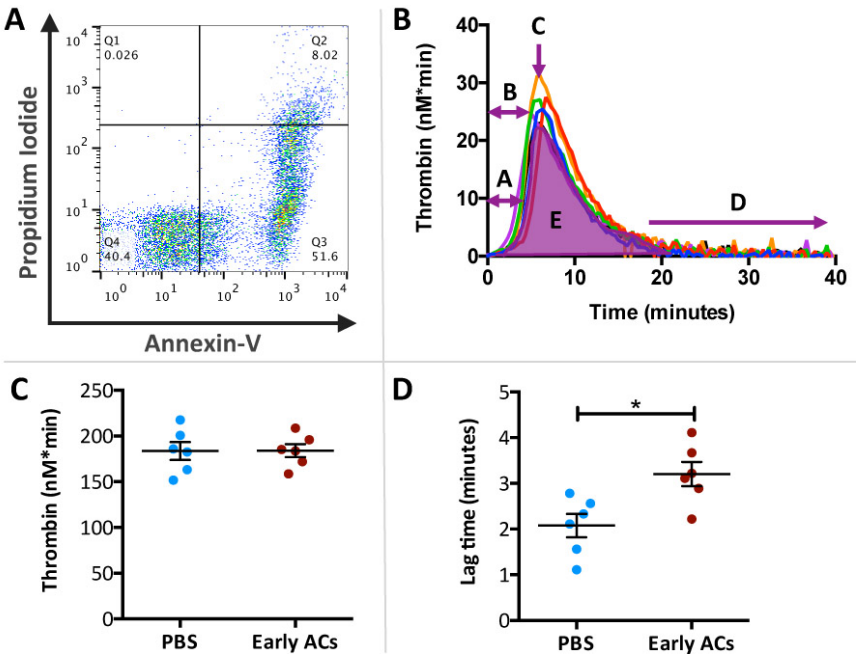

Figure 4.4 – Apoptotic cell (AC) administration to mice modulates thrombin generation. A thrombin generation assay (TGA) was performed on citrated platelet-poor-plasma obtained 24-hours after Balb/c mice received 20x10^6 early ACs or PBS. Cell viability was assessed by AnnV and PI staining and flow cytometry. **A**) Early apoptotic cells were approximately 51% Annexin-V$^+$ PI$^-$. **B**) TGA readouts: A = Lag time; B = Peak Time; C = Peak; D = Tail; E = endogenous thrombin potential. **C**) Endogenous thrombin potential remained similar in both PBS and AC treated mice. **D**) AC treated mice exhibit significantly delayed thrombin generation. Data expressed as mean ±SEM and analysed by student's *t*-test. * = P ≤ 0.05. P PBS (*n* = 6), apoptotic cell (*n* = 6).

AnnV$^+$PI$^+$; Figure 4.4A). The TGA was performed by Dr Roger Preston (Department of Clinical Medicine, Trinity College Dublin). In a TGA a fluorogenic substrate is used to measure thrombin generation; this is performed in parallel to a sample with a known thrombin activity. The results of this assay are presented as a thrombogram (Figure 4.4B). In this figure A illustrates the lag time, also known as clotting time, which represents the time until thrombin is first generated, the peak time indicated by the letter B is the time taken until maximum thrombin generated. C represents the peak, which is the maximum amount of thrombin generated during the assay, which tails off as shown by D. The area under the curve, labeled E, represents the endogenous thrombin potential that is the total amount of thrombin generated during the assay. The TGA revealed that although early apoptotic cell-treated mice produced a similar amount of thrombin as control mice (Figure 4.4C) its generation was delayed, as indicated by a significantly elevated lag time (Student's *t*-test; $P < 0.05$) (Figure 4.4D).

4.5 Overview of in vivo renal IRI experiments

The remaining results presented in this chapter were obtained from *in vivo* experiments that centered on the renal IRI murine model summarized in figure 4.5.

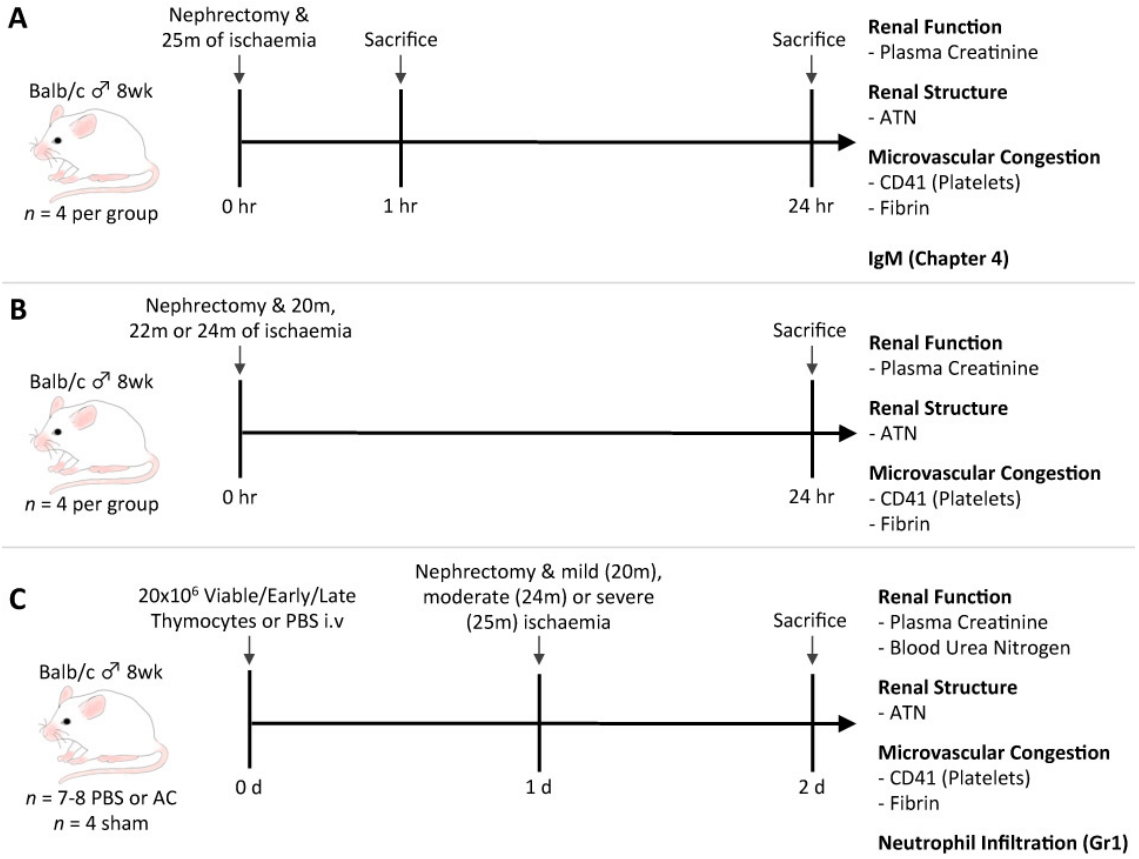

Figure 4.5 – Overview of *in vivo* experiments. A) Investigation of baseline injury and microvascular congestion 1-hour and 24-hours post renal IRI. Male Balb/c mice aged 8 weeks underwent a right nephrectomy and the left renal pedicle was clamped for 25-minutes. Following renal IRI mice were sacrificed at either 1-hour (*n* = 4) or 24-hours (*n* = 4). Renal function and structure was assessed by plasma creatinine and acute tubular necrosis (ATN), respectively. Microvascular congestion inferred from CD41 (platelet) and fibrin deposition was assessed via IHC. IgM deposition was also assessed but is presented in chapter 4. **B) Renal injury titration**. To assess the length of ischaemia required to induce varying degrees of renal injury, male Balb/c mice aged 8 weeks underwent a right nephrectomy and the left renal pedicle was clamped for 20, 22 or 24-minutes (*n* = 4 per group). Following renal IRI mice were sacrificed 24-hours later and renal function, structure and microvascular congestion was assessed. **C) Investigation into the influence of apoptotic cells on renal injury.** Male Balb/c mice received an intravenous injection of either PBS (*n* = 7-8) or $20x10^6$ early or late apoptotic thymocytes (*n* = 8), or $20x10^6$ viable thymocytes (*n* = 5) 24-hours prior to renal IRI. Shams underwent a laparotomy (*n* = 4). Mice were sacrificed 24-hours post IRI and renal function, structure and microvascular congestion was assessed, along with neutrophil infiltration inferred by Gr1 IHC.

4.6 Twenty-five minutes of ischaemia resulted in significant renal dysfunction with ATN and fibrin and platelet deposition observed 1-hour following ischaemic injury

In preparation for experiments investigating the protective potential of apoptotic cells in renal IRI we aimed to characterise and obtain baseline values of injury and microvascular congestion 24-hours following ischaemic injury. We also examined the time point of 1-hour post renal IRI with the view that future experiments may be performed to try and further explore how apoptotic cells influence injury and microvascular congestion at early time points. Male 8-week Balb/c mice underwent a right nephrectomy and 25-minutes of ischaemia and were sacrificed at 1-hour (n = 4) or 24-hours (n = 4) following surgery (Figure 4.5A). An ischaemic time of 25-minutes was selected as this was known to induce significant injury and was the standard duration used in the lab.

Mice sacrificed at 1-hour (n = 4) had a normal plasma creatinine, those sacrificed at 24-hours (n = 4) had a significantly elevated plasma creatinine indicating renal dysfunction (Student's t-test, P <0.05) (Figure 4.6A). Widespread loss of healthy cells within the OSOM occurred at both time points resulting in significant ATN for mice sacrificed at both 1 and 24-hours (one-way ANOVA, P <0.01 and P <0.001, respectively) (Figure 4.6B).

As fibrin and platelets accumulate in the microvasculature following renal IRI their deposition was measured by IF and IHC, respectively, to evaluate whether these readouts could be used to infer microvascular congestion. Whilst non-injured kidneys remained negative, fibrin staining was observed in the microvasculature of ischaemic kidneys (Figure 4.7). Quantification of fibrin positive staining illustrated that significant fibrin deposition occurred 1-hour following renal IRI and was significantly reduced by 24-hours (one-way ANOVA, P <0.05) (Figure 4.7). IHC staining for CD41 demonstrated that microvascular platelet deposition remained significantly elevated at 1-hour and 24-hours following renal IRI (one-way ANOVA, P <0.05) (Figure 4.8). These data confirm that fibrin and platelet deposition could be used as parameters to infer microvascular congestion.

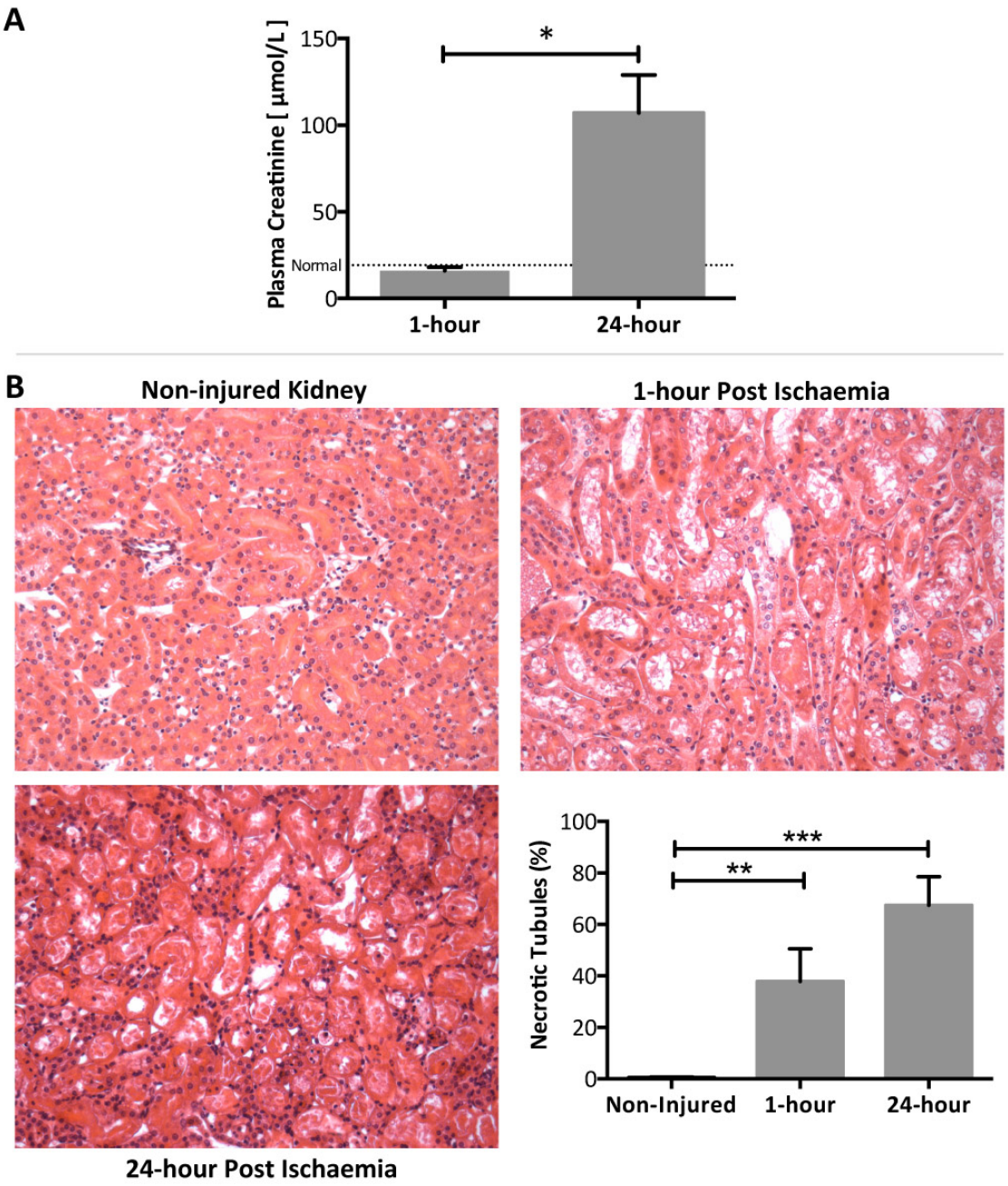

Figure 4.6 - Twenty-five minutes of ischaemia resulted in significant renal failure and ATN. To obtain baseline values of renal injury, fibrin and platelet deposition following renal IRI 8-week old male Balb/c mice underwent a right nephrectomy and 25-minutes of ischaemia. Mice were sacrificed either 1-hour (n = 4) or 24-hours (n = 4) following renal IRI. **A**) Mice sacrificed 24-hours after renal IRI had significantly impaired renal function, indicated by elevated plasma creatinine, in comparison to those sacrificed at 1-hour. The dotted line represents normal plasma creatinine levels in healthy male Balb/c mice aged 8-weeks. **B**) Scoring of ATN (expressed as the percentage of necrotic tubules in the OSOM) demonstrated that mice sacrificed 1-hour and 24-hour post IRI had significant ATN in comparison to non-injured kidneys. Magnification: x200. Data expressed as mean ±SEM and analysed by student t-test or one-way ANOVA. * = $P \leq 0.05$, ** = $P \leq 0.01$ and *** = $P \leq 0.001$

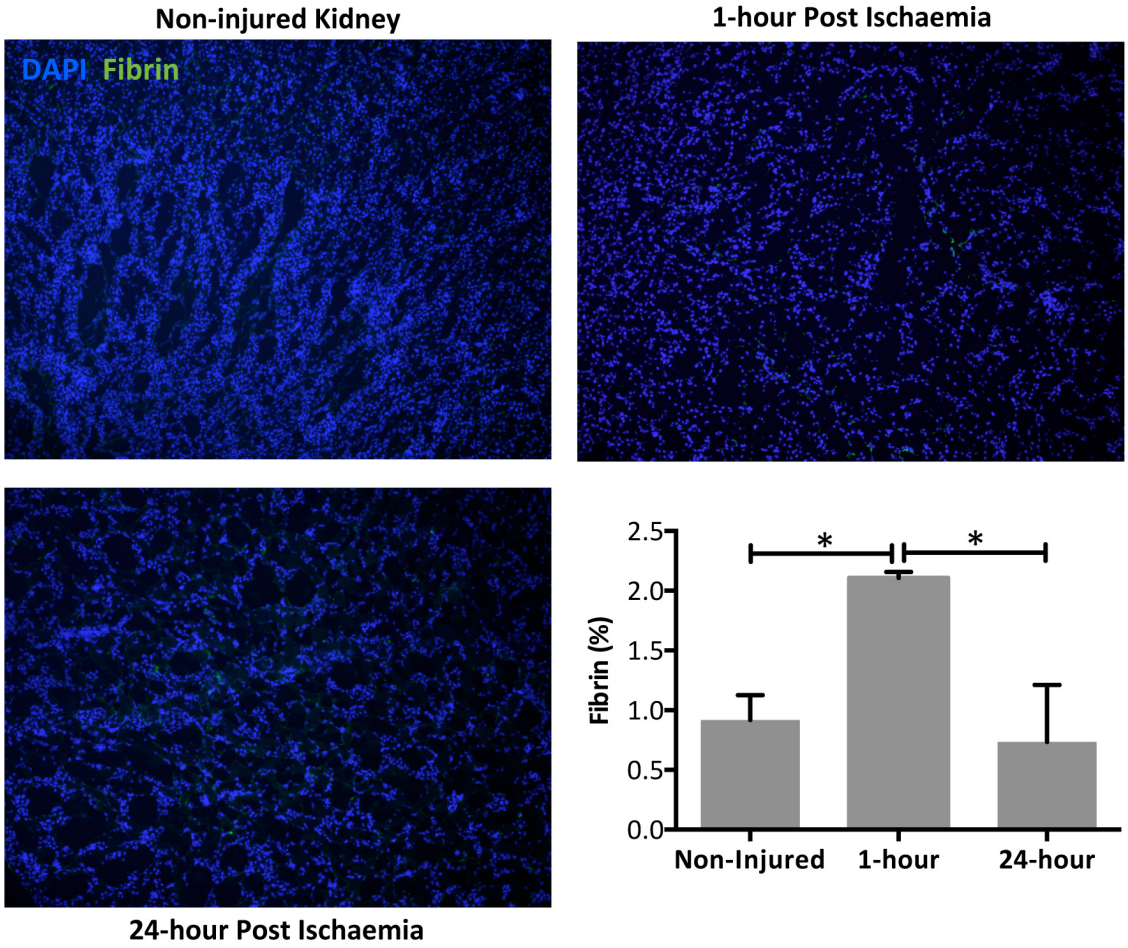

Figure 4.7 - Significant fibrin deposition occurs 1-hour following renal IRI. To obtain baseline values of renal injury, fibrin and platelet deposition following renal IRI 8-week old male Balb/c mice underwent a right nephrectomy and 25-minutes of ischaemia. Mice were sacrificed either 1-hour (n = 4) or 24-hours (n = 4) following renal IRI. Representative photomicrographs of the OSOM in non-injured and ischaemic kidney sections following fibrin IF staining reveals peritubular fibrin deposition. Quantification by compute image analysis of fibrin staining (expressed as fibrin^{+} area) demonstrates that deposition occurs 1-hour following renal IRI with a significantly less deposition at 24-hours. Magnification: x200. Data expressed as mean ±SEM and analysed by one-way ANOVA. * = $P \leq 0.05$

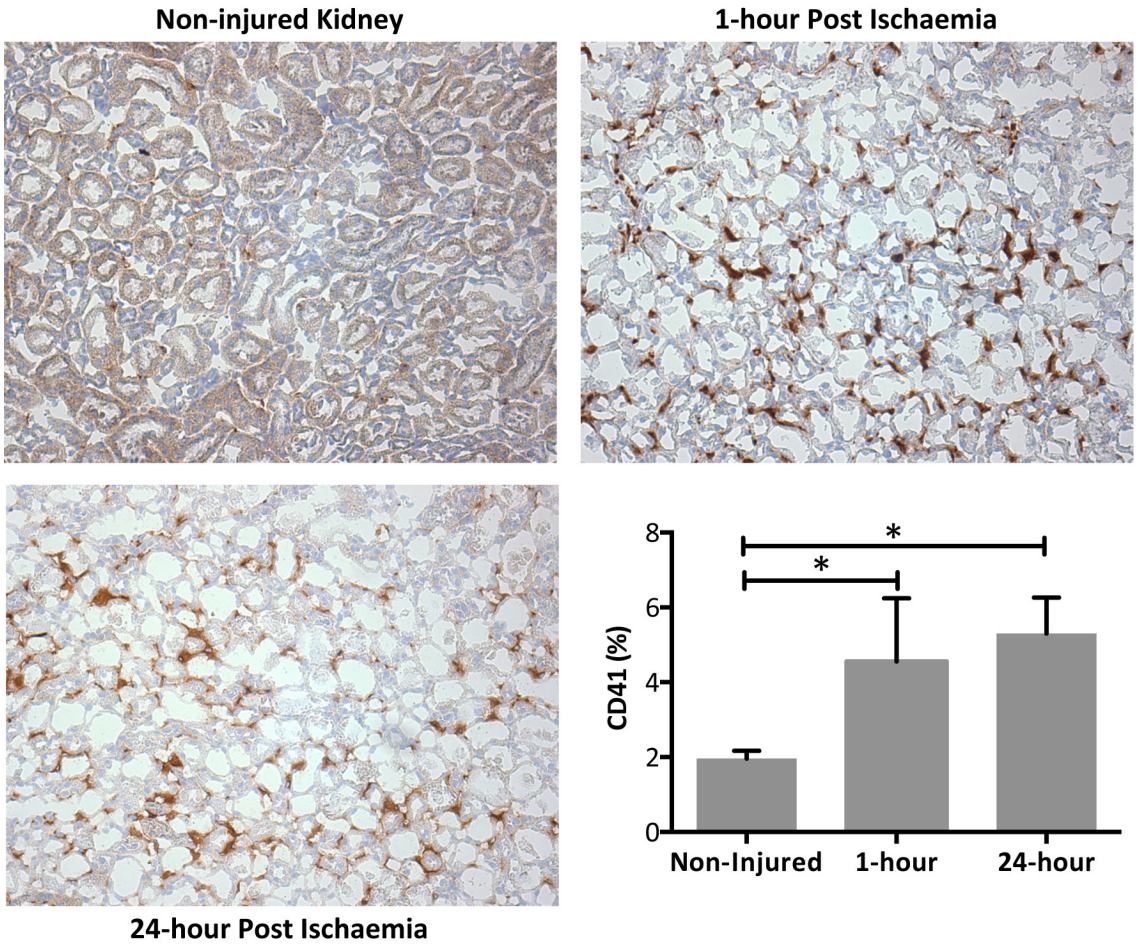

Figure 4.8 - Significant platelet deposition was observed 1-hour and 24-hours following renal IRI. To obtain baseline values of renal injury, fibrin and platelet deposition following renal IRI 8-week old male Balb/c mice underwent a right nephrectomy and 25-minutes of ischaemia. Mice were sacrificed either 1-hour (n = 4) or 24-hours (n = 4) following renal IRI. Representative photomicrographs of the OSOM in non-injured and ischaemic kidney sections following platelet (CD41) IHC staining reveal microvascular platelet deposition. Quantification by compute image analysis platelet staining (expressed as platelet^{+} area) demonstrates that significant platelet deposition is observed at both 1 and 24-hours post renal IRI. Magnification: x200. Data expressed as mean ±SEM and analysed by one-way ANOVA. * = $P \leq 0.05$

4.7 Renal dysfunction, injury and platelet deposition increased with prolonged ischaemia

With baseline values obtained, a titration of ischaemia was performed to assess the duration of ischaemia necessary to induce various degrees of renal injury in the hands of a new operator. Male 8-week old Balb/c mice underwent a right nephrectomy and 20, 22, or 24-mintues of ischaemia (*n* = 4 per group) and were sacrificed 24-hours later (Figure 4.5B). A progressive increase in the severity of renal dysfunction, assessed by plasma creatinine, was evident as the duration of ischaemia increased by 2-minute increments (Figure 4.9A). The ATN score (Figure 4.9B) follows a similar trend with more severe ATN accompanying more prolonged ischaemia (Figure 4.9C).

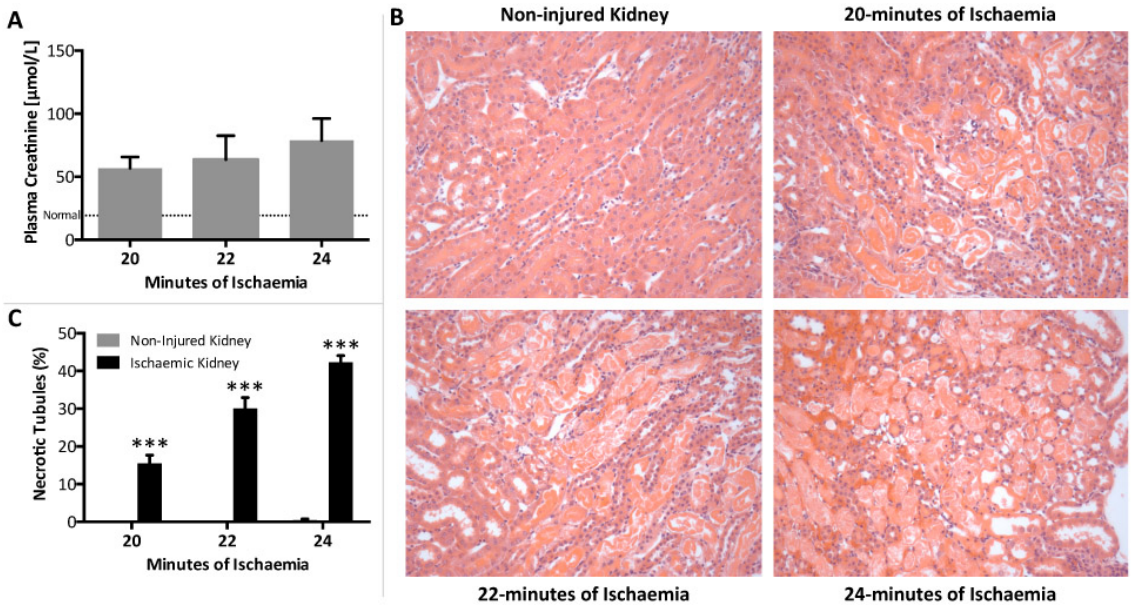

Figure 4.9 – Increased renal dysfunction and injury with increasing duration of ischaemia. To assess the duration of ischaemia required to induce varying degrees of renal injury 8-week old male Balb/c mice underwent a right nephrectomy and 20, 22 or 24-minutes of ischaemia (*n* = 4 per group). Mice were sacrificed 24-hours following renal IRI. **A**) Plasma creatinine shows an increasing trend of elevation, indicating increasing kidney dysfunction, as the length of ischaemia increased. The dotted line represents normal renal function in healthy male Balb/c mice aged 8-weeks. **B**) Representative photomicrographs (Magnification: x200) of the OSOM from H&E stained kidney sections of non-injured and ischaemic kidneys illustrate ATN. **C**) Formal scoring of ATN (expressed as the proportion of necrotic tubules) confirms the increased level of injury with increasing duration of ischaemia. Data expressed as mean ±SEM and analysed by one-way or two-way ANOVA. *** = $P \leq 0.001$

Fibrin and platelet deposition was determined to confirm that microvascular congestion occurred with all ischaemic periods. Although fibrin deposition occurred with all ischaemic durations (Figure 4.10A), quantification demonstrated that deposition varied as the length of ischaemia increased (Figure 4.10B). In contrast, platelet deposition (Figure 4.11A) followed an increasing trend with prolonged ischaemia (Figure 4.11B).

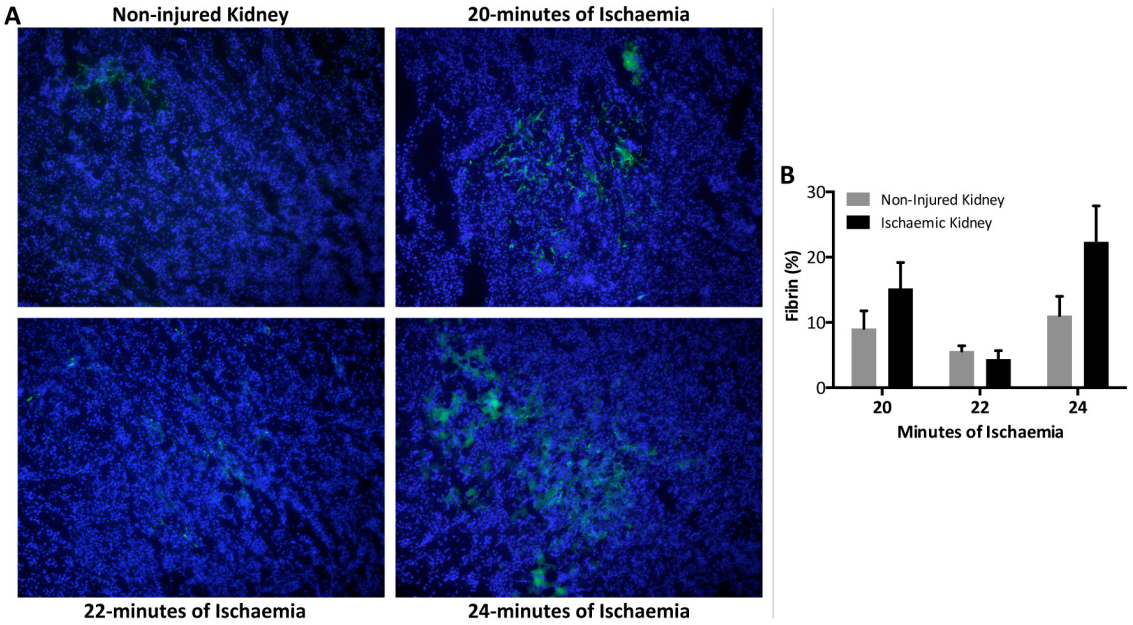

Figure 4.10 – Fibrin deposition was evident as the duration of ischaemia increased. To assess the lengths of ischaemia required to induce varying degrees of renal injury 8-week old male Balb/c mice underwent a right nephrectomy and 20, 22 or 24-minutes of ischaemia (*n* = 4 per group). Mice were sacrificed 24-hours following renal IRI. **A**) Representative photomicrographs (Magnification: x200) of the OSOM of kidney sections of non-injured and ischaemic kidneys illustrating fibrin deposition. **B**) Quantification of fibrin IF staining (expressed as fibrin^{+} area) demonstrates that deposition varied as the length of ischaemia increased. Data expressed as mean ±SEM and analysed by two-way ANOVA.

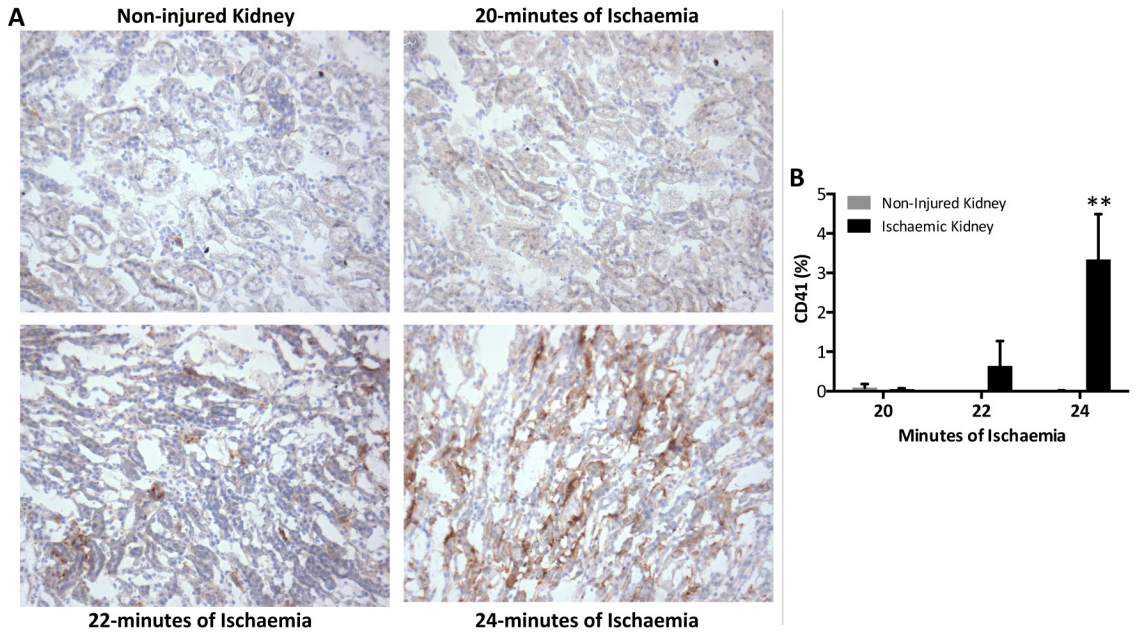

Figure 4.11 – Increased platelet deposition with increasing duration of ischaemia. To assess the duration of ischaemia required to induce varying degrees of renal injury 8-week old male Balb/c mice underwent a right nephrectomy and 20, 22 or 24-minutes of ischaemia (*n* = 4 per group). Mice were sacrificed 24-hours following renal IRI. **A**) Representative photomicrographs (Magnification: x200) of the OSOM of kidney sections of non-injured and ischaemic kidneys stained for CD41 to illustrate platelet deposition. **B**) Quantification of platelet IHC staining (expressed as platelet$^+$ area) demonstrates that deposition increased as the length of ischaemia increased. Data expressed as mean ±SEM and analysed by two-way ANOVA. ** = $P \leq 0.01$

4.8 Thymocytes used to generate apoptotic cells were either CD4$^+$, CD8α$^+$ or CD4$^+$CD8α$^+$

The phenotype of fresh thymocytes used to generate the apoptotic cells for use in *in vivo* experiments was examined by assessing the expression of CD3, CD4, CD8 (T cell markers), B220 (B cell marker) and CD11b (myeloid cell marker). The anti-CD3 antibody produced poor staining indicating that only approximately 61% of thymocytes were CD3$^+$ (Figure 4.12A). Despite this, minimal expression of B220 (Figure 4.12B) and CD11b (Figure 4.12C) confirmed that cell preparations consisted predominantly of thymocytes, 98% of which were either CD4$^+$, CD8α$^+$ or CD4$^+$CD8α$^+$ (Figure 4.12D).

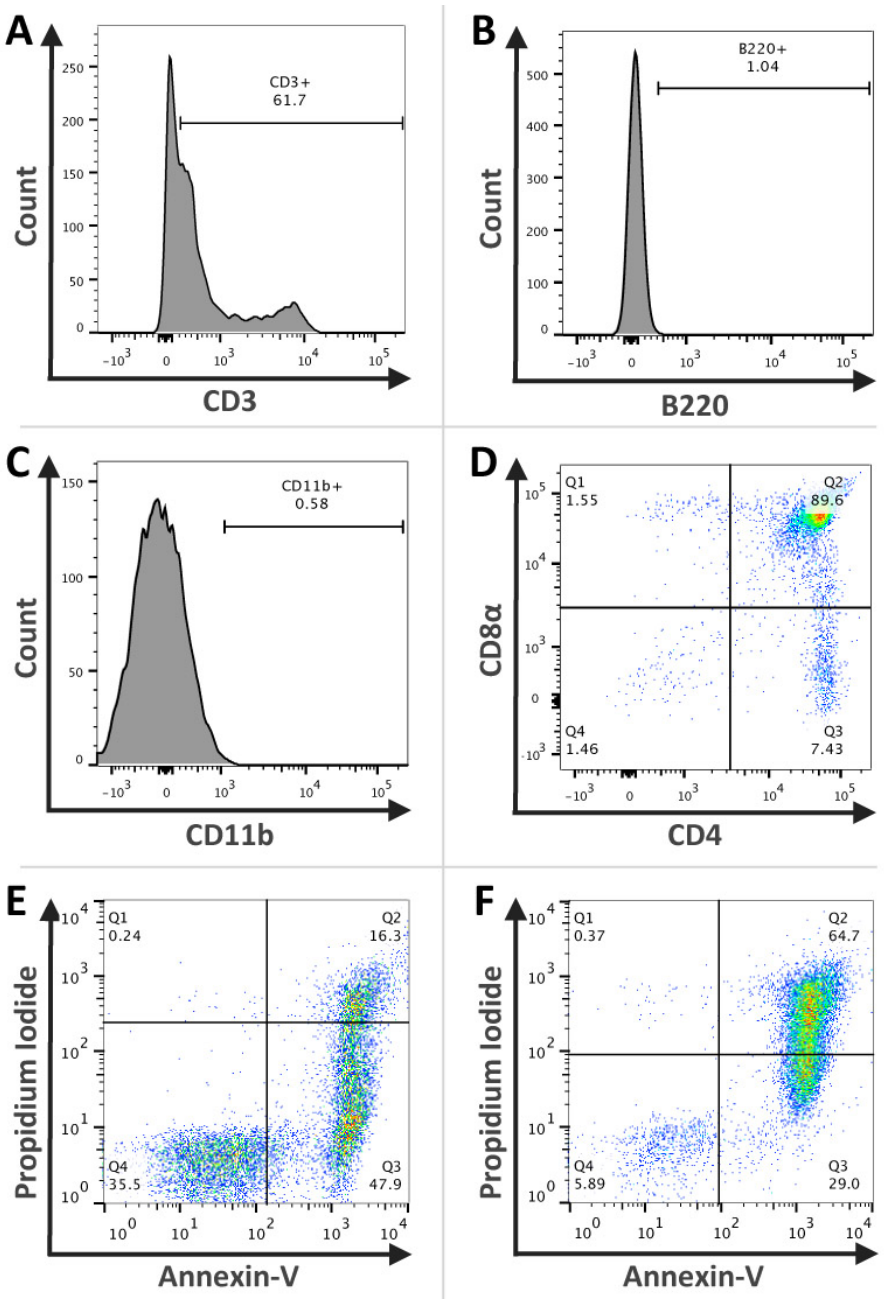

Figure 4.12 - Representative data illustrating the phenotype of thymocytes and classification of early and late apoptotic cells. Freshly isolated thymocytes were stained with CD3, CD11b, B220, CD4 and CD8α and analysed by flow cytometry to assess the phenotype of the cells used to generate apoptotic cells. Poor CD3 staining was observed with only 61.7% of total cell population being $CD3^+$ (**A**). Minimal staining for B220 (**B**) and CD11b (**C**) was found. Approximately 98% of cells gated to exclude debris are lymphocytes and either $CD4^+$, $CD8\alpha^+$ or $CD4^+CD8\alpha^+$ (**C**). Prior to administration of apoptotic cells to mice cell viability was assessed by Annexin-V and Propidium Iodide (PI) staining and flow cytometry. Overnight culture alone induced predominantly early apoptotic cells (47% Annexin-V^+ PI^-)(**E**) whilst the addition of 1μM dexamethasone elicited a population of late apoptotic cells (64.7% Annexin-V^+ PI^+)(**F**). Data representative of all apoptotic cell preparations.

4.9 Apoptotic cell administration prior to moderate and mild renal IRI impaired renal function

With data demonstrating apoptotic cells ability to modulate coagulation, the renal IRI model characterised and apoptotic cells phenotyped we were ready to assess the influence of apoptotic cell administration on renal ischaemic injury. To explore the effects of apoptotic cells upon renal IRI either PBS or 20×10^6 predominantly early apoptotic cells (Annexin-V^+ PI^-, Figure 4.12E) or predominantly late apoptotic cells (Annexin-V^+ PI^+, Figure 4.12F) were administered intravenously to mice 24-hours before renal IRI. Mice were then sacrificed 24-hours later (Figure 4.5C). In an initial experiment early apoptotic cells were administered prior to 25-minutes of ischaemia but no preservation of renal function was observed (Figure 4.13A). Note that this experiment was performed early during this thesis prior to the optimisation of this model; as such the lab standard 25-minutes of ischaemia was used. The resulting level of functional injury was unexpectedly high with markedly elevated levels of plasma creatinine and blood urea nitrogen and thus unlikely to be responsive to any therapeutic modulation. Further studies adopted a slightly reduced level of injury (classified according to plasma creatinine) induced by 24-minutes or 20-minutes of ischaemia. In light of work demonstrating that late apoptotic cells may exert anti-inflammatory effects (Miles et al., 2009) the influence of late apoptotic cells upon moderate kidney dysfunction was examined. In addition, the preliminary studies that demonstrated apoptotic cell derived protection from renal IRI appeared to use apoptotic cells at a more advanced stage of cell death. However, the administration of late apoptotic cells resulted in a significant increases in plasma creatinine and blood urea nitrogen indicative of a worsening of kidney function (Student's *t*-test, $P < 0.05$) (Figure 4.13B). This suggested that the administration of cells with significant PI positivity was detrimental and we therefore focused upon early apoptotic cells in a milder model of renal injury. Somewhat unexpectedly the administration of early apoptotic cells also resulted in a significant increase in plasma creatinine with no protection evident (Student's *t*-test, $P < 0.05$) (Figure 4.13C). On the basis of these data,

we did not examine the effects of early apoptotic cells in moderate injury or late apoptotic cells in mild injury.

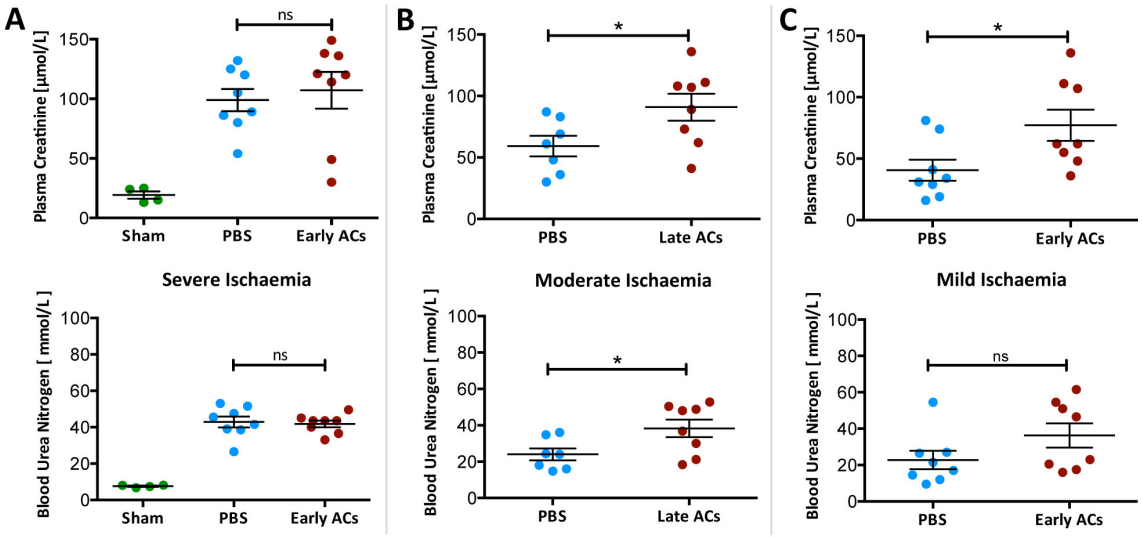

Figure 4.13 - Apoptotic cell (AC) administration prior to moderate and mild renal IRI impaired renal function. Renal IRI was induced in 8-week old male Balb/c mice by a right nephrectomy and ischaemia induced by occlusion of the left renal pedicle. Sham mice underwent a laparotomy only. Either PBS or $20x10^6$ early or late ACs were administered intravenously 24-hours prior to mild (20-minutes ischaemia), moderate (24-minutes) or severe (25-minutes) ischaemic injury. Mice were sacrificed 24-hours following IRI. **A**) Administration of early ACs did not preserve renal function from severe IRI. **B**) In contrast, administration of late ACs significantly worsened renal function in mice with moderate IRI. **C**) Similarly, early ACs administered prior to mild ischaemia significantly worsened renal function. Analysed by one-way ANOVA or students *t*-test * = P ≤ 0.05, ns = non-significant. Sham (*n* = 4), PBS (*n* = 7-8), AC (*n* = 8).

4.10 ATN following ischaemia was unaffected following apoptotic cell administration

ATN was evident with widespread tubular injury in the ischaemic kidneys of PBS and apoptotic cell treated mice (Figure 4.14A). Despite the deleterious effect of early or late apoptotic cell administration upon renal function in mild or moderate renal IRI, ATN scores of PBS and apoptotic cell treated mice were comparable (Figure 4.14B).

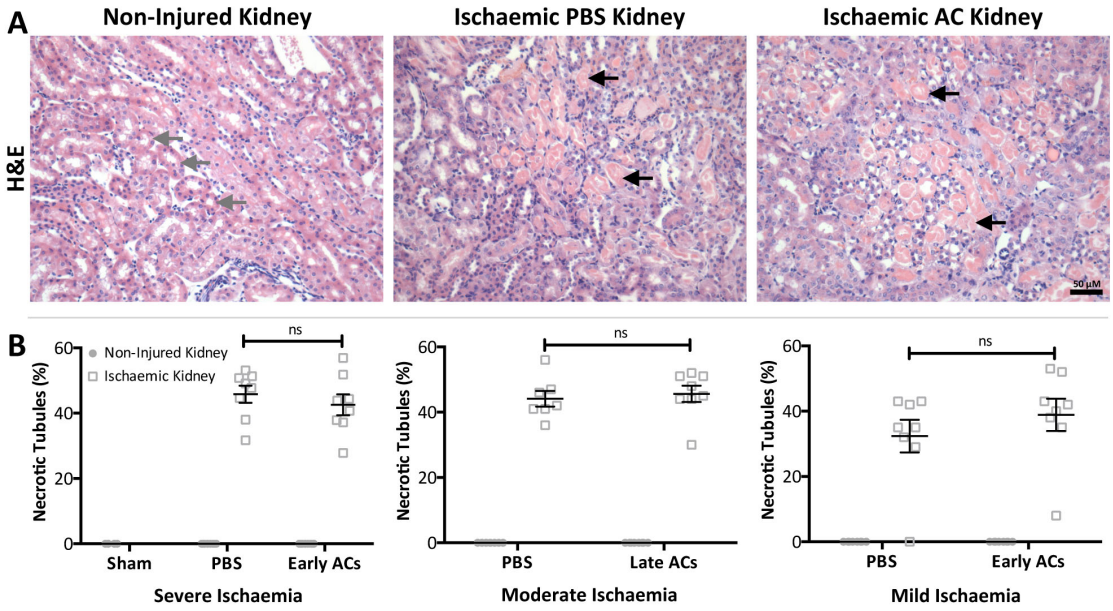

Figure 4.14 - Acute tubular necrosis (ATN) following ischaemia was unaffected following apoptotic cell (AC) administration. Renal IRI was induced in 8-week old male Balb/c mice by a right nephrectomy and ischaemia induced by occluding the left renal pedicle for 20 (mild ischaemia), 24 (moderate) or 25-minutes (severe). Sham mice underwent a laparotomy. Either PBS or $20x10^6$ early or late ACs were administered 24-hours prior to renal IRI. Mice were sacrificed 24-hours following IRI. **A**) Representative images of the OSOM in non-injured and ischaemic kidney sections stained with H&E. Tubules within the OSOM were classified as necrotic (black arrow) or healthy (grey arrow) according to cell morphology and integrity. (Magnification: x200; Scale Bar: 50 µM) **B**) ATN scoring (expressed as the percentage of necrotic tubules) demonstrates that the structural injury remained similar between PBS and AC treated mice with severe, moderate and mild ischaemic injury. ● = Non-injured kidney □ = Ischaemic kidney. Data expressed as mean ±SEM and analysed by two-way ANOVA. ns = non-significant. Sham (*n* = 4), PBS (*n* = 7-8), AC (*n* = 8).

4.11 Administration of viable thymocytes prior to renal IRI had no influence on renal function or ATN

It is evident from the lower left quadrants of figure 4.12 E & F that both early and late apoptotic cells contained populations of viable non-apoptotic cells and that these cells might be responsible for the worsening of renal dysfunction. However, the administration of 20×10^6 viable thymocytes (~95% Annexin-V^- PI^-) (Figure 4.15A) prior to renal IRI had no significant effect upon renal function measured by plasma creatinine (Figure 4.15B) and blood urea nitrogen (Figure 4.15C) or ATN (Figure 4.15D).

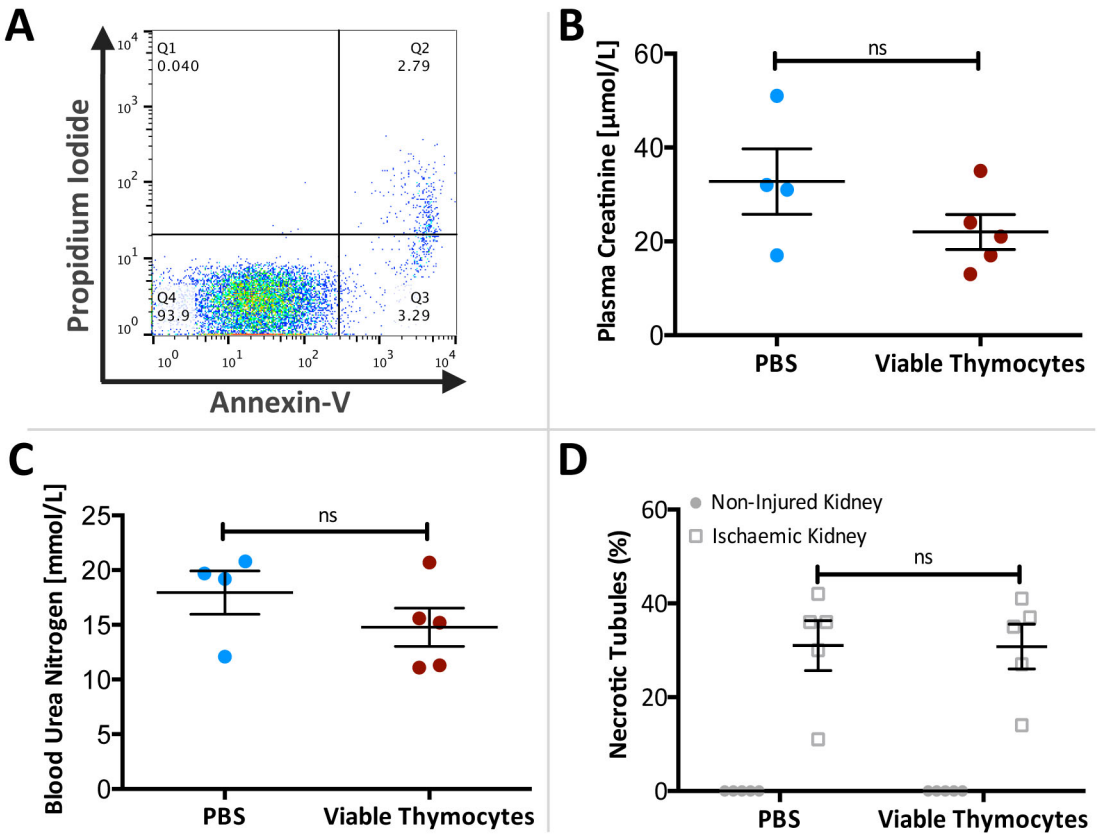

Figure 4.15 - Administration of viable thymocytes prior to renal IRI had no influence on renal function or ATN. Dissociated thymocytes were prepared from 4-week old male Balb/c mice. Cell viability was assessed by Annexin-V and Propidium Iodide (PI) staining and flow cytometry. Either PBS or $20x10^6$ viable non-apoptotic thymocytes were administered to 8-week old male Balb/c mice 24-hours prior to renal IRI induced by a right nephrectomy and occlusion of the left renal pedicle for 20 mins. Mice were sacrificed 24-hours following IRI. **A)** Viable thymocytes were approximately 94% Annexin-V$^-$ PI$^-$. **B & C)** Administration of viable thymocytes prior to renal IRI had no significant influence on renal function measured by plasma creatinine (**B**) and blood urea nitrogen (**C**). **D)** Scoring of ATN (acute tubular necrosis) (expressed as the percentage of necrotic tubules in the OSOM) demonstrates that the structural injury remained similar between mice that received PBS or viable thymocytes prior to renal IRI. ● = Non-injured kidney □ = Ischaemic kidney. Data expressed as mean ±SEM and analysed by student's *t*-test. ns = non-significant. PBS (*n* = 5), Viable thymocytes (*n* = 5).

4.12 Microvascular congestion remained unaffected following apoptotic cell administration

The finding of unexpectedly worse renal function without an increased ATN score in apoptotic cell treated mice suggested that apoptotic cells might have detrimentally reduced renal microvascular flow, contrary to our hypothesis. The coagulation cascade is activated following ischaemic injury (Jennewein et al., 2011) and the microvasculature becomes congested with erythrocytes and platelet/fibrin aggregates which aggravates tissue hypoxia and limits the perfusion of residual viable and potentially functional nephrons (Patschan et al., 2012a, Enestrom et al., 1988). Apoptotic cells expressing PtdSer are pro-coagulant and might therefore contribute to this pro-coagulant milieu (Casciola-Rosen et al., 1996). To investigate this $CD41^+$ platelet and fibrin deposition was assessed by IHC and IF, respectively. $CD41^+$ platelets and fibrin deposition was observed in the OSOM of PBS and apoptotic cell treated ischaemic kidneys (Figure 4.16A & C), but no significant differences between apoptotic cell treated and control mice were found following quantification (Figure 4.16B & D). Anti-CD41 specificity was confirmed using matched isotype control antibodies in non-injured and ischaemic kidney sections (Figure 4.18). With the finding that apoptotic cell administration did not influence microvascular congestion post IRI we did not use our established flow cytometry assays (platelet-apoptotic cell binding and platelet counts) for any further investigation.

4.13 Neutrophil infiltration occurred following ischaemia but was unaffected by apoptotic cell administration

With increased microvascular congestion not explaining this surprising result it was speculated that apoptotic cell administration might have increased immune cell infiltration thereby elevating pro-inflammatory responses post renal IRI. Neutrophils rapidly accumulate after renal ischaemic injury (Kinsey et al., 2008). They adhere to the microvascular endothelium where they may obstruct the renal microvasculature and potentially damage tubular cells by releasing reactive oxygen species (Friedewald and Rabb, 2004). To gain an insight into the inflammatory status, neutrophil infiltration

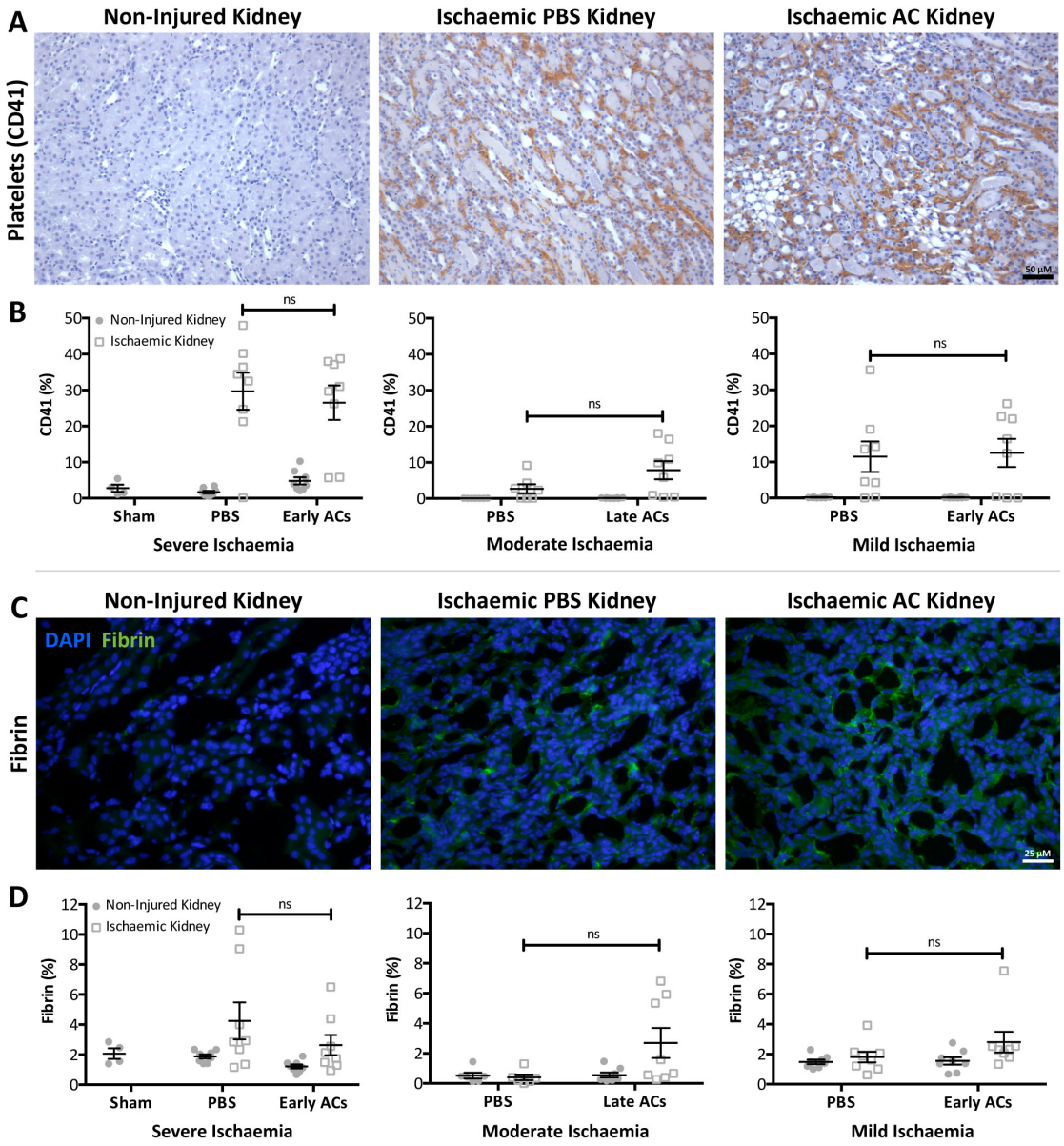

Figure 4.16 - Microvascular congestion remained unaffected following apoptotic cell (AC) administration. Renal IRI was induced in 8-week old male Balb/c mice by a right nephrectomy and ischaemia induced by occluding the left renal pedicle for 20 (mild ischaemia), 24 (moderate) or 25-minutes (severe). Sham mice underwent a laparotomy. PBS or $20x10^6$ early or late ACs were administered 24-hours prior to renal IRI. Mice were sacrificed 24-hours following IRI. **A & C**) Representative images of the OSOM in non-injured and ischaemic kidney sections following platelet (CD41) IHC (**A**) and fibrin IF (**C**) staining. In ischaemic kidneys microvascular congestion was observed as indicated by platelet and fibrin deposition. (CD41 - Magnification: x200 & Scale Bar: 50 µM; Fibrin - Magnification: x400 & Scale Bar: 25 µM) **B & D**) Scoring of platelet (**B**) and fibrin (**D**) staining (expressed as platelet/fibrin$^+$ area) demonstrates that microvascular congestion remained similar between PBS and AC treated mice with severe, moderate and mild ischaemic injury. ● = Non-injured kidney □ = Ischaemic kidney. Data expressed as mean ±SEM and analysed by two-way ANOVA. ns = non-significant. Sham (*n* = 4), PBS (*n* = 7-8), AC (*n* = 8).

was determined following IHC staining for Gr1. Neutrophil infiltration was observed in the OSOM of all ischaemic kidneys of PBS and apoptotic cell treated mice (Figure 4.17A), however this remained equivalent in all apoptotic cell treated mice and their corresponding PBS controls (Figure 4.17B). Anti-Gr1 specificity was confirmed using matched isotype control antibodies in non-injured and ischaemic kidney sections (Figure 4.18).

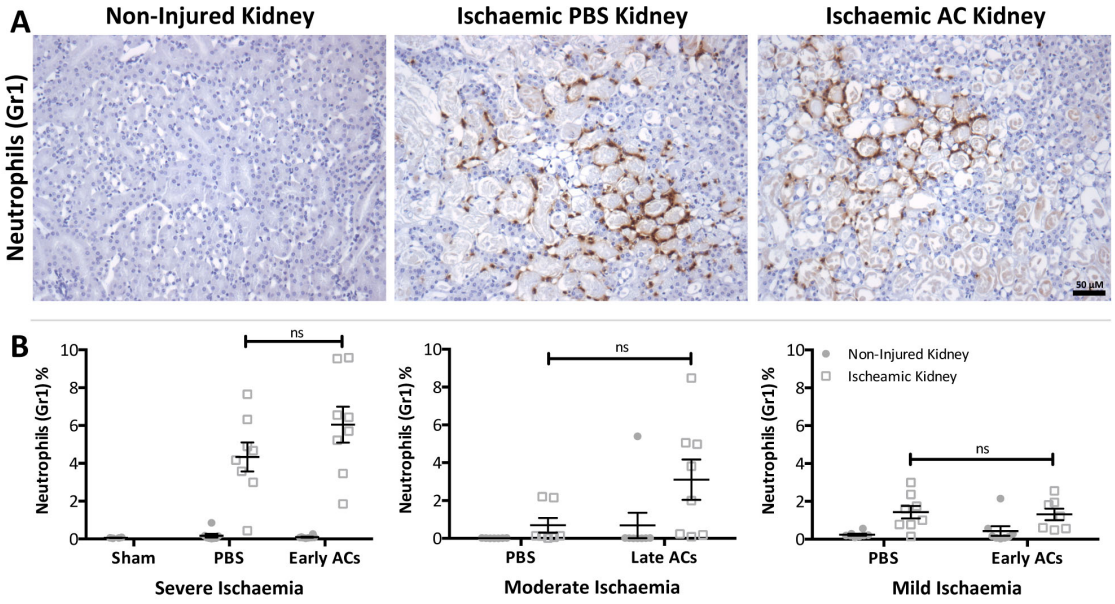

Figure 4.17 - Neutrophil infiltration occurred following ischaemia but was unaffected by apoptotic cell (AC) administration. Renal IRI was induced in 8-week old male Balb/c mice by a right nephrectomy and ischaemia induced by occluding the left renal pedicle for 20 (mild ischaemia), 24 (moderate) or 25-minutes (severe). Sham mice underwent a laparotomy only. Either PBS or $20x10^6$ early or late ACs were administered intravenously 24-hours prior to renal IRI. Mice were sacrificed 24-hours following IRI. **A**) Representative images of the OSOM in non-injured and ischaemic kidney sections following Gr1 staining. In ischaemic kidneys neutrophil infiltration was observed in areas of necrosis. (Magnification: x200; Scale Bar: 50 µM) **B**) Scoring of Gr1 staining (expressed as $Gr1^+$ area) demonstrates that neutrophil infiltration remained similar between PBS and AC treated mice with severe, moderate and mild ischaemic injury. ● = Non-injured kidney □ = Ischaemic kidney. Data expressed as mean ±SEM and analysed by two-way ANOVA. ns = non-significant. Sham (*n* = 4), PBS (*n* = 7-8), AC (*n* = 8).

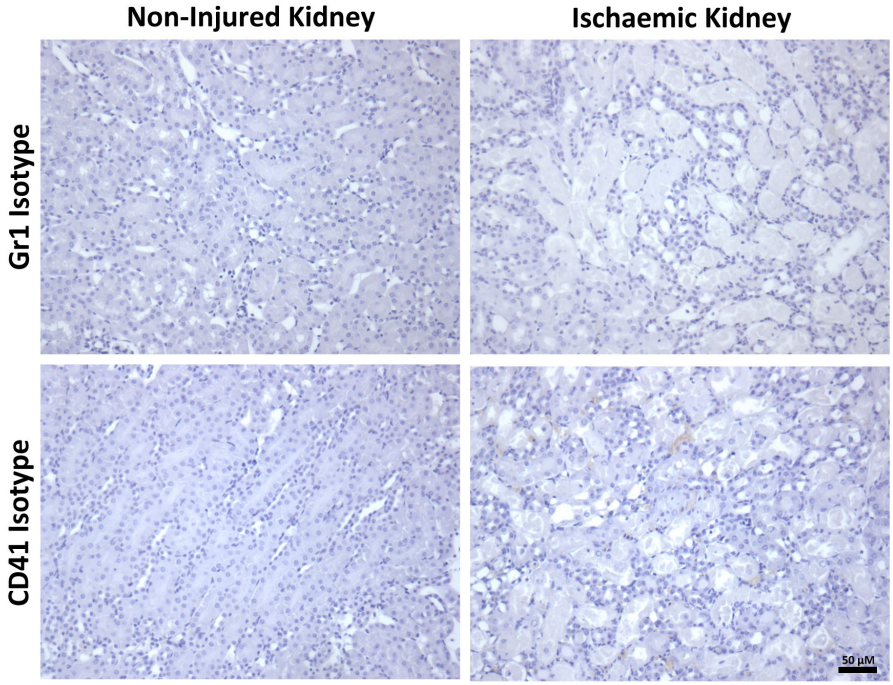

Figure 4.18 - Isotype controls for Gr1 and CD41 were negative on non-injured and ischaemic kidney. Renal IRI was induced in 8-week old male Balb/c mice by a right nephrectomy and ischaemia induced by occluding the left renal pedicle for 24 mins. Representative images of the OSOM in non-injured and ischaemic kidney sections following staining with isotype control antibodies for CD41 and Gr1. Both isotype control antibodies exhibit no staining in non-injured and ischaemic kidneys. (Magnification: x200; Scale Bar: 50 µM)

Summary

In this chapter we examined if apoptotic cells administered prior to the induction of renal ischaemia reperfusion injury were protective. In contrast to the preliminary data and protection derived from apoptotic cell administration observed in other models, our data indicates that apoptotic cells do not protect from renal ischaemic injury. Indeed, depending upon the severity of the ischaemic injury, apoptotic cells may act to further worsen renal function. These data represents an important message for the field in that the administration of apoptotic cells is not inherently anti-inflammatory in all models of acute inflammation. Our data suggests that 'apoptotic cell therapy' is not translationally relevant for patients with acute kidney injury induced by ischaemic injury.

Interestingly, we found that apoptotic cells can modulate coagulation status, in regards to thrombin generation; with apoptotic cell treated mice demonstrating significantly delayed clotting times. In support of this, apoptotic cells were also found to be able to bind platelets, which are instrumental in the regulation of coagulation and thrombin generation (Monroe et al., 2002). Despite platelet/apoptotic cell interaction and delayed thrombin having no discernable influence on microvascular congestion following ischaemia, these data still provides further insight into how apoptotic cells may alter coagulation status.

Chapter 5. Circulating IgM requires plasma membrane disruption in order to bind cells

Introduction

Despite data presented in chapters 3 and 4 indicating that apoptotic thymocyte administration prior to renal IRI is not protective, and that IgM antibodies deposition was not prominent following renal ischaemic injury, IgM binding to injured or apoptotic cells remained an intriguing area that we wanted to explore. We were also optimistic that our studies in this area may provide us with an insight into the mechanism behind the disparity between IgM deposition in ischaemic liver and kidney tissue.

IgM antibodies mediate and promote apoptotic cell clearance (Peng et al., 2005, Ogden et al., 2005, Litvack et al., 2010, Litvack et al., 2011), and bind to a diverse range of non-self and self-antigens (reviewed in Table 1.3). Many of these are thought to be antigens that have been modified or that are only accessible following apoptosis. Although it has been suggested that IgM antibodies illustrate a distinct preference for "late" apoptotic cells (Litvack et al., 2010, Fu et al., 2007, Zwart et al., 2004, Ciurana and Hack, 2006, Porcheray et al., 2013), it should be noted that heterogeneity exists between investigators in the classification of "late" apoptotic cells. Restricting classification to the use of AnnV and PI viability dyes alone, "late" apoptotic cells have been classified as $AnnV^{+}PI^{-}$, $AnnV^{+}PI^{+}$ or simply PI^{+}. Some would argue that PI^{+} events should be designated as cellular fragments. Despite this classification ambiguity it can at least be concluded that IgM antibodies bind cells at an advanced stage of cell death.

In this chapter we sought to carefully explore the binding of circulating IgM to apoptotic cells, both human and murine, at different stages of apoptosis, with thoughtful consideration to controls to ensure the specificity and accuracy of our results.

Results

5.1 Establishment of an assay to detect circulating IgM binding to cells

First, an IgM detection assay was established in order to characterise and explore circulating IgM binding to non-apoptotic and apoptotic cells. Initial experiments induced apoptosis in murine thymocytes by a 20-hour incubation in RMPI supplemented with 1 µM Dexamethasone (Dex), which elicited a predominately late apoptotic cell population (78% $AnnV^{+}PI^{+}$) (Figure 5.1A). To investigate IgM binding apoptotic thymocytes were exposed to either PBS or undiluted Balb/c plasma (as a source of IgM) for 30-minutes. Following this samples were incubated with a fluorochrome conjugated anti-IgM antibody for 30-minutes before IgM binding was assessed by flow cytometry. Apoptotic thymocytes exposed to Balb/c plasma demonstrated a shift towards IgM positivity compared to PBS treated samples, indicating bound IgM (Figure 5.1B). Following successful detection of IgM binding an anti-IgM antibody titration was performed to determine the optimum antibody dilution for IgM detection. Median fluorescent intensity (MFI) was determined on cells gated for IgM positivity in samples exposed to Balb/c plasma compared to PBS treated samples. This demonstrated that a 1:100 dilution was appropriate as the MFI was drastically reduced at a 1:200 dilution (Figure 5.1C). Next a plasma dilution series was performed to determine the optimum dilution necessary to allow binding and detection of circulating IgM, but preserve plasma stock that was limited. MFI was determined on cells gated for IgM positivity in samples exposed to Balb/c plasma compared to PBS treated samples. On the basis of MFI a 1:8 dilution was selected as dilutions 1:5 and 1:10 resulted in acceptable MFI values (Figure 5.1D). Cell number was not optimised as the standard 500,000 cells used for flow cytometry generated acceptable results.

With conditions for the assay optimised, a time course of apoptosis in murine thymocytes was performed. This was performed to ascertain which conditions elicited a cell population consisting of various levels of cell death (non-apoptotic, early and late apoptotic). This would allow the assessment of IgM binding to thymocytes at variable

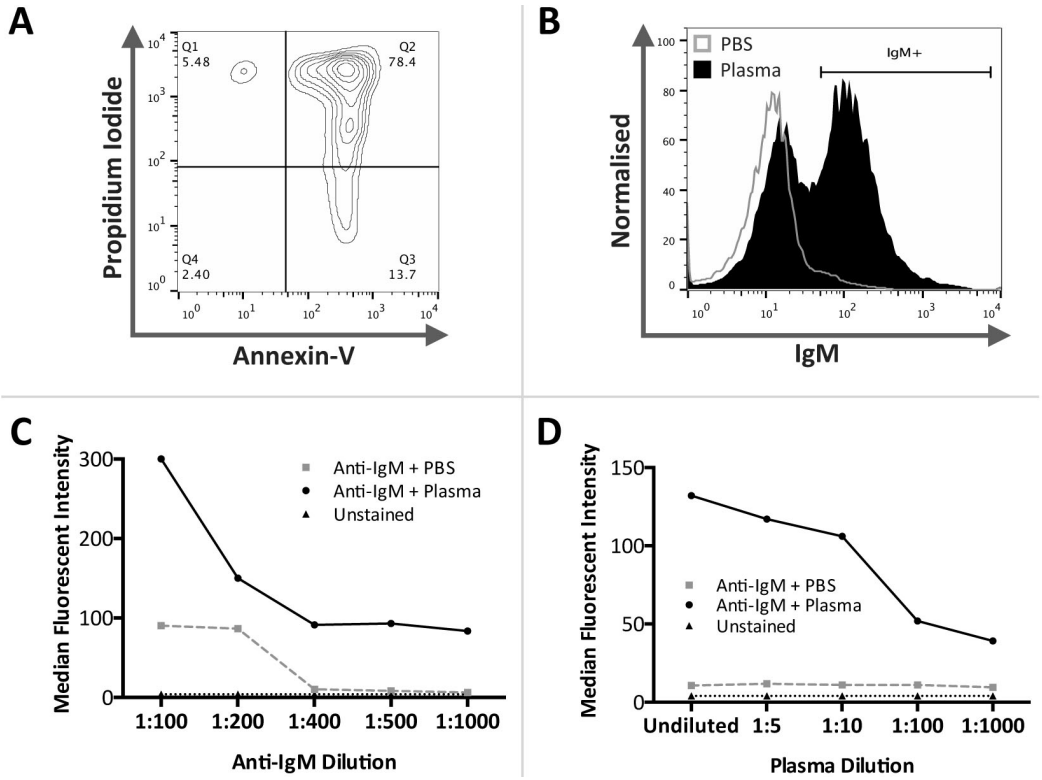

Figure 5.1 – Establishing and optimising an assay to detect circulating IgM binding to cells. A) Murine thymocytes were rendered apoptotic by a 20-hour incubation with 1 µM Dex, which resulted in a predominantly $AnnV^+$ PI^+ apoptotic cell population. **B**) Apoptotic thymocytes were then exposed to either PBS or undiluted Balb/c plasma (as a source of IgM). IgM binding was then assessed by flow cytometry. A marked shift towards IgM positivity was observed in samples treated with Balb/c plasma compared to PBS treated samples. **C**) An anti-IgM antibody titration was performed to determine the correct antibody dilution for IgM detection. Median fluorescent intensity was determined on cells gated for IgM positivity in samples exposed to Balb/c plasma compared to PBS treated samples. **D**) A plasma dilution series was performed to determine the correct dilution necessary to allow IgM to bind, but preserve plasma stock. Median fluorescent intensity was determined on cells gated for IgM positivity in samples exposed to Balb/c plasma compared to PBS treated samples.

stages of apoptosis. Dissociated murine thymocytes were incubated with RPMI alone, or RMPI supplemented with 1% FCS or 1% BSA. Murine thymocytes were then aged or treated with 1µM Dex and sampled at 0, 4, 8, 16, 20 and 24-hours and apoptosis was determined by AnnV and PI staining assessed by flow cytometry. A 16-hour incubation in RMPI alone elicited a cell population of approximately 35% $AnnV^-PI^-$, 40% $AnnV^+PI^-$, 25% $AnnV^+PI^+$ (highlighted in blue in Figure 5.2) and was selected for future experiments. In addition, culture of murine thymocytes in RMPI eliminated any potential pre-exposure to cell culture serum protein supplements.

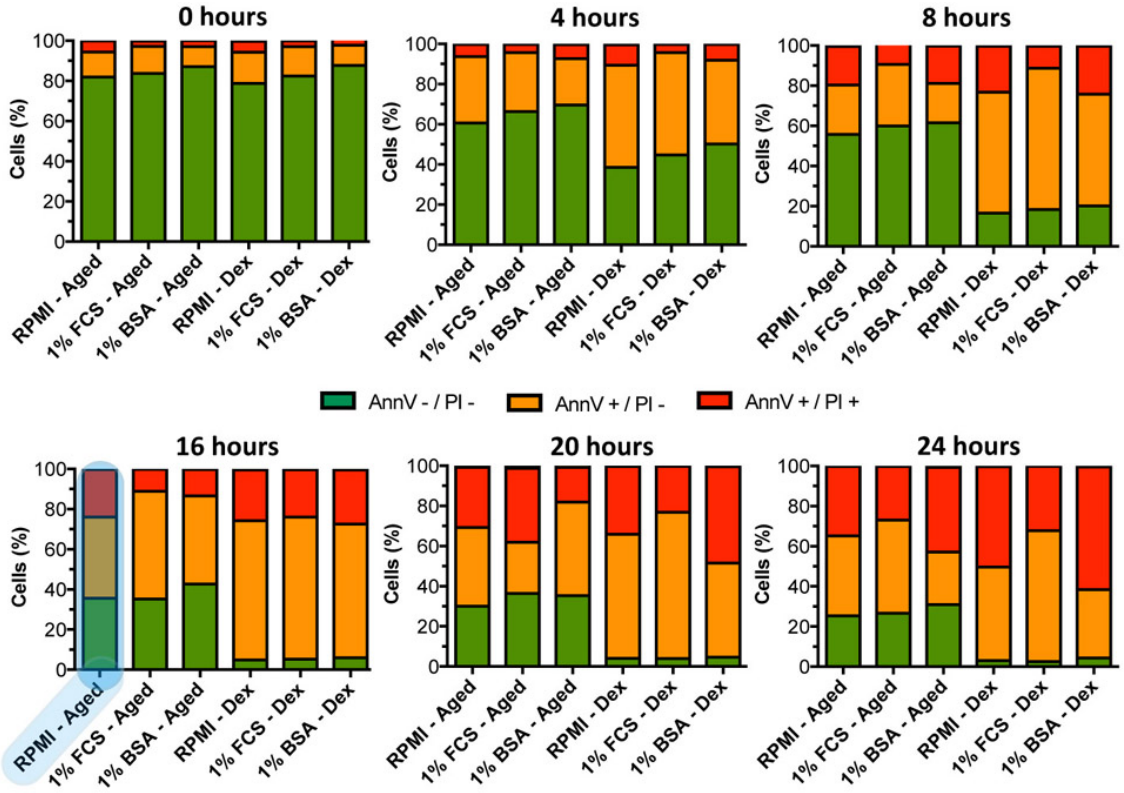

Figure 5.2 – Time course of apoptosis in murine thymocytes. A time course of apoptosis was performed to determine appropriate conditions necessary to induce a cell population with mixed levels of apoptosis. Dissociated murine thymocytes were incubated with RPMI alone, or RMPI supplemented with 1% FCS or 1% BSA. Thymocytes were then aged or treated with 1 µM Dex and sampled at 0, 4, 8, 16, 20 and 24-hours. Apoptosis was determined by AnnV and PI staining assessed by flow cytometry. Selected time point and conditions used for future experiments was 16-hours aged in RPMI alone (highlighted in blue).

5.2 Circulating murine IgM preferentially binds a distinct subpopulation of $AnnV^+PI^+$ thymocytes

We next examined IgM binding to murine thymocytes with mixed levels of apoptosis. Thymocytes were exposed to either PBS, Balb/c plasma (as a source of circulating IgM) or control plasma from immunoglobulin deficient RAG-1 mice. As previous work suggested that IgM binds apoptotic cells (Litvack et al., 2010, Fu et al., 2007, Zwart et al., 2004, Ciurana and Hack, 2006, Porcheray et al., 2013), we therefore focused our attention on $AnnV^+$ thymocytes and assessed the percentage of $AnnV^+IgM^+$ thymocytes (Figure 5.3A-B). IgM binding of thymocytes by control isotype antibody (Mouse (Balb/c) IgM κ isotype control) or following incubation in RAG1-deficient mice

plasma or PBS remained non-significant whilst samples exposed to Balb/c plasma exhibited significant binding with 32.1 ±3.1% of cells being $AnnV^+IgM^+$ (Kruskal–Wallis one-way ANOVA; $P < 0.0001$; $n = 5$ isotype, $n = 6$ RAG1-deficient mice plasma + Anti-IgM, $n = 8$ PBS + Anti-IgM and Balb/c plasma + Anti-IgM) (Figure 5.3B).

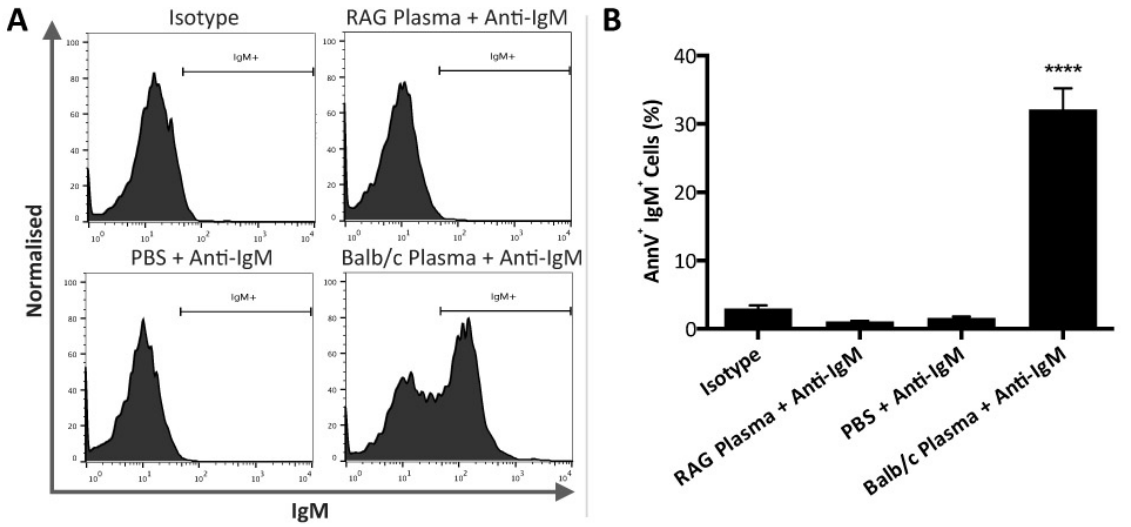

Figure 5.3 - IgM specifically binds to a distinct population of $AnnV^+$ murine thymocytes. Murine thymocytes were rendered apoptotic by overnight culture. Thymocytes were exposed to either murine anti-human isotype control antibodies, PBS, Balb/c plasma (as a source of IgM) or plasma from immunodeficient RAG-1 deficient mice. IgM binding was assessed by flow cytometry. AnnV and PI staining, assessed by flow cytometry, was used to determine the level of non-apoptotic ($AnnV^-PI^-$), early ($AnnV^+PI^-$) or late apoptotic ($AnnV^+PI^+$) thymocytes. **A**) Representative histograms illustrating IgM binding to $AnnV^+$ apoptotic thymocytes within treatment groups. **B**) Apoptotic thymocytes were gated on the basis of AnnV positivity and the percentage of $AnnV^+IgM^+$ thymocytes was assessed. IgM binding in isotype, RAG1-deficient mice plasma and PBS treatment groups remained non-significant whilst samples exposed to Balb/c plasma exhibited significant binding. However, surprisingly only approximately 68% were IgM^-.

Approximately 68% of $AnnV^+$ cells were IgM^- and further examination of the cell populations present within samples exposed to Balb/c plasma revealed three distinct populations: $AnnV^-IgM^-$, $AnnV^+IgM^-$ and $AnnV^+IgM^+$ cells (Figure 5.4A). Analysis of $AnnV^+IgM^-$ and $AnnV^+IgM^+$ FSC/SSC contour plots revealed contrasting profiles, yet comparable AnnV/PI staining (Figure 5.4B). As expected the $AnnV^-IgM^-$ population exhibited no PI positivity. Interestingly, $AnnV^+IgM^-$ and $AnnV^+IgM^+$ populations demonstrated disparate FSC/SSC profiles, yet both populations were predominantly

AnnV$^+$PI$^+$ (Figure 5.4B). Apoptotic thymocytes incrementally incubated in Balb/c plasma indicated that circulating IgM bound rapidly to cells localised within the region defined as AnnV$^+$IgM$^+$ on FSC/SSC contour plots (*n* = 4) (Figure 5.4C).

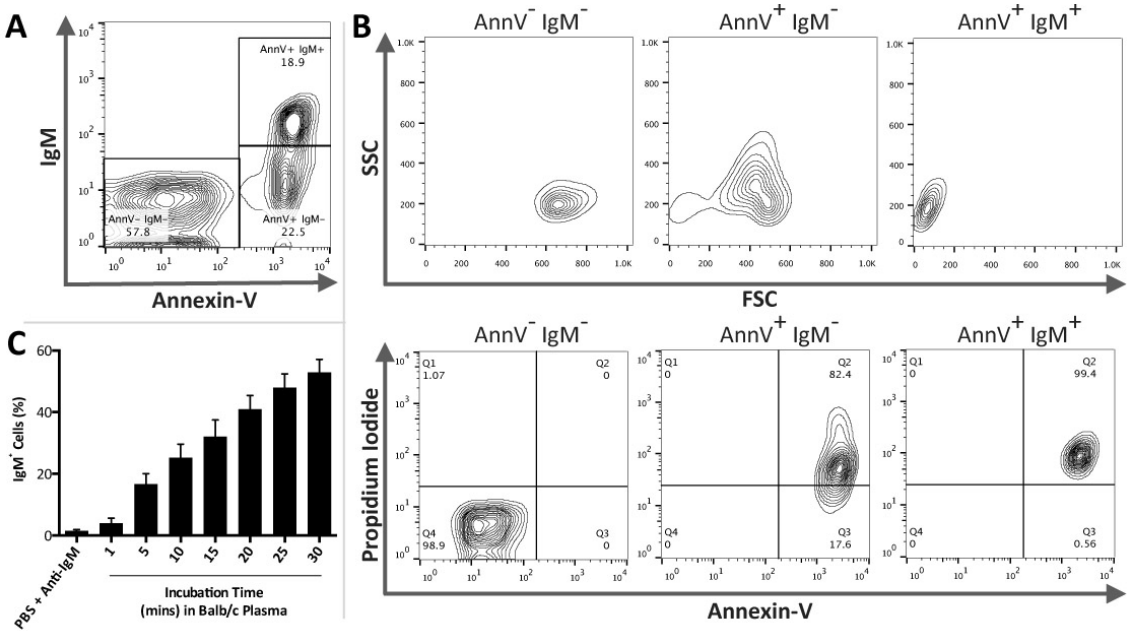

Figure 5.4 - IgM rapidly binds to a distinct population of AnnV$^+$ PI$^+$ murine thymocytes. Murine thymocytes were rendered apoptotic by overnight culture. Thymocytes were exposed to either murine anti-human isotype control antibodies, PBS, Balb/c plasma (as a source of IgM) or plasma from immunodeficient RAG-1 deficient mice. IgM binding was assessed by flow cytometry. AnnV and PI staining, assessed by flow cytometry, was used to determine the level of non-apoptotic (AnnV$^-$ PI$^-$), early (AnnV$^+$PI$^-$) or late apoptotic (AnnV$^+$PI$^+$) thymocytes. **A**) Samples exposed to Balb/c plasma consisted of three distinct populations: AnnV$^-$IgM$^-$, AnnV$^+$IgM$^-$ and AnnV$^+$IgM$^+$. **B**) The three distinct populations present in samples exposed to Balb/c plasma were further characterised by examining the FSC/SSC profile and AnnV and PI positivity. Although both AnnV$^+$IgM$^-$ and AnnV$^+$IgM$^+$ populations were predominantly AnnV$^+$ PI$^+$ they occupied distinct separate regions of FSC/SSC contour plots. **C**) Within the AnnV$^+$IgM$^+$ population IgM binding occurred rapidly. Data expressed as means ±SEM.

These data suggested that murine IgM antibodies were appearing to bind to a distinct subset of apoptotic thymocytes that have exposed PtdSer (AnnV positive) and a distinct FSC SSC profile. Our next objectives at this point were:

a) confirm whether cell surface C3 deposition accompanied IgM binding, in line with other investigators findings, and

b) further characterize these distinct populations of IgM^- and IgM^+ apoptotic thymocytes.

To do this we aimed to determine whether these distinct populations were formed due to the action of IgM antibody binding or complement mediated cell disruption or whether the IgM^+ cells had any obvious morphological differences detectable by microscopy. We hoped that through these studies we would be able to discern why IgM antibodies appeared to bind such a distinct population of thymocytes.

5.3 C3 deposition is present on aged $AnnV^-IgM^-$, $AnnV^+IgM^-$ and $AnnV^+IgM^+$ murine thymocytes

As previous studies illustrated, IgM binding is often accompanied by complement deposition on the cell surface. We therefore sought to confirm whether C3 deposition occurred on IgM bound cells in our assay (Figure 5.3A-B). Murine apoptotic thymocytes were incubated in PBS, Balb/c plasma (as a source of C3) or heat inactivated Balb/c plasma. C3 deposition was assessed by flow cytometry and sample populations were identified and designated as detailed in Figure 5.3 and 5.4. C3 deposition was detected on $AnnV^+IgM^-$ and $AnnV^+IgM^+$ aged cell populations incubated in Balb/c plasma (Figure 5.5A-B). Interestingly and unexpectedly, aged thymocytes not yet expressing PtdSer, and as such classified as $AnnV^-$, appeared to demonstrate C3 deposition. Intrigued by this we sought to investigate C3 deposition on fresh murine thymocytes exposed to Balb/c plasma immediately following dissociation (fresh). As expected fresh thymocytes remained convincingly C3 negative (Figure 5A-B). Minimal C3 deposition was detected in all samples exposed to PBS and heat inactivated plasma (Figure 5.5B, Representative histograms (n = 2-3)). Although admittedly brief this finding is striking as despite a high daily burden of apoptotic cells is generated, apoptotic cells are rarely observed in healthy tissue (Mochizuki et al., 1996, Scott et al., 2001, Elliott et al., 2009, Yang et al., 2006, Schrijvers et al., 2005, Gregory and Devitt, 2004). This data suggests that membrane alterations occur before traditionally defined apoptosis is evident, enabling complement opsonisation and subsequent phagocytosis early than previously thought.

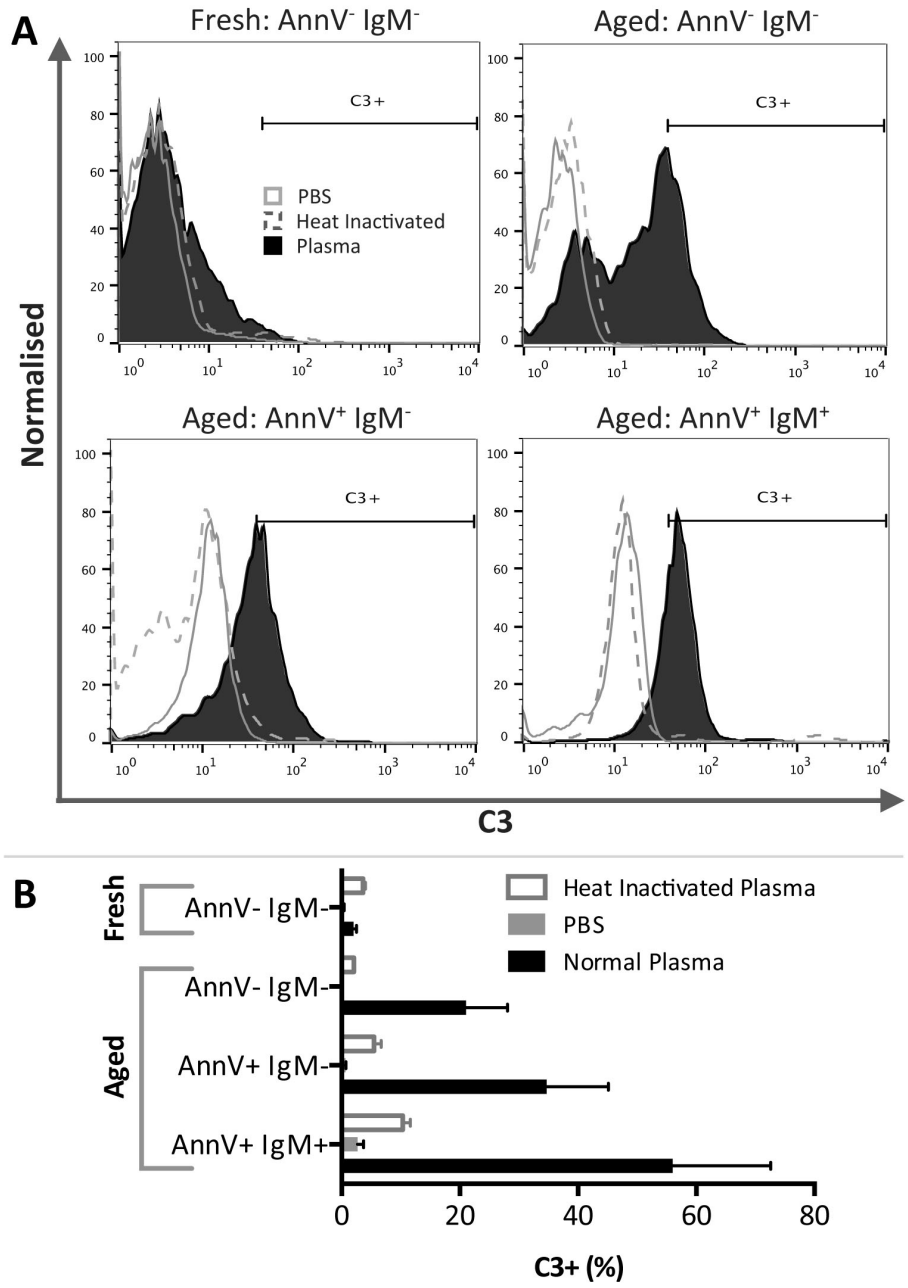

Figure 5.5 – C3 deposition present on aged AnnV$^-$IgM$^-$, AnnV$^+$IgM$^-$ and AnnV$^+$IgM$^+$. Murine thymocytes were used immediately (fresh) or rendered apoptotic by overnight culture before being incubated in PBS, Balb/c plasma (as a source of C3) or heat inactivated Balb/c plasma. C3 deposition was detected by flow cytometry. Sample populations were identified and designated as detailed in figure 5.3 and 5.4. **A**) Representative histograms. **B**) C3 deposition was detected on AnnV$^+$IgM$^-$ and AnnV$^+$IgM$^+$ aged cell populations incubated in Balb/c plasma. Interestingly, AnnV$^-$IgM$^-$ cell populations exposed to Balb/c plasma exhibited low C3 deposition when used fresh. However, some C3 binding was evident in thymocytes aged *in vitro* despite the absence of a well established marker of apoptosis (AnnV positivity). Minimal C3 deposition was detected in all samples exposed to PBS and heat inactivated plasma. Representative histograms (*n* = 2-3).

5.4 Formation of AnnV$^+$ IgM$^+$ population located on FSC/SSC plots appears plasma dependent

We next wanted to further characterise the three distinct cell populations evident on FSC SSC contour plots, as described in figure 5.4B. The formation of these three populations appeared to be plasma dependent, as when diluted 1:1000 the apoptotic thymocytes largely remain as one population (Figure 5.6A). Fresh thymocytes exposed to plasma also largely remained as one population (Figure 5.6B). We were next interested in investigating whether the formation of these three populations was partly dependent upon complement mediated cell disruption. As illustrated in figure 5.5 we found that C3 was deposited on the cell surface of IgM$^+$ cells. However, the populations were still present on FSC SSC contour plots of apoptotic murine thymocytes exposed to heat inactivated Balb/c plasma (Figure 5.6C). In addition, the populations were present in samples exposed to immunodeficient RAG-1 plasma, suggesting that formation of this population is immunoglobulin independent (Figure 5.6D).

5.5 Circulating IgM binds to murine apoptotic thymocytes with evidence of a disrupted cell membrane

We explored whether apoptotic thymocytes that bound IgM demonstrated any morphological features that might explain the disparity of IgM binding to AnnV$^+$PI$^+$ cells and the differing FSC/SSC profiles of the AnnV$^+$IgM$^+$ and AnnV$^+$IgM$^-$ cell populations. CellTracker Green labelled thymocytes were FACS sorted into AnnV$^-$IgM$^-$, AnnV$^+$IgM$^-$ and AnnV$^+$IgM$^+$ populations on the basis of FSC SSC populations (illustrated in Figure 5.4B) by FACS. Post FACS sorting checks were performed to assess whether the fragile apoptotic thymocytes remained intact/morphologically normal according to FSC SSC following a high-pressure sort. Figure 5.7 indicates that all sorted cell populations lie predominantly within their corresponding gate following FACS sorting. The apoptotic AnnV$^+$IgM$^-$ population (Figure 5.7 – lower right yellow/orange boxed panel) moved further towards the right, this is expected due to ongoing apoptosis related morphological changes during FACS sorting. Sorted cells populations were then

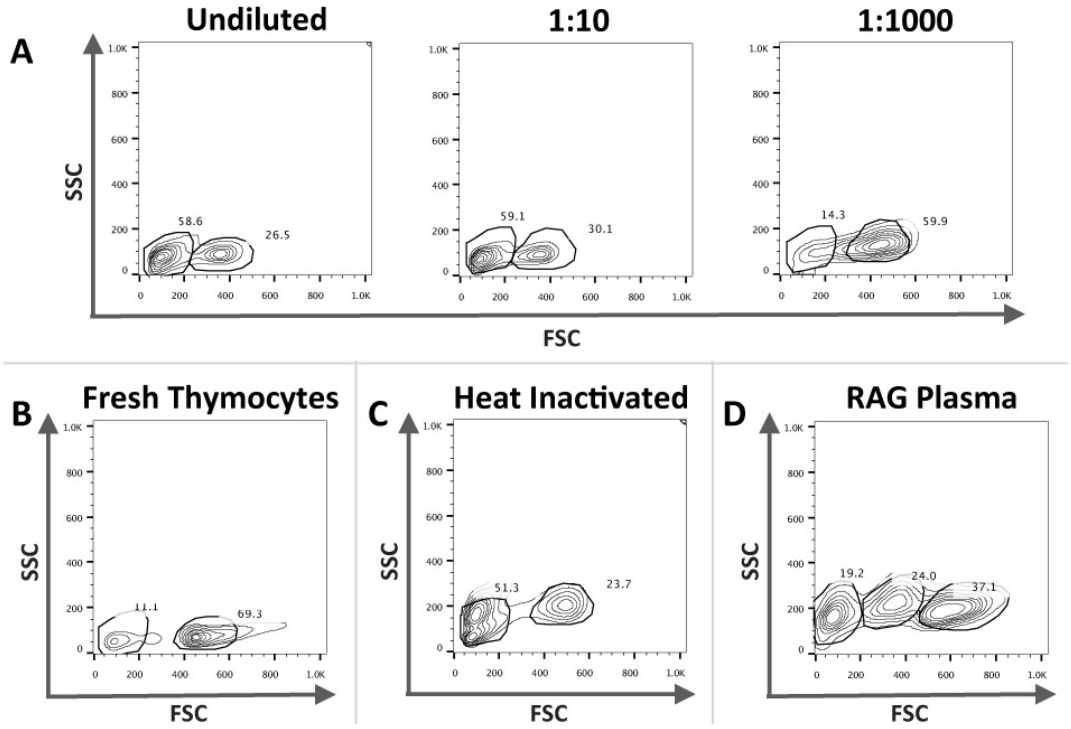

Figure 5.6 – Formation of AnnV$^+$IgM$^+$ population located on FSC/SSC plots appears plasma dependent. Murine thymocytes were rendered apoptotic by overnight culture before being incubated in immunodeficient RAG-1 plasma, Balb/c plasma or heat inactivated Balb/c plasma. Samples were then analysed by flow cytometry and FSC SSC contour plots were examined to identify and gate the three distinct populations as illustrated in figure 5.4B. **A**) The formation of the three FSC SSC populations appears to be plasma dependent, as when diluted 1:1000 the thymocytes largely remain as one population on FSC SSC contour plots. **B**) Fresh thymocytes remain largely as one population on FSC SSC contour plots. **C**) Heat inactivation of plasma does not inhibit the formation of the three distinct populations. **D**) Formation of the three distinct populations appears immunoglobulin independent, as the three distinct FSC SSC populations remains present in samples exposed to RAG-1 plasma. Representative of several experiments.

examined by confocal microscopy. Unsurprisingly AnnV and IgM staining was absent in sorted AnnV$^-$IgM$^-$ cell populations (Figure 5.8A). Similarly, AnnV$^+$IgM$^-$ cells only displayed AnnV staining that appeared restricted to the membrane with no obvious morphological differences to AnnV$^-$IgM$^-$ cells (Figure 5.8B). Some AnnV$^+$IgM$^+$ cells appeared disrupted with abnormal cellular morphology and some cells appearing to have large 'openings' in the membrane (Figure 5.8C) Therefore, electron microscopy was used to investigate the cellular and membrane morphology in detail (Figure 5.9A-C). AnnV$^-$IgM$^-$ cells (Figure 5.9A) appeared non-apoptotic with an intact membrane

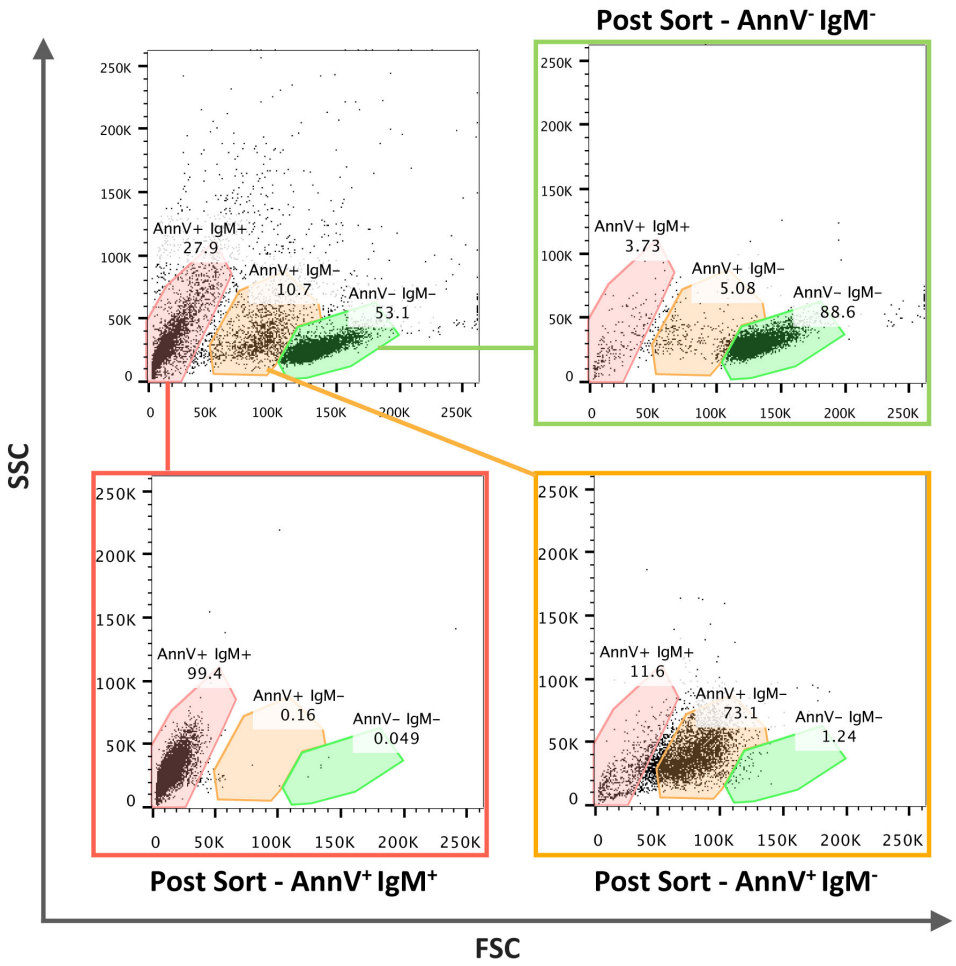

Figure 5.7 – Post FACS sorting checks demonstrate that sorted murine apoptotic cells remain in designated pre-sort defined populations. Murine thymocytes rendered apoptotic by overnight culture were FACS sorted into $AnnV^{+}IgM^{+}$, $AnnV^{+}IgM^{-}$, $AnnV^{-}IgM^{-}$ cell populations for confocal or electron microscopy studies. Post FACS sorted FSC/SSC dot plots demonstrate that the apoptotic thymocytes remain within the designated pre-sort gates.

whilst $AnnV^{+}IgM^{-}$ cells (Figure 5.9B) exhibited nuclear pyknosis with preservation of cytoplasmic and membrane integrity. However, the membrane of $AnnV^{+}IgM^{+}$ cells (Figure 5.9C) was severely disrupted compared to either $AnnV^{-}IgM^{-}$ cells or $AnnV^{+}IgM^{-}$ cells. Despite marked membrane disruption $AnnV^{+}IgM^{+}$ cells appeared to maintain sufficient cellular integrity to prevent the overt loss of organelles, such as mitochondria as evident in figure 5.9C.

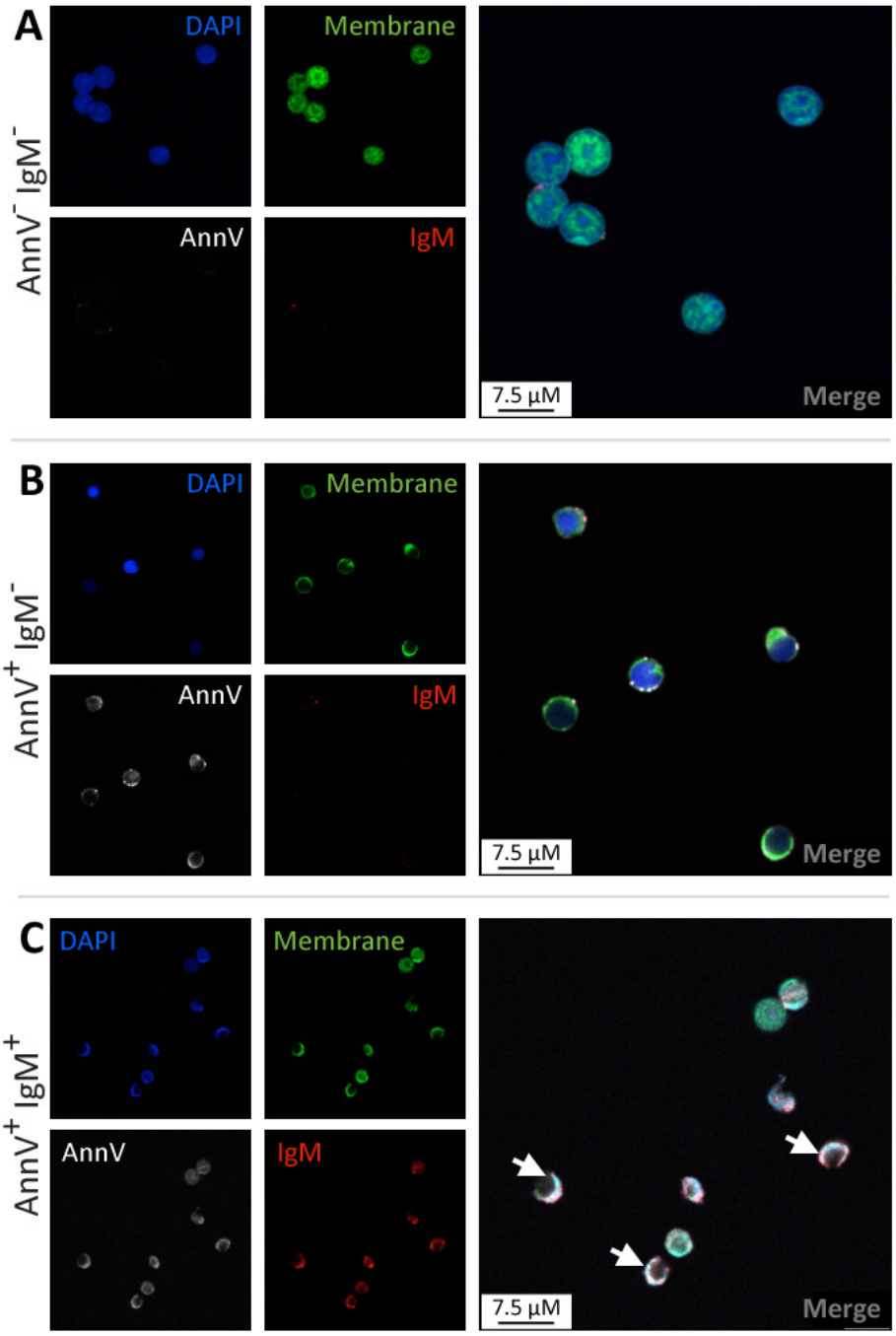

Figure 5.8 - IgM bound murine apoptotic thymocytes appear disrupted. Murine thymocytes were stained with a membrane cell tracker and then rendered apoptotic by overnight culture. Thymocytes were then exposed to Balb/c plasma prior to incubation with anti-IgM antibody, AnnV and DAPI. On the basis of FSC/SSC thymocytes were then sorted into $AnnV^-IgM^-$ (**A**), $AnnV^+IgM^-$ (**B**) and $AnnV^+IgM^+$ (**C**) populations, as illustrated in figure 5.4B, by FACS and examined by confocal microscopy. **A**) $AnnV^-IgM^-$ thymocytes were AnnV and IgM negative. **B**) $AnnV^+IgM^-$ thymocytes exhibited AnnV membrane staining but remained IgM negative and morphologically appeared intact. **C**) $AnnV^+IgM^+$ thymocytes were AnnV positive and appeared disrupted with irregular cellular morphology (arrowhead) with an apparent IgM^+ membrane.

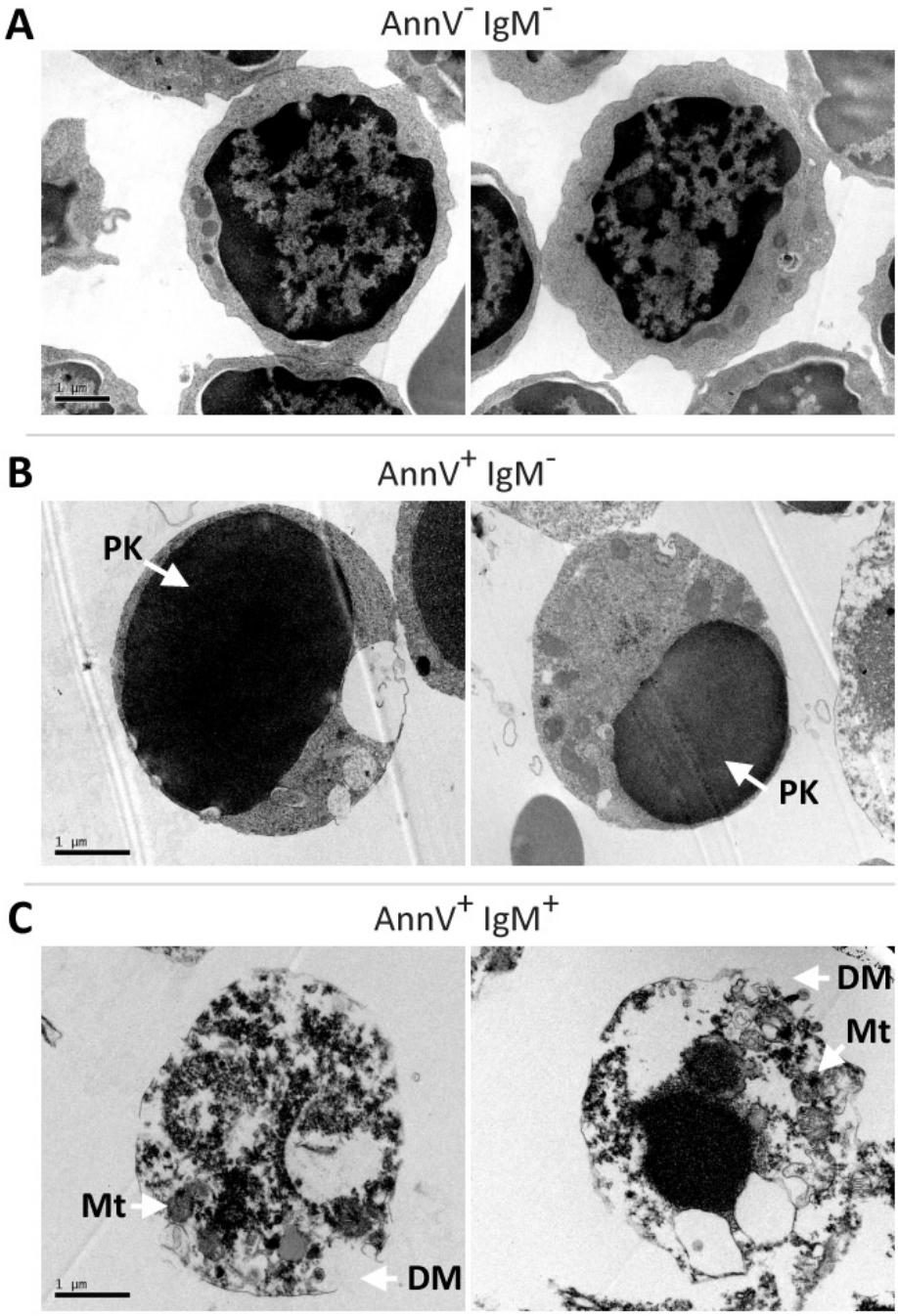

Figure 5.9 - IgM bound murine apoptotic thymocytes appear to have a disrupted plasma membrane. Murine thymocytes were rendered apoptotic by overnight culture and then exposed to Balb/c plasma prior to incubation with anti-IgM antibody and AnnV. On the basis of FSC/SSC thymocytes were then sorted into $AnnV^-IgM^-$ (**A**), $AnnV^+IgM^-$ (**B**) and $AnnV^+IgM^+$ (**C**) populations, as illustrated in figure 5.4B, by FACS and examined by electron microscopy **A**) $AnnV^-IgM^-$ cells appeared non-apoptotic with normal nuclei and intact plasma membranes. **B**) $AnnV^+IgM^-$ cells exhibited nuclear pyknosis (PK, arrowed) with preservation of cytoplasmic and membrane integrity. **C**) Electron microscopy studies confirmed that $AnnV^+IgM^+$ cells had a disrupted membrane (DM, arrowed) with cellular disorganisation, but retention of mitochondria (Mt, arrowed). Representative images.

5.6 Circulating IgM binds strongly to saponin permeabilised murine thymocytes

In light of the previous results we hypothesized that circulating IgM may be interacting with intracellular epitopes only accessible following significant loss of plasma membrane integrity and that these epitopes were not necessarily generated during apoptosis by caspases and other enzymes. We then examined whether IgM bound non-apoptotic thymocytes, which are consistently IgM negative, following permeabilisation with saponin. IgM binding of permeabilised non-apoptotic thymocytes was assessed following exposure to PBS, or plasma from either Balb/c or RAG-1 deficient mice (*n* = 3 per group). Saponin treated non-apoptotic thymocytes were PI^+ indicating successful permeabilisation and demonstrated a dramatic shift in IgM positivity whilst control non-saponin treated non-apoptotic thymocytes remained negative for both PI and IgM (Figure 5.10A).

We next assessed if IgM would bind more strongly to saponin treated apoptotic thymocytes, a large percentage of which remain IgM negative as evident in figure 5.4A (*n* = 4 per group). A small proportion of apoptotic thymocytes were PI positive representing late apoptotic thymocytes but nearly all cells became PI positive (>99%) following permeabilisation with saponin (Figure 5.10B). In the absence of permeabilisation a minority of apoptotic thymocytes were IgM^+ representing the PI positive population shown in figure 5.10B. However, following permeabilisation the majority of cells (>98%) became IgM positive (Figure 5.10B). Inclusion of isotype control IgM antibodies (Mouse (Balb/c) IgM κ isotype control) confirmed that IgM binding of permeabilised cells was not due to a non-specific interaction (Figure 5.10A-B). Furthermore, confocal microscopy confirmed these results as permeabilised non-apoptotic thymocytes were $AnnV^+$, indicating permeability, and IgM^+. IgM appeared to mostly bind in the region of the cellular membrane (Figure 5.10C).

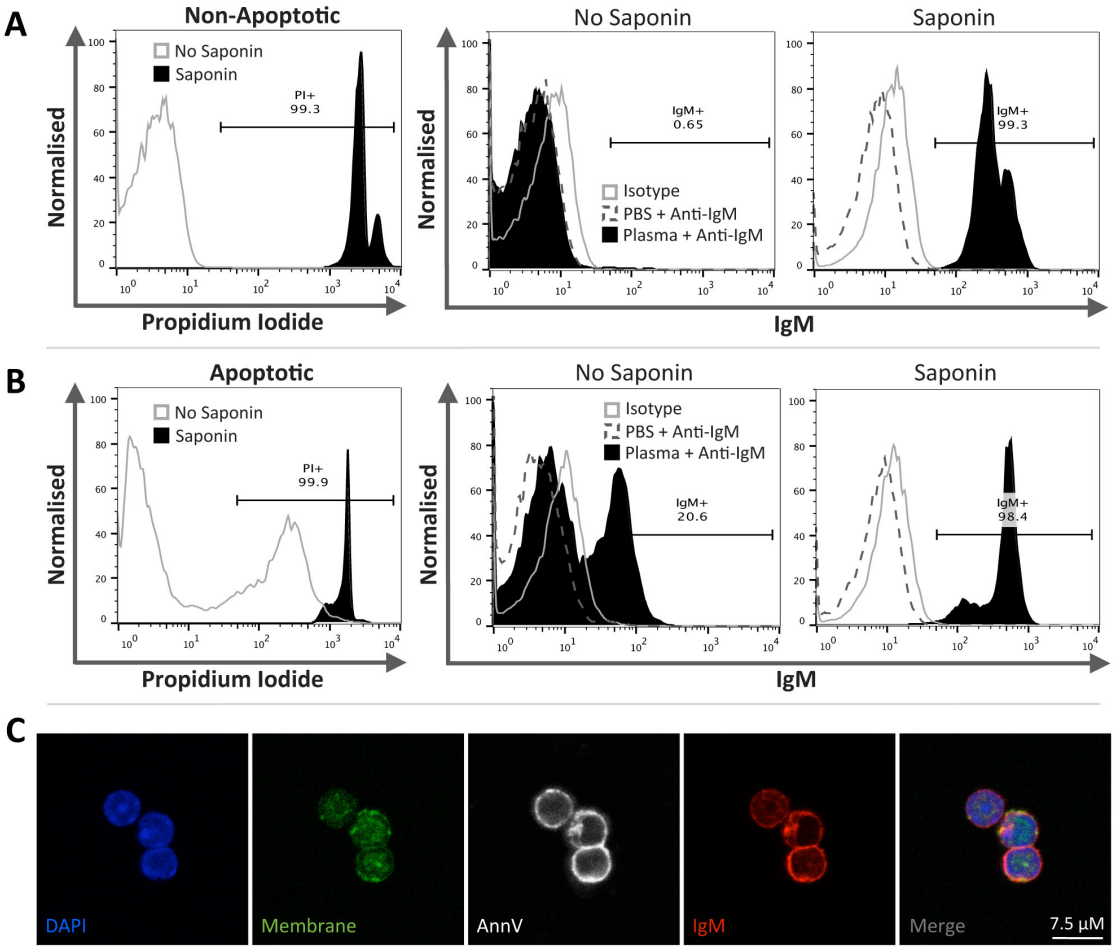

Figure 5.10 - IgM binds strongly to permeabilised non-apoptotic and apoptotic thymocytes. Non-apoptotic and apoptotic thymocytes, induced by overnight culture, were permeabilised with saponin prior to incubation with Balb/c plasma. Permeability was confirmed by PI staining and IgM binding was assessed by flow cytometry. **A**) Following permeablisation non-apoptotic thymocytes were predominantly PI positive. Non-permeable non-apoptotic thymocytes remained consistently IgM negative, whilst the majority of permeable thymocytes were IgM positive. Inclusion of isotype control IgM antibodies confirmed that IgM binding was not due to a non-specific interaction of IgM. **B**) A small proportion of apoptotic thymocytes were PI positive representing late apoptotic thymocytes; however following permeabilisation with saponin the cell population became PI positive. Whilst a minority of apoptotic thymocytes were IgM positive, representing the $AnnV^{+}IgM^{+}$ population discussed in figure 5.3C-E, with permeabilisation the population became IgM positive. **C**) Confocal microscopy demonstrates that permeabilised non-apoptotic thymocytes were AnnV positive, used to indicate permeability, with IgM appearing to bind the cellular membrane, with some intracellular staining evident. Representative histograms (Non-apoptotic thymocytes *n* = 3; Apoptotic thymocytes *n* = 4).

5.7 A 16-hour incubation with 0.5µM camptothecin elicited mixed levels of apoptosis in human Jurkat cells

We then explored the relevance of these findings to human biology using human Jurkat cells. As with the murine apoptotic cell studies we aimed to obtain a population of Jurkat cells at various stages of apoptosis to probe IgM binding. Camptothecin was used to induce apoptosis and a titration was performed. Human Jurkat cells at a density of $2x10^6$/mL were treated with 0, 0.5, 1.5 and 2 µM camptothecin for 16-hours. AnnV and PI staining, assessed by flow cytometry, was used to determine the level of apoptosis. Untreated Jurkat cells remained $AnnV^-PI^-$; whilst all camptothecin treated cells had a large but similar populations of $AnnV^+PI^+$ cells, and a small transient population that could be $AnnV^+PI^-$ (Figure 5.11). The difference in $AnnV^+PI^+$ population sizes was negligible and the lower camptothecin concentration of 0.5 µM was selected for future experiments as this induced an acceptable level of apoptosis.

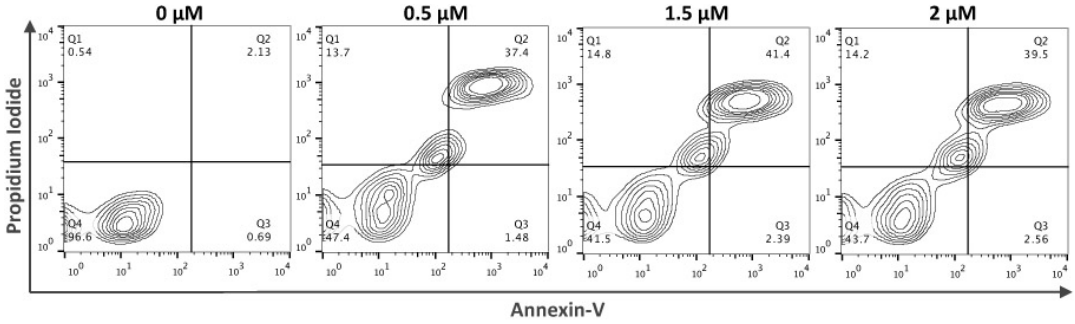

Figure 5.11 – Titration of camptothecin induced apoptosis in human Jurkat cells. Human Jurkat cells at a density of $2x10^6$/mL were treated with 0, 0.5, 1.5 and 2 µM camptothecin for 16-hours to induce apoptosis. AnnV and PI staining, assessed by flow cytometry, was used to determine the level of non-apoptotic ($AnnV^-PI^-$), early ($AnnV^+PI^-$) or late apoptotic ($AnnV^+PI^+$) Jurkat cells. Non-camptothecin Jurkat cells remained $AnnV^-PI^-$; whilst all camptothecin treated cells had a large population of $AnnV^+PI^+$ cells, and a small transient population that could be $AnnV^+PI^-$. Gates were defined on the basis of single stained controls. Representative dot plots.

5.8 Circulating human IgM preferentially bind a subpopulation of $AnnV^+PI^+$ Jurkat cells

We then aimed to ascertain whether human Jurkat cells would demonstrate a similar IgM binding profile to that observed in murine thymocytes. Jurkat cells were treated with camptothecin for 16-hours to induce apoptosis and exposed to PBS or 30% pooled normal human serum as a source of IgM. Apoptotic Jurkat cells were gated on the basis of AnnV positivity and the percentage of $AnnV^+IgM^+$ Jurkat cells was

determined (Figure 5.12A-C). A significant proportion of apoptotic Jurkat cells exposed to human serum were IgM^+ (Student's *t*-test; $P < 0.0001$; $n = 4$) compared to those incubated in PBS (Figure 5.12B). As observed in murine apoptotic thymocytes, Jurkat cells exposed to human serum also consisted of three distinct populations (Figure 5.12C) including an $AnnV^-IgM^-$ population that comprised of non-apoptotic cells. In addition, despite all $AnnV^+$ cells being PI^+, two $AnnV^+$ populations were evident being either $AnnV^+IgM^-$ or $AnnV^+IgM^+$. These $AnnV^+IgM^-$ and $AnnV^+IgM^+$ cell populations occupied relatively distinct regions of FSC/SSC contour plots (Figure 5.12D), although the downward shift of $AnnV^+IgM^+$ cells in relation to $AnnV^+IgM^-$ cells was subtler than that observed in murine thymocytes (Figure 5.4B).

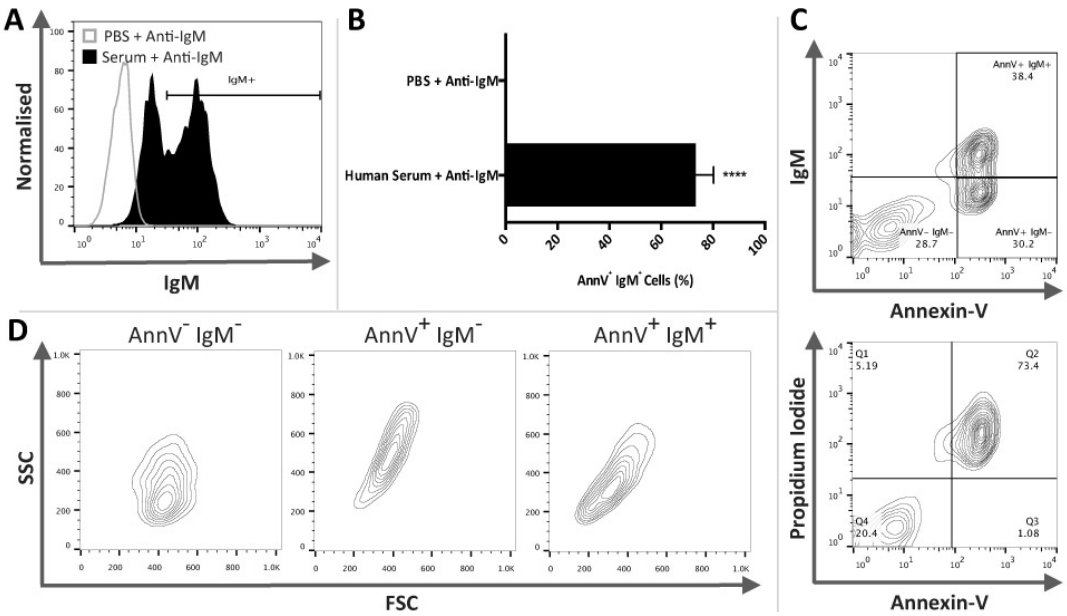

Figure 5.12 - IgM binds $AnnV^+$ PI^+ human Jurkat cells. Human Jurkat cells were treated with 0.5 µM camptothecin for 16-hours to induce apoptosis and exposed to PBS or 30% normal human serum as a source of IgM. AnnV and PI staining was used to determine the level of non-apoptotic ($AnnV^-PI^-$), early ($AnnV^+PI^-$) or late apoptotic ($AnnV^+PI^+$) Jurkat cells. Staining was assessed by flow cytometry. **A**) Representative histogram illustrating IgM binding to $AnnV^+$ apoptotic Jurkat cells within human serum and PBS treatment groups. **B**) Apoptotic Jurkat cells were gated on the basis of AnnV positivity and the percentage of $AnnV^+IgM^+$ Jurkat cells was assessed. Apoptotic Jurkat cells exposed to human serum exhibited significant IgM binding. ($n = 4$) **C**) Samples exposed to human plasma consisted of three distinct populations: $AnnV^-IgM^-$, $AnnV^+IgM^-$ and $AnnV^+IgM^+$. Apoptotic Jurkat cells were largely $AnnV^+PI^+$. **D**) The three distinct populations present in samples exposed to human serum were further characterised by examining FSC/SSC profiles. Although both $AnnV^+IgM^-$ and $AnnV^+IgM^+$ populations were $AnnV^+PI^+$ they occupy distinct and separate regions of FSC/SSC contour plots.

5.9 Circulating IgM binding to apoptotic human Jurkat cells appears membrane restricted

The morphology of IgM bound apoptotic Jurkat cells was analysed by confocal microscopy. As figure 5.13 illustrates apoptotic Jurkat cells exhibited AnnV and some IgM positive staining that appeared restricted to the membrane, whilst non-apoptotic Jurkat cells displayed no positive staining as expected. Some IgM staining that appeared intracellular was also evident.

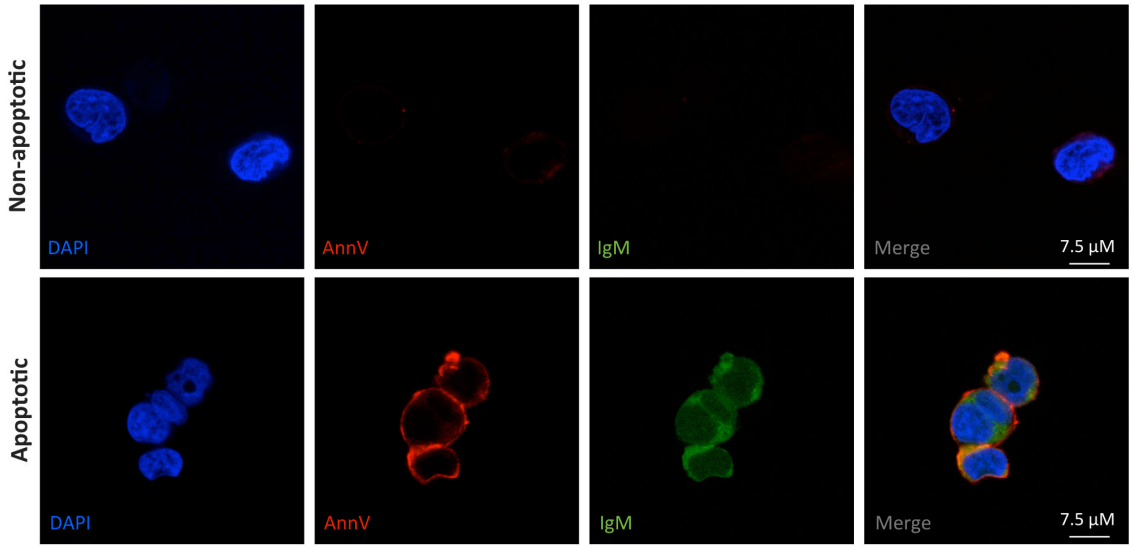

Figure 5.13 - IgM binding to apoptotic human Jurkat cells appears membrane restricted. Human Jurkat cells were treated with camptothecin for 16-hours to induce apoptosis. Jurkat cells were then exposed to 30% human serum as a source of IgM. Confocal microscopy revealed that whilst non-apoptotic Jurkat cells remained negative, late apoptotic Jurkat cells exhibited AnnV staining which appeared to be restricted to the membrane. Non-apoptotic Jurkat cells were also IgM negative. IgM staining on late apoptotic Jurkat cells appeared in the region of the plasma membrane with intracellular staining also evident. Representative images.

5.10 Circulating IgM binds strongly to saponin permeabilised human Jurkat cells

IgM binding to saponin permeabilised non-apoptotic Jurkat cells was assessed to determine if human IgM could bind intracellular epitopes within normal cells (n = 3 per group). Following permeabilisation non-apoptotic Jurkat cells were predominantly PI and IgM positive (>98%), whilst non-saponin treated non-apoptotic Jurkat cells remained consistently PI and IgM negative (Figure 5.14A). Confocal microscopy further

confirmed these results as permeabilised non-apoptotic Jurkat cells were AnnV^{+}, indicating permeability, and IgM^{+} with IgM appearing to bind in the region of the cell membrane (Figure 5.14B). IgM staining that appeared to be intracellular was also evident.

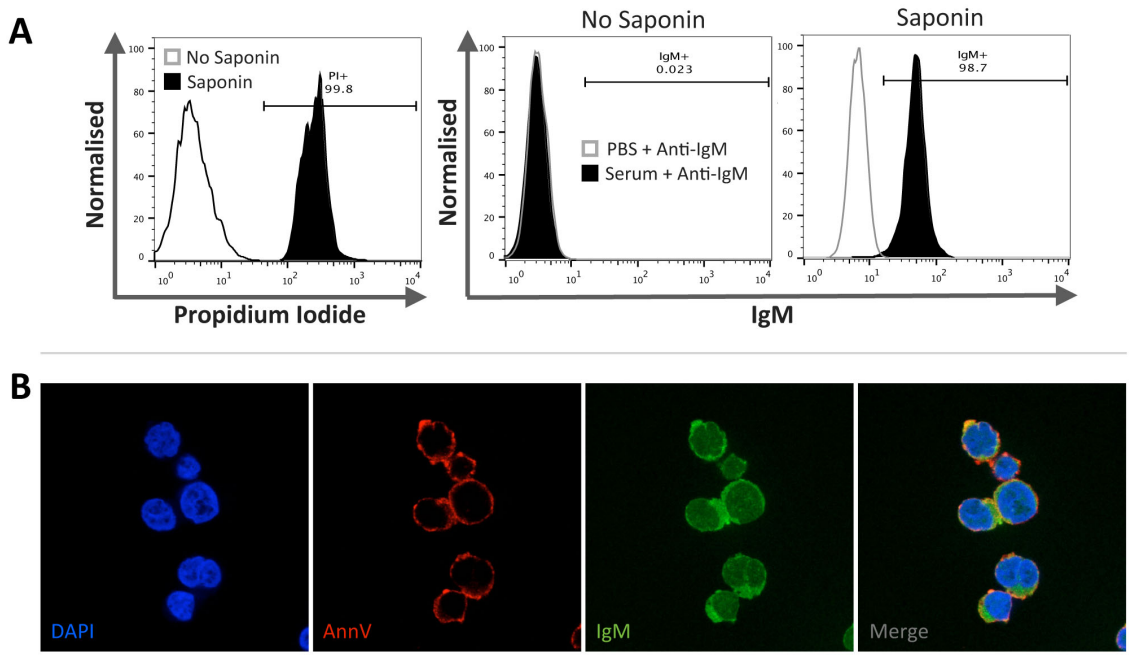

Figure 5.14 - IgM binds permeabilised non-apoptotic human Jurkat cells. Non-apoptotic Jurkat cells were permeabilised with saponin prior to incubation with human serum. **A**) Permeability was confirmed by PI staining and IgM binding was assessed by flow cytometry. Following permeabilisation non-apoptotic Jurkat cells were predominantly PI positive. Non-permeable non-apoptotic Jurkat cells remained consistently IgM negative, whilst permeable Jurkat cells were IgM positive. Representative histograms (*n* = 3 per group). **B**) Confocal microscopy revealed that permeabilised Jurkat cells exhibited AnnV staining that appears membrane restricted. IgM appeared to bind strongly in the plasma membrane region, but intracellular IgM staining was also evident. Representative images.

5.11 A 2-hour incubation with 25 µM H_2O_2 elicited mixed levels of apoptosis in human Jurkat cells

We sought to replicate the observed pattern of IgM binding to human Jurkat cells using a different apoptosis-inducing agent to further support our findings and confirm that binding was not specific for apoptosis induced by camptothecin. H_2O_2 was thus used to induce apoptosis and a titration was performed. Human Jurkat cells at a

density of $2x10^6$/mL were treated with 0, 0.5, 2.5, 5 and 25 µM H_2O_2 for 1-hour. AnnV and PI staining, assessed by flow cytometry, was used to determine the level of apoptosis. Non-H_2O_2 Jurkat cells remained $AnnV^-PI^-$ (Figure 5.15). The majority of Jurkat cells treated with 0.5 to 5 µM H_2O_2 remained $AnnV^-PI^-$ similar to non-treated samples (data not shown). Only Jurkat cells treated with 25 µM H_2O_2 demonstrated apoptosis with a small $AnnV^+PI^-$ population. In light of this data Jurkat cells were treated with 25 µM H_2O_2 for 2-hours and this elicited a population with mixed levels of apoptosis (approximately 38% $AnnV^-PI^-$, 30% $AnnV^+PI^-$ and 25% $AnnV^+PI^+$). Future experiments induced apoptosis in Jurkat cells by a 2-hour incubation in 25 µM H_2O_2.

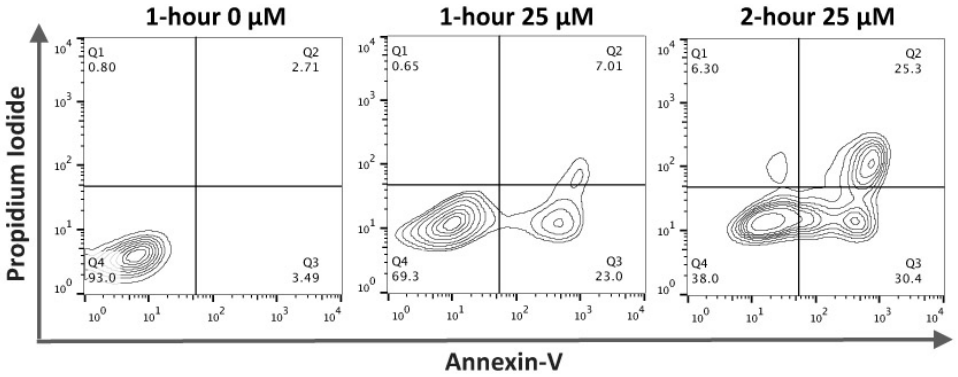

Figure 5.15 – Titration of H_2O_2 induced apoptosis in human Jurkat cells. Human Jurkat cells at a density of $2x10^6$/mL were treated with 0, 0.5, 1.5, 2, 5 and 25 µM H_2O_2 for 1-hour to induce apoptosis. AnnV and PI staining, assessed by flow cytometry, was used to determine the level of non-apoptotic ($AnnV^-PI^-$), early ($AnnV^+PI^-$) or late apoptotic ($AnnV^+PI^+$) Jurkat cells. Non-H_2O_2 Jurkat cells remained $AnnV^-PI^-$. Jurkat cells treated with 0.5 to 5 µM H_2O_2 remained $AnnV^-PI^-$ (not shown), only cells treated with 25µM H_2O_2 had a small $AnnV^+PI^-$ population. On the basis of this Jurkat cells were treated with 25 µM for 2-hours which induced a population with mixed levels of apoptosis. Representative dot plots.

5.12 Circulating IgM appears to bind $AnnV^+PI^+$ human Jurkat cells following H_2O_2 induced apoptosis, however FSC SSC contour plots of $AnnV^-IgM^-$ cells appear abnormal

IgM binding to non-apoptotic cells and Jurkat cells treated with 25 µM H_2O_2 exposed to PBS or human serum was assessed by flow cytometry. Apoptotic Jurkat cells were gated on the basis of AnnV positivity and the percentage of $AnnV^+IgM^+$ Jurkat cells was determined (Figure 5.16A-C). Apoptotic Jurkat cells demonstrated a shift towards IgM positivity (Figure 5.16A). As previously observed in camptothecin treated Jurkat cells (Figure 5.15C), two distinct $AnnV^+$ populations were present, $AnnV^+IgM^-$ and

$AnnV^+IgM^+$, with apoptotic Jurkat cells being predominantly $AnnV^+PI^+$ (Figure 5.16B). Analysis of FSC SSC contour plots revealed that $AnnV^-IgM^-$ (also PI^-) cells had an abnormal morphology. As cells progress through apoptosis they move towards the lower left portion of FSC SSC plots, reflecting a loss of complexity and cell size indicative of apoptosis related morphological changes including cell shrinkage. The H_2O_2 $AnnV^-IgM^-$ population located to a region in which cells at an advanced stage of apoptosis are expected. This suggests that H_2O_2 had adversely affected cells. It was decided that the data obtained from this assay would be unreliable, and attempts to replicate IgM binding to H_2O_2 treated Jurkat cells were not continued.

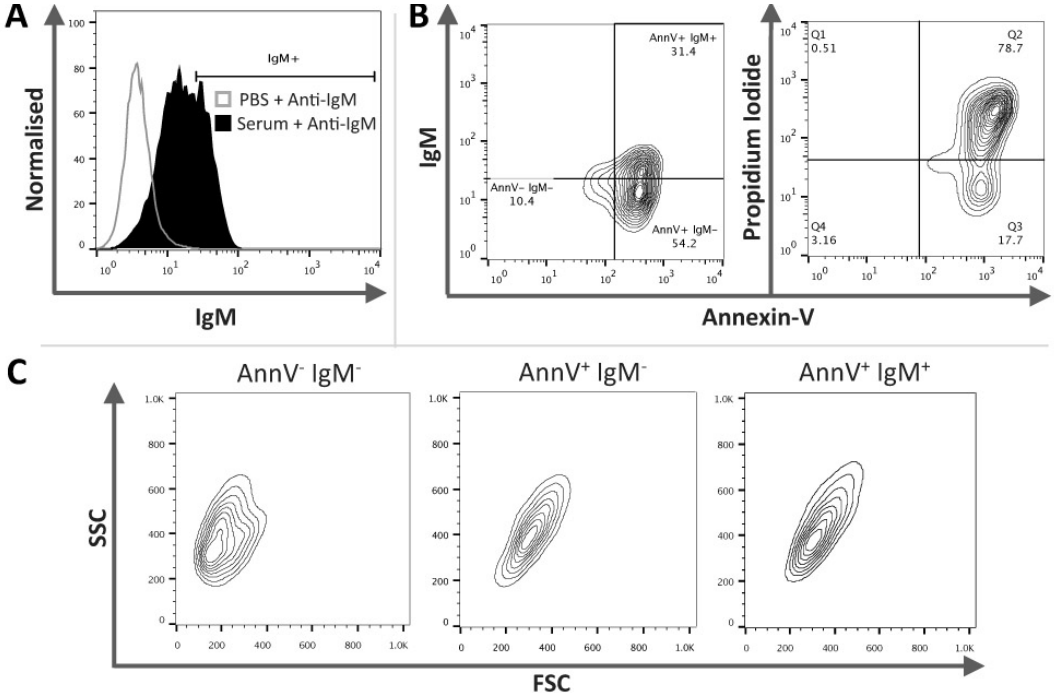

Figure 5.16 – IgM appears to bind $AnnV^+PI^+$ human Jurkat cells following H_2O_2 induced apoptosis, however FSC SSC contour plots of $AnnV^-IgM^-$ cells appear abnormal. Human Jurkat cells were treated with 25 µM H_2O_2 for 2-hours to induce apoptosis. Jurkat cells were then exposed to PBS or human serum (as a source of IgM). IgM binding was then assessed by flow cytometry. AnnV and PI staining, assessed by flow cytometry, was used to determine the level of non-apoptotic ($AnnV^-PI^-$), early ($AnnV^+PI^-$) or late apoptotic ($AnnV^+PI^+$) Jurkat cells. **A**) Representative histogram illustrating IgM binding to $AnnV^+$ apoptotic Jurkat cells within human serum and PBS treatment groups. **B**) Samples exposed to human plasma consisted of two populations: $AnnV^+IgM^-$ and $AnnV^+IgM^+$. Apoptotic Jurkat cells were largely $AnnV^+PI^+$. **D**) The two populations present in samples exposed to human serum were further characterised by examining FSC SSC. $AnnV^-IgM^-$ cells had an abnormal FSC SSC contour plot indicative of cell fragmentation and poor cellular morphology. Representative histograms and contour plots (*n* = 1 (in triplicate)).

5.13 Circulating IgM in human serum binds saponin permeabilised human proximal tubular epithelial cells

To determine if circulating IgM could interact with intracellular antigens present within non-lymphoid cells we examined IgM binding to saponin permeabilised human proximal tubular epithelial (HK-2) cells; a cell line derived from normal adult human kidney (Ryan et al., 1994) (Figure 5.17A). A distinct shift in PI positivity confirmed permeabilisation of saponin treated HK-2 cells (Figure 5.17B). Control non-permeabilised HK-2 cells remained consistently IgM^- whilst permeabilised HK-2 cells were IgM^+ (Figure 5.17C) (*n* = 3 per group).

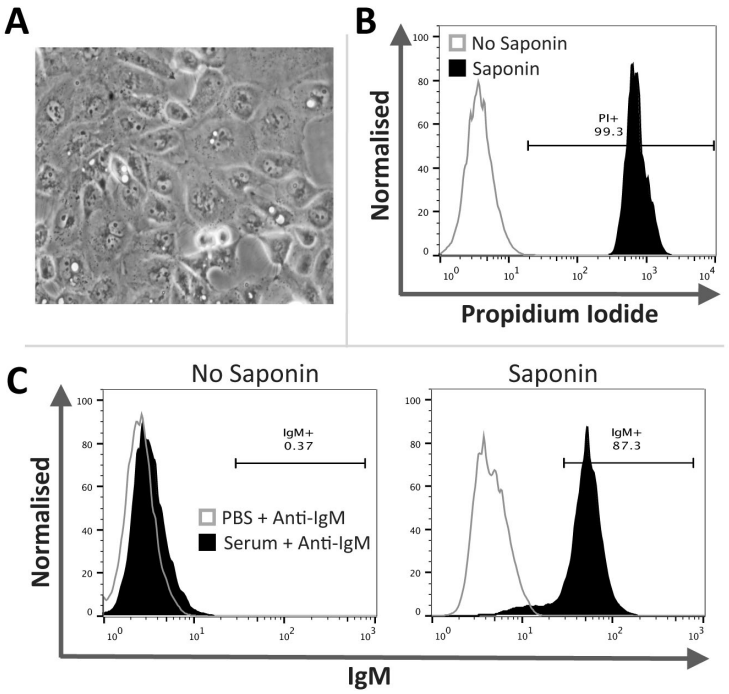

Figure 5.17 - IgM binds to permeable human proximal tubule epithelial (HK-2) cells. Non-apoptotic HK-2 cells (**A**) were permeabilised with saponin prior to incubation with human serum (as a source of IgM). Permeability was confirmed by PI staining and IgM binding was assessed by flow cytometry. **B**) Saponin treated HK-2 cells demonstrated a distinct shift in PI positivity indicating successful permeabilisation. **C**) Non-permeable HK-2 cells remained consistently IgM negative, whilst HK-2 cells treated with saponin were IgM positive. Representative histograms (*n* = 3 per group).

5.14 Circulating murine IgM specifically binds permeabilised erythrocytes

Confocal microscopy studies of $AnnV^{+}IgM^{+}$ apoptotic thymocytes and apoptotic Jurkat cells suggested IgM binding to the cell membrane together with some intracellular binding and it was thus possible that IgM also bound intracellular organelles. We therefore used murine erythrocytes as a simple anucleate target with no intracellular organelles and determined if circulating IgM bound permeabilised erythrocytes. Murine erythrocytes were studied due to the availability of both control murine IgM isotype antibodies and RAG1-deficient mice plasma to evaluate the specificity of any IgM binding seen. Erythrocytes were stained with the erythrocyte marker Ter-119 prior to permeabilisation with saponin. Ter-119 positivity was used to identify erythrocytes (Figure 5.18A). Successful permeabilisation of saponin treated erythrocytes was confirmed by AnnV positivity (Figure 5.18B) and the percentage of $Ter\text{-}119^{+}$ IgM^{+} erythrocytes was assessed (Figure 5.18C-D). IgM binding to control and saponin treated erythrocytes in isotype antibody treated or RAG1-deficient mice plasma and PBS treatment groups remained non-significant whilst permeabilised erythrocytes exposed to Balb/c plasma exhibited significant binding with 43.1 ±8.4% of erythrocytes being IgM^{+} (two-way ANOVA; $P < 0.0001$; $n = 4$).

5.15 IgM binding to apoptotic murine and apoptotic Jurkat cells appears to be calcium independent

In chapter 4 data presented demonstrated that ischaemic injured HK-2 cells did not bind IgM. Earlier IgM studies suggested that IgM binding might be influenced by calcium (McMullen et al., 2006). As the cell dissociation buffer and trypsin used to detach the HK-2 cells were diluted in EDTA (calcium chelator) (final concentration 0.4 mM EDTA) this may have resulted in IgM failing to remain bound thus leading to a false negative result. To assess whether the EDTA impaired IgM binding, our robust IgM binding detection assay was used to assess IgM positivity of apoptotic murine thymocytes and human Jurkat cells exposed to EDTA-diluted Balb/c plasma or EDTA-diluted human serum, respectively. The results suggest that it is unlikely that EDTA

influenced the previous findings as both apoptotic cell types incubated in EDTA-diluted plasma/serum demonstrated IgM positivity (Figure 5.19A&B).

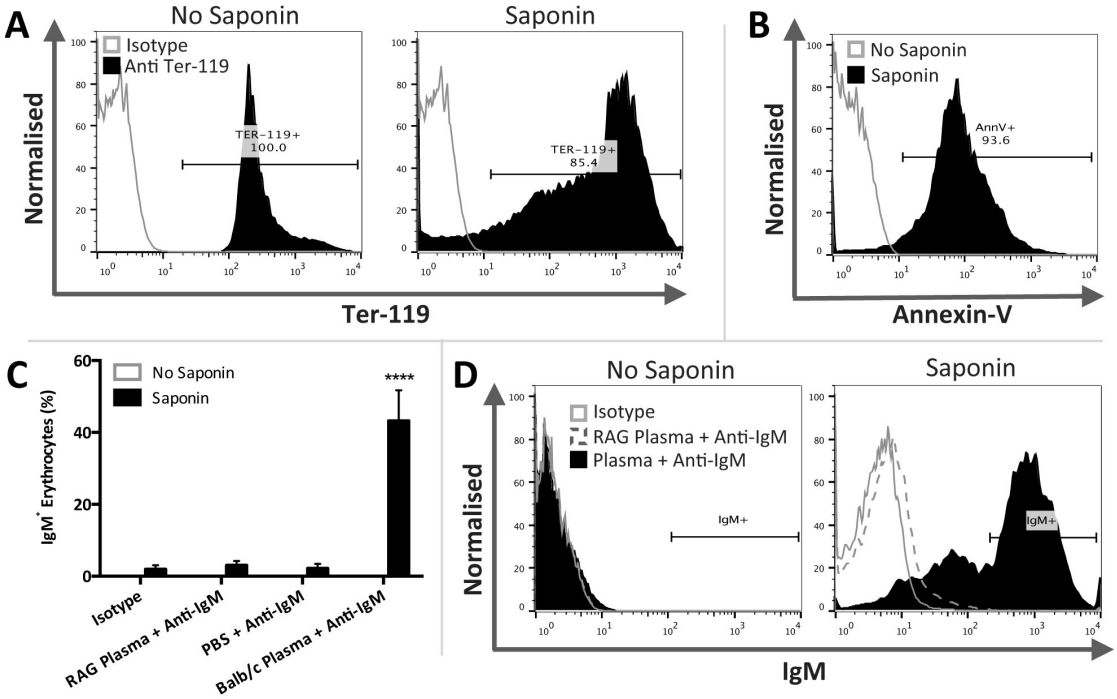

Figure 5.18 - IgM binds permeabilised murine erythrocytes. Murine erythrocytes were stained with the erythrocyte marker Ter-119 prior to permeabilisation with saponin. Annexin-V (AnnV) staining was used to confirm permeability. Non-permeable and permeable erythrocytes were then exposed to either murine IgM isotype control antibodies, PBS, Balb/c plasma (as a source of IgM) or plasma from immunodeficient RAG1-deficient mice. Staining was assessed by flow cytometry. **A**) Both non-permeable and permeable erythrocytes were identified and gated on the basis of Ter-119 positivity. **B**) Permeable Ter-119^{+} erythrocytes demonstrated a distinct shift in AnnV positivity indicating successful permeabilisation. **C**) Non-permeable and permeable erythrocytes were gated on the basis of Ter-119 positivity and the percentage of IgM^{+} erythrocytes was assessed. IgM binding to non-permeable and permeable erythrocytes in isotype antibody treated, RAG1-deficient mice plasma and PBS treatment groups remained non-significant. Permeable erythrocytes exposed to Balb/c plasma exhibited significant binding (n = 4 per group). **D**) Representative histograms illustrating IgM binding to non-permeable and permeable Ter-119^{+} erythrocytes within the treatment groups. Data expressed as means ±SEM.

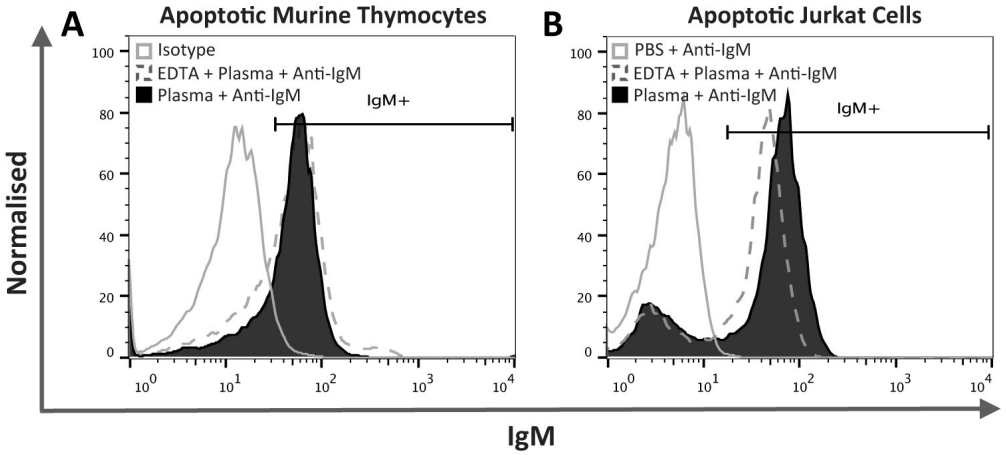

Figure 5.19 – IgM binding to apoptotic murine and apoptotic Jurkat cells is still detectable following EDTA-diluted plasma incubation. A) Murine thymocytes were rendered apoptotic by overnight culture. Thymocytes were exposed to murine anti-human isotype control antibodies, PBS, Balb/c plasma (as a source of IgM) or Balb/c plasma diluted in EDTA. IgM binding was detected in both EDTA-diluted and normal Balb/c plasma. **B**) Human Jurkat cells were treated with 0.5 µM camptothecin for 16-hours to induce apoptosis. Jurkat cells were then exposed to PBS or human serum as a source of IgM or human serum diluted in EDTA. IgM binding was then assessed by flow cytometry. IgM binding was detected in both EDTA-diluted and normal human serum. Representative histograms.

Summary

In this chapter, we have carefully characterised IgM binding to cells undergoing apoptosis and demonstrate robust binding of both human and murine IgM to a subset of cells that have exposed PtdSer (AnnV positive) and exhibit loss of membrane integrity (PI positive). Confocal and electron microscopy studies indicate that IgM binds to cells at a morphologically advanced stage of apoptosis with evident disruption of the plasma membrane. IgM binding thus requires loss of plasma membrane integrity allowing access to cytoplasmic or cell membrane antigens. In view of the non-redundant role for circulating IgM antibodies in the removal of dying cells and the prevention of autoimmunity, our findings provide important insights into the mechanism behind the preferential binding of IgM to subsets of apoptotic cells. Importantly, we show that IgM strongly binds non-apoptotic cells and erythrocytes that have undergone membrane permeabilisation suggesting that the epitopes bound are present within normal cells and not necessarily generated by the apoptotic process

per se. These findings suggest an important role for IgM in the recognition of nucleated cells and erythrocytes that have lost significant membrane integrity. These studies are thus relevant to the potential *in vivo* role of IgM antibodies in cell clearance during conditions characterised by severe cell damage such as ischaemic injury, sepsis and thrombotic microangiopathies.

The finding of C3 deposition being present on aged $AnnV^-$ murine thymocytes, but absent on fresh $AnnV^-$ thymocytes is quite interesting. Following traditional AnnV classification aged $AnnV^-$ cells would not be classified as apoptotic, as they have not yet exposed PtdSer, and would likely not be recognised by phagocytes. Yet fresh $AnnV^-$ PI^- remained C3 negative suggesting that additional novel membrane alterations occur early during apoptosis, prior to PtdSer exposure, which enable complement activation and opsonisation.

Chapter 6. Discussion

AKI induced by renal IRI is characterised by renal dysfunction, ATN, microvascular congestion and inflammation. The administration of exogenous apoptotic cells has been shown to reduce inflammation in experimental models of LPS-mediated shock, CIA, lung and liver inflammation. Preliminary data suggested that the intravenous administration of $20x10^6$ apoptotic thymocytes to FVB/n or Balb/c mice 24-hours prior to renal IRI protected renal function without affecting ATN 24-hours following IRI. In addition it appeared that IgM antibodies were deposited in the kidney 30-minutes following reperfusion. This thesis aimed to confirm these early finding and explore underlying testable hypothetical mechanisms. These examined if functional protection was conferred by apoptotic cell modulation of (a) circulating IgM antibodies, which are pathogenic in ischaemic injury in other organs or (b) coagulation status leading to improved intrarenal microvascular blood flow.

6.1 IgM antibody deposition is minimal following renal ischaemic injury, but is dramatic following hepatic ischaemia and in a model of AIH

IgM antibodies have an established role in the pathogenesis of intestinal, cardiac and skeletal muscle ischaemia where they bind neo-epitopes created in the injured reperfused tissue leading to complement activation that augments tissue injury. We sought to explore whether circulating IgM may be involved in the development of renal and hepatic ischaemia. We discovered striking differences in the kinetics of IgM deposition following both renal and hepatic ischaemic injury, and in a mouse model of AIH. Whilst IgM was minimally detected at 24-hours following renal injury, dramatic IgM deposition occurred 24-hours following both hepatic IRI and induction of AIH.

6.1.1 IgM antibodies are unlikely to play a direct role in the pathogenesis of renal ischaemia

In contrast to the numerous confirmatory studies illustrating how IgM antibodies augment intestinal, cardiac and skeletal muscle ischaemia, studies regarding IgM in

renal IRI are limited and contradictory (Burne-Taney et al., 2003, van der Pol et al., 2011, Lobo et al., 2012, Renner et al., 2010, Park et al., 2002). Park *et al.,* (2002) reported that Ig are not involved in renal IRI pathogenesis. This was based upon histological examination revealing the absence of Ig in kidneys harvested 1-30-minutes following bilateral renal IRI in C57BL/6 mice, and a lack of protection observed in RAG-1 mice. However, despite published work demonstrating the pathogenic nature of IgM in tissue ischaemia, a paper published in 2012 by Lobo *et al.,* suggested that IgM antibodies were in fact protective after renal IRI and cardiac allograft rejection. sIgM KO mice had more pronounced renal inflammation and dysfunction following bilateral renal IRI. Following reconstitution with purified IgM Lobo *et al,.* observed attenuation of renal inflammation. This protection was thought to be the result of IgM antibodies limiting T cell differentiation into pro-inflammatory Th-1 and Th-17 cells. This effect was accompanied by inhibition of TLR4 induced NF-kB nuclear translocation with a subsequent reduction in inflammatory pathways. It is important to note that the sIgM KO mice used in this study develop a clear autoimmune phenotype similar to SLE (Boes et al., 2000, Ehrenstein et al., 2000) with elevated production of IgG autoantibodies and the development of glomerulonephritis (Boes et al., 2000). This complicates the study of renal injury in these mice and comparison of injury to wild type mice is not a clear-cut approach.

The ambiguity surrounding the role of immunoglobulins in renal IRI is best illustrated by two contradictory studies by Burne-Taney *et al.,* (2003) and Renner *et al.,* (2010). Both studies induced bilateral renal ischaemia in B-cell deficient µMT mice, but while Renner *et al.,* observed increased renal dysfunction, Burne-Taney *et al.,* found µMT mice to be significantly protected from renal dysfunction. Our data in wild-type Balb/c mice suggest that IgM is unlikely to play a key direct role in the pathogenesis of renal IRI. Although statistically significantly IgM deposition was detected at 1-hour, the deposition was minimal and unlikely to have critical biological functional relevance. In addition, despite technical problems reducing the sample size, we also observed minimal C3 deposition.

We were unable to confirm the findings of van der Pol *et al.,* (2011) who demonstrated IgM binding, and subsequent C3 binding, to hypoxic human immortalized proximal tubular epithelial HK-2 cells. We used an assay similar to the hypoxia based one described, but induced oxidative injury by treatment with H_2O_2 and an additional ATP depletion assay using Antimycin A. Despite evident cellular apoptosis and a clear morphological injury, similar to that described by van der Pol *et al.,* IgM antibodies did not convincingly bind to injured HK-2 cells following H_2O_2 or Antimycin A treatment. These negative results were not due to the influence of EDTA or cleavage of IgM bound cell surface neo-epitopes. It is possible that the mode of cellular injury can alter/create different neo-epitopes to which IgM antibodies are able to bind thus explaining the detection of IgM binding to HK-2 cells injured by hypoxia by van der Pol *et al.* It is, however, important to note that van der Pol *et al.,* concluded that IgM and C3 bound to hypoxic HK-2 cells on the basis of an MFI of approximately 35, which would not be considered biologically relevant by some researchers.

The totality of our data suggests that IgM antibodies are unlikely to be directly involved in the development of renal injury following ischaemia. One possibility is that the lack of marked IgM deposition *in vivo* detected in kidney sections may be secondary to the sloughing of tubular cell that occurs following the ischaemic insult (Bonventre and Yang, 2011, Basile et al., 2012). Tubular cells undergo necrosis and may be shed into the tubular lumen and may thus be lost before IgM antibodies are able to bind. This seems unlikely as, despite remaining present throughout our *in vitro* assays, and progressing through apoptosis (Antimycin A treatment) or undergoing apparent primary necrosis (H_2O_2 treatment), human IgM failed to convincingly bind to injured HK-2 cells. It can be appreciated from the morphologically injury induced by 500mM H_2O_2 and 20µM Antimycin A that the HK-2 cells had drastically 'rounded'. It is possible, though unlikely, that this perhaps prevented access of the detection antibody to IgM bound epitopes.

IgM is a potent activator of the classical complement cascade and intestinal, cardiac

and skeletal muscle ischaemia are known to have strong complement involvement, most notably by the classical pathway (Chan et al., 2004, Weisman et al., 1990a, Hill et al., 1992, Lindsay et al., 1992, Weiser et al., 1996, Williams et al., 1999). However, similar to IgM, the involvement of complement in renal IRI is also controversial. Evidence is accumulating towards a dominant role for the alternative pathway, (Thurman et al., 2003, Zhou et al., 2000b, Thurman et al., 2005, Miwa et al., 2013), while other studies implicate MBL (van der Pol et al., 2012) or suggest no major role for complement (Park et al., 2001). Interestingly we did not find marked C3 deposition, which is generated following classical or alternative pathway activation, in ischaemic kidneys.

It is worth noting that the majority of studies establishing IgM antibodies to be pathogenic in intestinal, cardiac and skeletal ischaemia originate from one group, with supporting papers produced by affiliated groups (Austen et al., 2004, Zhang et al., 2004, Zhang et al., 2006a, Williams et al., 1999, Chan et al., 2004, Weiser et al., 1996, Zhang et al., 2006b, Zhang and Carroll, 2007, Haas et al., 2010, Chan et al., 2006). With the exception of different experimental readouts depending upon the ischaemic tissue type, and *in vitro* work, this group systematically studied IgM and complement deposition in wild type, reconstituted RAG-1 mice and complement deficient mice using similar techniques. This group discovered that a single IgM clone produced by a B-1 cell hybridoma ($IgM_{cm\text{-}22}$) bound NMHC-II and restored intestinal and cardiac ischaemic injury in RAG-1 mice. A non-affiliated study by Kulik *et al.,* (2009) also described an IgM clone (mAb B4) that was able to bind annexin IV and restore intestinal injury in RAG-1 mice. This is something that we had hoped to achieve in the renal IRI model, but was not pursued in light of our negative results indicating that IgM antibodies were not present following ischaemia. In contrast to studies of IgM antibodies in intestinal, cardiac and skeletal muscle ischaemia, our data suggests that IgM is unlikely to play a direct crucial role in renal IRI. It appears that IgM antibodies are not likely to be targets of novel therapeutics in the treatment of AKI induced by renal IRI.

6.1.2 IgM antibodies may be involved in the development of hepatic ischaemic injury and AIH

Unlike renal IRI there is no preceding ambiguity regarding the role of IgM antibodies in hepatic IRI, as their role is simply unknown. Although the role of Ig during and following hepatic IRI has not been directly studied, studies indicate that injury is reduced in RAG-1 mice suggesting that Ig may be partly involved in injury pathogenesis (Lappas et al., 2006, Feng et al., 2012).

In chapter 3 we determined whether IgM antibodies bound to injured liver tissue harvested between 0-hour and 7-days following hepatic IRI using robust, specific and carefully controlled IHC. The results were striking and in stark contrast to our renal IRI data. IgM was detected at 0-hours and accumulated progressively up to 24-hours post ischaemia, but appeared to have been resolved by 7-days. Moreover, tissue injury and IgM deposition illustrated a similar pattern and this finding does suggest that IgM antibodies were indeed binding to damaged tissue that may have neo-epitopes created/exposed following IRI. The finding of IgM deposition at 0-hours following hepatic ischaemia not only suggests that, residual blood prior to full reperfusion has sufficient IgM to allow binding detection, but indicates that neo-epitopes may be created/exposed during the ischaemic period. However, additional work is required to firmly establish this. It may be worth studying early time points in other models of ischaemia, as a similar finding was described during skeletal ischaemia (Chan et al., 2004). Other papers predominately study a 24-hour time point following reperfusion.

The pattern of IgM deposition following hepatic ischaemia was intriguing as it seemed to locate to the regions of the liver that may be vulnerable to hypoxic injury. Tissue injury was first evident around blood vessels with IgM appearing to infiltrate into the tissue at 0-hours following ischaemia. Both the injury and IgM staining became more pronounced in these regions at later time points.

It is possible to speculate that IgM antibodies may be involved, at least partially, in the

development of hepatic IRI, similar to intestinal, cardiac and skeletal muscle ischaemia. Studies demonstrate a strong role for complement in hepatic IRI with the administration of recombinant sCR1, a C3 inhibitor that blocks all complement pathways, attenuating injury in rats following hepatic IRI (Chavez-Cartaya et al., 1995, Lehmann et al., 2001, Lehmann et al., 1998). Similarly, C3 deficient mice exhibit attenuated injury following hepatic ischaemia (He et al., 2009a, He et al., 2009b) whilst inhibition of the classical pathway reduces hepatic ischaemic injury in rats (Heijnen et al., 2006). Some studies suggest that all 3 complement pathways are involved (Arumugam et al., 2004), all culminating in C5b-9 membrane attack complex (MAC) formation in cell membranes that kills liver cells (Fondevila et al., 2008). These studies indirectly support the possible involvement of IgM antibodies in hepatic IRI as IgM binding may be upstream of complement activation. Although the role of IgM during hepatic ischaemia requires further study a recent study by Diepnhorst *et al.,* (2014) described IgM deposition following hepatic IRI similar to our data. However in this study IgM reached a maximum at 12-hours and was reduced by 24-hours. C3 deposition followed a similar trend. The study did not examine what role IgM antibodies may play during injury.

It was important to determine whether IgM antibody deposition was found in a non-ischaemic form of hepatic injury in order to determine whether IgM may be involved in other forms of tissue injury. AIH, a chronic inflammatory condition, is characterised by the presence of autoantibodies that are thought to contribute to antibody-mediated cellular cytotoxicity and complement mediated tissue injury (Liberal et al., 2013, Krawitt, 2006, Mieli-Vergani and Vergani, 2011). Although the pathogenesis is thought to center around augmented pro-inflammatory $CD4^+$ and $CD8^+$ T-cell cytokine production, autoantibody generation is a characteristic of the ConA mouse model of AIH (Wang et al., 2012, Sass et al., 2002, Nakano et al., 2013). Interestingly, we demonstrated dramatic IgM deposition in ConA injured liver tissue. The pattern of IgM deposition was very similar to that observed following hepatic IRI with IgM antibodies deposited in areas of tissue necrosis suggesting neo-epitopes were created/exposed

during or following injury.

We have not extensively studied the role of IgM antibodies during hepatic ischaemia, or the mouse model of AIH. However, the detection of dramatic IgM deposition in both models suggests that it may play a role in the pathogenesis of injury as well as possibly the subsequent tissue repair. Whether IgM antibodies are protective, detrimental or neutral is yet to be determined.

6.1.3 Future Direction

Firstly, the low sample size of ischaemic and ConA injured liver tissue was a major limitation of these data and prevented any formal statistical analysis. This must be rectified before any meaningful conclusions can be drawn. In addition, it would be important to examine the human relevance of these data by assessing IgM antibody deposition in liver biopsy tissue harvested from patients. Possible tissue biopsy to be studied could include liver transplantation, AIH liver or paracetamol injured liver (as a source of necrotic tissue). Alternatively, another possibility would be to use primary human hepatocytes or human embryonic stem cell-derived hepatocytes (Medine et al., 2011) in an assay similar to that used to assess IgM binding to HK-2 cells. Also, if biopsy tissue is available it is crucial to determine whether AIH patients also demonstrate IgM binding to injured liver tissue, as autoantibodies in AIH are predominantly IgG (Krawitt, 2006). It is equally important to confirm that in humans hepatic ischaemia activates, at least in part, the classical complement pathway, as this has not been extensively studied (Straatsburg et al., 2000).

These data suggest that IgM antibodies may be involved in hepatic ischaemia and ConA induced AIH and their exact role be it pathogenic, protective or neutral needs to be dissected. This should consist of a systematic study utilizing various wild type, complement deficient and RAG-1 mice with subsequent IgM reconstitution. If IgM reconstitution restores the injury phenotype in RAG-1 mice this would suggest that IgM has a pathogenic role. In contrast, failure to restore injury may indicate that IgM

binding is a neutral event assuming that sufficient IgM can be replaced. It is possible that sIgM KO mice could be used in these studies although their tendency to develop SLE and altered immune state may complicate data interpretation in ConA induced AIH. An assessment of the deposition of key complement proteins including C3, C4 and MBL with regards to the location of IgM binding should also be determined as colocalisation would suggest that IgM is involved in the activation of complement.

How can we explain the differential deposition of IgM antibodies in injured renal and liver tissue? A rigorous assessment of endothelial permeability following ischaemic injury may shed light onto the disparate kinetics of IgM antibody deposition following renal and hepatic IRI. During intestinal and skeletal muscle ischaemia Williams *et al.,* (1999) and Chan *et al.,* (2004), respectively, reported that extravasation of ^{125}I-labeled bovine serum albumin and IgM binding to injured tissue followed a similar trend. This indicated that the microvascular endothelial cells need to be sufficiently permeable before IgM antibodies enter the tissue from the circulation to allow binding to occur. A similar line of investigation could be conducted for both renal and hepatic IRI, and possibly ConA induced AIH. If feasible in place of ^{125}I-labeled bovine serum albumin radiolabeled IgM antibodies could be used. This would be more informative given the size disparity between albumin (MW 69 kDa) and IgM (MW 970 kDa). It may be the case that IgM is readily able to enter the injured liver tissue but that it is not able to pass through the renal microvasculature.

These data has led us to conclude that IgM antibodies are unlikely to be directly involved in the pathogenesis of renal ischaemic injury. It is clear that further studies dissecting the role of complement during renal IRI are required. A thorough study utilizing various wild type, complement deficient mice and complement inhibitors with carefully controlled IHC is necessary. If these studies confirm that the alternative pathway is dominant throughout renal ischaemia then this would clarify the absence of IgM antibodies.

6.2 Apoptotic cell administration to mice modulates thrombin generation but is detrimental to renal function following renal ischaemia reperfusion injury

Exogenous apoptotic cell administration has been shown to reduce inflammation in experimental models of LPS-induced shock, CIA, bleomycin-induced lung inflammation and LPS-induced hepatitis (Lee et al., 2012, Gray et al., 2007, Ren et al., 2008, Zhang et al., 2011). With preliminary data suggesting that the administration of $20x10^6$ apoptotic thymocytes protected mice from renal dysfunction, but not ATN, following renal IRI we aimed to validate these early findings. We also intended to further explore the ability of apoptotic cells to influence coagulation status. We discovered that despite apoptotic cells being able to modulate thrombin generation, and in contrast to our preliminary data, apoptotic cell administration was not able to protect mice from renal IRI.

6.2.1 'Apoptotic cell therapy' is not translationally relevant for patients with ischaemic AKI

Although apoptotic cell administration is able to reduce inflammation in diverse experimental models (Lee et al., 2012, Gray et al., 2007, Ren et al., 2008, Zhang et al., 2011, Huynh et al., 2002, Marriott et al., 2006, Sun et al., 2004), the data presented in chapter 4 indicates that apoptotic cells do not protect mice from renal IRI. Whilst early apoptotic cells had no effect on severe renal IRI, the administration of early or late apoptotic cells prior to mild or moderate renal IRI respectively resulted in a further increase in plasma creatinine indicative of worse renal failure. This adverse effect was not the result of increased structural injury as ATN scores were comparable in PBS and apoptotic cell-treated mice.

While therapeutic interventions in the renal IRI model usually modulate both renal function and structure, functional protection alone has been observed in mice administered hemeoxygenase-1 overexpressing macrophages (Ferenbach et al., 2010). This protection was considered to be secondary to a dramatic reduction in $CD41^+$

platelet accumulation with improved microvascular blood flow and perfusion of non-injured functioning nephrons. As plasma creatinine values were higher in apoptotic cell treated mice than PBS treated controls in this study, it was hypothesised that apoptotic cell treated mice might exhibit an additional worsening of microvascular blood flow post ischaemia. However, this was found to be unlikely as microvascular congestion, inferred by renal fibrin and $CD41^+$ platelet IHC staining, was comparable in all PBS treated and apoptotic cell treated mice.

It is surprising that early apoptotic cells aggravated renal function as early apoptotic cells have generally been regarded as anti-inflammatory in comparison to late apoptotic cells which have been generally considered to be pro-inflammatory (Savill et al., 2002). However, Gray *et al.,* found apoptotic cells at an early or advanced stage of apoptosis provided equal protection from CIA (Gray et al., 2007). Importantly, apoptotic cell-derived protection does not appear to be restricted to one cell type. The administration of between $10x10^6$ to $30x10^6$ apoptotic neutrophils (Ren et al., 2008), thymocytes (Gray et al., 2007), splenocytes (Zhang et al., 2011) and human Jurkat T cells (Lee et al., 2012, Huynh et al., 2002) have all elicited protection from inflammation in mice. In this thesis $20x10^6$ apoptotic thymocytes were administered to mice 24-hours prior to renal IRI and it is unlikely that either the apoptotic cell type or number contributed to the neutral or detrimental effect on renal function.

Apoptosis and necrosis are key events in renal tubular cells following ischaemic injury (Daemen et al., 2002) with inhibition of apoptosis attenuating renal inflammation (Daemen et al., 1999). However, the level of ATN did not differ between PBS and apoptotic cell-treated mice indicating that increased necrosis/apoptosis of renal tubular cells did not occur following ischaemic injury. Furthermore, no discernable difference in neutrophil infiltration was observed, suggesting that apoptotic cell administration did not result in increased renal inflammation.

Despite previously published work demonstrating the striking ability of apoptotic cells

to modulate inflammation in multiple organs (Fadok et al., 1998, Gray et al., 2007, Lee et al., 2012, Ren et al., 2008, Zhang et al., 2011, Huynh et al., 2002, Marriott et al., 2006, Sun et al., 2004) these data indicate that both early and late apoptotic cells were not protective in renal IRI. Indeed, depending upon the severity of ischaemic injury, the administration of both early and late apoptotic cells may further impair renal function with this effect unlikely to be secondary to any contaminating viable non-apoptotic cells in the cell populations administered.

These studies have not extensively probed the potential mechanisms involved in the worsening of acute kidney dysfunction by early or late apoptotic cells. Apoptotic cells express PtdSer which, in addition to being involved in the phagocytic removal of apoptotic cells, may activate the coagulation system (Vance and Steenbergen, 2005). Also, thymocytes typically undergo marked cell blebbing during the apoptotic process and it is possible that they may generate many millions of small microparticles that express PtdSer following intravenous administration. It is thus possible that apoptotic cell administration might modulate the coagulation status of recipient mice and affect the microvascular response to renal IRI. In support of this we demonstrated platelet/apoptotic cell interaction *in vitro* and delayed thrombin generation in apoptotic cell treated mice not undergoing renal IRI. Interestingly, we did see a trend to increased platelet and fibrin deposition in mild renal IRI following administration of early apoptotic cells and moderate renal IRI following administration of late apoptotic cells but it was non-significant.

Early apoptotic cells contained some PI positive cells that have lost membrane integrity whilst the majority of late apoptotic cells were PI positive. Admittedly we did not undertake a direct head-to-head comparison of the effects of early and late apoptotic cells, and it is possible that the adverse effects of late apoptotic cells might involve the release of intracellular damage-associated molecular pattern molecules such as high-mobility group box chromosomal protein 1 that may activate cells via Toll-like receptor 4 (Zhao et al., 2014).

In contrast to the apoptotic cell-derived protection observed in other diverse inflammatory models, these data indicate 'apoptotic cell therapy' does not have translational relevance for patients with AKI induced by IRI. It was hoped that apoptotic cells could be administered to patients prior to surgery, such as cardiac surgery, in an attempt to limit pot-operative AKI. It thus appears that apoptotic cell administration is not inherently anti-inflammatory in all models of acute inflammation.

6.2.2 Apoptotic cells modulate blood coagulation

The influence of apoptotic cells on coagulation status is a thought provoking yet overlooked area. Exposure of PtdSer confers apoptotic cells with a striking ability to influence diverse pathways, but most notably in this thesis – coagulation status (Vance and Steenbergen, 2005). It is known that phospholipids promote blood coagulation by acting as catalytic surfaces that facilitate interactions between coagulation factors (Barton, 1967, Zwaal et al., 1998, Pickering et al., 2008). PtdSer is able to regulate the central blood clotting cascade protein thrombin and is considered a potent modulator of coagulation (Zwaal et al., 1998, Gerads et al., 1990, Casciola-Rosen et al., 1996). For instance PtdSer externalisation on activated platelets is known to promote the conversion of prothrombin to thrombin via coagulation factor Xa (Bevers et al., 1983, Monroe et al., 2002). Platelets are important regulators of coagulation and thrombin generation and interestingly we found that apoptotic thymocytes were able to bind to murine platelets *in vitro.* Such an interaction could lead to an extensive amplification of catalytic surfaces available to coagulation factors.

In a Russell viper venom assay apoptotic HeLa cells and human endothelial cells were found to be considerably procoagulant by Casciola-Rosen *et al.,* (1996). We discovered that apoptotic thymocyte treated mice exhibited significantly delayed thrombin generation, whilst the total amount of thrombin produced remained unchanged. Although preliminary, this data hints towards another pathway whereby apoptotic cells may be able to influence coagulation status.

With apoptotic cells rich in externalised phospholipids able to interact with coagulation cascade factors, that in addition to PtdSer include phosphatidylcholine and phosphatidylethanolamine, it is widely accepted that apoptotic cells influence coagulation. Despite this, however, the numbers of studies that directly show or study the effects of apoptotic cells modulation of coagulation are limited (Casciola-Rosen et al., 1996). Although brief these data further confirm that apoptotic cells are able to significantly alter coagulation status. With the increased prevalence of studies interested in 'apoptotic cell therapy', this is a topic that merits further investigation.

6.2.3 Future Direction

In regards to apoptotic cells and coagulation it would be useful to discern whether the observed phenotype was the result of PtdSer exposure alone, other apoptotic cell-coagulation protein interactions or a combination. Casciola-Rosen *et al.,* (1996) revealed that the ability of apoptotic HeLa cells and human endothelial cells to influence coagulation was solely due to PtdSer exposure. Anti-PtdSer antibody abolished any procoagulant effect. A similar approach could be adopted for future experiments in which the coagulability of plasma samples from mice receiving apoptotic cells treated with various anti-phospholipid antibodies is assessed. It is also important to confirm that our results are not restricted to apoptotic thymocytes, and that non-apoptotic cells do not alter coagulation. In addition, although technically more challenging, it is crucial that the human relevance of these finding is determined. One such approach could be to treat human blood samples with human apoptotic Jurkat cells, or apoptotic neutrophils and measure coagulability by a TGA. However, careful consideration regarding the selection of the anti-coagulants used in the collection of blood is required.

6.3 Circulating IgM antibodies requires membrane disruption to bind apoptotic and non-apoptotic cells, and may promote the clearance of disrupted nucleated cells and erythrocytes

Circulating IgM antibodies play a non-redundant role in apoptotic cell clearance, evident by the development of autoimmune disease in IgM-deficient mice (Boes et al., 2000, Ehrenstein et al., 2000). IgM binding to late apoptotic cells (Litvack et al., 2010, Fu et al., 2007, Zwart et al., 2004, Ciurana and Hack, 2006, Porcheray et al., 2013) leads to complement activation and subsequent opsonisation of IgM^+ cells by complement components that may be recognised by phagocytes (Chen et al., 2009c, Quartier et al., 2005, Chen et al., 2009a, Ogden et al., 2005). In chapter 5 we carefully explored the binding of circulating IgM to apoptotic cells, both human and murine, at different apoptotic stages. We demonstrated that IgM antibody binding requires significant plasma membrane disruption thereby allowing access to cytoplasmic or cell membrane antigens.

6.3.1 Circulating IgM antibodies illustrate a preference for late apoptotic cells due to plasma membrane disruption

Apoptosis consists of multiple temporal stages defined by morphological changes such as nuclear pyknosis, cytoplasmic vacuolation, cell shrinkage and the presence or absence of plasma membrane integrity (Elmore, 2007, Kerr et al., 1972, Galluzzi et al., 2007). A key finding of this work is that IgM binds a subpopulation of $AnnV^+PI^+$ apoptotic thymocytes with IgM^+ cells exhibiting a different FSC/SSC profile to $AnnV^+PI^+$ apoptotic thymocytes that were IgM^-. IgM binding specificity was confirmed by the absence of binding to $AnnV^+PI^+$ thymocytes in experiments using immunoglobulin-deficient plasma from RAG1-deficient mice or isotype IgM antibodies.

These data suggested a fundamental difference in the properties of $IgM^+AnnV^+PI^+$ apoptotic thymocytes, with potential epitopes bound by IgM either being absent or inaccessible in $IgM^-AnnV^+PI^+$ thymocytes. Confocal microscopy imaging analysis of FACS sorted cells suggested that IgM may bind the cell membrane of $AnnV^+IgM^+$ thymocytes and that the membrane of these cells was disrupted. Electron microscopy studies of FACS sorted cells were therefore undertaken, revealing important morphological

features of these distinct cell populations. Non-apoptotic $AnnV^-PI^-IgM^-$ cells exhibited a normal nucleus together with organelles and an intact plasma membrane. Apoptotic $AnnV^+PI^+IgM^-$ cells exhibited a pyknotic nucleus with intracellular organelles and a predominantly intact cell membrane. Apoptotic $AnnV^+PI^+IgM^+$ cells exhibited nuclear pyknosis and intracellular organelles accompanied by marked disruption of the cell membrane with obvious 'holes' evident. The profound morphological changes evident in these IgM^+ apoptotic $AnnV^+PI^+$ cells are likely to account for their different FSC/SSC profile evident on flow cytometry.

These flow cytometry and morphological studies of IgM^+ or IgM^- apoptotic cells suggest that the binding of IgM (MW 970kDa) requires physical access to the cellular interior via a severely disrupted cell membrane. Such access is not provided by the loss of cell membrane integrity that is defined by positive staining with propidium iodide (MW 0.67kDa). This model is schematically depicted in Figure 6.1 in which apoptotic cells undergo a progressive and increasing loss of cell membrane integrity that culminates in large pentameric IgM (Czajkowsky and Shao, 2009, Feinstein and Munn, 1969) molecules being able to access and bind internal epitopes.

The relevance of our carefully controlled murine IgM binding data to human cells was provided by similar findings in studies of apoptotic Jurkat cells. IgM binding was confined to a subset of apoptotic $AnnV^+PI^+$ Jurkat cells that also exhibited a different FSC/SSC profile to $IgM^-AnnV^+PI^+$ cells. Similar to thymocytes, confocal microscopy suggested that IgM bound to apoptotic cells with plasma membrane disruption.

Our confocal imaging studies appeared to suggest that IgM antibodies bound in the region of the plasma membrane. However, we were not able to confirm this or discern which side of the plasma membrane IgM bound. The combined diameter of the mean plasma membrane (≈4-7nM) and pentameric IgM (≈30nM) (Czajkowsky and Shao, 2009) is beyond the standard distance in which techniques such as fluorescence resonance energy transfer (FRET) and immunogold are typically used. We decided that

convincing confirmatory localisation of IgM binding by FRET or immunogold labeling might be possible, but would be extremely challenging and was unfortunately not possible to perform during this thesis due to time constraints.

6.3.2 Epitopes bound by circulating IgM antibodies do not need to be modified by apoptosis

A key question concerned the nature of the epitopes recognized by IgM and whether these epitopes were generated *de novo* during apoptosis by caspases or other enzymes, or by other forms of cell stress, such as oxidation. Examination of IgM binding to saponin permeabilised cells revealed that all thymocytes became strongly IgM^+ following permeabilisation irrespective of whether they were non-apoptotic or apoptotic. Moreover no significant binding of IgM control isotype antibody was evident. Also, non-apoptotic Jurkat cells and human renal tubular (HK-2) cells became strongly IgM^+ following permeabilisation providing relevance to human disease. This also indicated that the presence of intracellular epitopes capable of IgM recognition is not confined to lymphoid cells.

Experiments examining IgM binding to permeabilised murine erythrocytes were undertaken as these cells represent a structurally simple target. Erythrocytes are anucleate with few organelles and a biochemically less complicated cell membrane compared to nucleated cells, such as lymphocytes. We found that IgM bound a significant proportion of permeabilised erythrocytes. Specificity of IgM binding was again demonstrated by the complete lack of binding of isotype IgM antibody and the absence of IgM binding to erythrocytes incubated in RAG1-deficient plasma. These data suggested that at least a proportion of epitopes recognised and bound by IgM are cell membrane associated.

It can be appreciated from Table 1.3 that IgM antibodies bind a diverse range of epitopes. Although it is clear that studies predominantly report binding to phospholipids that are modified during the apoptotic process such as by oxidation. Our

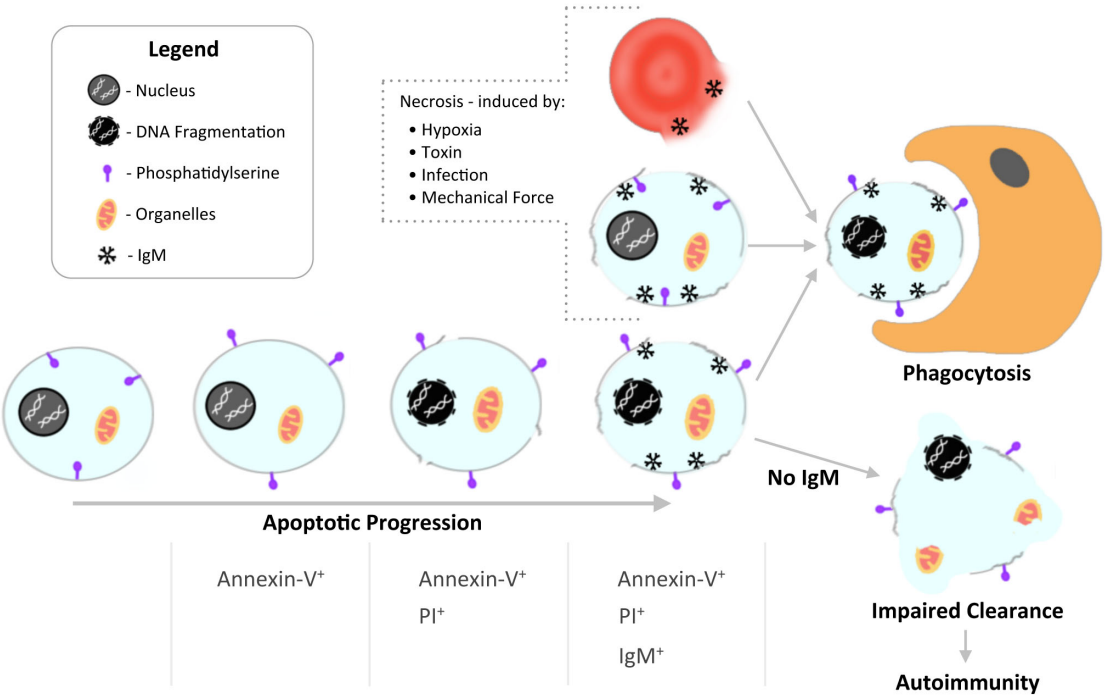

Figure 6.1 - Schematic diagram of IgM binding to apoptotic or disrupted cells. As cells progress through apoptosis IgM binding occurs at a point following phosphatidylserine exposure (AnnV binding) and loss of membrane integrity (PI binding). At this point IgM is able to bind intracellular cell membrane or cytoplasmic antigens. Similarly, IgM may bind any cells including lymphocytes or erythrocytes that have lost cellular integrity and have become permeable following cell necrosis or fragmentation. IgM binding represents an important signal for phagocytosis and thus promotes engulfment of cells (including nuclear material and organelles) before complete cellular disintegration that would promote the development of autoimmunity.

data suggests that IgM bound epitopes, such as membrane phospholipids, do not need to have been modified during apoptosis for IgM to bind. This is quite a pertinent finding as work by Kim *et al.,* (2002) indicates that IgM binding occurs following the activation of a specific phospholipase (iPLA2). This phospholipase remodels apoptotic cell membranes exposing IgM bound phospholipids. This further supports the notion that IgM binding is restricted by accessibility to IgM bound epitopes.

One point of concern for these studies was the use of saponin to permeabilise the plasma membrane and whether this artificially modified or damaged membrane phospholipids. This is unlikely to have occurred. Unlike organic solvents methanol and

acetone that permeablise by dissolving lipids, or the non-ionic detergent Triton-X, which extracts proteins and lipids, saponin, is a plant glycoside detergent that is able to permeablise by solubilizing cholesterol (Jamur and Oliver, 2010, Jacob et al., 1991). This allows saponin to selectively leave approximately 1μM sized holes in the membrane, leaving membrane architecture and antigens as well as and intracellular antigens largely unaltered (Hudder et al., 2003, Jamur and Oliver, 2010, Seeman et al., 1973, Jacob et al., 1991).

6.3.3 IgM binding may promote the clearance of nucleated cells and erythrocytes that have significantly disrupted membrane integrity

These data indicate that IgM is able to recognise and bind epitopes present within both normal and apoptotic nucleated cells. This suggests that IgM bound epitopes are not generated by the activation of caspase cascades associated with apoptosis. Indeed, the presence of such apoptosis-independent epitopes within normal cells could provide the substrate for IgM binding to cells that have undergone any form of cell lysis such as primary necrosis secondary to ischaemia etc. or cell injury induced by granzyme/perforin or complement (Figure 6.1). The binding of IgM to permeabilised erythrocytes is intriguing as previous work has shown that natural autologous IgG1 antibodies and complement are implicated in the recognition and clearance of senescent erythrocytes (Lutz and Bogdanova, 2013). Furthermore, natural IgM antibodies have been shown to bind exosomes derived from reticulocytes (Blanc et al., 2007a). There is little data available regarding the clearance of the fragmented normal erythrocytes generated in patients with conditions such as microangiopathic haemolytic anaemia. These fragmented erythrocytes may account for up to 6.9% of all circulating erythrocytes (Toba et al., 2004) and thus represent a significant cellular load that requires clearance by the reticuloendothelial system. Based upon our observations, we would speculate that IgM might play a role in the recognition and clearance of damaged erythrocytes that exhibit significant disruption of cell membrane integrity (Figure 6.1), though this will require further studies.

In conclusion, these flow cytometric and morphological studies indicate that circulating IgM specifically binds to cells that have progressed through apoptosis such that they have developed marked plasma membrane disruption that allows IgM to access intracellular epitopes. Studies of IgM binding to permeabilised lymphoid and parenchymal tissue cells indicate that both normal and apoptotic cells possess intracellular epitopes that can be recognised by IgM. Lastly, permeabilised erythrocytes also exhibit specific IgM binding. The totality of these data suggest that an important function of circulating IgM is to recognise and tag any nucleated circulating or resident tissue cell or erythrocytes that is severely damaged and exhibits significant plasma membrane disruption. Subsequent activation of complement and opsonisation would promote clearance of these severely damaged cells by phagocytes. Further work is required to define the role of circulating IgM in the specific clearance of nucleated cells and erythrocytes with severely compromised cell membranes *in vivo* in conditions such as ischemic injury, sepsis and thrombotic microangiopathies.

6.3.4 Complement protein C3 binds to aged thymocytes prior to PtdSer exposure

The efficiency of phagocytosis appears to be impressive as, despite an incidence of over 10^9 apoptotic cells per day, it is rare to observe apoptotic cells in normal tissue (Mochizuki et al., 1996, Scott et al., 2001, Elliott et al., 2009, Yang et al., 2006, Schrijvers et al., 2005, Gregory and Devitt, 2004). Reports in *Caenorhabditis elegans* indicated that apoptotic cells might be cleared before advanced stages of apoptosis are reached. These studies aided the discovery of 'find-me' and 'eat-me' signals on the apoptotic cell plasma membrane that act to communicate their status to phagocytes (Reddien et al., 2001, Hoeppner et al., 2001, Ravichandran, 2003, Lauber et al., 2003). A crucial and widely accepted 'eat-me' signal and hallmark of early apoptosis is PtdSer, exposure of which on apoptotic cell surfaces appears a requirement for clearance (Fadok et al., 2000, Fadok et al., 2001, Fadok et al., 1992, Kagan et al., 2002). Complement proteins are also involved in apoptotic cell recognition, promoting clearance by acting as molecular bridges between apoptotic and phagocyte cell surfaces although this is thought to occur late during apoptosis (Gaipl et al., 2001).

Unsurprisingly we found that C3 bound to thymocytes that had exposed PtdSer on their cell surface and would be considered apoptotic ($AnnV^+$). However, it was surprising to detect C3 bound to thymocytes not yet expressing PtdSer ($AnnV^-$) with the extent of deposition being markedly elevated in comparison to fresh thymocytes. This suggests that molecular determinants on dying cell plasma membranes may be recognised by complement proteins very early during apoptosis and prior to PtdSer exposure. With C3b present at low levels in the serum, due to spontaneous conversion of C3 to C3b, cells express membrane bound complement regulatory proteins. These regulators, such as CD59 and complement decay-accelerating factor (DAF or CD55) actively prevent C3b binding to protect the cell from complement activation (Zipfel and Skerka, 2009, Spendlove et al., 2006, Kimberley et al., 2007). During apoptosis these membrane complement regulators are lost meaning that C3b is able to bind and facilitate cell clearance by opsonization (Zipfel and Skerka, 2009). It is possible to hypothesise that phagocytes may be able to clear dying cells earlier than what is currently thought. These data, despite an admittedly low sample size, are quite intriguing and requires further investigation.

6.3.5 Future Direction

As discussed these studies did not define the epitopes bound by IgM antibodies on the plasma membrane or decipher which aspect of the plasma membrane binds IgM. However, on the basis of permeable cell experiments, it is likely that IgM bound to the inner plasma membrane though this should be confirmed in future studies. However, this is likely to be technically challenging. Although once optimized, techniques such as immunogold labeling or FRET could be used to dissect whether IgM antibodies used in these studies bound to phospholipids or intracellular membrane proteins. Alternatively, it may be possible to discern which cellular region (membrane, nuclear or cytoplasm) IgM antibodies bound.

It is well established that IgM binding promotes opsonisation of IgM^+ cells by

complement components and subsequent phagocytosis (Chen et al., 2009c, Quartier et al., 2005, Chen et al., 2009a, Ogden et al., 2005). Further work is necessary to demonstrate that $AnnV^{+}IgM^{+}$ are actively cleared by phagocytes in preference to $AnnV^{+}IgM^{-}$ cells. The generation of an adequate number of $AnnV^{+}IgM^{+}$ cells to enable electron microscopy was challenging, factoring in their fragile nature and the experimental length, and it may be difficult to acquire enough of these cells to enable phagocytosis assays. The same is true for permeabilised erythrocytes.

These data suggest that circulating IgM may be involved in the clearance of fragmented normal erythrocytes generated in patients with conditions such as microangiopathic haemolytic anaemia. Therefore, it must be confirmed that IgM are also able to recognise and bind to permeabilised or damaged human erythrocytes. Due to antibody 'stickiness' of erythrocytes in this thesis we opted to study IgM binding to permeabilised murine erythrocytes due to the availability of isotype antibody and RAG-1 plasma controls to ensure specificity of binding. Controls to ensure the specificity of human erythrocyte experiments could include the use of IgM depleted human plasma/serum.

Further studies probing C3 deposition on fresh, aged and apoptotic murine thymocytes are of course necessary to enable formal statistical analysis. It should also be confirmed that human Jurkat cells exhibit a similar finding, and whether other complement proteins, such as C1q, also bind prior to PtdSer exposure. Once this is confirmed macrophage phagocytic assay will need to be performed to demonstrate the relevance of this finding for dead cell clearance.

6.4 Overall Summary of Major Findings

This thesis set out to determine if preliminary data suggesting that apoptotic cells were able to limit renal dysfunction post renal ischaemia was the result of either of two hypothetical mechanisms of apoptotic cell-mediated functional protection. These were

to examine whether functional protection was conferred by apoptotic cell modulation of (a) circulating IgM antibodies, which are pathogenic in ischaemic injury in other organs or (b) coagulation status leading to improved intrarenal microvascular blood flow.

It became apparent that IgM antibodies were unlikely to play a direct role in injury pathogenesis, as IgM was not detected following renal IRI. This was found to be in stark contrast to the dramatic deposition of IgM antibodies following hepatic ischaemia and in a mouse model of AIH. The reason for this disparity remains unclear. It is possible that tissue accessibility may be a factor. Our cellular *in vitro* investigation indicates that the preferential binding of IgM antibodies to late apoptotic cells could be the result of apoptotic related membrane disruption that enables IgM to access intracellular antigens.

As it was unlikely that administered apoptotic cells reduced self-reactive IgM antibody levels thereby limiting complement augmented injury post ischaemia, as per our hypothesis, we focused our attention upon the ability of apoptotic cells to modulate coagulation status. We discovered that as well as binding platelets, apoptotic cells were able to delay thrombin generation. Despite this, unexpectedly, and in contrast to preliminary data, we found apoptotic cell administration to be neutral to renal functional following ischaemia, and depending upon injury severity may further impair renal dysfunction.

These data indicate that IgM antibodies are not likely to be targets of novel therapeutics, and that 'apoptotic cell therapy' is not translationally relevant in the treatment of AKI induced by renal ischaemia.

References

ALPER, C. A., JOHNSON, A. M., BIRTCH, A. G. & MOORE, F. D. 1969. Human C'3: evidence for the liver as the primary site of synthesis. *Science,* 163**,** 286-8.

ANANIA, C., GUSTAFSSON, T., HUA, X., SU, J., VIKSTROM, M., DE FAIRE, U., HEIMBURGER, M., JOGESTRAND, T. & FROSTEGARD, J. 2010. Increased prevalence of vulnerable atherosclerotic plaques and low levels of natural IgM antibodies against phosphorylcholine in patients with systemic lupus erythematosus. *Arthritis Res Ther,* 12**,** R214.

ARAGNO, M., CUTRIN, J. C., MASTROCOLA, R., PERRELLI, M. G., RESTIVO, F., POLI, G., DANNI, O. & BOCCUZZI, G. 2003. Oxidative stress and kidney dysfunction due to ischemia/reperfusion in rat: attenuation by dehydroepiandrosterone. *Kidney Int,* 64**,** 836-43.

ARUMUGAM, T. V., SHIELS, I. A., WOODRUFF, T. M., GRANGER, D. N. & TAYLOR, S. M. 2004. The role of the complement system in ischemia-reperfusion injury. *Shock,* 21**,** 401-9.

AUSTEN, W. G., JR., ZHANG, M., CHAN, R., FRIEND, D., HECHTMAN, H. B., CARROLL, M. C. & MOORE, F. D., JR. 2004. Murine hindlimb reperfusion injury can be initiated by a self-reactive monoclonal IgM. *Surgery,* 136**,** 401-6.

AVRAMEAS, S. 1991. Natural autoantibodies: from 'horror autotoxicus' to 'gnothi seauton'. *Immunol Today,* 12**,** 154-9.

AVRAMEAS, S., DIGHIERO, G., LYMBERI, P. & GUILBERT, B. 1983. Studies on natural antibodies and autoantibodies. *Ann Immunol (Paris),* 134D**,** 103-13.

BARTON, P. G. 1967. Sequence theories of blood coagulation re-evaluated with reference to lipid-protein interactions. *Nature,* 215**,** 1508-9.

BASILE, D. P. 2011. A GAP in our knowledge of vascular signaling in acute kidney injury. *Kidney international,* 80**,** 233-235.

BASILE, D. P., ANDERSON, M. D. & SUTTON, T. A. 2012. Pathophysiology of acute kidney injury. *Compr Physiol,* 2**,** 1303-53.

BECHERUCCI, F., MAZZINGHI, B., RONCONI, E., PEIRED, A., LAZZERI, E., SAGRINATI, C., ROMAGNANI, P. & LASAGNI, L. 2009. The role of endothelial progenitor cells in acute kidney injury. *Blood purification,* 27**,** 261-270.

BELLOMO, R., KELLUM, J. A. & RONCO, C. 2012. Acute kidney injury. *Lancet,* 380**,** 756-766.

BERNAL, W., AUZINGER, G., DHAWAN, A. & WENDON, J. 2010. Acute liver failure. *Lancet,* 376**,** 190-201.

BERNAL, W. & WENDON, J. 2013. Acute liver failure. *N Engl J Med,* 369**,** 2525-2534.

BEVERS, E. M., COMFURIUS, P. & ZWAAL, R. F. 1983. Changes in membrane phospholipid distribution during platelet activation. *Biochim Biophys Acta,* 736**,** 57-66.

BLANC, L., BARRES, C., BETTE-BOBILLO, P. & VIDAL, M. 2007a. Reticulocyte-secreted exosomes bind natural IgM antibodies: involvement of a ROS-activatable endosomal phospholipase iPLA2. *Blood,* 110**,** 3407-16.

BLANC, L., BARRES, C., BETTE-BOBILLO, P. & VIDAL, M. 2007b. Reticulocyte-secreted exosomes bind natural IgM antibodies: involvement of a ROS-activatable endosomal phospholipase iPLA2. *Blood,* 110**,** 3407-3416.

BOES, M., SCHMIDT, T., LINKEMANN, K., BEAUDETTE, B. C., MARSHAK-ROTHSTEIN, A. & CHEN, J. 2000. Accelerated development of IgG autoantibodies and autoimmune disease in the absence of secreted IgM. *Proc Natl Acad Sci U S A,* 97**,** 1184-9.

BONVENTRE, J. V. & YANG, L. 2011. Cellular pathophysiology of ischemic acute kidney injury. *J Clin Invest,* 121**,** 4210-21.

BONVENTRE, J. V. & ZUK, A. 2004. Ischemic acute renal failure: an inflammatory disease? *Kidney international,* 66**,** 480-485.

BREGGIA, A. C. & HIMMELFARB, J. 2008. Primary mouse renal tubular epithelial cells have variable injury tolerance to ischemic and chemical mediators of oxidative stress. *Oxid Med Cell Longev,* 1**,** 33-8.

BRILES, D. E., FORMAN, C., HUDAK, S. & CLAFLIN, J. L. 1982. Anti-phosphorylcholine antibodies of the T15 idiotype are optimally protective against Streptococcus pneumoniae. *J Exp Med,* 156**,** 1177-85.

BRILES, D. E., NAHM, M., SCHROER, K., DAVIE, J., BAKER, P., KEARNEY, J. & BARLETTA, R. 1981. Antiphosphocholine antibodies found in normal mouse serum are protective against intravenous infection with type 3 streptococcus pneumoniae. *J Exp Med,* 153**,** 694-705.

BURNE-TANEY, M. J., ASCON, D. B., DANIELS, F., RACUSEN, L., BALDWIN, W. & RABB, H. 2003. B cell deficiency confers protection from renal ischemia reperfusion injury. *Journal of immunology (Baltimore, Md. : 1950),* 171**,** 3210-3215.

BUSCHE, M. N., PAVLOV, V., TAKAHASHI, K. & STAHL, G. L. 2009. Myocardial ischemia and reperfusion injury is dependent on both IgM and mannose-binding lectin. *American journal of physiology. Heart and circulatory physiology,* 297**,** H1853-9.

CAMPBELL, N. A. & REECE, J. B. 2011. *Campbell Biology,* San Francisco, Calif: Benjamin Cummings.

CAMUS, S. M., GAUSSERÈS, B., BONNIN, P., LOUFRANI, L., GRIMAUD, L., CHARUE, D., DE MORAES, J. A., RENARD, J.-M., TEDGUI, A., BOULANGER, C. M., THARAUX, P.-L. & BLANC-BRUDE, O. P. 2012. Erythrocyte microparticles can induce kidney vaso-occlusions in a murine model of sickle cell disease. *Blood,* 120**,** 5050-5058.

CASALI, P. & NOTKINS, A. L. 1989. CD5+ B lymphocytes, polyreactive antibodies and the human B-cell repertoire. *Immunol Today,* 10**,** 364-8.

CASCIOLA-ROSEN, L., ROSEN, A., PETRI, M. & SCHLISSEL, M. 1996. Surface blebs on apoptotic cells are sites of enhanced procoagulant activity: implications for coagulation events and antigenic spread in systemic lupus erythematosus. *Proceedings of the National Academy of Sciences of the United States of America,* 93**,** 1624-1629.

CHAN, R. K., DING, G., VERNA, N., IBRAHIM, S., OAKES, S., AUSTEN, W. G., HECHTMAN, H. B. & MOORE, F. D. 2004. IgM binding to injured tissue precedes complement activation during skeletal muscle ischemia-reperfusion. *The Journal of surgical research,* 122**,** 29-35.

CHAN, R. K., VERNA, N., AFNAN, J., ZHANG, M., IBRAHIM, S., CARROLL, M. C. & MOORE, F. D. 2006. Attenuation of skeletal muscle reperfusion injury with intravenous 12 amino acid peptides that bind to pathogenic IgM. *Surgery,* 139**,** 236-243.

CHAVEZ-CARTAYA, R. E., DESOLA, G. P., WRIGHT, L., JAMIESON, N. V. & WHITE, D. J. 1995. Regulation of the complement cascade by soluble complement receptor type 1. Protective effect in experimental liver ischemia and reperfusion. *Transplantation,* 59**,** 1047-52.

CHEN, G., ZHANG, D., FUCHS, T. A., MANWANI, D., WAGNER, D. D. & FRENETTE, P. S. 2014. Heme-induced neutrophil extracellular traps contribute to the pathogenesis of sickle cell disease. *Blood,* 123**,** 3818-3827.

CHEN, Y., KHANNA, S., GOODYEAR, C. S., PARK, Y. B., RAZ, E., THIEL, S., GRONWALL, C., VAS, J., BOYLE, D. L., CORR, M., KONO, D. H. & SILVERMAN, G. J. 2009a. Regulation of dendritic cells and macrophages by an anti-apoptotic cell natural antibody that suppresses TLR responses and inhibits inflammatory arthritis. *J Immunol,* 183**,** 1346-59.

CHEN, Y., PARK, Y. B., PATEL, E. & SILVERMAN, G. J. 2009b. IgM antibodies to apoptosis-associated determinants recruit C1q and enhance dendritic cell phagocytosis of apoptotic cells. *Journal of immunology (Baltimore, Md. : 1950),* 182**,** 6031-6043.

CHEN, Y., PARK, Y. B., PATEL, E. & SILVERMAN, G. J. 2009c. IgM antibodies to apoptosis-associated determinants recruit C1q and enhance dendritic cell phagocytosis of apoptotic cells. *J Immunol,* 182**,** 6031-43.

CHIKAZAWA, M., OTAKI, N., SHIBATA, T., YASUEDA, T., MATSUDA, T. & UCHIDA, K. 2013. An apoptosis-associated mammary protein deficiency leads to enhanced production of IgM antibodies against multiple damage-associated molecules. *PloS one,* 8**,** e68468.

CHOU, M.-Y., FOGELSTRAND, L., HARTVIGSEN, K., HANSEN, L. F., WOELKERS, D., SHAW, P. X., CHOI, J., PERKMANN, T., BÄCKHED, F., MILLER, Y. I., HÖRKKÖ, S., CORR, M., WITZTUM, J. L. & BINDER, C. J. 2009a. Oxidation-specific epitopes are

dominant targets of innate natural antibodies in mice and humans. *The Journal of clinical investigation,* 119**,** 1335-1349.

CHOU, M. Y., FOGELSTRAND, L., HARTVIGSEN, K., HANSEN, L. F., WOELKERS, D., SHAW, P. X., CHOI, J., PERKMANN, T., BACKHED, F., MILLER, Y. I., HORKKO, S., CORR, M., WITZTUM, J. L. & BINDER, C. J. 2009b. Oxidation-specific epitopes are dominant targets of innate natural antibodies in mice and humans. *J Clin Invest,* 119**,** 1335-49.

CIURANA, C. L. F. & HACK, C. E. 2006. Competitive binding of pentraxins and IgM to newly exposed epitopes on late apoptotic cells. *Cellular immunology,* 239**,** 14-21.

COLMAN, R. W. 1969. Fragmentation of erythrocytes. *N Engl J Med,* 280**,** 563.

CONNOLLY, A. M., PESTRONK, A., MEHTA, S., YEE, W. C., GREEN, B. J., FELLIN, C., OLNEY, R. K., MILLER, R. G. & DEVOR, W. N. 1997. Serum IgM monoclonal autoantibody binding to the 301 to 314 amino acid epitope of beta-tubulin: clinical association with slowly progressive demyelinating polyneuropathy. *Neurology,* 48**,** 243-8.

CVETKOVIC, J. T., WALLBERG-JONSSON, S., AHMED, E., RANTAPAA-DAHLQVIST, S. & LEFVERT, A. K. 2002. Increased levels of autoantibodies against copper-oxidized low density lipoprotein, malondialdehyde-modified low density lipoprotein and cardiolipin in patients with rheumatoid arthritis. *Rheumatology (Oxford),* 41**,** 988-95.

CZAJKOWSKY, D. M. & SHAO, Z. 2009. The human IgM pentamer is a mushroom-shaped molecule with a flexural bias. *Proceedings of the National Academy of Sciences of the United States of America,* 106**,** 14960-14965.

DAEMEN, M. A., VAN 'T VEER, C., DENECKER, G., HEEMSKERK, V. H., WOLFS, T. G., CLAUSS, M., VANDENABEELE, P. & BUURMAN, W. A. 1999. Inhibition of apoptosis induced by ischemia-reperfusion prevents inflammation. *The Journal of clinical investigation,* 104**,** 541-549.

DAEMEN, M. A. R. C., DE VRIES, B. & BUURMAN, W. A. 2002. Apoptosis and inflammation in renal reperfusion injury. *Transplantation,* 73**,** 1693-1700.

DAHA, M. R. & VAN KOOTEN, C. 2000. Is the proximal tubular cell a proinflammatory cell? *Nephrology, dialysis, transplantation : official publication of the European Dialysis and Transplant Association - European Renal Association,* 15 Suppl 6**,** 41-43.

DHALIWAL, G., CORNETT, P. A. & TIERNEY, L. M. 2004. Hemolytic anemia. *American family physician,* 69**,** 2599-2606.

DIEPENHORST, G. M., DE GRAAF, W., NIESSEN, H. W., VAN VLIET, A. K., HACK, C. E. & VAN GULIK, T. M. 2014. Immunoglobulin M, C-reactive protein and complement activation in rat hepatic ischemia-reperfusion injury. *Eur Surg Res,* 52**,** 50-62.

DIEUDÉ, M., SENÉCAL, J.-L., RAUCH, J., HANLY, J. G., FORTIN, P., BRASSARD, N. & RAYMOND, Y. 2002. Association of autoantibodies to nuclear lamin B1 with thromboprotection in systemic lupus erythematosus: lack of evidence for a direct role of lamin B1 in apoptotic blebs. *Arthritis and rheumatism,* 46**,** 2695-2707.

EHRENSTEIN, M. R., COOK, H. T. & NEUBERGER, M. S. 2000. Deficiency in serum immunoglobulin (Ig)M predisposes to development of IgG autoantibodies. *J Exp Med,* 191**,** 1253-8.

EHRENSTEIN, M. R. & NOTLEY, C. A. 2010. The importance of natural IgM: scavenger, protector and regulator. *Nature reviews. Immunology,* 10**,** 778-786.

ELLIOTT, M. R., CHEKENI, F. B., TRAMPONT, P. C., LAZAROWSKI, E. R., KADL, A., WALK, S. F., PARK, D., WOODSON, R. I., OSTANKOVICH, M., SHARMA, P., LYSIAK, J. J., HARDEN, T. K., LEITINGER, N. & RAVICHANDRAN, K. S. 2009. Nucleotides released by apoptotic cells act as a find-me signal to promote phagocytic clearance. *Nature,* 461**,** 282-6.

ELLIOTT, M. R. & RAVICHANDRAN, K. S. 2010. Clearance of apoptotic cells: implications in health and disease. *The Journal of cell biology,* 189**,** 1059-1070.

ELMORE, S. 2007. Apoptosis: a review of programmed cell death. *Toxicologic pathology,* 35**,** 495-516.

ELTZSCHIG, H. K. & ECKLE, T. 2011. Ischemia and reperfusion--from mechanism to translation. *Nat Med,* 17**,** 1391-401.

ENESTRÖM, S., DRUID, H. & RAMMER, L. 1988. Fibrin deposition in the kidney in post-ischaemic renal damage. *British journal of experimental pathology,* 69**,** 387-394.

EPPIHIMER, M. J. & GRANGER, D. N. 1997. Ischemia/reperfusion-induced leukocyte-endothelial interactions in postcapillary venules. *Shock,* 8**,** 16-25.

ERWIG, L. P. & HENSON, P. M. 2007. Immunological consequences of apoptotic cell phagocytosis. *Am J Pathol,* 171**,** 2-8.

FADEEL, B. 2004. Plasma membrane alterations during apoptosis: role in corpse clearance. *Antioxid Redox Signal,* 6**,** 269-75.

FADOK, V. A., BRATTON, D. L., KONOWAL, A., FREED, P. W., WESTCOTT, J. Y. & HENSON, P. M. 1998. Macrophages that have ingested apoptotic cells in vitro inhibit proinflammatory cytokine production through autocrine/paracrine mechanisms involving TGF-beta, PGE2, and PAF. *The Journal of clinical investigation,* 101**,** 890-898.

FADOK, V. A., BRATTON, D. L., ROSE, D. M., PEARSON, A., EZEKEWITZ, R. A. & HENSON, P. M. 2000. A receptor for phosphatidylserine-specific clearance of apoptotic cells. *Nature,* 405**,** 85-90.

FADOK, V. A., DE CATHELINEAU, A., DALEKE, D. L., HENSON, P. M. & BRATTON, D. L. 2001. Loss of phospholipid asymmetry and surface exposure of phosphatidylserine is required for phagocytosis of apoptotic cells by macrophages and fibroblasts. *J Biol Chem,* 276**,** 1071-7.

FADOK, V. A., VOELKER, D. R., CAMPBELL, P. A., COHEN, J. J., BRATTON, D. L. & HENSON, P. M. 1992. Exposure of phosphatidylserine on the surface of apoptotic lymphocytes triggers specific recognition and removal by macrophages. *Journal of immunology (Baltimore, Md. : 1950),* 148**,** 2207-2216.

FEINSTEIN, A. & MUNN, E. A. 1969. Conformation of the free and antigen-bound IgM antibody molecules. *Nature,* 224**,** 1307-9.

FENG, M., LI, G., QIAN, X., FAN, Y., HUANG, X., ZHANG, F. & LU, L. 2012. IL-17A-producing NK cells were implicated in liver injury induced by ischemia and reperfusion. *Int Immunopharmacol,* 13**,** 135-40.

FERENBACH, D. A., RAMDAS, V., SPENCER, N., MARSON, L., ANEGON, I., HUGHES, J. & KLUTH, D. C. 2010. Macrophages expressing heme oxygenase-1 improve renal function in ischemia/reperfusion injury. *Molecular therapy : the journal of the American Society of Gene Therapy,* 18**,** 1706-1713.

FONDEVILA, C., SHEN, X. D., TSUCHIHASHI, S., UCHIDA, Y., FREITAS, M. C., KE, B., BUSUTTIL, R. W. & KUPIEC-WEGLINSKI, J. W. 2008. The membrane attack complex (C5b-9) in liver cold ischemia and reperfusion injury. *Liver Transpl,* 14**,** 1133-41.

FRIEDEWALD, J. J. & RABB, H. 2004. Inflammatory cells in ischemic acute renal failure. *Kidney international,* 66**,** 486-491.

FU, M., FAN, P.-S., LI, W., LI, C.-X., XING, Y., AN, J.-G., WANG, G., FAN, X.-L., GAO, T.-W., LIU, Y.-F. & IKEDA, S. 2007. Identification of poly-reactive natural IgM antibody that recognizes late apoptotic cells and promotes phagocytosis of the cells. *Apoptosis : an international journal on programmed cell death,* 12**,** 355-362.

FURUICHI, K., WADA, T., KANEKO, S. & MURPHY, P. M. 2008. Roles of chemokines in renal ischemia/reperfusion injury. *Front Biosci,* 13**,** 4021-8.

GAIPL, U. S., KUENKELE, S., VOLL, R. E., BEYER, T. D., KOLOWOS, W., HEYDER, P., KALDEN, J. R. & HERRMANN, M. 2001. Complement binding is an early feature of necrotic and a rather late event during apoptotic cell death. *Cell Death Differ,* 8**,** 327-34.

GAIPL, U. S., VOLL, R. E., SHERIFF, A., FRANZ, S., KALDEN, J. R. & HERRMANN, M. 2005. Impaired clearance of dying cells in systemic lupus erythematosus. *Autoimmunity reviews,* 4**,** 189-194.

GALLUZZI, L., MAIURI, M. C., VITALE, I., ZISCHKA, H., CASTEDO, M., ZITVOGEL, L. & KROEMER, G. 2007. Cell death modalities: classification and pathophysiological implications. *Cell Death Differ,* 14**,** 1237-43.

GEORGE, J. N. & NESTER, C. M. 2014. Syndromes of thrombotic microangiopathy. *N Engl J Med,* 371**,** 654-66.

GERADS, I., GOVERS-RIEMSLAG, J. W., TANS, G., ZWAAL, R. F. & ROSING, J. 1990. Prothrombin activation on membranes with anionic lipids containing phosphate, sulfate, and/or carboxyl groups. *Biochemistry,* 29**,** 7967-74.

GERSHOV, D., KIM, S., BROT, N. & ELKON, K. B. 2000. C-Reactive protein binds to apoptotic cells, protects the cells from assembly of the terminal complement components, and sustains an antiinflammatory innate immune response: implications for systemic autoimmunity. *J Exp Med,* 192**,** 1353-64.

GLADWIN, M. T., KANIAS, T. & KIM-SHAPIRO, D. B. 2012. Hemolysis and cell-free hemoglobin drive an intrinsic mechanism for human disease. *The Journal of clinical investigation,* 122**,** 1205-1208.

GLADWIN, M. T. & OFORI-ACQUAH, S. F. 2014. Erythroid DAMPs drive inflammation in SCD. *Blood,* 123**,** 3689-3690.

GRAY, M., MILES, K., SALTER, D., GRAY, D. & SAVILL, J. 2007. Apoptotic cells protect mice from autoimmune inflammation by the induction of regulatory B cells. *Proceedings of the National Academy of Sciences of the United States of America,* 104**,** 14080-14085.

GREENE, E. L. & PALLER, M. S. 1994. Calcium and free radicals in hypoxia/reoxygenation injury of renal epithelial cells. *Am J Physiol,* 266**,** F13-20.

GREGORY, C. D. & DEVITT, A. 2004. The macrophage and the apoptotic cell: an innate immune interaction viewed simplistically? *Immunology,* 113**,** 1-14.

GRÖNWALL, C., AKHTER, E., OH, C., BURLINGAME, R. W., PETRI, M. & SILVERMAN, G. J. 2012. IgM autoantibodies to distinct apoptosis-associated antigens correlate with protection from cardiovascular events and renal disease in patients with SLE. *Clinical immunology (Orlando, Fla.),* 142**,** 390-398.

HAAS, M. S., ALICOT, E. M., SCHUERPF, F., CHIU, I., LI, J., MOORE, F. D. & CARROLL, M. C. 2010. Blockade of self-reactive IgM significantly reduces injury in a murine model of acute myocardial infarction. *Cardiovascular research,* 87**,** 618-627.

HART, S. P., SMITH, J. R. & DRANSFIELD, I. 2004. Phagocytosis of opsonized apoptotic cells: roles for 'old-fashioned' receptors for antibody and complement. *Clin Exp Immunol,* 135**,** 181-5.

HARTVIGSEN, K., CHOU, M. Y., HANSEN, L. F., SHAW, P. X., TSIMIKAS, S., BINDER, C. J. & WITZTUM, J. L. 2009. The role of innate immunity in atherogenesis. *J Lipid Res,* 50 Suppl**,** S388-93.

HE, S., ATKINSON, C., EVANS, Z., ELLETT, J. D., SOUTHWOOD, M., ELVINGTON, A., CHAVIN, K. D. & TOMLINSON, S. 2009a. A role for complement in the enhanced susceptibility of steatotic livers to ischemia and reperfusion injury. *J Immunol,* 183**,** 4764-72.

HE, S., ATKINSON, C., QIAO, F., CIANFLONE, K., CHEN, X. & TOMLINSON, S. 2009b. A complement-dependent balance between hepatic ischemia/reperfusion injury and liver regeneration in mice. *J Clin Invest,* 119**,** 2304-16.

HEIJNEN, B. H., STRAATSBURG, I. H., PADILLA, N. D., VAN MIERLO, G. J., HACK, C. E. & VAN GULIK, T. M. 2006. Inhibition of classical complement activation attenuates liver ischaemia and reperfusion injury in a rat model. *Clin Exp Immunol,* 143**,** 15-23.

HELLBERG, P. O., BAYATI, A., KÄLLSKOG, O. & WOLGAST, M. 1990. Red cell trapping after ischemia and long-term kidney damage. Influence of hematocrit. *Kidney international,* 37**,** 1240-1247.

HESKETH, E. E., CZOPEK, A., CLAY, M., BORTHWICK, G., FERENBACH, D., KLUTH, D. & HUGHES, J. 2014. Renal ischaemia reperfusion injury: a mouse model of injury and regeneration. *Journal of visualized experiments : JoVE*.

HILL, J., LINDSAY, T. F., ORTIZ, F., YEH, C. G., HECHTMAN, H. B. & MOORE, F. D., JR. 1992. Soluble complement receptor type 1 ameliorates the local and remote organ injury after intestinal ischemia-reperfusion in the rat. *J Immunol,* 149**,** 1723-8.

HOEPPNER, D. J., HENGARTNER, M. O. & SCHNABEL, R. 2001. Engulfment genes cooperate with ced-3 to promote cell death in Caenorhabditis elegans. *Nature,* 412**,** 202-6.

HUDDER, A., NATHANSON, L. & DEUTSCHER, M. P. 2003. Organization of mammalian cytoplasm. *Mol Cell Biol,* 23**,** 9318-26.

HUYNH, M. L., FADOK, V. A. & HENSON, P. M. 2002. Phosphatidylserine-dependent ingestion of apoptotic cells promotes TGF-beta1 secretion and the resolution of inflammation. *J Clin Invest,* 109**,** 41-50.

IWATA, M., HERRINGTON, J. & ZAGER, R. A. 1995. Protein synthesis inhibition induces cytoresistance in cultured human proximal tubular (HK-2) cells. *Am J Physiol,* 268**,** F1154-63.

JACOB, M. C., FAVRE, M. & BENSA, J. C. 1991. Membrane cell permeabilization with saponin and multiparametric analysis by flow cytometry. *Cytometry,* 12**,** 550-8.

JAMUR, M. & OLIVER, C. 2010. Permeabilization of Cell Membranes. *In:* OLIVER, C. & JAMUR, M. C. (eds.) *Immunocytochemical Methods and Protocols.* Humana Press.

JANG, H. R., GANDOLFO, M. T., KO, G. J., SATPUTE, S. R., RACUSEN, L. & RABB, H. 2010. B cells limit repair after ischemic acute kidney injury. *Journal of the American Society of Nephrology : JASN,* 21**,** 654-665.

JENNEWEIN, C., TRAN, N., PAULUS, P., ELLINGHAUS, P., EBLE, J. A. & ZACHAROWSKI, K. 2011. Novel aspects of fibrin(ogen) fragments during inflammation. *Molecular medicine (Cambridge, Mass.),* 17**,** 568-573.

KAGAN, V. E., GLEISS, B., TYURINA, Y. Y., TYURIN, V. A., ELENSTROM-MAGNUSSON, C., LIU, S. X., SERINKAN, F. B., ARROYO, A., CHANDRA, J., ORRENIUS, S. & FADEEL, B. 2002. A role for oxidative stress in apoptosis: oxidation and externalization of phosphatidylserine is required for macrophage clearance of cells undergoing Fas-mediated apoptosis. *J Immunol,* 169**,** 487-99.

KAUSHAL, G. P., BASNAKIAN, A. G. & SHAH, S. V. 2004. Apoptotic pathways in ischemic acute renal failure. *Kidney Int,* 66**,** 500-6.

KERR, J. F., WYLLIE, A. H. & CURRIE, A. R. 1972. Apoptosis: a basic biological phenomenon with wide-ranging implications in tissue kinetics. *British journal of cancer,* 26**,** 239-257.

KERR, M., BEDFORD, M., MATTHEWS, B. & O'DONOGHUE, D. 2014. The economic impact of acute kidney injury in England. *Nephrology, dialysis, transplantation : official publication of the European Dialysis and Transplant Association - European Renal Association,* 29**,** 1362-1368.

KHATOON, F., MOINUDDIN, ALAM, K. & ALI, A. 2012. Physicochemical and immunological studies on 4-hydroxynonenal modified HSA: implications of protein damage by lipid peroxidation products in the etiopathogenesis of SLE. *Hum Immunol,* 73**,** 1132-9.

KIM, J. 2010. Identification of a human monoclonal natural IgM antibody that recognizes early apoptotic cells and promotes phagocytosis. *Hybridoma (Larchmt),* 29**,** 275-81.

KIM, S. J., GERSHOV, D., MA, X., BROT, N. & ELKON, K. B. 2002. I-PLA(2) activation during apoptosis promotes the exposure of membrane lysophosphatidylcholine leading to binding by natural immunoglobulin M antibodies and complement activation. *The Journal of experimental medicine,* 196**,** 655-665.

KIMBERLEY, F. C., SIVASANKAR, B. & PAUL MORGAN, B. 2007. Alternative roles for CD59. *Mol Immunol,* 44**,** 73-81.

KINA, T., IKUTA, K., TAKAYAMA, E., WADA, K., MAJUMDAR, A. S., WEISSMAN, I. L. & KATSURA, Y. 2000. The monoclonal antibody TER-119 recognizes a molecule associated with glycophorin A and specifically marks the late stages of murine erythroid lineage. *Br J Haematol,* 109**,** 280-7.

KINDT, T. J., GOLDSBY, R. A., OSBORNE, B. A. & KUBY, J. 2007. *Kuby immunology,* New York, W.H. Freeman.

KINSEY, G. R., LI, L. & OKUSA, M. D. 2008. Inflammation in acute kidney injury. *Nephron. Experimental nephrology,* 109**,** e102-7.

KRAWITT, E. L. 2006. Autoimmune hepatitis. *N Engl J Med,* 354**,** 54-66.

KULIK, L., FLEMING, S. D., MORATZ, C., REUTER, J. W., NOVIKOV, A., CHEN, K., ANDREWS, K. A., MARKARYAN, A., QUIGG, R. J., SILVERMAN, G. J., TSOKOS, G. C. & HOLERS, V. M. 2009. Pathogenic natural antibodies recognizing annexin IV

are required to develop intestinal ischemia-reperfusion injury. *J Immunol,* 182**,** 5363-73.

KUMAR, S., ALLEN, D. A., KIESWICH, J. E., PATEL, N. S., HARWOOD, S., MAZZON, E., CUZZOCREA, S., RAFTERY, M. J., THIEMERMANN, C. & YAQOOB, M. M. 2009. Dexamethasone ameliorates renal ischemia-reperfusion injury. *J Am Soc Nephrol,* 20**,** 2412-25.

KYRIAKIDES, C., WANG, Y., AUSTEN, W. G., JR., FAVUZZA, J., KOBZIK, L., MOORE, F. D., JR. & HECHTMAN, H. B. 2001. Moderation of skeletal muscle reperfusion injury by a sLe(x)-glycosylated complement inhibitory protein. *Am J Physiol Cell Physiol,* 281**,** C224-30.

LAMEIRE, N. H., BAGGA, A., CRUZ, D., DE MAESENEER, J., ENDRE, Z., KELLUM, J. A., LIU, K. D., MEHTA, R. L., PANNU, N., VAN BIESEN, W. & VANHOLDER, R. 2013. Acute kidney injury: an increasing global concern. *Lancet,* 382**,** 170-179.

LAPPAS, C. M., DAY, Y. J., MARSHALL, M. A., ENGELHARD, V. H. & LINDEN, J. 2006. Adenosine A2A receptor activation reduces hepatic ischemia reperfusion injury by inhibiting CD1d-dependent NKT cell activation. *J Exp Med,* 203**,** 2639-48.

LAUBER, K., BOHN, E., KROBER, S. M., XIAO, Y. J., BLUMENTHAL, S. G., LINDEMANN, R. K., MARINI, P., WIEDIG, C., ZOBYWALSKI, A., BAKSH, S., XU, Y., AUTENRIETH, I. B., SCHULZE-OSTHOFF, K., BELKA, C., STUHLER, G. & WESSELBORG, S. 2003. Apoptotic cells induce migration of phagocytes via caspase-3-mediated release of a lipid attraction signal. *Cell,* 113**,** 717-30.

LEE, A. Y. & LEVINE, M. N. 1999. The thrombophilic state induced by therapeutic agents in the cancer patient. *Seminars in thrombosis and hemostasis,* 25**,** 137-145.

LEE, H. T. & EMALA, C. W. 2002. Preconditioning and adenosine protect human proximal tubule cells in an in vitro model of ischemic injury. *J Am Soc Nephrol,* 13**,** 2753-61.

LEE, Y.-J., MOON, C., LEE, S.-H., PARK, H.-J., SEOH, J.-Y., CHO, M.-S. & KANG, J. L. 2012. Apoptotic cell instillation after bleomycin attenuates lung injury through hepatocyte growth factor induction. *The European respiratory journal,* 40**,** 424-435.

LEHMANN, T. G., KOEPPEL, T. A., KIRSCHFINK, M., GEBHARD, M. M., HERFARTH, C., OTTO, G. & POST, S. 1998. Complement inhibition by soluble complement receptor type 1 improves microcirculation after rat liver transplantation. *Transplantation,* 66**,** 717-22.

LEHMANN, T. G., KOEPPEL, T. A., MUNCH, S., HEGER, M., KIRSCHFINK, M., KLAR, E. & POST, S. 2001. Impact of inhibition of complement by sCR1 on hepatic microcirculation after warm ischemia. *Microvasc Res,* 62**,** 284-92.

LEIBUNDGUT, G., WITZTUM, J. L. & TSIMIKAS, S. 2013. Oxidation-specific epitopes and immunological responses: Translational biotheranostic implications for atherosclerosis. *Current opinion in pharmacology*.

LIBERAL, R., GRANT, C. R., MIELI-VERGANI, G. & VERGANI, D. 2013. Autoimmune hepatitis: a comprehensive review. *J Autoimmun,* 41**,** 126-39.

LINDSAY, T. F., HILL, J., ORTIZ, F., RUDOLPH, A., VALERI, C. R., HECHTMAN, H. B. & MOORE, F. D., JR. 1992. Blockade of complement activation prevents local and pulmonary albumin leak after lower torso ischemia-reperfusion. *Ann Surg,* 216**,** 677-83.

LITVACK, M. L., DJIADEU, P., RENGANATHAN, S. D. S., SY, S., POST, M. & PALANIYAR, N. 2010. Natural IgM and innate immune collectin SP-D bind to late apoptotic cells and enhance their clearance by alveolar macrophages in vivo. *Molecular immunology,* 48**,** 37-47.

LITVACK, M. L., POST, M. & PALANIYAR, N. 2011. IgM promotes the clearance of small particles and apoptotic microparticles by macrophages. *PloS one,* 6**,** e17223.

LOBO, P. I., BAJWA, A., SCHLEGEL, K. H., VENGAL, J., LEE, S. J., HUANG, L., YE, H., DESHMUKH, U., WANG, T., PEI, H. & OKUSA, M. D. 2012. Natural IgM Anti-Leukocyte Autoantibodies Attenuate Excess Inflammation Mediated by Innate and Adaptive Immune Mechanisms Involving Th-17. *Journal of immunology (Baltimore, Md. : 1950),* 188**,** 1675-1685.

LOBO, P. I., SCHLEGAL, K. H., VENGAL, J., OKUSA, M. D. & PEI, H. 2010. Naturally occurring IgM anti-leukocyte autoantibodies inhibit T-cell activation and chemotaxis. *Journal of clinical immunology,* 30 Suppl 1**,** S31-6.

LUTZ, H. U. & BOGDANOVA, A. 2013. Mechanisms tagging senescent red blood cells for clearance in healthy humans. *Front Physiol,* 4**,** 387.

LUTZ, J., THÜRMEL, K. & HEEMANN, U. 2010. Anti-inflammatory treatment strategies for ischemia/reperfusion injury in transplantation. *Journal of inflammation (London, England),* 7**,** 27.

MADI, A., BRANSBURG-ZABARY, S., KENETT, D. Y., BEN-JACOB, E. & COHEN, I. R. 2012. The natural autoantibody repertoire in newborns and adults: a current overview. *Adv Exp Med Biol,* 750**,** 198-212.

MADI, A., HECHT, I., BRANSBURG-ZABARY, S., MERBL, Y., PICK, A., ZUCKER-TOLEDANO, M., QUINTANA, F. J., TAUBER, A. I., COHEN, I. R. & BEN-JACOB, E. 2009. Organization of the autoantibody repertoire in healthy newborns and adults revealed by system level informatics of antigen microarray data. *Proc Natl Acad Sci U S A,* 106**,** 14484-9.

MARRIOTT, H. M., HELLEWELL, P. G., CROSS, S. S., INCE, P. G., WHYTE, M. K. & DOCKRELL, D. H. 2006. Decreased alveolar macrophage apoptosis is associated with increased pulmonary inflammation in a murine model of pneumococcal pneumonia. *J Immunol,* 177**,** 6480-8.

MASON, J., WELSCH, J. & TORHORST, J. 1987. The contribution of vascular obstruction to the functional defect that follows renal ischemia. *Kidney international,* 31**,** 65-71.

MASSBERG, S., ENDERS, G., LEIDERER, R., EISENMENGER, S., VESTWEBER, D., KROMBACH, F. & MESSMER, K. 1998. Platelet-endothelial cell interactions during ischemia/reperfusion: the role of P-selectin. *Blood,* 92**,** 507-515.

MCMULLEN, M. E., HART, M. L., WALSH, M. C., BURAS, J., TAKAHASHI, K. & STAHL, G. L. 2006. Mannose-binding lectin binds IgM to activate the lectin complement pathway in vitro and in vivo. *Immunobiology,* 211**,** 759-66.

MEDINE, C. N., LUCENDO-VILLARIN, B., ZHOU, W., WEST, C. C. & HAY, D. C. 2011. Robust generation of hepatocyte-like cells from human embryonic stem cell populations. *Journal of visualized experiments : JoVE***,** e2969.

MENDES-BRAZ, M., ELIAS-MIRO, M., JIMENEZ-CASTRO, M. B., CASILLAS-RAMIREZ, A., RAMALHO, F. S. & PERALTA, C. 2012. The current state of knowledge of hepatic ischemia-reperfusion injury based on its study in experimental models. *J Biomed Biotechnol,* 2012**,** 298657.

MERCOLINO, T. J., ARNOLD, L. W. & HAUGHTON, G. 1986. Phosphatidyl choline is recognized by a series of Ly-1+ murine B cell lymphomas specific for erythrocyte membranes. *J Exp Med,* 163**,** 155-65.

MIELI-VERGANI, G. & VERGANI, D. 2011. Autoimmune hepatitis. *Nature reviews. Gastroenterology & hepatology,* 8**,** 320-9.

MILES, K., CLARKE, D. J., LU, W., SIBINSKA, Z., BEAUMONT, P. E., DAVIDSON, D. J., BARR, T. A., CAMPOPIANO, D. J. & GRAY, M. 2009. Dying and necrotic neutrophils are anti-inflammatory secondary to the release of alpha-defensins. *Journal of immunology (Baltimore, Md. : 1950),* 183**,** 2122-2132.

MITTAL, M., SIDDIQUI, M. R., TRAN, K., REDDY, S. P. & MALIK, A. B. 2014. Reactive oxygen species in inflammation and tissue injury. *Antioxid Redox Signal,* 20**,** 1126-67.

MIWA, T., SATO, S., GULLIPALLI, D., NANGAKU, M. & SONG, W. C. 2013. Blocking properdin, the alternative pathway, and anaphylatoxin receptors ameliorates renal ischemia-reperfusion injury in decay-accelerating factor and CD59 double-knockout mice. *J Immunol,* 190**,** 3552-9.

MOCHIZUKI, H., GOTO, K., MORI, H. & MIZUNO, Y. 1996. Histochemical detection of apoptosis in Parkinson's disease. *J Neurol Sci,* 137**,** 120-3.

MONROE, D. M., HOFFMAN, M. & ROBERTS, H. R. 2002. Platelets and thrombin generation. *Arteriosclerosis, thrombosis, and vascular biology,* 22**,** 1381-1389.

MOORE, K. 1999. Renal failure in acute liver failure. *Eur J Gastroenterol Hepatol,* 11**,** 967-75.

MORRELL, C. N., SUN, H., SWAIM, A. M. & BALDWIN, W. M. 2007. Platelets an inflammatory force in transplantation. *American journal of transplantation : official journal of the American Society of Transplantation and the American Society of Transplant Surgeons,* 7**,** 2447-2454.

MUNSHI, R., HSU, C. & HIMMELFARB, J. 2011. Advances in understanding ischemic acute kidney injury. *BMC medicine,* 9**,** 11.

NAKANO, T., GOTO, S., LAI, C.-Y., HSU, L.-W., TSENG, H.-P., CHEN, K.-D., CHIU, K.-W., WANG, C.-C., CHENG, Y.-F. & CHEN, C.-L. 2013. Induction of antinuclear antibodies by de novo autoimmune hepatitis regulates alloimmune responses in rat liver transplantation. *Clinical & developmental immunology,* 2013**,** 413928.

OGDEN, C. A., DECATHELINEAU, A., HOFFMANN, P. R., BRATTON, D., GHEBREHIWET, B., FADOK, V. A. & HENSON, P. M. 2001. C1q and mannose binding lectin engagement of cell surface calreticulin and CD91 initiates macropinocytosis and uptake of apoptotic cells. *J Exp Med,* 194**,** 781-95.

OGDEN, C. A., KOWALEWSKI, R., PENG, Y., MONTENEGRO, V. & ELKON, K. B. 2005. IGM is required for efficient complement mediated phagocytosis of apoptotic cells in vivo. *Autoimmunity,* 38**,** 259-264.

OPELZ, G. & TERASAKI, P. I. 1978. Improvement of kidney-graft survival with increased numbers of blood transfusions. *N Engl J Med,* 299**,** 799-803.

OPELZ, G., VANRENTERGHEM, Y., KIRSTE, G., GRAY, D. W., HORSBURGH, T., LACHANCE, J. G., LARGIADER, F., LANGE, H., VUJAKLIJA-STIPANOVIC, K., ALVAREZ-GRANDE, J., SCHOTT, W., HOYER, J., SCHNUELLE, P., DESCOEUDRES, C., RUDER, H., WUJCIAK, T. & SCHWARZ, V. 1997. Prospective evaluation of pretransplant blood transfusions in cadaver kidney recipients. *Transplantation,* 63**,** 964-7.

OXBURGH, L. & DE CAESTECKER, M. P. 2012. Ischemia-reperfusion injury of the mouse kidney. *Methods Mol Biol,* 886**,** 363-79.

PARK, P., HAAS, M., CUNNINGHAM, P. N., ALEXANDER, J. J., BAO, L., GUTHRIDGE, J. M., KRAUS, D. M., HOLERS, V. M. & QUIGG, R. J. 2001. Inhibiting the complement system does not reduce injury in renal ischemia reperfusion. *J Am Soc Nephrol,* 12**,** 1383-90.

PARK, P., HAAS, M., CUNNINGHAM, P. N., BAO, L., ALEXANDER, J. J. & QUIGG, R. J. 2002. Injury in renal ischemia-reperfusion is independent from

immunoglobulins and T lymphocytes. *American journal of physiology. Renal physiology,* 282**,** F352-7.

PARK, S. W., KIM, J. Y., HAM, A., BROWN, K. M., KIM, M., D'AGATI, V. D. & LEE, H. T. 2012. A1 adenosine receptor allosteric enhancer PD-81723 protects against renal ischemia-reperfusion injury. *Am J Physiol Renal Physiol,* 303**,** F721-32.

PATSCHAN, D., PATSCHAN, S. & MÜLLER, G. A. 2012a. Inflammation and microvasculopathy in renal ischemia reperfusion injury. *Journal of transplantation,* 2012**,** 764154.

PATSCHAN, D., PATSCHAN, S. & MÜLLER, G. A. 2012b. Microvasculopathy in ischemic acute kidney injury: consequences and therapeutic implications. *Panminerva medica,* 54**,** 45-52.

PENG, Y., KOWALEWSKI, R., KIM, S. & ELKON, K. B. 2005. The role of IgM antibodies in the recognition and clearance of apoptotic cells. *Molecular immunology,* 42**,** 781-787.

PICKERING, W., GRAY, E., GOODALL, A. H. & BARROWCLIFFE, T. W. 2008. Effects of apoptosis and lipid peroxidation on T-lymphoblastoid phospholipid-dependent procoagulant activity. *Journal of thrombosis and haemostasis : JTH,* 6**,** 1122-1130.

PORCHERAY, F., FRASER, J. W., GAO, B., MCCOLL, A., DEVITO, J., DARGON, I., HELOU, Y., WONG, W., GIROUARD, T. C., SAIDMAN, S. L., COLVIN, R. B., PALMISANO, A., MAGGIORE, U., VAGLIO, A., SMITH, R. N. & ZORN, E. 2013. Polyreactive antibodies developing amidst humoral rejection of human kidney grafts bind apoptotic cells and activate complement. *Am J Transplant,* 13**,** 2590-600.

QUARTIER, P., POTTER, P. K., EHRENSTEIN, M. R., WALPORT, M. J. & BOTTO, M. 2005. Predominant role of IgM-dependent activation of the classical pathway in the clearance of dying cells by murine bone marrow-derived macrophages in vitro. *European journal of immunology,* 35**,** 252-260.

RADHI, M. & CARPENTER, S. L. 2012. Thrombotic microangiopathies. *ISRN hematology,* 2012**,** 310596.

RAMESH, G. & REEVES, W. B. 2004. Inflammatory cytokines in acute renal failure. *Kidney international. Supplement*, S56-61.

RAPAKA, R. R., RICKS, D. M., ALCORN, J. F., CHEN, K., KHADER, S. A., ZHENG, M., PLEVY, S., BENGTEN, E. & KOLLS, J. K. 2010. Conserved natural IgM antibodies mediate innate and adaptive immunity against the opportunistic fungus Pneumocystis murina. *J Exp Med,* 207**,** 2907-19.

RAVICHANDRAN, K. S. 2003. "Recruitment signals" from apoptotic cells: invitation to a quiet meal. *Cell,* 113**,** 817-20.

REDDIEN, P. W., CAMERON, S. & HORVITZ, H. R. 2001. Phagocytosis promotes programmed cell death in C. elegans. *Nature,* 412**,** 198-202.

REN, Y., XIE, Y., JIANG, G., FAN, J., YEUNG, J., LI, W., TAM, P. K. H. & SAVILL, J. 2008. Apoptotic cells protect mice against lipopolysaccharide-induced shock. *Journal of immunology (Baltimore, Md. : 1950),* 180**,** 4978-4985.

RENNER, B., STRASSHEIM, D., AMURA, C. R., KULIK, L., LJUBANOVIC, D., GLOGOWSKA, M. J., TAKAHASHI, K., CARROLL, M. C., HOLERS, V. M. & THURMAN, J. M. 2010. B cell subsets contribute to renal injury and renal protection after ischemia/reperfusion. *Journal of immunology (Baltimore, Md. : 1950),* 185**,** 4393-4400.

RIEDEMANN, N. C. & WARD, P. A. 2003. Complement in ischemia reperfusion injury. *The American journal of pathology,* 162**,** 363-367.

ROSENES, Z., MOK, Y.-F., YANG, S., GRIFFIN, M. D. W., MULHERN, T. D., HATTERS, D. M., HENSEL, F. & HOWLETT, G. J. 2013. Simultaneous Binding of the Anti-Cancer IgM Monoclonal Antibody PAT-SM6 to Low Density Lipoproteins and GRP78. *PloS one,* 8**,** e61239.

ROUHL, R. P., VAN OOSTENBRUGGE, R. J., THEUNISSEN, R. O., KNOTTNERUS, I. L., STAALS, J., HENSKENS, L. H., KROON, A. A., DE LEEUW, P. W., LODDER, J., TERVAERT, J. W. & DAMOISEAUX, J. G. 2010. Autoantibodies against oxidized low-density lipoprotein in cerebral small vessel disease. *Stroke,* 41**,** 2687-9.

RYAN, M. J., JOHNSON, G., KIRK, J., FUERSTENBERG, S. M., ZAGER, R. A. & TOROK-STORB, B. 1994. HK-2: an immortalized proximal tubule epithelial cell line from normal adult human kidney. *Kidney Int,* 45**,** 48-57.

SASS, G., HEINLEIN, S., AGLI, A., BANG, R., SCHÜMANN, J. & TIEGS, G. 2002. Cytokine expression in three mouse models of experimental hepatitis. *Cytokine,* 19**,** 115-120.

SAVILL, J. 1994. Apoptosis in disease. *Eur J Clin Invest,* 24**,** 715-23.

SAVILL, J., DRANSFIELD, I., GREGORY, C. & HASLETT, C. 2002. A blast from the past: clearance of apoptotic cells regulates immune responses. *Nature reviews. Immunology,* 2**,** 965-975.

SCHRIJVERS, D. M., DE MEYER, G. R., KOCKX, M. M., HERMAN, A. G. & MARTINET, W. 2005. Phagocytosis of apoptotic cells by macrophages is impaired in atherosclerosis. *Arterioscler Thromb Vasc Biol,* 25**,** 1256-61.

SCOTT, R. S., MCMAHON, E. J., POP, S. M., REAP, E. A., CARICCHIO, R., COHEN, P. L., EARP, H. S. & MATSUSHIMA, G. K. 2001. Phagocytosis and clearance of apoptotic cells is mediated by MER. *Nature,* 411**,** 207-11.

SEEMAN, P., CHENG, D. & ILES, G. H. 1973. Structure of membrane holes in osmotic and saponin hemolysis. *J Cell Biol,* 56**,** 519-27.

SENECAL, J. L., RAUCH, J., GRODZICKY, T., RAYNAULD, J. P., UTHMAN, I., NAVA, A., GUIMOND, M. & RAYMOND, Y. 1999. Strong association of autoantibodies to human nuclear lamin B1 with lupus anticoagulant antibodies in systemic lupus erythematosus. *Arthritis Rheum,* 42**,** 1347-53.

SERHAN, C. N. & SAVILL, J. 2005. Resolution of inflammation: the beginning programs the end. *Nature immunology,* 6**,** 1191-1197.

SHAW, P. X., GOODYEAR, C. S., CHANG, M. K., WITZTUM, J. L. & SILVERMAN, G. J. 2003. The autoreactivity of anti-phosphorylcholine antibodies for atherosclerosis-associated neo-antigens and apoptotic cells. *J Immunol,* 170**,** 6151-7.

SHAW, P. X., HÖRKKÖ, S., CHANG, M. K., CURTISS, L. K., PALINSKI, W., SILVERMAN, G. J. & WITZTUM, J. L. 2000. Natural antibodies with the T15 idiotype may act in

atherosclerosis, apoptotic clearance, and protective immunity. *The Journal of clinical investigation,* 105**,** 1731-1740.

SHI, C. & PAMER, E. G. 2011. Monocyte recruitment during infection and inflammation. *Nat Rev Immunol,* 11**,** 762-74.

SIMONSON, S. G., ZHANG, J., CANADA, A. T., JR., SU, Y. F., BENVENISTE, H. & PIANTADOSI, C. A. 1993. Hydrogen peroxide production by monoamine oxidase during ischemia-reperfusion in the rat brain. *J Cereb Blood Flow Metab,* 13**,** 125-34.

SMIT SIBINGA, C. T. 1999. Immune effects of blood transfusion. *Curr Opin Hematol,* 6**,** 442-5.

SORICE, M., CIRCELLA, A., MISASI, R., PITTONI, V., GAROFALO, T., CIRELLI, A., PAVAN, A., PONTIERI, G. M. & VALESINI, G. 2000. Cardiolipin on the surface of apoptotic cells as a possible trigger for antiphospholipids antibodies. *Clin Exp Immunol,* 122**,** 277-84.

SPENDLOVE, I., RAMAGE, J. M., BRADLEY, R., HARRIS, C. & DURRANT, L. G. 2006. Complement decay accelerating factor (DAF)/CD55 in cancer. *Cancer Immunol Immunother,* 55**,** 987-95.

STRAATSBURG, I. H., BOERMEESTER, M. A., WOLBINK, G. J., VAN GULIK, T. M., GOUMA, D. J., FREDERIKS, W. M. & HACK, C. E. 2000. Complement activation induced by ischemia-reperfusion in humans: a study in patients undergoing partial hepatectomy. *J Hepatol,* 32**,** 783-91.

SUN, E., GAO, Y., CHEN, J., ROBERTS, A. I., WANG, X., CHEN, Z. & SHI, Y. 2004. Allograft tolerance induced by donor apoptotic lymphocytes requires phagocytosis in the recipient. *Cell Death Differ,* 11**,** 1258-64.

SUTTON, T. A., FISHER, C. J. & MOLITORIS, B. A. 2002. Microvascular endothelial injury and dysfunction during ischemic acute renal failure. *Kidney international,* 62**,** 1539-1549.

TCHAIKOVSKI, S. N., VAN VLIJMEN, B. J. M., ROSING, J. & TANS, G. 2007. Development of a calibrated automated thrombography based thrombin generation test in mouse plasma. *Journal of thrombosis and haemostasis : JTH,* 5**,** 2079-2086.

THURMAN, J. M. 2007. Triggers of inflammation after renal ischemia/reperfusion. *Clinical immunology (Orlando, Fla.),* 123**,** 7-13.

THURMAN, J. M., LJUBANOVIC, D., EDELSTEIN, C. L., GILKESON, G. S. & HOLERS, V. M. 2003. Lack of a functional alternative complement pathway ameliorates ischemic acute renal failure in mice. *J Immunol,* 170**,** 1517-23.

THURMAN, J. M., LUCIA, M. S., LJUBANOVIC, D. & HOLERS, V. M. 2005. Acute tubular necrosis is characterized by activation of the alternative pathway of complement. *Kidney Int,* 67**,** 524-30.

TIEGS, G., HENTSCHEL, J. & WENDEL, A. 1992. A T cell-dependent experimental liver injury in mice inducible by concanavalin A. *The Journal of clinical investigation,* 90**,** 196-203.

TOBA, K., TSUCHIYAMA, J., HASHIMOTO, S., ICHIDA, T., KATO, K., WATANABE, K., FURUKAWA, T., NARITA, M., TAKAHASHI, M. & AIZAWA, Y. 2004. Sensitive measurement of fragmented red cell population using flow cytometry, and its application for estimating thrombotic microangiopathy after stem cell transplantation. *Cytometry B Clin Cytom,* 58**,** 39-46.

TSIANTOULAS, D., GRUBER, S. & BINDER, C. J. 2012. B-1 cell immunoglobulin directed against oxidation-specific epitopes. *Frontiers in immunology,* 3**,** 415.

TU, Z., LI, Q., CHOU, H. S., HSIEH, C. C., MEYERSON, H., PETERS, M. G., BU, H., FUNG, J. J., QIAN, S., LU, L. & LIN, F. 2011. Complement mediated hepatocytes injury in a model of autoantibody induced hepatitis. *Immunobiology,* 216**,** 528-34.

TUOMINEN, A., MILLER, Y. I., HANSEN, L. F., KESÄNIEMI, Y. A., WITZTUM, J. L. & HÖRKKÖ, S. 2006. A natural antibody to oxidized cardiolipin binds to oxidized low-density lipoprotein, apoptotic cells, and atherosclerotic lesions. *Arteriosclerosis, thrombosis, and vascular biology,* 26**,** 2096-2102.

VAN DER POL, P., ROOS, A., BERGER, S. P., DAHA, M. R. & VAN KOOTEN, C. 2011. Natural IgM antibodies are involved in the activation of complement by hypoxic human tubular cells. *American journal of physiology. Renal physiology,* 300**,** F932-40.

VAN DER POL, P., SCHLAGWEIN, N., VAN GIJLSWIJK, D. J., BERGER, S. P., ROOS, A., BAJEMA, I. M., DE BOER, H. C., DE FIJTER, J. W., STAHL, G. L., DAHA, M. R. & VAN KOOTEN, C. 2012. Mannan-binding lectin mediates renal ischemia/reperfusion injury independent of complement activation. *Am J Transplant,* 12**,** 877-87.

VAN HINSBERGH, V. W. M. 2012. Endothelium--role in regulation of coagulation and inflammation. *Seminars in immunopathology,* 34**,** 93-106.

VAN PROOIJEN, H. C., VISSER, J. J., VAN OOSTENDORP, W. R., DE GAST, G. C. & VERDONCK, L. F. 1994. Prevention of primary transfusion-associated cytomegalovirus infection in bone marrow transplant recipients by the removal of white cells from blood components with high-affinity filters. *Br J Haematol,* 87**,** 144-7.

VANCE, J. E. & STEENBERGEN, R. 2005. Metabolism and functions of phosphatidylserine. *Progress in lipid research,* 44**,** 207-234.

VAS, J., GRÖNWALL, C., MARSHAK-ROTHSTEIN, A. & SILVERMAN, G. J. 2012. Natural antibody to apoptotic cell membranes inhibits the proinflammatory properties of lupus autoantibody immune complexes. *Arthritis and rheumatism,* 64**,** 3388-3398.

VERGANI, D. & MIELI-VERGANI, G. 2003. Autoimmune hepatitis. *Autoimmunity reviews,* 2**,** 241-7.

VINAY, K., ABBAS, A. K. & ASTER, J. C. 2012. *Robbins Basic Pathology,* Philadelphia, Elsevier.

WANG, H. X., LIU, M., WENG, S. Y., LI, J. J., XIE, C., HE, H. L., GUAN, W., YUAN, Y. S. & GAO, J. 2012. Immune mechanisms of Concanavalin A model of autoimmune hepatitis. *World J Gastroenterol,* 18**,** 119-25.

WANG, J., WEISS, I., SVOBODA, K. & KWAAN, H. C. 2001. Thrombogenic role of cells undergoing apoptosis. *British journal of haematology,* 115**,** 382-391.

WEI, Q. & DONG, Z. 2012. Mouse model of ischemic acute kidney injury: technical notes and tricks. *Am J Physiol Renal Physiol,* 303**,** F1487-94.

WEISER, M. R., WILLIAMS, J. P., MOORE, F. D., KOBZIK, L., MA, M., HECHTMAN, H. B. & CARROLL, M. C. 1996. Reperfusion injury of ischemic skeletal muscle is mediated by natural antibody and complement. *The Journal of experimental medicine,* 183**,** 2343-2348.

WEISMAN, H. F., BARTOW, T., LEPPO, M. K., MARSH, H. C., CARSON, G. R., CONCINO, M. F., BOYLE, M. P., ROUX, K. H., WEISFELDT, M. L. & FEARON, D. T. 1990a. Soluble human complement receptor type 1: in vivo inhibitor of complement suppressing post-ischemic myocardial inflammation and necrosis. *Science (New York, N.Y.),* 249**,** 146-151.

WEISMAN, H. F., BARTOW, T., LEPPO, M. K., MARSH, H. C., JR., CARSON, G. R., CONCINO, M. F., BOYLE, M. P., ROUX, K. H., WEISFELDT, M. L. & FEARON, D. T. 1990b. Soluble human complement receptor type 1: in vivo inhibitor of complement suppressing post-ischemic myocardial inflammation and necrosis. *Science,* 249**,** 146-51.

WELLMANN, U., LETZ, M., HERRMANN, M., ANGERMULLER, S., KALDEN, J. R. & WINKLER, T. H. 2005. The evolution of human anti-double-stranded DNA autoantibodies. *Proc Natl Acad Sci U S A,* 102**,** 9258-63.

WILLIAMS, J. P., PECHET, T. T., WEISER, M. R., REID, R., KOBZIK, L., MOORE, F. D., CARROLL, M. C. & HECHTMAN, H. B. 1999. Intestinal reperfusion injury is mediated by IgM and complement. *Journal of applied physiology (Bethesda, Md. : 1985),* 86**,** 938-942.

WITTE, T. 2008. IgM antibodies against dsDNA in SLE. *Clin Rev Allergy Immunol,* 34**,** 345-7.

WYLLIE, A. H., KERR, J. F. & CURRIE, A. R. 1980. Cell death: the significance of apoptosis. *Int Rev Cytol,* 68**,** 251-306.

YANG, S. K., ATTIPOE, S., KLAUSNER, A. P., TIAN, R., PAN, D., RICH, T. A., TURNER, T. T., STEERS, W. D. & LYSIAK, J. J. 2006. In vivo detection of apoptotic cells in the testis using fluorescence labeled annexin V in a mouse model of testicular torsion. *J Urol,* 176**,** 830-5.

YOSHIDA, T., SUGIURA, H., MITOBE, M., TSUCHIYA, K., SHIROTA, S., NISHIMURA, S., SHIOHIRA, S., ITO, H., NOBORI, K., GULLANS, S. R., AKIBA, T. & NITTA, K. 2008. ATF3 protects against renal ischemia-reperfusion injury. *J Am Soc Nephrol,* 19**,** 217-24.

ZACHAROWSKI, K., OTTO, M., HAFNER, G., MARSH, H. C., JR. & THIEMERMANN, C. 1999. Reduction of myocardial infarct size with sCR1sLe(x), an alternatively glycosylated form of human soluble complement receptor type 1 (sCR1), possessing sialyl Lewis x. *Br J Pharmacol,* 128**,** 945-52.

ZHAI, Y., PETROWSKY, H., HONG, J. C., BUSUTTIL, R. W. & KUPIEC-WEGLINSKI, J. W. 2013. Ischaemia-reperfusion injury in liver transplantation--from bench to bedside. *Nature reviews. Gastroenterology & hepatology,* 10**,** 79-89.

ZHANG, M., ALICOT, E. M., CHIU, I., LI, J., VERNA, N., VORUP-JENSEN, T., KESSLER, B., SHIMAOKA, M., CHAN, R., FRIEND, D., MAHMOOD, U., WEISSLEDER, R., MOORE, F. D. & CARROLL, M. C. 2006a. Identification of the target self-antigens in reperfusion injury. *The Journal of experimental medicine,* 203**,** 141-152.

ZHANG, M., AUSTEN, W. G., CHIU, I., ALICOT, E. M., HUNG, R., MA, M., VERNA, N., XU, M., HECHTMAN, H. B., MOORE, F. D. & CARROLL, M. C. 2004. Identification of a specific self-reactive IgM antibody that initiates intestinal ischemia/reperfusion injury. *Proceedings of the National Academy of Sciences of the United States of America,* 101**,** 3886-3891.

ZHANG, M. & CARROLL, M. C. 2007. Natural antibody mediated innate autoimmune response. *Molecular immunology,* 44**,** 103-110.

ZHANG, M., MICHAEL, L. H., GROSJEAN, S. A., KELLY, R. A., CARROLL, M. C. & ENTMAN, M. L. 2006b. The role of natural IgM in myocardial ischemia-reperfusion injury. *Journal of molecular and cellular cardiology,* 41**,** 62-67.

ZHANG, M., XU, S., HAN, Y. & CAO, X. 2011. Apoptotic cells attenuate fulminant hepatitis by priming Kupffer cells to produce interleukin-10 through membrane-bound TGF-β. *Hepatology (Baltimore, Md.),* 53**,** 306-316.

ZHAO, H., PEREZ, J. S., LU, K., GEORGE, A. J. T. & MA, D. 2014. Role of Toll-like receptor-4 in renal graft ischemia-reperfusion injury. *AJP: Renal Physiology,* 306**,** F801-11.

ZHOU, W., FARRAR, C. A., ABE, K., PRATT, J. R., MARSH, J. E., WANG, Y., STAHL, G. L. & SACKS, S. H. 2000a. Predominant role for C5b-9 in renal ischemia/reperfusion injury. *The Journal of clinical investigation,* 105**,** 1363-1371.

ZHOU, W., FARRAR, C. A., ABE, K., PRATT, J. R., MARSH, J. E., WANG, Y., STAHL, G. L. & SACKS, S. H. 2000b. Predominant role for C5b-9 in renal ischemia/reperfusion injury. *J Clin Invest,* 105**,** 1363-71.

ZIEGLER, U. & GROSCURTH, P. 2004. Morphological features of cell death. *News in physiological sciences : an international journal of physiology produced jointly by the International Union of Physiological Sciences and the American Physiological Society,* 19**,** 124-128.

ZIPFEL, P. F. & SKERKA, C. 2009. Complement regulators and inhibitory proteins. *Nat Rev Immunol,* 9**,** 729-40.

ZONG, W. X. & THOMPSON, C. B. 2006. Necrotic death as a cell fate. *Genes Dev,* 20**,** 1-15.

ZWAAL, R. F., COMFURIUS, P. & BEVERS, E. M. 1998. Lipid-protein interactions in blood coagulation. *Biochim Biophys Acta,* 1376**,** 433-53.

ZWART, B., CIURANA, C., RENSINK, I., MANOE, R., HACK, C. E. & AARDEN, L. A. 2004. Complement activation by apoptotic cells occurs predominantly via IgM and is limited to late apoptotic (secondary necrotic) cells. *Autoimmunity,* 37**,** 95-102.

Appendix of publications

Publications included are as follows:

Hesketh EE, Kluth DC, Hughes J: Apoptotic cell administration is detrimental in murine renal ischaemia reperfusion injury. *Journal of inflammation (London, England)* 2014, **11**:31.

Hesketh EE, Czopek A, Clay M, Borthwick G, Ferenbach D, Kluth D, Hughes J: Renal ischaemia reperfusion injury: a mouse model of injury and regeneration. *JoVE* 2014, **88**:e51816

Hesketh *et al. Journal of Inflammation* 2014, **11**:31
http://www.journal-inflammation.com/content/11/1/31

JOURNAL OF INFLAMMATION

SHORT REPORT **Open Access**

Apoptotic cell administration is detrimental in murine renal ischaemia reperfusion injury

Emily E Hesketh*, David C Kluth and Jeremy Hughes

Abstract

Background: Acute kidney injury induced by renal ischaemia reperfusion injury (IRI) is characterised by renal failure, acute tubular necrosis (ATN), inflammation and microvascular congestion. The administration of apoptotic cells (ACs) has been shown to reduce inflammation in various organs including the liver and kidney. This study explored whether AC administration prior to the induction of renal IRI was protective.

Findings: Renal IRI was induced in Balb/c mice by clamping the renal blood vessels for either 20, 24 or 25 minutes to induce mild, moderate or severe kidney dysfunction respectively. Renal function and injury was determined 24 hours following IRI by measurement of plasma creatinine and ATN scoring respectively. ACs were generated from Balb/c thymocytes and classified as either predominantly early or late apoptotic by Annexin-V and propidium iodide staining. Early AC administration prior to severe IRI had no influence on plasma creatinine or ATN severity. In contrast, administration of early or late ACs significantly worsened renal function in mice with mild or moderate renal IRI, respectively, compared to PBS treated controls, though ATN scores were comparable. Despite ACs exerting pro-coagulant effects, the worsening of renal function was not secondary to increased microvascular congestion, inferred by fibrin and platelet (CD41) deposition, or inflammation, assessed by neutrophil infiltration.

Conclusions: Despite the AC-derived protection demonstrated in other organs, ACs do not protect mice from renal IRI. ACs may in fact further impair renal function depending on injury severity. These data suggest that AC-derived protection is not translationally relevant for patients with acute kidney injury induced by ischaemic injury.

Keywords: Ischaemia reperfusion injury, Acute kidney injury, Apoptotic cells, Inflammation, Microvasculature

Findings

Introduction

Acute kidney injury (AKI) induced by renal ischaemia reperfusion injury (IRI) is a significant risk factor for patients undergoing renal transplantation or any major surgery that may transiently reduce renal blood flow. Ischaemic AKI has a complex pathogenesis involving acute inflammatory responses, endothelial and tubular cell injury that determine injury severity [1-3]. Inflammatory responses lead to further endothelial dysfunction and injury with increased leukocyte infiltration and reduced microvascular blood flow [2]. Pro-inflammatory cytokines such as tumour necrosis factor-α (TNF-α) and interleukin (IL)-1β are released by infiltrating leukocytes and injured tubular epithelial cells which act to potentiate inflammation and associated injury [4,5]. As inflammation plays a key role following renal IRI it is not surprising that the resultant injury may be attenuated by anti-inflammatory treatments [6]. There is an urgent need for novel treatments for AKI that reduce inflammation as current clinical treatments are purely supportive with no specific therapy available.

Increased numbers of apoptotic cells (ACs) are found at sites of inflammation. Surface exposure of phosphatidylserine (PS) on the AC surface promotes AC clearance by macrophages [7] which facilitates the resolution of inflammation [8]. Macrophages that ingest ACs adopt an anti-inflammatory phenotype with secretion of transforming growth factor-β (TGF-β) and IL-10 [9]. Exogenous AC administration reduces inflammation in various experimental models including lipopolysaccharide (LPS)-induced shock [10], collagen induced arthritis (CIA) [11] as well as lung [12] and liver inflammation [13]. The anti-inflammatory mechanisms of exogenous AC administration are diverse and include (i) the induction of

* Correspondence: E.E.Hesketh@sms.ed.ac.uk
MRC Centre for Inflammation Research, Queen's Medical Research Institute, University of Edinburgh, 47 Little France Crescent, Edinburgh EH16 4TJ, UK

BioMed Central

© 2014 Hesketh et al.; licensee BioMed Central Ltd. This is an Open Access article distributed under the terms of the Creative Commons Attribution License (http://creativecommons.org/licenses/by/4.0), which permits unrestricted use, distribution, and reproduction in any medium, provided the original work is properly credited. The Creative Commons Public Domain Dedication waiver (http://creativecommons.org/publicdomain/zero/1.0/) applies to the data made available in this article, unless otherwise stated.

IL-10 production by Kupffer cells by TGF-β bound to the AC surface [13], (ii) the induction of IL-10 producing $CD19^+$ regulatory B cells that stimulate a population of IL-10 secreting antigen-specific $CD4^+$ T cells in CIA [11] and (iii) binding of LPS to ACs accompanied by reduced serum TNF-α levels and increased serum IL-10 levels in LPS shock [10]. Ren *et al.* also observed suppressed neutrophil infiltration in the kidney following AC administration in LPS-induced shock [10]. In addition, it has been shown that both apoptotic and necrotic cells exert anti-inflammatory effects [14] suggesting that these effects are not confined to intact ACs.

In view of these previous studies AC administration may represent a novel pretreatment for AKI secondary to renal IRI and act to limit the resultant inflammation and tissue injury. This short study explored whether ACs administered 24 hr prior to the induction of renal IRI could protect Balb/c mice from functional and structural renal injury. The findings contrast with the AC-derived protection observed in other organs and suggest that AC administration is either neutral or, depending upon the severity of the ischaemic injury, may act to worsen renal function.

Methods

Mice

Experiments were performed on male Balb/c mice aged between 4–8 weeks (Harlan). All animal procedures were performed under a Project License in accordance with guidelines set out by the United Kingdom's Home Office under the Animal (Scientific Procedures) Act of 1986 and the University of Edinburgh's Biological Services Department.

Preparation and administration of viable and apoptotic thymocytes

Dissociated thymocytes harvested from the thymi of Balb/c mice aged 4-weeks were used fresh or incubated for 20 hr in RPMI 1640 (PAA Laboratories) or RMPI 1640 supplemented with 1 μM dexamethasone (Oragon). Cell viability was assessed by Annexin-V (BioLegend) and Propidium Iodide (PI; Invitrogen) staining assessed by flow cytometry on a BD Calibur cytometer. ACs were classified as either early (Annexin-V^+ PI^-) or late (Annexin-V^+ PI^+) apoptotic. Either PBS (control) or $20{\times}10^6$ viable thymocytes or ACs was administered intravenously to mice 24 hr prior to renal IRI.

Thymocyte phenotyping

Fresh thymocytes were prepared as described and stained with the following anti-mouse antibodies: PE CD4 (1:200, Clone: RM4-5, BD Pharmingen), APC CD8α (1:200, Clone: 53-6.7, eBioscience), PerCp-Cy5.5 CD11b (1:200, Clone: M1/70, eBiosciences) and Pacific Blue B220 (1:200, Clone: RA3-6B2, BD Pharmingen) before analysis by flow cytometry on a BD LSR Fortessa. Isotype controls were used to determine staining positivity.

Renal IRI and assessment of renal function and acute tubular necrosis (ATN)

Detailed methodology is described in Hesketh *et al.*, [15]. In brief male 8-week Balb/c mice underwent a contralateral right nephrectomy before the renal pedicle was clamped with an atraumatic clamp for 22 (mild), 24 (moderate) or 25 minutes (severe injury). Body temperature was maintained at 37°C by a homeostatically controlled blanket (Harvard Apparatus, Boston MA) during the ischaemic period. The peritoneum was then sutured and the skin closed with metallic clips and the anaesthesia reversed. Sham mice underwent a laparotomy with manipulation of the left and right renal pedicle only. Tissue and blood was collected 24 hr post-surgery under terminal anaesthesia. Creatinine concentration [μmol/L] was assessed in plasma samples using a creatininase based method on a Cobas Fara Centrifugal Analyser (Roche Diagnostics, UK) [15]. To determine the ATN score the number of viable (intact cell membrane) and necrotic tubules (compromised cell membrane) were marked and counted in deparaffinised 4 μm kidney sections stained with H&E [15]. The number of necrotic tubules was expressed as a percentage of the total number of tubules (necrotic tubules %). ATN was assessed in 5 images taken at ×200 magnification of the outer stripe of the outer medulla (OSOM) per mouse. ATN was scored in a blinded manner.

Immunohistochemistry (IHC)

Deparaffinised or frozen kidney sections, fixed in 70% methanol, cut at a thickness of 4 μM were prepared. Endogenous peroxidase activity was blocked using 0.3% H_2O_2 diluted in methanol. Endogenous avidin and biotin activity was blocked using an Avidin/Biotin Blocking Kit (Vector Laboratories). Non-specific binding was blocked using protein block serum-free ready-to-use (Dako). Primary antibodies used were rat anti-mouse CD41 (1:250, Clone: MWReg30, AbDserotec) and rat anti-mouse Gr1 (1:300, Clone: RB6-8C5, BioLegend). A biotinylated secondary rabbit anti-rat IgG (Vector Laboratories) was applied (1:300). R.T.U Vectastain Kit Elite Reagent (Vector Laboratories) was applied before sections were exposed to Dako Liquid DAB + Substrate Chromogen System. Sections were counterstained with Haematoxylin. Frozen sections were mounted with ProLong Gold Antifade Reagent (Life Technologies) and paraffin sections were dehydrated and mounted with Pertex. Negative controls without the primary antibody and control isotype antibodies were included (Additional file 1).

Fibrin direct immunofluorescence (IF)

Frozen kidney sections cut at a thickness of 4 μM were fixed with 4% PFA 2% Acetic acid before incubation with rabbit serum (Sigma). Polyclonal Rabbit Anti-Human Fibrinogen/FITC (1:200, Dako Cytomation) which cross-reacts with mouse fibrin was applied before sections were stained with DAPI (Life Technologies). Sections were mounted with ProLong Gold Antifade Reagent (Life Technologies). Positive control tissue was included.

Quantification of IF and IHC staining

For each stained section 5 images of the OSOM were taken and positive staining was selected using ImageJ (NIH). The number of positive pixels was expressed as a percentage of the total number of pixels [16]. Sections were examined using either a Zeiss Axioskop 2mot + and Hamamatsu Orca-ER camera or a Zeiss Axioskop microscope and QImaging Micropublisher 3.3 RTV camera. Quantification was performed in a blinded manner.

Statistics

Data are expressed as mean ± SEM. Significance was assessed by using unpaired students *t* test, one- or two-way ANOVA where appropriate using Prism software (Graphpad). P values <0.05 were considered significant.

Results

The phenotype of the fresh thymocytes used to generate the ACs was examined by assessing the expression of CD4, CD8, B220 (B cell marker) and CD11b (myeloid cell marker). Minimal expression of B220 (Figure 1A) and CD11b (Figure 1B) confirmed that cell preparations consisted predominantly of thymocytes, 98% of which were either $CD4^+$, $CD8\alpha^+$ or $CD4^+CD8\alpha^+$ (Figure 1C).

To explore the effects of ACs upon renal IRI either PBS or 20×10^6 predominantly early ACs (Annexin-V^+ PI^-, Figure 1D) or predominantly late ACs (Annexin-V^+ PI^+, Figure 1E) were administered intravenously to mice 24 hr before renal IRI. Mice were then sacrificed 24 hr later. In

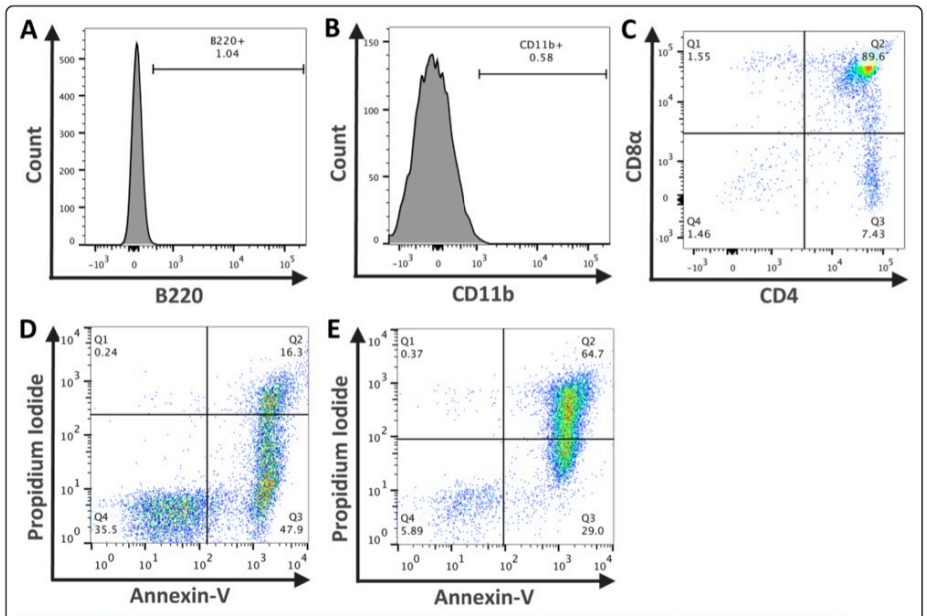

Figure 1 Representative data illustrating the phenotype of thymocytes and classification of early and late ACs. Freshly isolated thymocytes were stained with CD11b, B220, CD4 and CD8α and analysed by flow cytometry to assess the phenotype of the cells used to generate ACs. Minimal staining for B220 **(A)** and CD11b **(B)** was found. Approximately 98% of cells gated to exclude debris are lymphocytes and either $CD4^+$, $CD8\alpha^+$ or $CD4^+CD8\alpha^+$ **(C)**. Prior to administration of ACs cell viability was assessed by Annexin-V and Propidium Iodide (PI) staining and flow cytometry. Overnight culture alone induced predominantly early ACs (47% Annexin-V^+ PI^-) **(D)** whilst the addition of 1 μM dexamethasone elicited a population of late ACs (64.7% Annexin-V^+ PI^+) **(E)**. Data representative of all AC preparations.

an initial experiment early ACs were administered prior to 25 mins of ischaemia but no preservation of renal function was observed (Figure 2A). The resulting level of functional injury was high with markedly elevated levels of plasma creatinine and thus unlikely to be responsive to any therapeutic modulation. Further studies adopted a slightly reduced level of injury (classified according to plasma creatinine). In light of work demonstrating that late ACs may exert anti-inflammatory effects [14] the influence of late ACs upon moderate kidney dysfunction was examined. However, the administration of late ACs resulted in a significant increase in plasma creatinine indicative of a worsening of kidney function (Figure 2B). This suggested that the administration of cells with significant PI positivity was detrimental and we therefore focused upon early ACs in a milder model of renal injury. Somewhat unexpectedly the administration of early ACs also resulted in a significant increase in plasma creatinine with no protection evident (Figure 2C). On the basis of these data, we did not examine the effects of early ACs in moderate injury or late ACs in mild injury. ATN was evident with widespread tubular injury in the OSOM in the ischaemic kidneys of all PBS and AC treated mice (Figure 3A). Despite the deleterious effect of early or late AC administration upon renal function in mice with mild or moderate renal IRI, the ATN scores of PBS treated and AC treated mice were comparable (Figure 3B). It is evident from the lower left quadrants of Figure 1D and E that both early and late ACs contained populations of viable non-apoptotic cells and that these cells might be responsible for the worsening of plasma creatinine. However, the administration of 20×10^6 viable thymocytes (~95% Annexin-V$^-$ PI$^-$) prior to renal IRI had no significant effect upon renal function measured by plasma creatinine or ATN (Additional file 2).

The finding of unexpectedly worse renal function without an increased ATN score in AC treated mice suggested that ACs might have detrimentally reduced renal microvascular flow. The coagulation cascade is activated following ischaemic injury [17] and the microvasculature becomes congested with erythrocytes and platelet/fibrin aggregates which aggravates tissue hypoxia and limits the perfusion of residual viable and potentially functional nephrons [1,18]. ACs expressing PS are procoagulant and might therefore contribute to this procoagulant milieu [19]. To investigate this CD41$^+$ platelets and fibrin were selected as markers of microvascular congestion and their deposition assessed by IHC and IF, respectively. CD41$^+$ platelets and fibrin deposition was observed in the OSOM of PBS and AC treated ischaemic kidneys (Figure 4A & C), but no significant differences between AC treated and control mice were found following quantification (Figure 4B & D).

With increased microvascular congestion not explaining this surprising result it was speculated that AC administration might have increased immune cell infiltration thereby elevating pro-inflammatory responses post renal IRI. Neutrophils rapidly accumulate after renal ischaemic injury [3]. They adhere to the microvascular endothelium where they may obstruct the renal microvasculature and potentially damage tubular cells by releasing reactive oxygen species [20]. To gain an insight into the inflammatory status, neutrophil infiltration was determined following IHC staining for Gr1. Neutrophil infiltration was observed in the OSOM of all ischaemic kidneys of PBS and AC treated mice (Figure 5A), however this remained equivalent in all AC treated mice and their corresponding PBS controls (Figure 5B).

Discussion

Although AC administration has been demonstrated to reduce inflammation in diverse experimental models [10-13], the data presented in this report indicates that

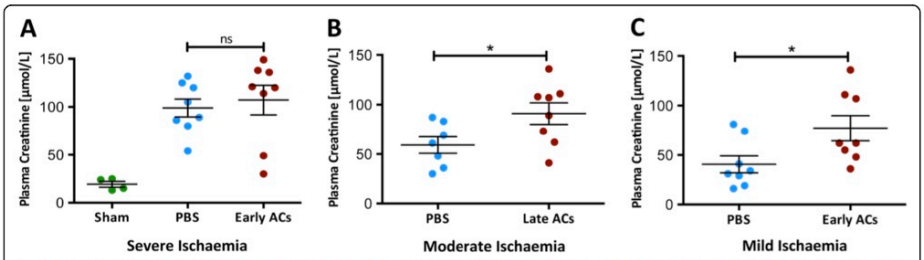

Figure 2 AC administration prior to moderate and mild renal IRI impaired renal function. Renal IRI was induced in 8-week old male Balb/c mice by a right nephrectomy and ischaemia induced by occlusion of the left renal pedicle. Sham mice underwent a laparotomy only. Either PBS or 20×10^6 early or late ACs were administered 24 hr prior to mild (20 mins ischaemia), moderate (24 mins) or severe (25 mins) ischaemic injury. Mice were sacrificed 24 hr following IRI. **(A)** Administration of early ACs did not preserve renal function from severe IRI. **(B)** In contrast, administration of late ACs significantly worsened renal function in mice with moderate IRI. **(C)** Similarly, early ACs administered prior to mild ischaemia significantly worsened renal function. Analysed by one-way ANOVA or students *t*-test * = P ≤ 0.05, ns = non-significant. Sham ($n = 4$), PBS ($n = 7–8$), AC ($n = 8$).

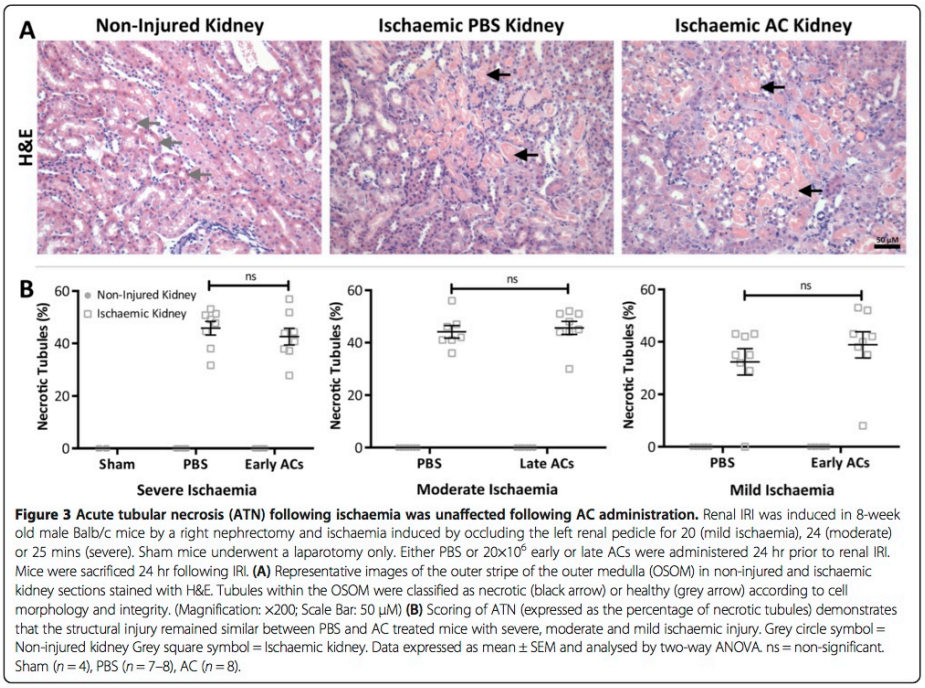

Figure 3 Acute tubular necrosis (ATN) following ischaemia was unaffected following AC administration. Renal IRI was induced in 8-week old male Balb/c mice by a right nephrectomy and ischaemia induced by occluding the left renal pedicle for 20 (mild ischaemia), 24 (moderate) or 25 mins (severe). Sham mice underwent a laparotomy only. Either PBS or 20×10^6 early or late ACs were administered 24 hr prior to renal IRI. Mice were sacrificed 24 hr following IRI. **(A)** Representative images of the outer stripe of the outer medulla (OSOM) in non-injured and ischaemic kidney sections stained with H&E. Tubules within the OSOM were classified as necrotic (black arrow) or healthy (grey arrow) according to cell morphology and integrity. (Magnification: ×200; Scale Bar: 50 μM) **(B)** Scoring of ATN (expressed as the percentage of necrotic tubules) demonstrates that the structural injury remained similar between PBS and AC treated mice with severe, moderate and mild ischaemic injury. Grey circle symbol = Non-injured kidney Grey square symbol = Ischaemic kidney. Data expressed as mean ± SEM and analysed by two-way ANOVA. ns = non-significant. Sham ($n = 4$), PBS ($n = 7–8$), AC ($n = 8$).

ACs do not protect mice from renal IRI. Whilst early ACs had no effect on severe renal IRI, the administration of early or late ACs prior to mild or moderate renal IRI respectively resulted in a further increase in plasma creatinine indicative of worse renal failure. This adverse effect was not the result of increased structural injury as ATN scores were comparable in PBS and AC treated mice.

While therapeutic interventions in the renal IRI model usually modulate both renal function and structure, functional protection alone has been observed in mice administered hemeoxygenase-1 overexpressing macrophages [21]. This protection was considered to be secondary to a dramatic reduction in $CD41^+$ platelet accumulation with improved microvascular blood flow and perfusion of non-injured functioning nephrons. As plasma creatinine values were higher in AC treated mice than PBS treated controls in this study, it was hypothesized that AC treated mice might exhibit an additional worsening of microvascular blood flow post ischaemia. However, this was found to be unlikely as microvascular congestion, inferred by renal fibrin and $CD41^+$ platelet IHC staining, was comparable in all PBS treated and AC treated mice.

It is surprising that early ACs aggravated renal function as early ACs have generally been regarded as anti-inflammatory in comparison to late ACs which are generally considered to be pro-inflammatory [9]. However, Gray *et al.*, found ACs at an early or advanced stage of apoptosis provided equal protection from CIA [11]. Importantly, AC-derived protection does not appear to be restricted to one cell type. The administration of between 10×10^6 to 30×10^6 apoptotic neutrophils [10], thymocytes [11], splenocytes [13] and human Jurkat T cells [12] have all elicited protection from inflammation in mice. In the current short report 20×10^6 apoptotic thymocytes were administered to mice 24 hr prior to renal IRI and it is unlikely that either the AC type or number contributed to the neutral or detrimental effect on renal function.

Apoptosis and necrosis are key events in renal tubular cells following ischaemic injury [22] with inhibition of apoptosis attenuating renal inflammation [23]. However, the level of ATN did not differ between PBS and AC treated mice indicating that increased necrosis/apoptosis of renal tubular cells did not occur following ischaemic injury. Furthermore, no discernable difference in neutrophil infiltration was observed, suggesting that

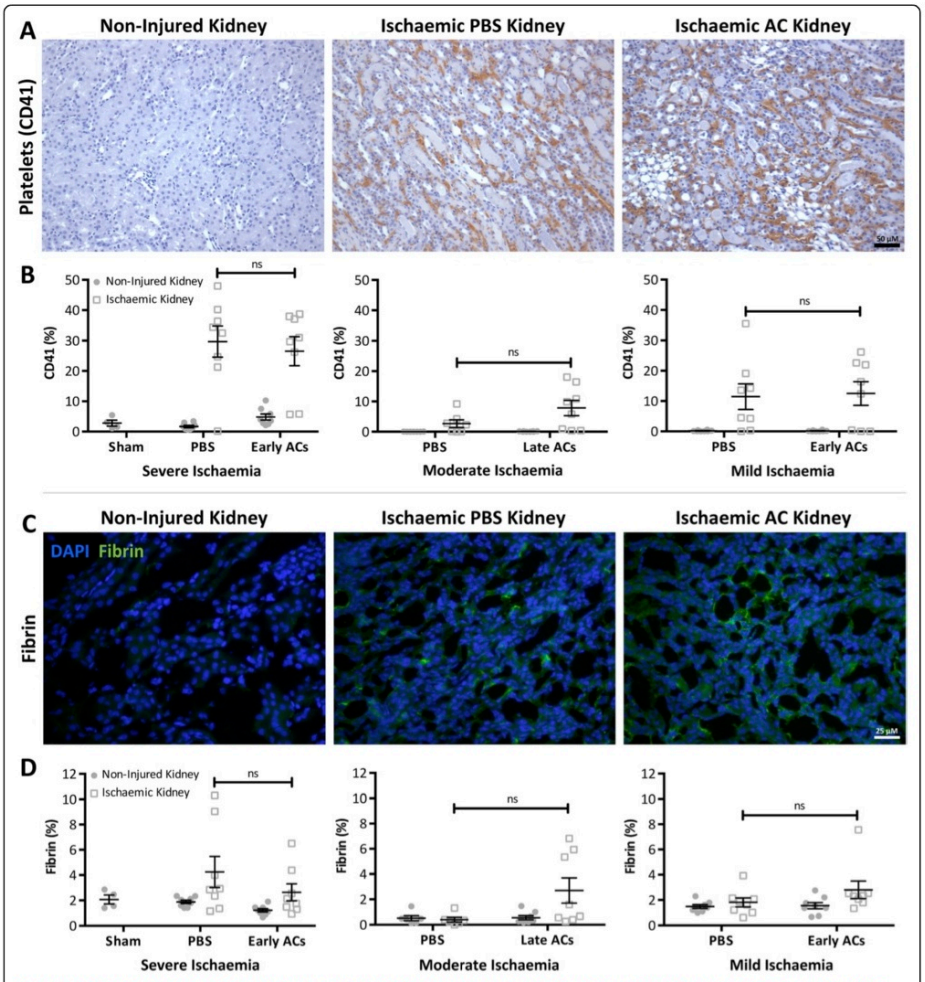

Figure 4 Microvascular congestion remained unaffected following AC administration. Renal IRI was induced in 8-week old male Balb/c mice by a right nephrectomy and ischaemia induced by occluding the left renal pedicle for 20 (mild ischaemia), 24 (moderate) or 25 mins (severe). Sham mice underwent a laparotomy only. Either PBS or 20×10^6 early or late ACs were administered 24 hr prior to renal IRI. Mice were sacrificed 24 hr following IRI. **A & C**) Representative images of the outer stripe of the outer medulla in non-injured and ischaemic kidney sections following platelet (CD41) immunohistochemistry **(A)** and fibrin immunofluorescence **(C)** staining. In ischaemic kidneys microvascular congestion was observed as indicated by platelet and fibrin deposition. (CD41 - Magnification: ×200 & Scale Bar: 50 μM; Fibrin - Magnification: ×400 & Scale Bar: 25 μM) **B & D**) Scoring of platelet **(B)** and fibrin **(D)** staining (expressed as platelet/fibrin$^+$ area) demonstrates that microvascular congestion remained similar between PBS and AC treated mice with severe, moderate and mild ischaemic injury. Grey circle symbol = Non-injured kidney Grey square symbol = Ischaemic kidney. Data expressed as mean ± SEM and analysed by two-way ANOVA. ns = non-significant. Sham ($n = 4$), PBS ($n = 7$–8), AC ($n = 8$).

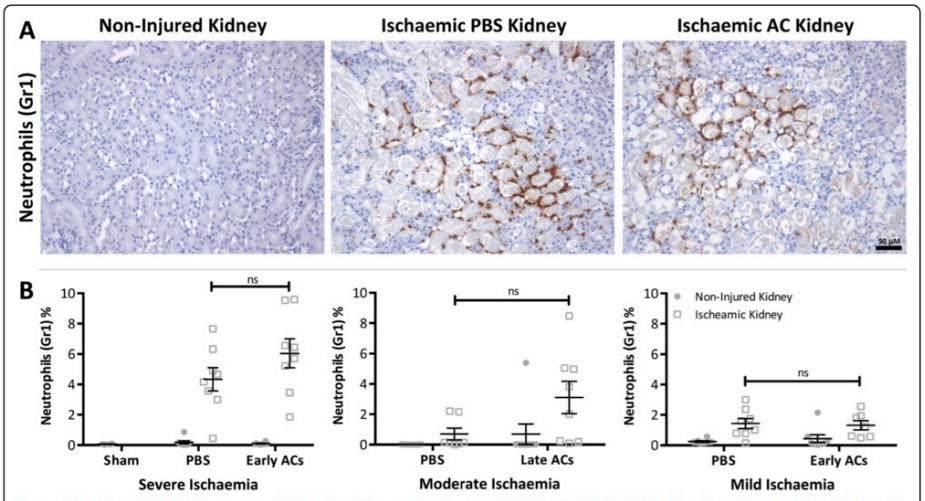

Figure 5 Neutrophil infiltration occurred following ischaemia but was unaffected by AC administration. Renal IRI was induced in 8-week old male Balb/c mice by a right nephrectomy and ischaemia induced by occluding the left renal pedicle for 20 (mild ischaemia), 24 (moderate) or 25 mins (severe). Sham mice underwent a laparotomy only. Either PBS or 20×10^6 early or late ACs were administered 24 hr prior to renal IRI. Mice were sacrificed 24 hr following IRI. **(A)** Representative images of the outer stripe of the outer medulla in non-injured and ischaemic kidney sections following Gr1 staining. In ischaemic kidneys neutrophil infiltration was observed in areas of necrosis. (Magnification: ×200; Scale Bar: 50 μM) **(B)** Scoring of Gr1 staining (expressed as $Gr1^+$ area) demonstrates that neutrophil infiltration remained similar between PBS and AC treated mice with severe, moderate and mild ischaemic injury. Grey circle symbol = Non-injured kidney Grey square symbol = Ischaemic kidney. Data expressed as mean ± SEM and analysed by two-way ANOVA. ns = non-significant. Sham ($n = 4$), PBS ($n = 7$–8), AC ($n = 8$).

AC administration did not result in increased renal inflammation.

Despite previously published work demonstrating the striking ability of ACs to modulate inflammation in multiple organs [8,10-13] this data indicates that both early and late ACs were not protective in renal IRI. Indeed, depending upon the severity of ischaemic injury, administration of both early and late ACs may further impair renal function with this effect unlikely to be secondary to any contaminating viable non-apoptotic cells in the cell populations administered. These studies have not extensively probed the potential mechanisms involved in the worsening of acute kidney dysfunction by early or late ACs. ACs express PS which, in addition to being involved in the phagocytic removal of ACs, may activate the coagulation system [24]. Also, thymocytes typically undergo marked cell blebbing during the apoptotic process and it is possible that they may generate many millions of small microparticles that express PS following intravenous administration. It is thus possible that AC administration might modulate the coagulation status of recipient mice and affect the microvascular response to renal IRI. Interestingly, we did see a trend to increased platelet and fibrin deposition in mild renal IRI following administration of early ACs and moderate renal IRI following administration of late ACs but it was non-significant. Early ACs contained some PI positive cells that have lost membrane integrity whilst the majority of late ACs were PI positive. Although we did not undertake a direct head-to-head comparison of the effects of early and late ACs, it is possible that the adverse effects of late ACs might involve the release of intracellular damage-associated molecular pattern molecules such as high-mobility group box chromosomal protein 1 that may activate cells via Toll-like receptor 4 [25]. This work contrasts with the AC-derived protection observed in other organs and suggests that AC administration does not have translational potential for patients with AKI secondary to renal hypoperfusion.

Additional files

Additional file 1: Isotype controls for Gr1 and CD41 were negative on non-injured and ischaemic kidney. Renal IRI was induced in 8-week old male Balb/c mice by a right nephrectomy and ischaemia induced by occluding the left renal pedicle for 24 mins. Representative images of the outer stripe of the outer medulla in non-injured and ischaemic kidney sections following staining with isotype control antibodies for CD41 and

Gr1. Both isotype control antibodies exhibit no staining in non-injured and ischaemic kidneys. (Magnification: ×200; Scale Bar: 50 μM).

Additional file 2: Administration of viable thymocytes prior to renal IRI had no influence on renal function or ATN. Dissociated thymocytes were prepared from 4-week old male Balb/c mice. Cell viability was assessed by Annexin-V and Propidium Iodide (PI) staining and flow cytometry. Either PBS or 20×10^6 viable non-apoptotic thymocytes were administered to 8-week old male Balb/c mice 24 hr prior to renal IRI induced by a right nephrectomy and occlusion of the left renal pedicle for 20 mins. Mice were sacrificed 24 hr following IRI. **A)** Viable thymocytes were approximately 94% Annexin-V$^-$ PI$^-$. **B)** Administration of viable thymocytes prior to renal IRI had no significant influence on renal function measured by plasma creatinine. **C)** Scoring of ATN (acute tubular necrosis) (expressed as the percentage of necrotic tubules in the outer stripe of the outer medulla) demonstrates that the structural injury remained similar between mice that received PBS or viable thymocytes prior to renal IRI. Grey circle symbol = Non-injured kidney Grey square symbol = Ischaemic kidney. Data expressed as mean ± SEM and analysed by either student's *t*-test or one-way ANOVA. ns = non-significant. PBS ($n = 5$), Viable thymocytes ($n = 5$).

Abbreviations

AC(s): Apoptotic cell(s); AKI: Acute kidney injury; ATN: Acute tubular necrosis; CIA: Collagen induced arthritis; IF: Immunofluorescence; IHC: Immunohistochemistry; IL: Interleukin; IRI: Ischaemia reperfusion injury; LPS: Lipopolysaccharide; OSOM: Outer stripe of the outer medulla; PI: Propidium iodide; PS: Phosphatidylserine; TGF-β: Transforming growth factor-β; TNF-α: Tumour necrosis factor-α.

Competing interests

The authors declare that they have no competing interests.

Authors' contributions

EEH designed the study, acquired the data, performed the data analysis and interpretation and drafted the manuscript. DK participated in the design of the study. JH participated in the design of the study and contributed to the data interpretation and manuscript preparation. All authors have read and approved the final manuscript.

Acknowledgements

The authors would like to thank Gary Borthwick and Spike Clay for their technical assistance with the surgical renal ischaemic reperfusion injury model. The present study was supported by grants from Kidney Research UK (ST4/2011), the Mrs. AE Hogg Charitable Trust for Kidney Research and the Renal Endowment Fund of the Royal Infirmary of Edinburgh.

Received: 7 April 2014 Accepted: 1 October 2014
Published online: 10 October 2014

References

1. Patschan D, Patschan S, Müller GA: **Inflammation and microvasculopathy in renal ischemia reperfusion injury.** *J Transplant* 2012, **2012**:764154.
2. Bonventre JV, Zuk A: **Ischemic acute renal failure: an inflammatory disease?** *Kidney Int* 2004, **66**:480–485.
3. Kinsey GR, Li L, Okusa MD: **Inflammation in acute kidney injury.** *Nephron Exp Nephrol* 2008, **109**:e102–e107.
4. Daha MR, van Kooten C: **Is the proximal tubular cell a proinflammatory cell?** *Nephrol Dial Transplant* 2000, **15**(Suppl 6):41–43.
5. Ramesh G, Reeves WB: **Inflammatory cytokines in acute renal failure.** *Kidney Int* 2004, **66**(Suppl):S56–S61.
6. Lutz J, Thürmel K, Heemann U: **Anti-inflammatory treatment strategies for ischemia/reperfusion injury in transplantation.** *J Inflamm (Lond)* 2010, **7**:27.
7. Fadok VA, Voelker DR, Campbell PA, Cohen JJ, Bratton DL, Henson PM: **Exposure of phosphatidylserine on the surface of apoptotic lymphocytes triggers specific recognition and removal by macrophages.** *J Immunol* 1992, **148**:2207–2216.
8. Fadok VA, Bratton DL, Konowal A, Freed PW, Westcott JY, Henson PM: **Macrophages that have ingested apoptotic cells in vitro inhibit proinflammatory cytokine production through autocrine/paracrine mechanisms involving TGF-beta, PGE2, and PAF.** *J Clin Invest* 1998, **101**:890–898.
9. Savill J, Dransfield I, Gregory C, Haslett C: **A blast from the past: clearance of apoptotic cells regulates immune responses.** *Nat Rev Immunol* 2002, **2**:965–975.
10. Ren Y, Xie Y, Jiang G, Fan J, Yeung J, Li W, Tam PKH, Savill J: **Apoptotic cells protect mice against lipopolysaccharide-induced shock.** *J Immunol* 2008, **180**:4978–4985.
11. Gray M, Miles K, Salter D, Gray D, Savill J: **Apoptotic cells protect mice from autoimmune inflammation by the induction of regulatory B cells.** *Proc Natl Acad Sci U S A* 2007, **104**:14080–14085.
12. Lee Y-J, Moon C, Lee S-H, Park H-J, Seoh J-Y, Cho M-S, Kang JL: **Apoptotic cell instillation after bleomycin attenuates lung injury through hepatocyte growth factor induction.** *Eur Respir J* 2012, **40**:424–435.
13. Zhang M, Xu S, Han Y, Cao X: **Apoptotic cells attenuate fulminant hepatitis by priming Kupffer cells to produce interleukin-10 through membrane-bound TGF-β.** *Hepatology* 2011, **53**:306–316.
14. Miles K, Clarke DJ, Lu W, Sibinska Z, Beaumont PE, Davidson DJ, Barr TA, Campopiano DJ, Gray M: **Dying and necrotic neutrophils are anti-inflammatory secondary to the release of alpha-defensins.** *J Immunol* 2009, **183**:2122–2132.
15. Hesketh EE, Czopek A, Clay M, Borthwick G, Ferenbach D, Kluth D, Hughes J: **Renal ischaemia reperfusion injury: a mouse model of injury and regeneration.** *J Vis Exp* 2014, **8**. doi:10.3791/51816.
16. Tse GH, Marson LP: **A comparative study of 2 computer-assisted methods of quantifying brightfield microscopy images.** *Appl Immunohistochem Mol Morphol* 2013, **21**:464–470.
17. Jennewein C, Tran N, Paulus P, Ellinghaus P, Eble JA, Zacharowski K: **Novel aspects of fibrin(ogen) fragments during inflammation.** *Mol Med* 2011, **17**:568–573.
18. Eneström S, Druid H, Rammer L: **Fibrin deposition in the kidney in post-ischaemic renal damage.** *Br J Exp Pathol* 1988, **69**:387–394.
19. Casciola-Rosen L, Rosen A, Petri M, Schlissel M: **Surface blebs on apoptotic cells are sites of enhanced procoagulant activity: implications for coagulation events and antigenic spread in systemic lupus erythematosus.** *Proc Natl Acad Sci U S A* 1996, **93**:1624–1629.
20. Friedewald JJ, Rabb H: **Inflammatory cells in ischemic acute renal failure.** *Kidney Int* 2004, **66**:486–491.
21. Ferenbach DA, Ramdas V, Spencer N, Marson L, Anegon I, Hughes J, Kluth DC: **Macrophages expressing heme oxygenase-1 improve renal function in ischemia/reperfusion injury.** *Mol Ther* 2010, **18**:1706–1713.
22. Daemen MARC, de Vries B, Buurman WA: **Apoptosis and inflammation in renal reperfusion injury.** *Transplantation* 2002, **73**:1693–1700.
23. Daemen MA, Van't Veer C, Denecker G, Heemskerk VH, Wolfs TG, Clauss M, Vandenabeele P, Buurman WA: **Inhibition of apoptosis induced by ischemia-reperfusion prevents inflammation.** *J Clin Invest* 1999, **104**:541–549.
24. Vance JE, Steenbergen R: **Metabolism and functions of phosphatidylserine.** *Prog Lipid Res* 2005, **44**:207–234.
25. Zhao H, Perez JS, Lu K, George AJT, Ma D: **Role of Toll-like receptor-4 in renal graft ischemia-reperfusion injury.** *Am J Physiol Renal Physiol* 2014, **306**:F801–F811.

doi:10.1186/s12950-014-0031-6
Cite this article as: Hesketh *et al.*: Apoptotic cell administration is detrimental in murine renal ischaemia reperfusion injury. *Journal of Inflammation* 2014 **11**:31.

Video Article

Renal Ischaemia Reperfusion Injury: A Mouse Model of Injury and Regeneration

Emily E. Hesketh[1], Alicja Czopek[1], Michael Clay[1], Gary Borthwick[1], David Ferenbach[1], David Kluth[1], Jeremy Hughes[1]

[1]MRC Centre for Inflammation Research, University of Edinburgh

Correspondence to: Emily E. Hesketh at E.E.Hesketh@sms.ed.ac.uk

URL: http://www.jove.com/video/51816
DOI: doi:10.3791/51816

Keywords: Medicine, Issue 88, Murine, Acute Kidney Injury, Ischaemia, Reperfusion, Nephrectomy, Regeneration, Laparotomy

Date Published: 6/7/2014

Citation: Hesketh, E.E., Czopek, A., Clay, M., Borthwick, G., Ferenbach, D., Kluth, D., Hughes, J. Renal Ischaemia Reperfusion Injury: A Mouse Model of Injury and Regeneration. *J. Vis. Exp.* (88), e51816, doi:10.3791/51816 (2014).

Abstract

Renal ischaemia reperfusion injury (IRI) is a common cause of acute kidney injury (AKI) in patients and occlusion of renal blood flow is unavoidable during renal transplantation. Experimental models that accurately and reproducibly recapitulate renal IRI are crucial in dissecting the pathophysiology of AKI and the development of novel therapeutic agents. Presented here is a mouse model of renal IRI that results in reproducible AKI. This is achieved by a midline laparotomy approach for the surgery with one incision allowing both a right nephrectomy that provides control tissue and clamping of the left renal pedicle to induce ischaemia of the left kidney. By careful monitoring of the clamp position and body temperature during the period of ischaemia this model achieves reproducible functional and structural injury. Mice sacrificed 24 hr following surgery demonstrate loss of renal function with elevation of the serum or plasma creatinine level as well as structural kidney damage with acute tubular necrosis evident. Renal function improves and the acute tissue injury resolves during the course of 7 days following renal IRI such that this model may be used to study renal regeneration. This model of renal IRI has been utilized to study the molecular and cellular pathophysiology of AKI as well as analysis of the subsequent renal regeneration.

Video Link

The video component of this article can be found at http://www.jove.com/video/51816/

Introduction

Ischaemia reperfusion injury (IRI) is a common mode of injury for multiple organs including the kidney, heart and brain. Renal IRI may lead to acute kidney injury (AKI) in patients and no specific treatment is available. AKI as a result of IRI has a complicated pathogenesis involving both the innate and adaptive immune response[1]. An experimental model of renal IRI offers the potential to dissect the key cells and mediators involved in the pathogenesis of AKI as well as the subsequent renal regeneration that ensues over subsequent days. Furthermore the effects of novel therapeutic agents upon disease processes can be assessed.

The overall goal of the experimental model of renal IRI described here is to induce both acute functional and structural kidney injury. Some investigators have utilized a model that involves the induction of bilateral IRI[2]. Although the bilateral renal IRI model is of use, the unilateral renal IRI model has the advantage of a right nephrectomy being undertaken at the time of surgery. The right nephrectomy tissue serves as valuable control tissue in studies involving a pretreatment step that either induces or suppresses the expression of a gene or protein. For example, we have used this model to assess the preconditioning effects of heme arginate (HA) injection 24 hours before renal IRI[3]. The successful induction of the cytoprotective enzyme heme-oxygenase-1 (HO-1) by HA before IRI was confirmed in the right nephrectomy control tissue[4]. HA reduced renal IRI in aged mice in part via an HO-1 dependent mechanism. Similarly, we have used the model in macrophage depletion studies to examine the role of macrophages in renal IRI[5]. Immunohistochemical analysis of the right nephrectomy tissue can be used to confirm the efficacy of the ablation methodology. The right nephrectomy tissue can therefore be used to both confirm and quantify the level of induction or inhibition of the molecule of interest in each individual experimental animal. This model will be of interest to researchers who are using drugs or other compounds to modulate the expression of genes or proteins etc. prior to the induction of renal IRI.

Other studies have used flank incisions to access the kidneys. The model described here uses a single midline abdominal surgery to perform both the right nephrectomy and induce ischaemia reperfusion of the left kidney. This surgical approach provides excellent visualization of the surgical field including the renal pedicles and color changes that follow renal pedicle clamping. Our published experience with the model[4-6] indicates that mice quickly recover from the surgery with a near 100% survival rate.

Lastly, kinetic analysis of the model over a period of 7 days indicates that this model exhibits restoration of both renal function and tubular integrity, with significant tubular cell proliferation.

Copyright © 2014 Journal of Visualized Experiments

Protocol

NOTE: Animal experiments were performed in accordance with the guidelines and regulations imposed by the Animals (Scientific Procedures) Act 1986. Procedures were conducted using sterile (autoclaved) surgical instruments and consumables. Whilst the murine model of renal IRI presented here was performed on an 8-week-old male Balb/c mouse it can be reproducibly performed on a variety of murine strains of either gender typically aged between 7 – 15 weeks, with the optimum age being 8 weeks. The data presented in the representative results section was obtained from both Balb/c and FVB mice. The application of warmed saline is used to keep the intestines and surgical area moist but it should be carefully monitored and kept to a minimum as the excessive application of fluids can lead to an artifactual lowering of the serum or plasma creatinine levels, which is an important experimental readout.

1. Animal Preparation and Laparotomy

1. Anesthetize the mouse with ketamine hydrochloride (70 mg/kg) and medetomidine hydrochloride (1 mg/kg) intraperitoneally and confirm the depth of anesthesia by loss of reflexes *e.g.* toe pinch. The duration of the resulting anesthetic plane is 4 hours. This is sufficient to perform the entire surgical procedure and no supplemental anesthesia is required.
2. Remove the hair surrounding the incision area, ensure that the area is free of loose hair, and sanitize the abdominal skin using a dilute chlorhexidine solution.
3. Place the mouse on a heated surgical pad in a supine position and fix the upper and lower limbs to the pad using low-tack adhesive tape. Ensure that the upper extremities are maintained in a normal position to prevent lung compression. Throughout the procedure monitor the mouse for thermal burns. If possible it is recommended that a non-electric heat source be used.
4. Administer the analgesic buprenorphine hydrochloride (0.06 mg/kg) subcutaneously and apply eye lubricant to the eyes to prevent corneal drying. Analgesics are administered pre-operatively in order to aid the post-surgical recovery.
5. Using tissue separating scissors or a scalpel blade make a midline laparotomy incision and bluntly separate the skin from the peritoneum. This allows the skin and peritoneum to be sutured separately during wound closure. An incision of the avascular linea alba is made giving access to the peritoneal cavity.
6. To create a clear view of the surgical area insert a retractor and drape the mouse.

2. Ureter Division and Right Nephrectomy

1. Gently push the intestines towards the left side of the abdominal cavity using autoclaved sterilized cotton swabs moistened with saline to expose the right kidney and ureter. Cover the intestines with moistened drapes to prevent drying.
2. Lift the right ureter with angled forceps. Ligate the right ureter twice using 6/0 silk-braided suture. For long term experiments, use absorbable sutures for all abdominal surgeries.
3. Divide the ureter between the sutures. Whilst the vesico-ureteric junction should prevent urine from leaking into the peritoneum from the bladder the ureter is ligated as a safeguard against any leakage post-operatively during long-term experiments.
4. To allow easier access when performing the right nephrectomy, gently push the liver up and to the right using a moistened cotton swab and hold in place using moistened gauze to expose the right renal artery and vein.
5. Bluntly dissect the connective tissue and fat along the medial aspect of the right kidney as far as the right renal artery and vein.
6. Create a channel underneath the renal artery and vein by carefully sliding the angled forceps underneath the blood vessels. Guide the forceps underneath with the tips closed and gently remove with the tips open in order to facilitate the formation of the channel.
7. Repeat step 2.6 until the tips of the forceps are visible through the connective tissues just above the renal artery and vein. Once visible gently rub the tips of the forceps against the tips of another set of angled forceps to gently break the connective tissue.
8. With the renal artery and vein clearly accessible they can now be occluded. Carefully slide angled forceps underneath the renal artery and vein with the tips closed. Once in place open the tips of the forceps and guide the haemostatic clip applicator between the tips and firmly apply a haemostatic clip onto the renal artery and vein close to the kidney. Alternatively the renal artery and vein can be ligated using 6/0 silk braided suture.
9. Divide the occluded renal artery and vein close to the kidney, which can now be removed with any remaining adherent connective tissue.
10. Remove any gauze used to hold the liver and replace the intestines with cotton swabs.

3. Left Kidney Ischaemia and Reperfusion

1. Gently push the intestines towards the right side of the abdominal cavity with cotton swabs to expose the left kidney and ureter and cover with moistened drapes. If necessary the pancreas can be deflected with moistened gauze to allow easier access.
2. Use blunt dissection to gently break the connective tissues anterior and posterior to the left renal artery and vein, and then create a channel underneath the vessels in a similar manner to that described in Ureter Division and Right Nephrectomy step 2.4.
3. Induce ischaemia of the left kidney by applying a micro serrafine clip onto the renal artery and vein. Successful ischaemia can be visually confirmed by a gradual uniform darkening of the kidney. Blood vessels in addition to the left renal artery and vein may occasionally supply the kidney. If present, these additional blood vessels will also need to be occluded using micro serrafine clips in order to successfully induce ischaemia of the entire kidney.
4. Replace the intestines and carefully ensure that there are no abrupt twists that may lead to intestinal ischaemia compromising results. Temporarily close the peritoneum with a single suture.
5. Following ischaemia induction immediately place the mouse on a homeothermic blanket with a rectal thermistor attached to a control unit that will maintain the body temperature at 37 °C for the required duration of ischaemia. To define the appropriate length of ischaemia necessary to induce the desired degree of renal injury and kidney failure it is recommended that a titration be performed for each strain and surgical operator.

Copyright © 2014 Journal of Visualized Experiments

6. Shortly before the end of the ischaemic period re-open the peritoneum and carefully position the intestines to allow access to the clamp and view the kidney. Insertion of the retractor, as shown in the video, is not necessary and was solely performed for presentational purposes.
7. Remove the clamp after the period of ischaemia has concluded. Immediately after removal the kidney will rapidly change color from a dark maroon to a healthy dark pink indicating successful reperfusion.
8. Again ensure that the intestines are not twisted prior to closing the peritoneum with a blanket stitch using 6/0 braided silk suture. Then close the skin using metallic skin clips.
9. To minimize the risk of post-operative infection, apply an antiseptic such as iodine/alcohol solution to the surgical area.

4. Post-operative Recovery and Care

1. Partially reverse anesthesia with atipamezole hydrochloride (2 mg/kg) subcutaneously and administer fluids with a subcutaneous injection of 1 ml warmed saline to prevent dehydration following surgery.
2. Carefully monitor mice until they have recovered consciousness, appear alert and are able to right themselves.
3. Allow mice to recover in a heated box kept at 29 °C, located in a quiet environment, for 24 hr. Mice will have an impaired ability to thermoregulate due to the anesthesia and it is therefore crucial that they are housed at an elevated temperature to enable effective recovery. Moistened food can also be provided to encourage fluid and nutrition intake.
4. For long-term recovery experiments provide ongoing analgesics and remove skin clips 7 days following surgery.

5. Assessing Functional and Structural Kidney Injury and Regeneration

1. Blood may be collected from the tail vein during experiments or by cardiac puncture at the time of euthanasia at the end of the experiment. Measure renal function by serum creatinine, using a creatinase based method, and blood urea nitrogen (BUN) on a biochemical centrifugal analyzer as described previously[7]. The renal function of normal healthy mice needs to be determined before establishing a model of renal failure as this can vary markedly depending on the analysis method used *e.g.* the Jaffe reaction and creatinase based methods for measuring creatinine give different results.
2. Examine renal structure by histopathology on paraffin embedded kidney tissue sections stained with Haematoxylin and Eosin (H&E) or Periodic Acid Schiff (PAS). Capture between 5 – 10 images at 200x magnification within the outer stripe of the outer medulla (OSOM) for each mouse. Assess the level of injury in the OSOM as this region is injured in this model because it is highly vulnerable to hypoxia.
3. Use either of the two scoring systems detailed below to measure acute tubular necrosis (ATN) or regeneration. Representative morphology of the classifications used in these systems is illustrated in **Figure 1**.
4. Use a simple binary system to score ATN. On the basis of cellular integrity and morphology mark and count tubules as either viable (intact cell morphology) or necrotic (compromised cell integrity, abnormal cell morphology or loss of cells).
    1. Express the number of necrotic tubules as a percentage of the total number of tubules (necrotic tubules %).
5. Classify regeneration using another system based on cell integrity, morphology and nuclei number. Mark and count tubules as healthy, necrotic, injured or recovering according to the criteria listed in the following steps.
    1. As with the ATN scoring system (detailed in step 5.4) mark tubules with intact normal cells as healthy whilst tubules showing compromised cell integrity, abnormal cell morphology or overt cell loss should be scored as necrotic.
    2. Classify tubules as injured if they have a thinned cytoplasm containing few nuclei. In contrast, designate tubules containing more nuclei with more normal cell morphology as recovering.
    3. Express each tubule classification as a percentage of the total tubule number.

Representative Results

Tubular injury and recovery may be assessed by H&E or PAS staining of tissue sections following renal IRI. Tubules located within the OSOM are classified as healthy, injured, necrotic or recovering according to cell morphology, integrity and nuclei number (**Figure 1**). The functional and structural injury in this model is dependent upon the duration of ischaemia. A progressive increase in the severity of renal dysfunction, assessed by plasma creatinine and BUN, is evident as the duration of ischaemia is increased by 2min increments (**Figure 2**). The extent of structural renal injury, inferred from the ATN score, follows a similar trend with more severe ATN accompanying more prolonged ischaemia (**Figure 3**). Following an initial titration of varying durations of ischaemia, this model of renal IRI should achieve a near 100% success rate, with all mice developing both functional and structural injury following surgery. This model of renal IRI also enables a fine level of control over the degree of injury with limited variation observed between animals (**Figures 2** and **3**). The use of different durations of ischaemia enables therapeutic interventions to be examined for their ability to modulate different levels of injury severity. For example on the basis of the length of ischaemia the resulting injury can be classed as mild (20 min), moderate (22 min) or high (24 min). These values are for male Balb/c mice aged 8 weeks and are included as guidance only. Investigators should establish their own experimental conditions as these will differ according to mouse strain, age, sex and the biochemical assay used to assess renal function.

This model has been successfully used to study regeneration following renal IRI with both renal function and structure recovering over the ensuing days. A gradual decline in plasma creatinine and BUN levels are observed, with plasma creatinine returning to basal levels by day 7 (**Figure 4**). An assessment of H&E stained tissue sections indicates that an increased number of tubules are classified as healthy or recovering at day 7 compared to day 4 indicating that tissue regeneration is taking place (**Figure 5**). The administration of 5-bromo-2'-deoxyuridine (BrdU) prior to sacrifice facilitates the immunostaining of kidney tissue for BrdU and subsequent quantification of tubular cell proliferation. Dramatic nuclear BrdU expression is observed 4 days following renal IRI indicating that the tubules are undergoing marked cell proliferation in order to restore tubule integrity and function (**Figure 6**). The combination of renal function assessment, scoring for structural improvement and BrdU immunostaining enables this model to be used to study regeneration following renal IRI. This allows the long-term effects of therapeutic interventions to be investigated.

Copyright © 2014 Journal of Visualized Experiments

Lastly, the utility of this model is dependent upon the induction of global ischaemia to the entire kidney and this may be jeopardized by the presence of blood vessels supplying the kidney in addition to the main left renal artery. If these additional vessels are not clamped then part of the kidney will not be subjected to ischaemic injury (**Figure 7**).

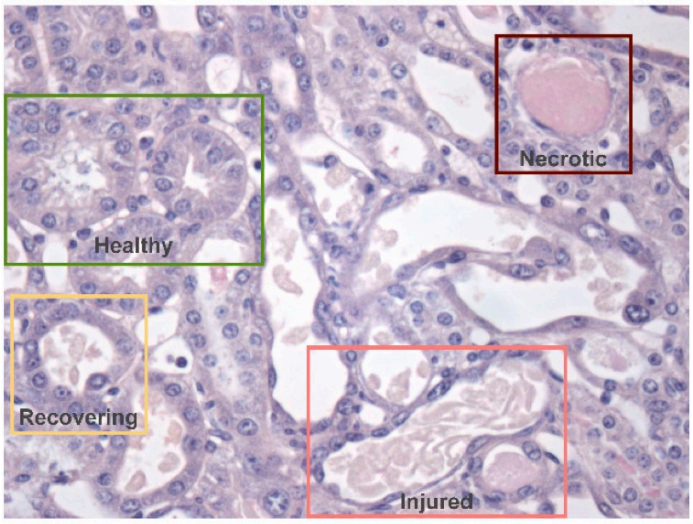

Figure 1. Scoring of structural tubular injury and regeneration – Representative morphology of healthy, recovering, injured and necrotic tubules. Tissue sections from a kidney removed 4 days following renal IRI are stained with PAS for assessment. Tubules located within the OSOM are classified as healthy, injured, necrotic or recovering according to cell morphology, integrity and nuclei number with representative examples highlighted. Healthy tubules are intact with a normal cellular morphology. Necrotic tubules exhibit a compromised monolayer with evident cell loss and loss of cell morphology. Injured tubules exhibit a thinned cellular monolayer and contain fewer nuclei. In contrast, recovering tubules exhibit a more normal cellular morphology and a similar number of nuclei to healthy tubules. Magnification: 400x. Please click here to view a larger version of this figure.

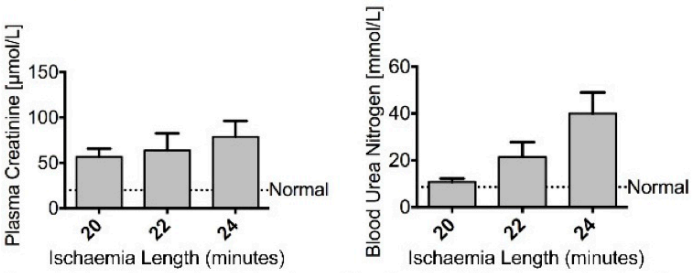

Figure 2. Injury – Renal ischaemia impairs renal function. Male Balb/c mice aged 8 weeks underwent a right nephrectomy and the left renal pedicle was clamped for 20, 22 or 24 min (n = 4 per group). Mice were sacrificed at 24 hr following renal IRI. Plasma creatinine and blood urea nitrogen show an increasing trend of severity as the length of ischaemia increased. The dashed line represents the levels of plasma creatinine and blood urea nitrogen found in normal control mice. Data presented as mean ± SEM and analyzed by one-way ANOVA. Please click here to view a larger version of this figure.

Copyright © 2014 Journal of Visualized Experiments

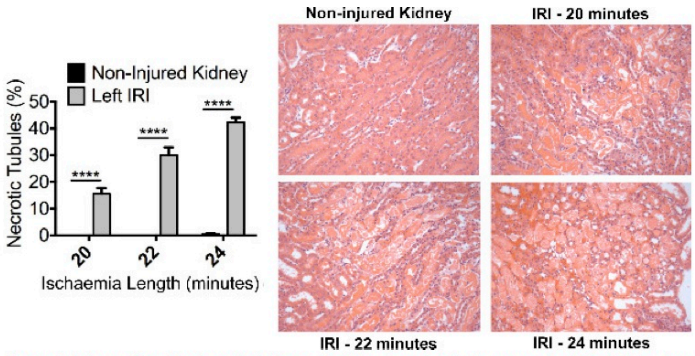

Figure 3. Injury – Renal ischaemia induces significant acute tubular necrosis. Male Balb/c mice aged 8 weeks underwent a right nephrectomy and the left renal pedicle was clamped for 20, 22 or 24 min (n = 4 per group). Mice were sacrificed at 24 hr following renal IRI. Representative photomicrographs (Magnification: 200x) of the OSOM from H&E stained kidney sections of control and injured kidneys illustrate ATN. Formal scoring of ATN (expressed as the proportion of necrotic tubules) confirms the increased level of injury with increasing duration of ischaemia. Data presented as mean ± SEM and analyzed by one-way ANOVA (**** = $P \leq 0.0001$). Please click here to view a larger version of this figure.

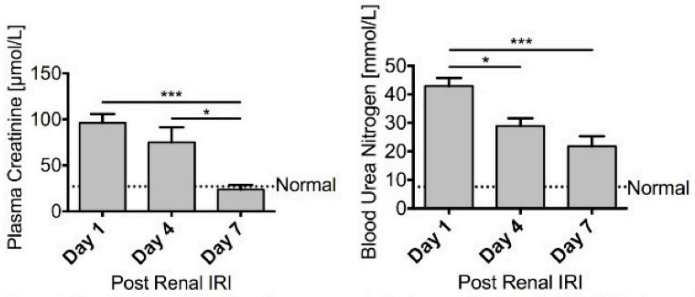

Figure 4. Regeneration – Renal function recovers following renal ischaemia. Male FVB mice aged 8 – 10 weeks underwent a right nephrectomy prior to 25 min of ischaemia to the left kidney. Mice were sacrificed 1 day (n = 10), 4 days (n = 10) or 7 days (n = 6) following renal IRI. Both plasma creatinine and blood urea nitrogen steadily decline over the course of 7 days, with plasma creatinine returning to basal levels, illustrating a recovery in renal function. Data presented as mean ± SEM and analyzed by one-way ANOVA (*** = $P \leq 0.001$, * = $P \leq 0.05$). Please click here to view a larger version of this figure.

Copyright © 2014 Journal of Visualized Experiments

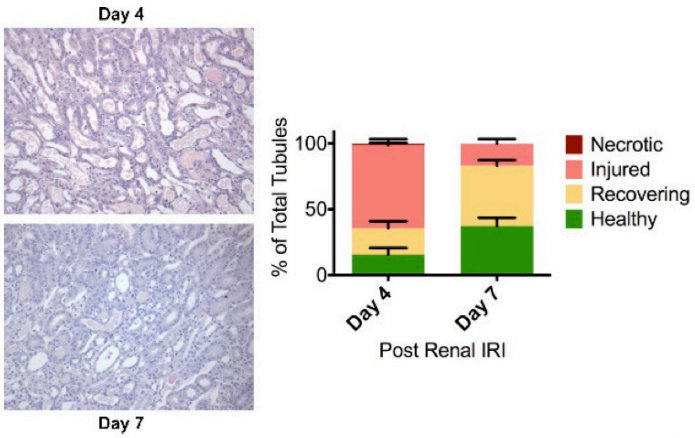

Figure 5. Regeneration – Renal tissue shows signs of recovery following renal ischaemia. Male FVB mice aged 8 – 10 weeks underwent a right nephrectomy prior to 25 min of ischaemia to the left kidney. Mice were sacrificed 4 days (n = 10) or 7 days (n = 6) following renal IRI. Representative photomicrographs (Magnification: 200x) of the OSOM following the induction of ischaemia are shown. Formal scoring of the number of healthy, recovering, injured or necrotic tubules within the OSOM was assessed in PAS stained paraffin sections. At day 4 following renal IRI a large proportion of tubules within the OSOM still appear injured. However by 7 days there is a considerable increase in the proportion of tubules that are classified as healthy or recovering indicative of renal regeneration. Data presented as mean ± SEM. Please click here to view a larger version of this figure.

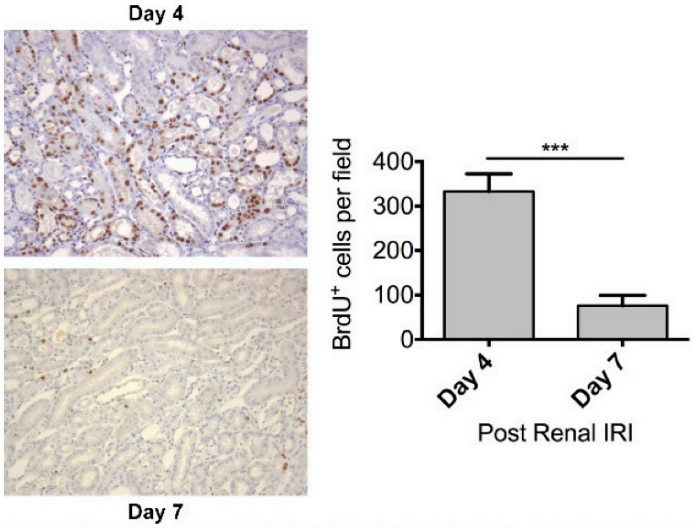

Figure 6. Regeneration – Dramatic tubular proliferation is evident 4 days following renal ischaemia. Male FVB mice aged 8 – 10 weeks underwent a right nephrectomy prior to 25 min of ischaemia to the left kidney. BrdU (50 mg/kg) was administered by intraperitoneal injection 24 hours prior to sacrifice. Mice were sacrificed 4 days (n = 10) or 7 days (n = 6) following renal IRI. Representative photomicrographs (Magnification: 200x) of the OSOM from mice sacrificed at day 4 and day 7 following the induction of ischaemia are shown. Tubular cell proliferation was assessed by immunohistochemical staining for BrdU on paraffin embedded kidney sections. Tubular cell proliferation was quantified by counting the number of BrdU positive nuclei in the OSOM with increased cell proliferation evident at day 4. Data presented as mean ± SEM and analyzed by students t-test (*** = $P \leq 0.001$). Please click here to view a larger version of this figure.

Copyright © 2014 Journal of Visualized Experiments

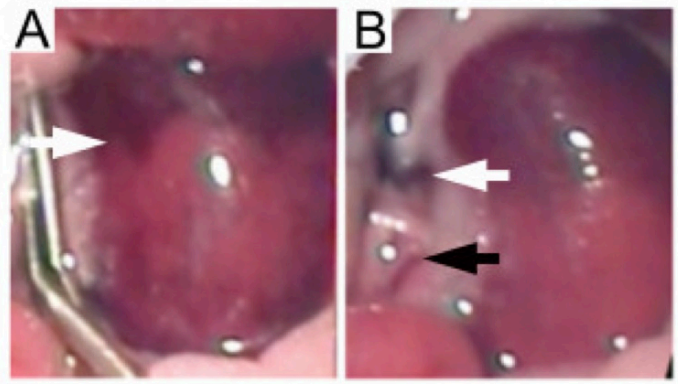

Figure 7. Left ischaemic kidney with non-occluded additional renal blood vessels. Failure to occlude additional blood vessels supplying the kidney leads to inconsistent ischaemia. (**A**) The absence of global kidney ischaemia is indicated by an uneven color change (white arrow) when the micro serrafine clip is in position. (**B**) Following removal of the micro serrafine clip, the main renal artery and vein are visible (white arrow) together with the additional blood vessel supplying the middle and lower pole of the kidney (black arrow). Please click here to view a larger version of this figure.

Discussion

Renal IRI is an important cause of AKI with no specific treatment available. The experimental study of renal IRI has been highly informative with previous work demonstrating the role of macrophages, dendritic cells, lymphocytes, regulatory T-cells as well as other cells and mediators in the induction of both the acute injury and healing phase[5,8-16]. In addition, experimental renal IRI has been used to assess the effect of various therapeutic agents[4,17-19].

The model of renal IRI detailed here uses a midline laparotomy approach to perform a right nephrectomy and induce ischaemia in the left kidney using clamps. As illustrated by the representative results, modifying the duration of ischaemia can control the severity of injury. Therefore this model can be adjusted to induce mild, moderate or a high level of kidney injury as required by the experimental question posed. However, a limitation of this model is that it is not suitable for the induction of very severe kidney injury by prolonged renal ischaemia. The resultant severe acute kidney dysfunction may lead to significant mortality.

There are several aspects of this model that are crucial in order to achieve predictable and reproducible renal injury. One major source of variability with this model can originate from the body temperature during the ischaemic period[20]. It is therefore essential that body temperature is maintained at a constant level and monitored throughout the ischaemic period. In this protocol a control unit with temperature probes and homoeothermic blanket was used to auto-regulate body temperature at 37 °C. The influence of body temperature on the susceptibility of the kidney to ischaemic injury is well described. Previous work has shown that body temperature affects the severity of renal IRI[20] and variation in the body temperature of the mice is a potential confounding factor that may affect the interpretation of the results. Another important consideration is that mice may exhibit anatomical variation with additional blood vessels that supply the left kidney. It is critical that such additional blood vessels are identified and occluded when performing the right nephrectomy and inducing global ischaemia in the left kidney. Failure to do so will result in inconsistent ischaemia throughout the kidney. Similarly, the color change of the left kidney following clamping of the left renal pedicle should be carefully scrutinized as the absence of a global color changes suggests the presence of an additional renal artery that had not initially been identified.

In contrast to models that utilize bilateral kidney ischaemia, this model will be of interest to researchers who are using the prophylactic administration of pharmaceutical drugs or other agents to modulate the expression of genes, proteins etc. prior to renal injury. The right nephrectomy tissue can be used to both confirm and quantify the level of induction or inhibition of the molecule of interest in each individual experimental animal. This model will also be of interest to researchers studying renal regeneration as the acute injury phase is followed by prominent tubular proliferation.

Some experimental models of renal inflammation are limited as significant disease can only be induced in certain strains of mice. In contrast, the model of renal IRI described here is versatile and can be applied to both male[5] and female[4] mice, different strains of mice as well as aged mice[4].

Disclosures

The authors have no competing or conflicting interests to disclose.

Copyright © 2014 Journal of Visualized Experiments

Acknowledgements

The present study was supported by grants from Kidney Research UK (ST4/2011), the Cunningham Trust (CT11/14) and the Mrs EA Hogg's Charitable Trust.

References

1. Kinsey, G. R., Li, L., & Okusa, M. D. Inflammation in acute kidney injury. *Nephron Exp Nephrol.* **109**, e102-107 (2008).
2. Wei, Q., & Dong, Z. Mouse model of ischemic acute kidney injury: technical notes and tricks. *Am J Physiol Renal Physiol.* **303**, F1487-1494, doi:10.1152/ajprenal.00352.2012 (2012).
3. Ferenbach, D. A., Kluth, D. C., & Hughes, J. Hemeoxygenase-1 and renal ischaemia-reperfusion injury. *Nephron Exp Nephrol.* **115**, e33-37, doi:10.1159/000313828 (2010).
4. Ferenbach, D. A. *et al.* The induction of macrophage hemeoxygenase-1 is protective during acute kidney injury in aging mice. *Kidney Int.* **79**, 966-976, doi:10.1038/ki.2010.535 (2011).
5. Ferenbach, D. A. *et al.* Macrophage/monocyte depletion by clodronate, but not diphtheria toxin, improves renal ischemia/reperfusion injury in mice. *Kidney Int.* **82**, 928-933, doi:10.1038/ki.2012.207 (2012).
6. Ferenbach, D. A. *et al.* Macrophages expressing heme oxygenase-1 improve renal function in ischemia/reperfusion injury. *Mol Ther.* **18**, 1706-1713, doi:10.1038/mt.2010.100 (2010).
7. Keppler, A. *et al.* Plasma creatinine determination in mice and rats: an enzymatic method compares favorably with a high-performance liquid chromatography assay. *Kidney Int.* **71**, 74-78, doi:10.1038/sj.ki.5001988 (2007).
8. Vinuesa, E. *et al.* Macrophage involvement in the kidney repair phase after ischaemia/reperfusion injury. *J Pathol.* **214**, 104-113. (2008).
9. Friedewald, J. J., & Rabb, H. Inflammatory cells in ischemic acute renal failure. *Kidney Int.* **66**, 486-491 (2004).
10. Gandolfo, M. T. *et al.* Foxp3+ regulatory T cells participate in repair of ischemic acute kidney injury. *Kidney Int.* **76**, 717-729, doi:10.1038/ki.2009.259 (2009).
11. Burne, M. J. *et al.* Identification of the CD4+ T cell as a major pathogenic factor in ischemic acute renal failure. *J Clin Invest.* **108**, 1283-1290 (2001).
12. Burne-Taney, M. J. *et al.* B cell deficiency confers protection from renal ischemia reperfusion injury. *J Immunol.* **171**, 3210-3215 (2003).
13. Kinsey, G. R. *et al.* Regulatory T cells suppress innate immunity in kidney ischemia-reperfusion injury. *J Am Soc Nephrol.* **20**, 1744-1753, doi:10.1681/ASN.2008111160 (2009).
14. Li, L., & Okusa, M. D. Macrophages, dendritic cells, and kidney ischemia-reperfusion injury. *Semin Nephrol.* **30**, 268-277 (2010).
15. Lin, S. L. *et al.* Macrophage Wnt7b is critical for kidney repair and regeneration. *Proc Natl Acad Sci U S A.* **107**, 4194-4199 (2010).
16. Lee, S. *et al.* Distinct macrophage phenotypes contribute to kidney injury and repair. *J Am Soc Nephrol.* **22**, 317-326 (2011).
17. Kumar, S. *et al.* Dexamethasone ameliorates renal ischemia-reperfusion injury. *J Am Soc Nephrol.* **20**, 2412-2425, doi:10.1681/ASN.2008080868 (2009).
18. Sharples, E. J. *et al.* Erythropoietin protects the kidney against the injury and dysfunction caused by ischemia-reperfusion. *J Am Soc Nephrol.* **15**, 2115-2124, doi:10.1097/01.ASN.0000135059.67385.5D (2004).
19. Gueler, F. *et al.* Statins attenuate ischemia-reperfusion injury by inducing heme oxygenase-1 in infiltrating macrophages. *Am J Pathol.* **170**, 1192-1199, doi:10.2353/ajpath.2007.060782 (2007).
20. Delbridge, M. S., Shrestha, B. M., Raftery, A. T., El Nahas, A. M., & Haylor, J. L. The effect of body temperature in a rat model of renal ischemia-reperfusion injury. *Transplant Proc.* **39**, 2983-2985, doi:10.1016/j.transproceed.2007.04.028 (2007).

Copyright © 2014 Journal of Visualized Experiments